

**Best
Available
Copy**

AD-761 648

ANALYTIC MODELING OF ROCK-STRUCTURE INTERACTION

Vol. 1

AGBABIAN ASSOCIATES

PREPARED FOR
ADVANCED RESEARCH PROJECTS AGENCY
BUREAU OF MINES

APRIL 1973

Distributed By:

NTIS

National Technical Information Service
U. S. DEPARTMENT OF COMMERCE

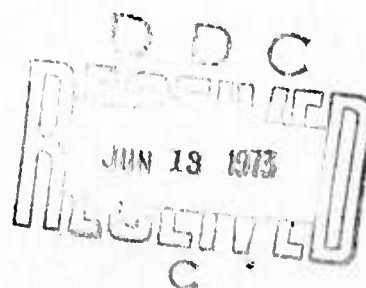
AD 761648



ANALYTIC MODELING OF ROCK-STRUCTURE INTERACTION

Final Technical Report
Volume 1
April 1973

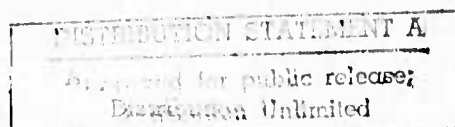
U. S. BUREAU OF MINES
Contract Number H0220035



Sponsored By
ADVANCED RESEARCH PROJECTS AGENCY
ARPA Order No. 1579, Amend. No. 3
Program Code 2F10

The views and conclusions contained in this document are those of the author and should not be interpreted as necessarily representing the official policies, either expressed or implied, of the Advanced Research Projects Agency or the U. S. Government.

Reproduction of this
NATIONAL TECHNICAL
INFORMATION SERVICE
U. S. Department of Commerce
Springfield, MA 01104



JEREMY ISENBURG
Principal Investigator

AGBABIAN ASSOCIATES
Engineering and Applied Sciences Division
250 N. Nash Street
El Segundo, California 90245

UNCLASSIFIED

Security Classification

DOCUMENT CONTROL DATA - R&D		
(Security classification of title, body of abstract and indexing annotation must be entered when the overall report is classified)		
1 ORIGINATING ACTIVITY (Corporate author) AGBABIAN ASSOCIATES 250 N. Nash St. El Segundo, Calif. 90245		2a REPORT SECURITY CLASSIFICATION UNCLASSIFIED
		2b GROUP
3 REPORT TITLE Analytic Modeling of Rock-Structure Interaction, Volume 1 of 3		
4 DESCRIPTIVE NOTES (Type of report and inclusive dates) Final Technical Report, 1 March 1972 to 30 April 1973		
5 AUTHOR(S) (Last name, first name, initial) ISENBERG, JEREMY		
6 REPORT DATE April 1973	7a. TOTAL NO. OF PAGES 203 221	7b. NO. OF REFS 57
8a CONTRACT OR GRANT NO. H0220035	9a. ORIGINATOR'S REPORT NUMBER(S)	
b. PROJECT NO.		
c.	9b. OTHER REPORT NO(S) (Any other numbers that may be assigned this report) R-7215-1-2701	
d.		
10. AVAILABILITY/LIMITATION NOTICES		
11. SUPPLEMENTARY NOTES		12. SPONSORING MILITARY ACTIVITY Advanced Research Projects Agency of the Department of Defense
13 ABSTRACT <p>A number of recent advances in finite element theory and computer technology are combined into a computer program for analyzing structures and cavities in rock. The program applies to general three-dimensional structures, considers nonlinear material properties, including joints, anisotropic and time-dependent material properties, gravity loading and sequence of construction or excavation.</p> <p>The computer program is applied to the analysis of deflections in the back of a chamber which was excavated in argillaceous quartzite at the Caladay Project, Osburn, Idaho. Auxiliary calculations were performed to help develop a viscoelastic model of argillite from in situ measurements. The final, three-dimensional calculation involves excavation and viscoelastic deformation and the results are compared with measurements.</p> <p>The computer program developed under this contract is available through DDC-TC and NTIS. Volume 2 of this report is entitled, "User's Guide to a Computer Program for Analytic Modeling of Rock-Structure Interaction". Volume 3, which consists primarily of a magnetic tape containing a version of the program for the Univac 1108, is entitled "Computer Program for Analytic Modeling of Rock-Structure Interaction."</p>		

DD FORM 1 JAN 64 1473

UNCLASSIFIED
Security Classification

14 KEY WORDS	LINK A		LINK B		LINK C	
	ROLE	WT	ROLE	WT	ROLE	WT
finite element						
rock/structure interaction						
joints						
anisotropy						
viscous properties						
plasticity						
automatic mesh generation						
bandwidth reduction						

INSTRUCTIONS

1. **ORIGINATING ACTIVITY:** Enter the name and address of the contractor, subcontractor, grantee, Department of Defense activity or other organization (*corporate author*) issuing the report.

2a. **REPORT SECURITY CLASSIFICATION:** Enter the overall security classification of the report. Indicate whether "Restricted Data" is included. Marking is to be in accordance with appropriate security regulations.

2b. **GROUP:** Automatic downgrading is specified in DoD Directive 5200.10 and Armed Forces Industrial Manual. Enter the group number. Also, when applicable, show that optional markings have been used for Group 3 and Group 4 as authorized.

3. **REPORT TITLE:** Enter the complete report title in all capital letters. Titles in all cases should be unclassified. If a meaningful title cannot be selected without classification, show title classification in all capitals in parenthesis immediately following the title.

4. **DESCRIPTIVE NOTES:** If appropriate, enter the type of report, e.g., interim, progress, summary, annual, or final. Give the inclusive dates when a specific reporting period is covered.

5. **AUTHOR(S):** Enter the name(s) of author(s) as shown on or in the report. Enter last name, first name, middle initial. If military, show rank and branch of service. The name of the principal author is an absolute minimum requirement.

6. **REPORT DATE:** Enter the date of the report as day, month, year, or month, year. If more than one date appears on the report, use date of publication.

7a. **TOTAL NUMBER OF PAGES:** The total page count should follow normal pagination procedures, i.e., enter the number of pages containing information.

7b. **NUMBER OF REFERENCES:** Enter the total number of references cited in the report.

8a. **CONTRACT OR GRANT NUMBER:** If appropriate, enter the applicable number of the contract or grant under which the report was written.

8b, 8c, & 8d. **PROJECT NUMBER:** Enter the appropriate military department identification, such as project number, subproject number, system numbers, task number, etc.

9a. **ORIGINATOR'S REPORT NUMBER(S):** Enter the official report number by which the document will be identified and controlled by the originating activity. This number must be unique to this report.

9b. **OTHER REPORT NUMBER(S):** If the report has been assigned any other report numbers (either by the originator or by the sponsor), also enter this number(s).

10. **AVAILABILITY/LIMITATION NOTICES:** Enter any limitations on further dissemination of the report, other than those

imposed by security classification, using standard statements such as:

- (1) "Qualified requesters may obtain copies of this report from DDC."
- (2) "Foreign announcement and dissemination of this report by DDC is not authorized."
- (3) "U. S. Government agencies may obtain copies of this report directly from DDC. Other qualified DDC users shall request through _____."
- (4) "U. S. military agencies may obtain copies of this report directly from DDC. Other qualified users shall request through _____."
- (5) "All distribution of this report is controlled. Qualified DDC users shall request through _____."

If the report has been furnished to the Office of Technical Services, Department of Commerce, for sale to the public, indicate this fact and enter the price, if known.

11. **SUPPLEMENTARY NOTES:** Use for additional explanatory notes.

12. **SPONSORING MILITARY ACTIVITY:** Enter the name of the departmental project office or laboratory sponsoring (paying for) the research and development. Include address.

13. **ABSTRACT:** Enter an abstract giving a brief and factual summary of the document indicated by the report, even though it may also appear elsewhere in the body of the technical report. If additional space is required, a continuation sheet shall be attached.

It is highly desirable that the abstract of classified reports be unclassified. Each paragraph of the abstract shall end with an indication of the military security classification of the information in the paragraph, represented as (TS), (S), (C), or (U).

There is no limitation on the length of the abstract. However, the suggested length is from 150 to 225 words.

14. **KEY WORDS:** Key words are technically meaningful terms or short phrases that characterize a report and may be used as index entries for cataloging the report. Key words must be selected so that no security classification is required. Identifiers, such as equipment model designation, trade name, military project code name, geographic location, may be used as key words but will be followed by an indication of technical context. The assignment of links, rules, and weights is optional.

ANALYTIC MODELING OF ROCK-STRUCTURE INTERACTION

Final Technical Report
Volume 1
April 1973

U. S. BUREAU OF MINES
Contract Number H0220035

Sponsored By
ADVANCED RESEARCH PROJECTS AGENCY
ARPA Order No. 1579, Amend. No. 3
Program Code 2F10

The views and conclusions contained in this document are those of the author and should not be interpreted as necessarily representing the official policies, either expressed or implied, of the Advanced Research Projects Agency or the U. S. Government.

JEREMY ISENBURG
Principal Investigator

AGBABIAN ASSOCIATES
Engineering and Applied Sciences Division
250 N. Nash Street
El Segundo, California 90245



R-7215-1-2701

FINAL TECHNICAL REPORT

VOLUME 1

ARPA Order Number: 1579, Amendment No. 3
Program Code Number: 2F10
Name of Contractor: Agbabian Associates
Effective Date of Contract: 1 March 1972
Contract Expiration Date: 1 May 1973
Amount of Contract: \$152,549
Contract Number: H0220035
Principal Investigator: Jeremy Isenberg
Phone Number: (213) 640-0576
Title of Work: Analytic Modeling of Rock-Structure Interaction,
Volume 1 of 3, Final Report.

This research was supported by the Advanced Research Projects Agency of the Department of Defense and was monitored by the Bureau of Mines under Contract No. H0220035.



TECHNICAL REPORT SUMMARY

The objective of this project is to combine a number of recent advances in finite element theory and computer technology for analyzing cavities and structures in rock. This computer program applies to general three-dimensional structures, considers nonlinear material properties, time dependent properties, gravity loading and sequence of excavation or construction.

The final report for this project is in three volumes as follows:

Volume 1 - "Analytical Modeling of Rock - Structure Interaction." Final Report, April 1973.

Volume 2 - "Users Guide for a Computer Program for Analytic Modeling of Rock - Structure Interaction." Final Report, April 1973.

Volume 3 - "Computer Program for Analytic Modeling of Rock - Structure Interaction." Final Report, April 1973.

All three volumes were prepared by Agbabian Associates, under contract H0220035 with U. S. Bureau of Mines. The project was sponsored by ARPA under ARPA Order Number 1579, Amend. No. 3, Program Code 2F10.

During this contract, work has been aimed at producing a user-oriented computer program. The work of writing the program was divided into three areas:

- a. Input
- b. Execution and output
- c. Material properties



The Input Section automatically generates the continuum part of the finite element mesh, including joint elements, allows the user to add other elements (beam, shell, truss) to the mesh, plots the result, reduces the bandwidth and reads loads, material properties, and other quantities necessary to the calculation. The Execution Section forms the global stiffness matrix and solves equations of equilibrium for displacements by an implicit method. The material properties are represented by subroutines within the Execution Section, which are written in a modular form so that if the general equations of nonlinear elasticity, viscoelasticity, viscoplasticity, or plasticity do not suit a particular problem they may be easily modified.

One of the guidelines for this project was to consolidate existing finite element technology into a single, general purpose computer program. Accordingly, the program uses existing finite elements, a proven form of the equation of equilibrium, existing material property descriptions, and an existing bandwidth reducer. However, a small amount of new work was done. A new joint element was developed and an existing concept for automatic mesh generation was greatly extended. Also, a form of Choleski decomposition was modified for efficient use of multibuffering, resulting in substantial improvement in efficiency of solving equations of equilibrium using peripheral storage.

During this study, some new work was reported by other ARPA/Bureau of Mines contractors which has been incorporated in the program. Among these are some creep data obtained by W. A. Wawersik of the University of Utah and strength/deformability data for faults by R. E. Goodman, F. E. Heuze, and Y. Ohnishi of the University of California, Berkeley.

The technical work reported in Volume 1 is divided into two main parts. The first part describes the range of possible application of the computer program to mining engineering problems and reports an extensive analytic study of the Caladay Project hoist room with which experimental data are compared. The second part discusses various aspects of the computer



R-7215-1-2701

program and its theoretical basis. Attention is given to the processing of input data and to options available to the user for mesh generation, sequential excavation or construction, automatic bandwidth reduction and plotting of the mesh. Example problems which have been solved during checkout of the program are described.

Volume 2 explains the overall operation of the computer program, defines how input should be submitted to the program, defines the material property models in detail, explains the data stored on each tape, and gives flow charts of some subroutines. This input definition is for the version of the program which operates on the UNIVAC 1108. This program is the primary content of Volume 3, and is available on seven track magnetic tape from DDC-TC, U. S. Department of Commerce, Springfield, Virginia 22151, telephone AC (703) 321-8517. The tape is unlabeled, even parity, external BCD and is written at 556 BPI. The tape has constant record sizes, each record being 1920 characters long (24-80 column card images per record). An end of file mark follows the last record on the tape.

Arrangements to obtain copies of Volumes 2 and 3 may also be made through Agbabian Associates, 250 North Nash Street, El Segundo, California 90245, telephone AC (213) 640-0576.

This contract was monitored by Dr. William J. Karwoski, Spokane Mining Research Center, U. S. Bureau of Mines.



FOREWORD

The principal contributors to the work reported here are listed below. All are members of the technical staff of Agbabian Associates.

A. K. Bhaumik

K. P. Chuang

J. M. Clark

K. T. Dill

J. Ghaboussi

J. Isenberg

E. M. Raney

The cooperation of the Callahan Mining Corporation in supplying engineering data for the study of the Caladay Project Hoist Room is gratefully acknowledged.



CONTENTS

<u>Section</u>		<u>Page</u>
1	INTRODUCTION	1
2	CAPABILITY OF COMPUTER PROGRAM AND ILLUSTRATIVE CASE HISTORY	3
2.1	Physical Aspects of Rock and Support Systems Which this Program Represents . .	3
2.2	Illustrative Case History--Caladay Hoist Room	5
2.3	Three-Dimensional Analysis of Hoist Room at Caladay Project	30
2.4	Discussion of Results	44
2.5	Summary and Conclusions	48
	REFERENCES	51
3	APPLICATION OF FINITE ELEMENT THEORY	52
3.1	Solution of Nonlinear Equations of Equilibrium	52
3.2	Equations of Equilibrium for Large Deformations	55
3.3	Structural Finite Elements	59
3.4	Joint Finite Element	70
	REFERENCES	77
4	REPRESENTATION OF PROPERTIES OF ROCK, INCLUDING ANISOTROPY, INELASTICITY, RATE EFFECTS AND PROPERTIES OF FAULTS OR JOINTS	78
4.1	Homogeneous Properties	79
4.2	Material Properties of Joints	119
	REFERENCES	128



CONTENTS

<u>Section</u>		<u>Page</u>
5	DESCRIPTION OF THE COMPUTER PROGRAM	131
	5.1 Processing of Input Data	131
	5.2 Execution Phase of Program	156
	REFERENCES	173
6	COMPARISON WITH CLOSED-FORM ANALYTIC SOLUTIONS .	174
	6.1 Sample Problems	174
	6.2 Computing Time Required for Solution . . .	189
	REFERENCES	191
<u>Appendix</u>		
A	LOGIC DIAGRAMS FOR MATERIAL PROPERTIES	A-1



ILLUSTRATIONS

<u>Figure</u>		<u>Page</u>
2-1	Two-Dimensional Tunnel with Excavation, Temporary Bracing and Joints	4
2-2	Excavation of Bank	6
2-3	Three-Dimensional Tunnel Analysis with Joints .	7
2-4	Fault Locations, Coeur D'Alene District	9
2-5	Plan View of Hoist Room and Connecting Drifts at Caladay Project Showing Dip of Bedding Fault . .	13
2-6	Idealization of Hoist Room Dimensions, Excava- tion Sequence and In Situ Stresses	14
2-7	Time Variation of Cumulative Displacement Between Toe and Collar of Each of the Three Extensometers Installed in the Back of the Hoist Room (Extension Positive).	15
2-8(a)	An Automatically Generated 2-D Mesh for Caladay Hoist Room	16
2-8(b)	Schematic Key Diagram for Mesh Shown in 2-8(c) .	17
2-8(c)	Actual Key Diagram with Input Nodal Point Coordinates for Preliminary Two-Dimensional Analysis	17
2-9	Results of Preliminary Two-Dimensional Elastic Analysis	19
2-10	Auxiliary Drift in Silver Summit Mine Used to Determine In Situ Viscoelastic Properties of Argillite	25
2-11	Comparison Between Measurements and Computation of Relative Displacements in Drift in Argillite, Silver Summit Mine (Compression Positive) . . .	27
2-12	Plane Strain Finite Element Analysis of Section SS-3 in Argillite	28
2-13	Three-Dimensional Finite Element Mesh with Original Configuration of Top Slice and First Bench Followed by Three Stages of Excavation . .	31



ILLUSTRATIONS (CONTINUED)

<u>Figure</u>		<u>Page</u>
2-14	Normal Stresses in Front and Back Layers of Elements	35
2-15	Measured and Calculated Relative Displacement Between Ends of Extensometers Located in Back of Hoist Room Versus Time (Extension Positive) . .	38
2-16	Vertical Normal Stresses (σ_y) in the Element Layer Over the Back	39
2-17	Absolute Deflection of Center of Back and First Bench Floor	41
2-18	Upheaval of First Bench Floor	43
2-19	Authors' Estimate of Results Which Would be Obtained if Model Were to be Refined and a Second Analysis Performed	47
3-1	Truss and Beam Element	60
3-2	Two-Dimensional Isoparametric Element	62
3-3	Eight-Point Three-Dimensional Element	65
3-4	Three-Dimensional Thick-Shell Element	67
3-5	Geometry of Joint Element	72
3-6	Coordinate Systems for Joint Element	74
4-1	Typical Laboratory Data on Rock from which Constitutive Equations are Derived	81
4-2	Model Bulk Modulus, Hydrostat and Yield Point in Uniaxial Strain Compared with Data	84
4-3	Shear Modulus Versus Pressure for NTS Granite .	86
4-4	Cap Model	91
4-5	Hydrostatic and Uniaxial Strain Behavior Cap Model Fit for Granitic Material	92
4-6	Triaxial Stress Behavior, Chamber Pressure = 0, 50, 100, 200 ksi, Cap Model Fit for Granitic Material	93



ILLUSTRATIONS

<u>Figure</u>		<u>Page</u>
4-7	Yield Strength Versus Mean Stress for NTS Granite	94
4-8	Orientation of Planes of Weakness Defining Anisotropic Behavior According to Jaeger	102
4-9	Comparison Between Failure Theories and Experimental Data for Anisotropic Rock (Reference 2-18)	103
4-10	Stress-Strain Curves for Green River Shale-2 for Various Confining Pressures, $\beta = 10$ Deg (Reference 2-18)	105
4-11	Present Model Subjected to Uniaxial Strain at Various Strain Rates	111
4-12	Compressive Stress/Strain Relations for Present Model Subjected to Proportional Loading at Different Stress Ratios	111
4-13	Compressive Stress/Strain Relations for Present Model Subjected to Proportional Loading	111
4-14	Compressive Stress/Strain Relations for Cedar City Tonalite at Various Strain Rates	112
4-15	Viscous Models Available in the Present Computer Program	114
4-16	Experimental Data on Viscoelastic Properties of Several Rocks	116
4-17	Comparison Between Present Creep Model and Experimental Data (References 4-30, 4-31)	117
4-18	Normal Stress-Strain Relation for Joints	121
4-19	Dilatant Joint	123
4-20	Geometry of Example Problem Using Plane Slip Element	124
4-21	Vertical Displacements for Example Wedge Problem	126



ILLUSTRATIONS (CONTINUED)

<u>Figure</u>		<u>Page</u>
4-22	Finite element Mesh in the Displaced Configuration for Wedge Problem in Final Equilibrium State	127
5-1	Operations of the Input Portion of the Present Computer Program	132
5-2	Quadrilateral Zone, Whose Shape and Coordinates are Expressed by Parabolic Shape Functions . . .	134
5-3	Key Diagram and Resulting Finite Element Mesh for a Dam and Foundation	136
5-4	Key Diagram and Resulting Finite Element Mesh for a Quadrant of a Square Plate with a Circular Hole	139
5-5	Key Diagram and Resulting Finite Element Mesh for a Tunnel	140
5-6	Key Diagram and Resulting Finite Element Mesh for a Dam on Foundation, Illustrating Capability to Join Any Two Edges in the Key Diagram	141
5-7	Key Diagram and Resulting Finite Element Mesh for a Tunnel, Illustrating Capability to Join Any Two Edges in the Key Diagram	142
5-8	Three-Dimensional Zone Whose Shape and Coordinates are Expressed by Parabolic Shape Functions	143
5-9	Automatically Generated Three-Dimensional Mesh .	145
5-10	Three-Dimensional Finite Element Mesh Representing a Tunnel (Preparation Time, Including Further Refinement of Any Section--About 1 Hour)	146
5-11	Example of Bandwidth Reducer	148
5-12	Procedure Used in Bandwidth Reducer (Reference 5-2)	149



ILLUSTRATIONS (CONTINUED)

<u>Figure</u>		<u>Page</u>
5-13	Procedure Used in Bandwidth Reducer (Reference 5-3)	150
5-14	Operation on Force, Displacement and Incremental Displacement Arrays	152
5-15	Generation of Global Stiffness Matrix from Element Data	154
5-16	Program BMCALC--Controls Main Operations of the Computation Section	157
5-17	Subroutine KFORM--Calls Subroutines to Compute the Load Vector and Global Stiffness	158
5-18	Subroutine BSTIF--Computer Element Stiffness [k] and Adds to Global [k]	161
5-19	Subroutine FWRT--Moves Data from Live Load Vector (FWORK) to F, u, du Output Buffer and to u Output File	162
5-20	Subroutine TDRUM--Adds in Element [k] which Overflowed from Previous Block of [k]	163
5-21	Subroutine FILLFU--Adds Live Loads to Load Vector, Updates Displacements, Fills Buffer Area with F, u, du Array	164
5-22	Typical Operation of Multibuffering Technique .	166
5-23	Method of Storing Stiffness Matrix Used in Present Program	169
5-24	Core Buffers for Stiffness Matrix Decomposition	170
5-25	Schematic Diagram of Stiffness Matrix Decomposition	171
5-26	Schematic Diagram of Solution Vector Evaluation	172
6-1	Problem 1--Stresses Around a Circular Hole . . .	176



ILLUSTRATIONS (CONTINUED)

<u>Figure</u>		<u>Page</u>
6-2	Finite Element Mesh for Stress Concentration Around Circular Hole	177
6-3	Comparison Between Present Finite Element Solution and Analytic Solution for Problem 1, Stresses Around a Circular Hole	178
6-4	Problem 2--Infinitely Long, Thick Elastic Cylinder Subject to Internal Pressure	179
6-5	Comparison Between Present Finite Element Solution and Analytic Solution for Problem 2, Thick Elastic Cylinder Subject to Internal Pressure	180
6-6	Comparison Between Present Finite Element Solution and Analytic Solution for Problem 3, Elastic/Plastic Cylinder Subject to Internal Pressure	181
6-7	Problem 4--Infinitely Long Reinforced Thick Viscoelastic Cylinder Subjected to Internal Pressure	183
6-8	Problem 4--Reinforced Viscoelastic Cylinder Subjected to Internal Pressure (Reference 6-4) .	184
6-9	Problem 5--Three-Dimensional Stress Concentration Around a Cylindrical Hole in a Semiinfinite Elastic Body	185
6-10	Problem 5--Finite Element Mesh (Only First Three Layers are Shown for Clarity. Complete Mesh Contains Eight Layers.)	186
6-11	Problem 5--Three-Dimensional Stress Concentration (Reference 6-4)	187



TABLES

<u>Table</u>		<u>Page</u>
2-1	Representative Elastic Properties of Pure Minerals Based on Laboratory Measurements	23
2-2	Properties of Analysis of Caladay Hoist Room . .	24
2-3	Twelve Steps Taken in the Final Three-Dimensional Calculation	33
4-1	Summary of Available Material Properties	79
4-1	Summary of Available Material Properties	79
4-2	Advantages and Disadvantages of Each Model . . .	80
4-3	Summary of Example Calculations	110
4-4	Properties Used in Present Examples	110
6-1	Problems Solved by Finite Element and Closed-Form Methods	175
6-2	Computing Time Required for Solutions	190



SECTION 1

INTRODUCTION

The purpose of this contract is to combine a number of recent advances in finite element theory and computer technology into a computer program for analyzing structures and cavities in rock. This computer program applies to general three-dimensional structures, considers nonlinear material properties including homogeneous deformation and inhomogeneous deformation due to joints, anisotropic and time-dependent material properties, gravity loading, and sequence of construction or excavation. Since the program is intended for practical analysis and design, great effort has been made to foresee difficulties in using it. For example, much tedious work, which formerly was done by the user, has been eliminated by sophisticated mesh generators and a bandwidth reducer. Also, since many prospective users may have access to small or medium-sized computers but may still wish to solve large problems (4000-6000 equations), the program uses up-to-date multibuffering techniques for accessing peripheral storage units, thus dramatically reducing computer run time for out-of-core problems. Finally, an attempt is made to lengthen the useful life of the program by making it simple to add new elements and to expand the material property description and by making the program efficient for and compatible with a wide variety of computers.

The capabilities and limitations of the computer program are summarized as follows:

- a. Two- and three-dimensional geometry
- b. Small deformations
- c. Inhomogeneous material properties
- d. Anisotropy



- e. Material nonlinearity including ideal and strain-hardening plasticity and variable moduli models
- f. Viscoelasticity and viscoplasticity
- g. Self-loading due to gravity
- h. Sequence of excavation and construction
- i. Static live loading

The purpose of this report is to discuss what the computer program does and to describe its application to a practical problem in mining engineering. Much of the description of the program is given from the standpoint of the prospective user. Mesh generation, the types of elements available, the types of loading and construction which may be done and the properties of continuous material and joints which are available are described. The theory underlying the present finite element formulation is described. The structure of the code is indicated by logic diagrams.

The application of the program to a practical mining situation is reported from the standpoint of a user approaching such a problem for the first time. The geologic conditions of the area, and the joint and fault pattern near the cavity which is being excavated are described. The candidate material properties are discussed. Calculations are made using candidate stress/strain properties and compared with measurements of wall deflections in an auxiliary drift. Parameters defining the stress/strain relations are varied until agreement between calculation and measurement is reached for the auxiliary drift. The same properties are used to analyze the three-dimensional response of a cavity in a similar geologic formation to excavation considering creep of the surrounding rock.



SECTION 2

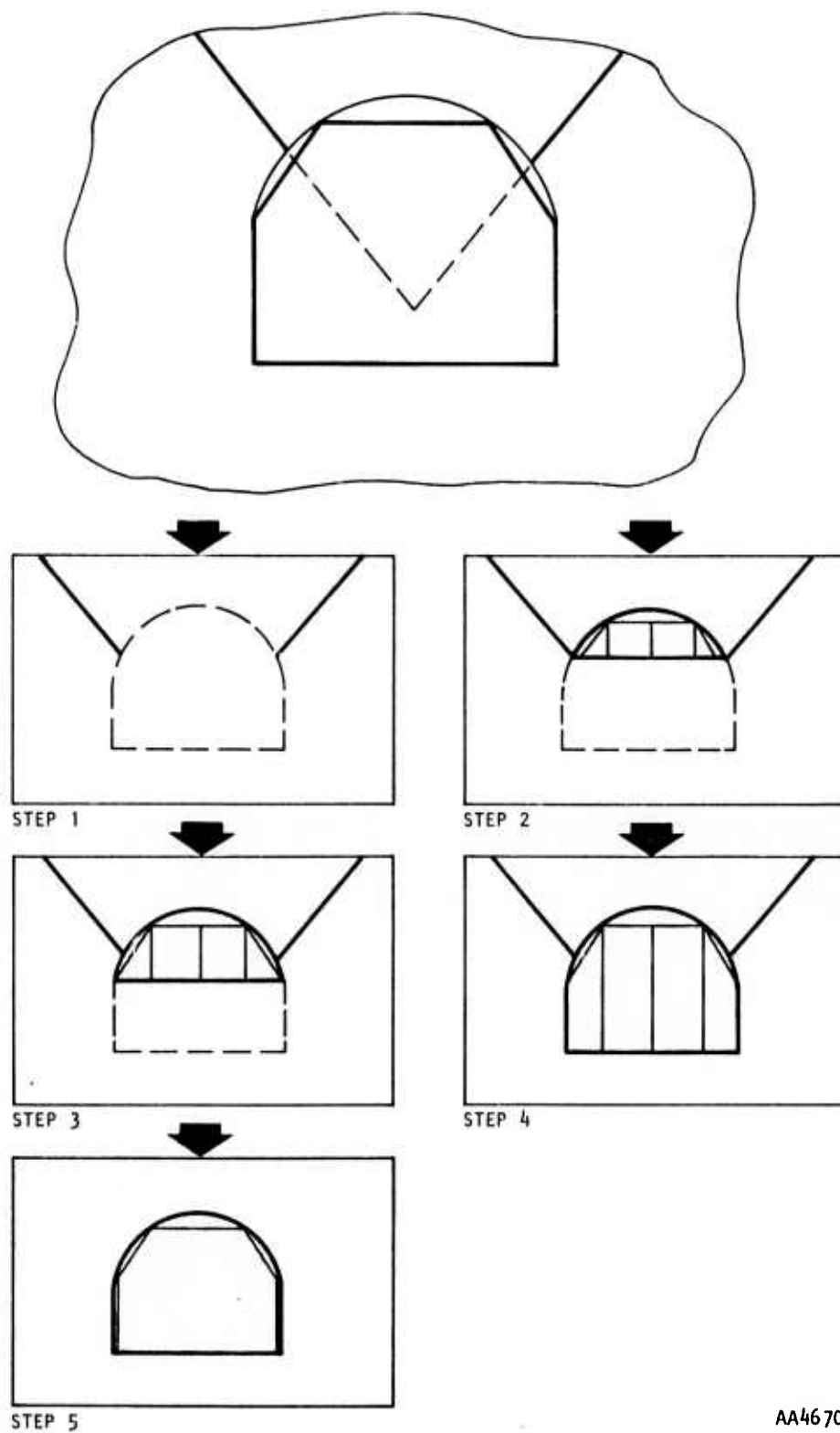
CAPABILITY OF COMPUTER PROGRAM AND ILLUSTRATIVE CASE HISTORY

This section mentions the physical aspects of rock and support systems which are represented by the computer program and illustrates part of this capability by analyzing the excavation of a chamber. The main purpose of this section is to show the scope of problems which the program is capable of analyzing and to illustrate how various options in the program are selected to solve a specific problem.

The main work reported in this section is an analysis of a hoist room roof at the Caladay project, Osburn, Idaho, which is excavated in argillaceous quartzite. Deflections which were measured during part of the excavation are compared with the results of the analysis. One goal in performing the analysis is to obtain as close an agreement as possible using the available data on sequence of construction, properties of rock and in situ stresses. The main benefit of analyses such as these performed for the Caladay hoist room is the insight which they provide into the pattern of stress and deformation. This insight, which the present computer program brings within reach of even modest computing facilities, has a role to play alongside empirical design, field measurements, and inspection.

2.1 PHYSICAL ASPECTS OF ROCK AND SUPPORT SYSTEMS WHICH THIS PROGRAM REPRESENTS

To illustrate the capability of the program, three hypothetical problems are described below. These problems have not actually been solved with the present program, but they could be solved at any time. The first is illustrated in Figure 2-1. A section of tunnel is to be excavated in a region containing a major joint. The properties of the joint are assumed to be known. The rock adjacent to the joint is assumed to be homogeneous and to



AA4670

FIGURE 2-1. TWO-DIMENSIONAL TUNNEL WITH EXCAVATION, TEMPORARY BRACING AND JOINTS



have viscous properties which can be represented by a visco-plastic model. In Step 1, the tunnel has not yet been excavated. Stress in the rock is computed by applying static overburden to the edges of the finite element mesh. Then the tunnel is excavated by removing appropriate elements. At each stage of the excavation, the tunnel roof is propped by truss and beam elements. Eventually, the tunnel is fully open and the final supports are installed. Each stage is associated with an elapsed time, during which the rock flows in a visco-plastic manner. At each intermediate stage and at a stage the user defines to be final, the stresses in the rock and in the support elements are printed.

The second problem is illustrated in Figure 2-2. A bank is to be excavated in a rock such as shale having nonlinear, anisotropic stress/strain properties and an anisotropic fracture criterion. In Step 1, the in situ states of stress are computed by applying gravitational forces in a step-by-step fashion throughout the grid. In subsequent steps, elements are removed in any sequence the user desires. Between excavation steps the remaining rock will be checked for fracture which would correspond to spalling and sliding in an actual field situation.

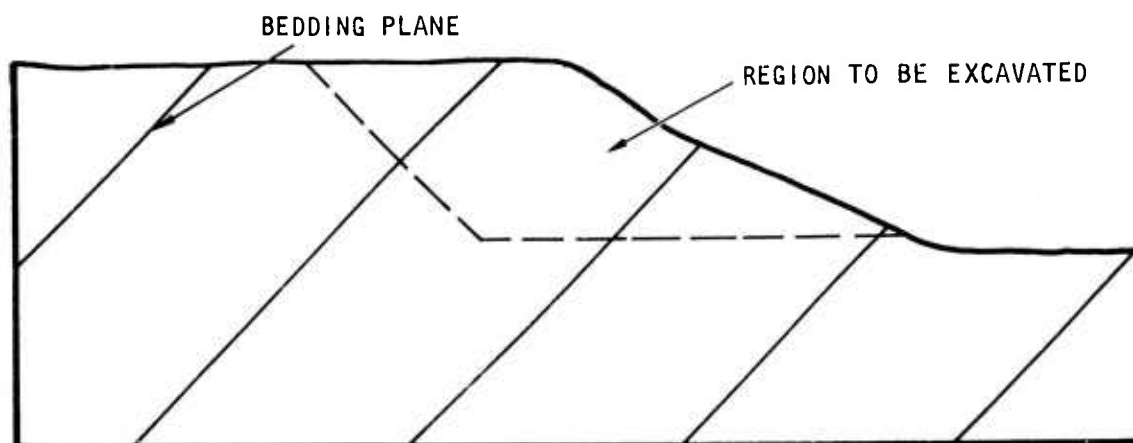
The third example is an extension to three dimensions of the first example. The final stage in the calculation, at which the section of tunnel under consideration is fully excavated, is illustrated in Figure 2-3. It was intended to develop a three-dimensional joint element as part of the present project. The theoretical aspects of this work are about 50 percent completed as of the date of this report.

2.2 ILLUSTRATIVE CASE HISTORY--CALADAY HOIST ROOM

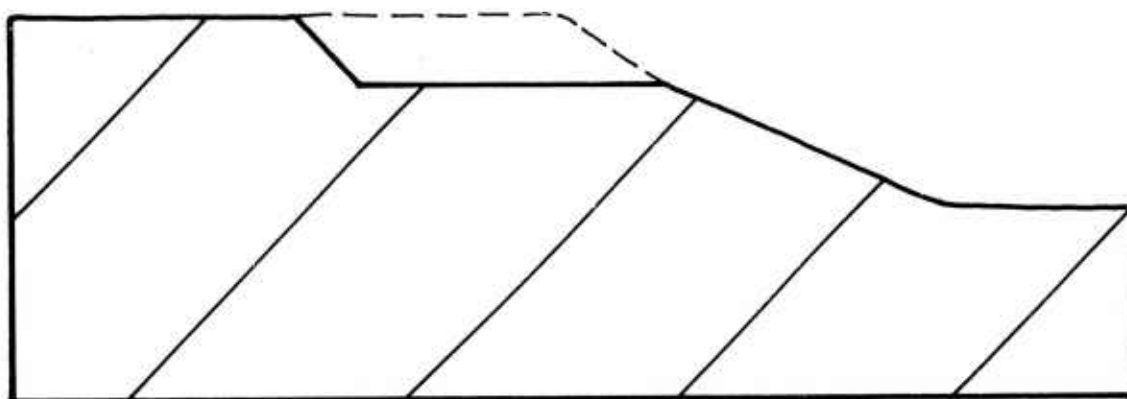
An analysis was made of the excavation of a hoist room at the Caladay Project near Osburn, Idaho. The location of the Caladay project is illustrated in Figure 2-4. The geology of the area may be described as follows:



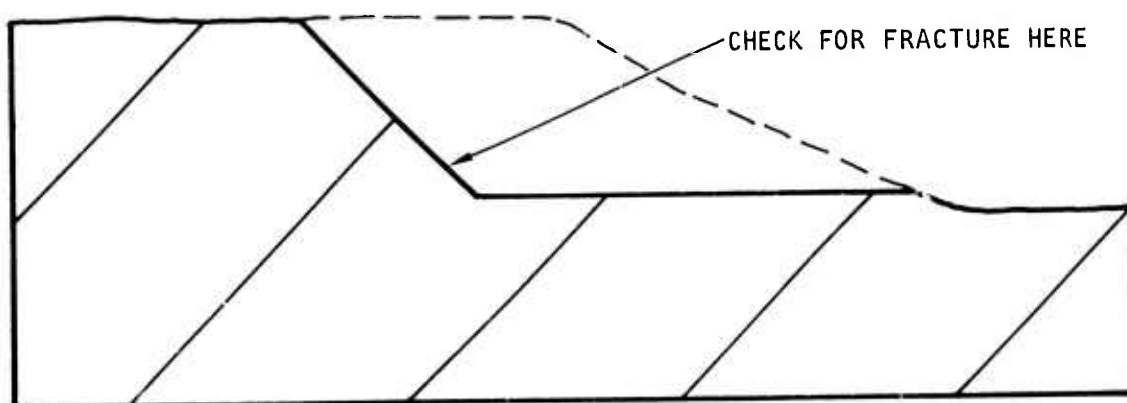
R-7215-1-2701



STEP 1. GRAVITY LOADING APPLIED TO ALL NODAL POINTS



STEP 2. EXCAVATION



STEP 3. EXCAVATION

FIGURE 2-2. EXCAVATION OF BANK



R-7215-1-2701

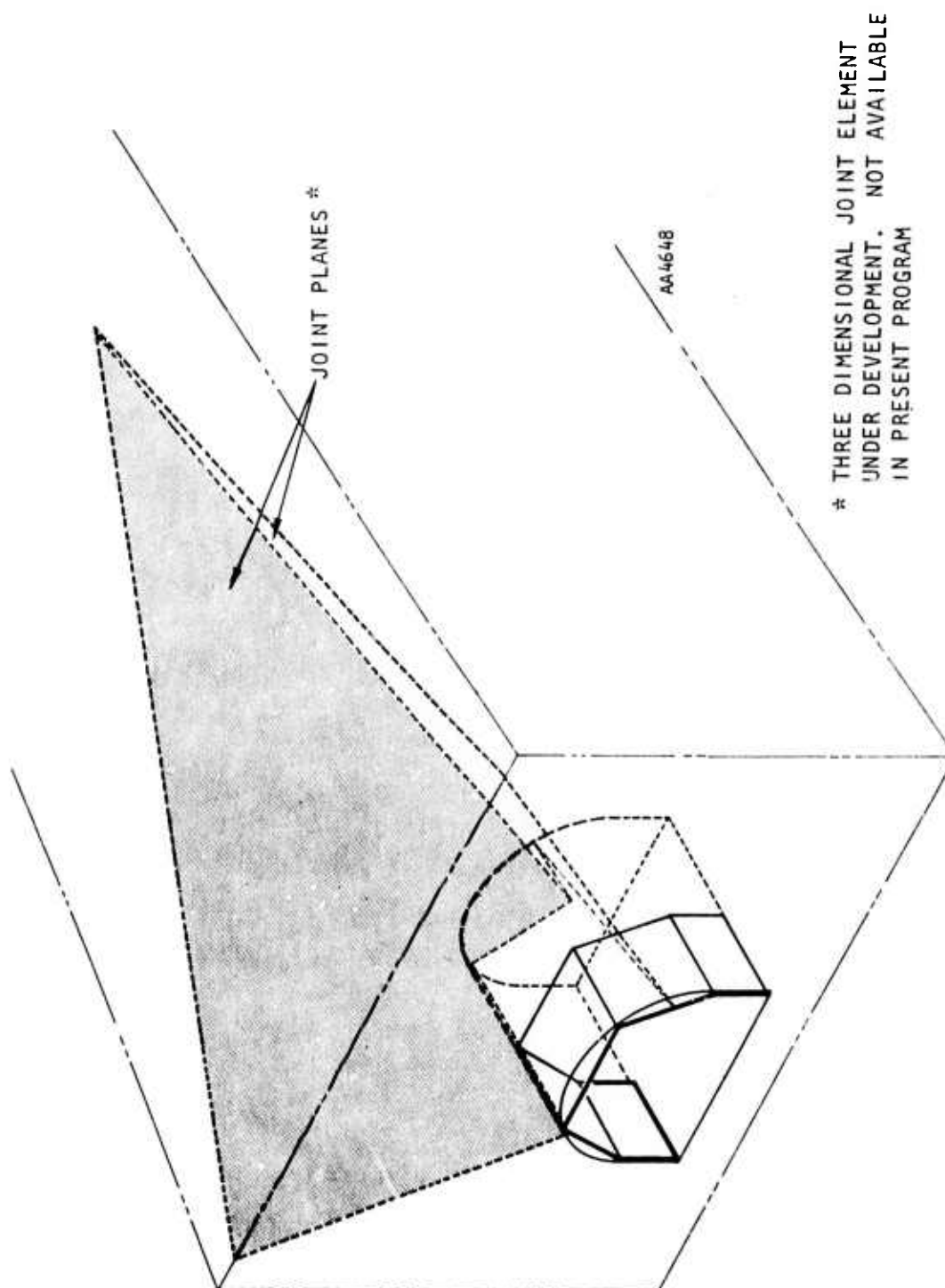


FIGURE 2-3. THREE-DIMENSIONAL TUNNEL ANALYSIS WITH JOINTS



2.2.1 GEOLOGIC DESCRIPTION

Figure 2-4 shows the general location of the Caladay underground hoist room project in the Coeur d'Alene mining district in Idaho. The Coeur d'Alene mining district (Reference 2-1), one of the preeminent lead-, zinc-, and silver-producing areas of the world, is near the base of the panhandle of northern Idaho. Spokane, Washington, is about 75 miles to the west, and Missoula, Montana, about 110 miles to the east of the district. The district lies wholly within the Coeur d'Alene Mountains which are a rugged, deeply dissected mountain mass. Rock units of the Coeur d'Alene district are metamorphosed sedimentary of the Precambrian Belt Series. This series consists of six formations. The three of interest are the Revett Quartzite, St. Regis, and Wallace Formations. They are in a complex anticline-syncline structural system. A very complex geologic history associated with strike-slip movements along the Osburn fault system has caused individual beds to be sharply contorted, crumpled, overturned, and faulted. Formation contacts are not well defined.

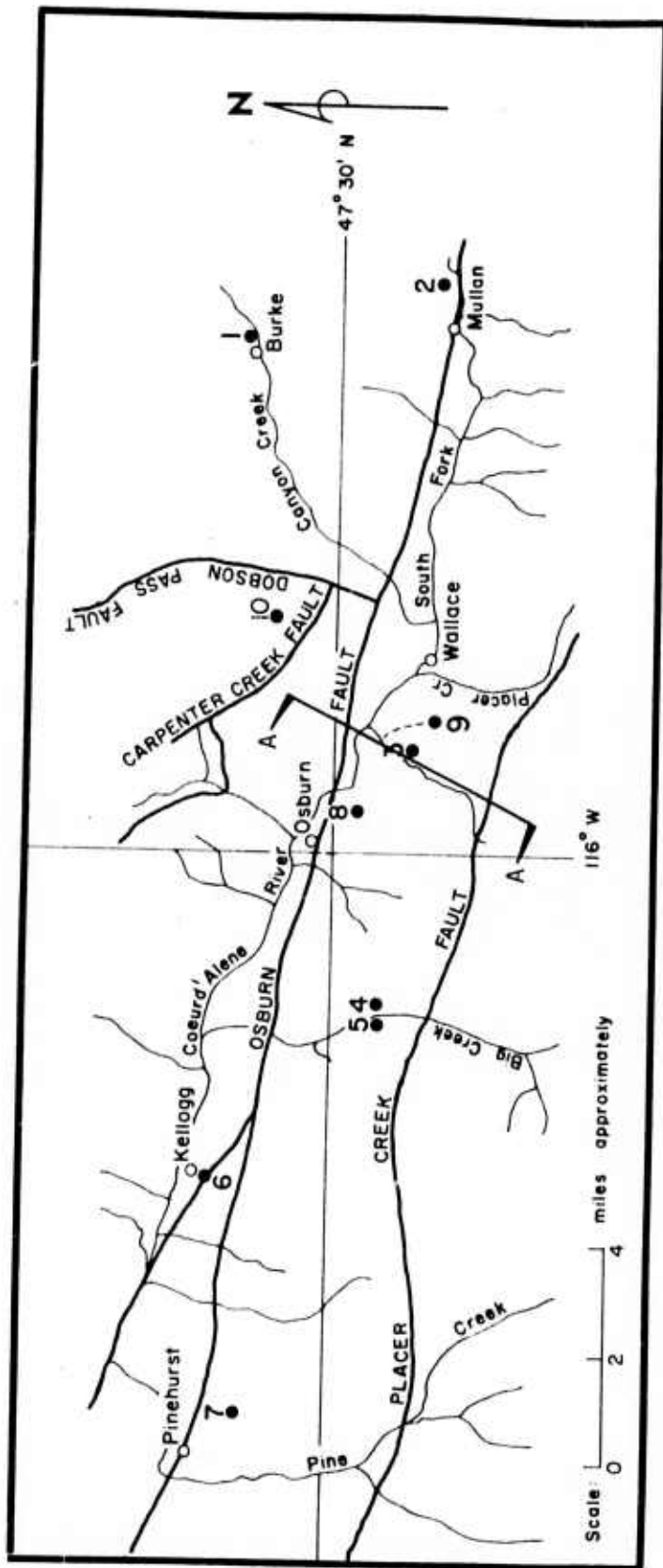
The Revett Quartzite, St. Regis, and Wallace are three of the oldest formations. The St. Regis forms its contact with the Revett Quartzite Formation and grades from interbedded quartzite and argillite upward into a dominantly thin-bedded argillite. The upper several hundred feet of the St. Regis are characterized by a finely laminated argillite. The Wallace Formation is a heterogeneous group of rock comprising quartzite, argillite, dolomite, and limestone.

The rock of the Belt series is fine grained, and the principal minerals are quartz and sericite with quartz the more abundant mineral.

Faults are the dominant structural features (Figure 2-4) in the area, and a myriad of them cut the country rock into a complex pattern of blocks. Hundreds can be seen underground. As a result of the regional faulting and folding, most of the beds dip greater than 45 deg. The rock of the district was intensely deformed in a complex pattern which can be



R-7215-1-2701



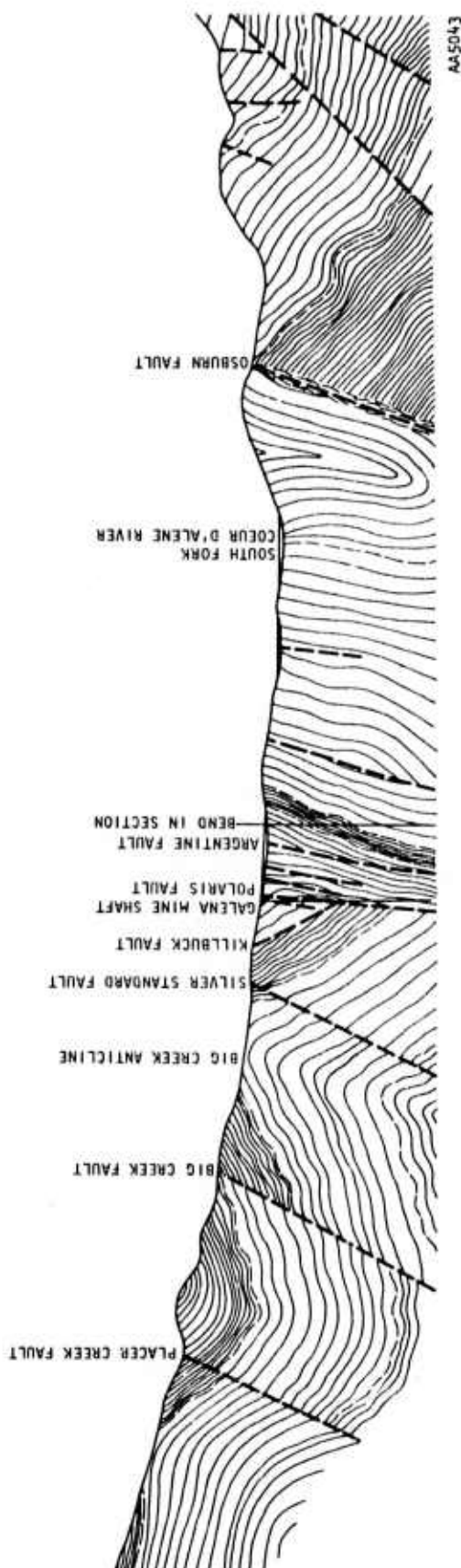
- | | | | |
|-----|---|----|--|
| 1 | Hecla Mining Company, Star Tunnel | 7 | American Smelting and Refining Company, Page Mine (inactive) |
| * 2 | Hecla Mining Company, Lucky Friday Mine | 8 | American Smelting and Refining Company, Coeur Shaft |
| * 3 | Callahan Mining Company, Galena Mine (operated by ASARCO) | 9 | Caladay Project, Callahan Mining Company |
| 4 | Sunshine Mining Company, Sunshine Mine | 10 | Day Mines, Dayrock Mine |
| * 5 | Bunker Hill Company, Crescent Mine | | |
| 6 | Bunker Hill Company, Bunker Hill Tunnel | | |
| | | * | Seismograph Station, U.S.B.M. |

(a) MINES LOCATION MAP - COEUR D'ALENE DISTRICT OF IDAHO

FIGURE 2-4. FAULT LOCATIONS, COEUR D'ALENE DISTRICT



R-7215-1-2701



(b) TYPICAL GEOLOGIC CROSS-SECTION (REFERENCE 2-1) NEAR CALADAY PROJECT SITE (SECTION A-A LOOKING NORTHWEST)



referred to as a structural knot. Much of this regional geology is similar to the local geology at the Caladay project site.

The Caladay project (Reference 2-2) was developed by driving an adit 5,200 ft into a mountainside. The adit begins in the Wallace Formation. At 2,900 ft the Wallace/St. Regis contact is found. The adit intersects the Polaris fault at approximately 3,200 ft where the Wallace Formation is reentered. The Wallace/St. Regis contact is encountered again at 4,800 ft. The hoist room is about 400 ft from this Wallace/St. Regis contact. Thus, the hoist room is in the upper several hundred feet of the St. Regis Formation.

Bedding in the hoist room dips nominally 65 deg and strikes normal to the long axis of the room. Bedding in the hoist room can be classed into three broad categories based on its mineral composition. Zone A is estimated to contain 60 percent argillite and 40 percent argillaceous quartzite. It is thin bedded with beds varying from less than 1 in. up to 6 in. in thickness. Zone B is estimated to contain 50 percent argillaceous quartzite, 40 percent argillite, and 10 percent quartz. The quartz content diminishes from bottom to top of the room. The bedding is 4 to 8 in. in thickness. Zone C is principally argillite with minor amounts of argillaceous quartzite, and this is generally thinly bedded.

Most of the faults in the area are slips along bedding planes. These faults contain a silt or silty clay-like gouge. One predominant fault (sheave room fault) projects over the top corner of the hoist room and into the sheave room. This fault is about 2 to 10 in. in thickness and does not appear to have asperities of any consequence. At the other end of the hoist room exists a large cross-bedding fault. This fault dips 85 deg across the bedding at 85 deg. Its shear zone is estimated at no less than 50 ft thick. The gouge material ranges from large chunks of broken rock to sand and silt-like materials.



2.2.2 PHYSICAL SITUATION AND MATHEMATICAL MODEL FOR CALADAY HOIST ROOM

Figure 2-5 shows the drift and tunnel complex surrounding the hoist room at the Caladay project. The figure also shows the local geologic structure including distribution of different kinds of rocks, location, and orientation of bedding faults and cross-cutting major faults. The two major types of rock encountered in the area are argillite and quartzite. These are found mostly as argillaceous quartzite. A major cross-bed fault, located next to the southwest wall of the hoist room, contains soft clay and shattered argillite.

Some details concerning the hoist room are given in Figure 2-6. The excavation of the room was started from the top of the room, which was reached through a raise dug upward from the entry drift. The excavation was then carried downward by presplitting and mucking horizontal layers of material until the bottom of the room was reached.

To monitor the response of the back of the hoist room, three extensometers of 30-ft length were installed in the back as soon as it was reached at the top of the access raise. Readings on these meters in the course of excavation were subsequently taken for a period of approximately seventy days until access to these meters was lost at the end of the top slice and first bench excavation. These readings were later processed into the form of strain rates and cumulative displacements between anchors located along the length of the extensometers. Figure 2-7 shows the time variation of cumulative displacement between the toe and collar of each one of the extensometers. One of the objectives of the finite element analyses to be presented herein is to check on these observed values.

To introduce the modeling procedure, one of the preliminary two-dimensional finite element meshes which is used only to investigate mesh fineness, loading and boundary supporting conditions suitable for eventual, three-dimensional modeling of the hoist room is shown in Figure 2-8(a). This 11 by 11 mesh was automatically generated and plotted by the code from the



R-7215-1-2701

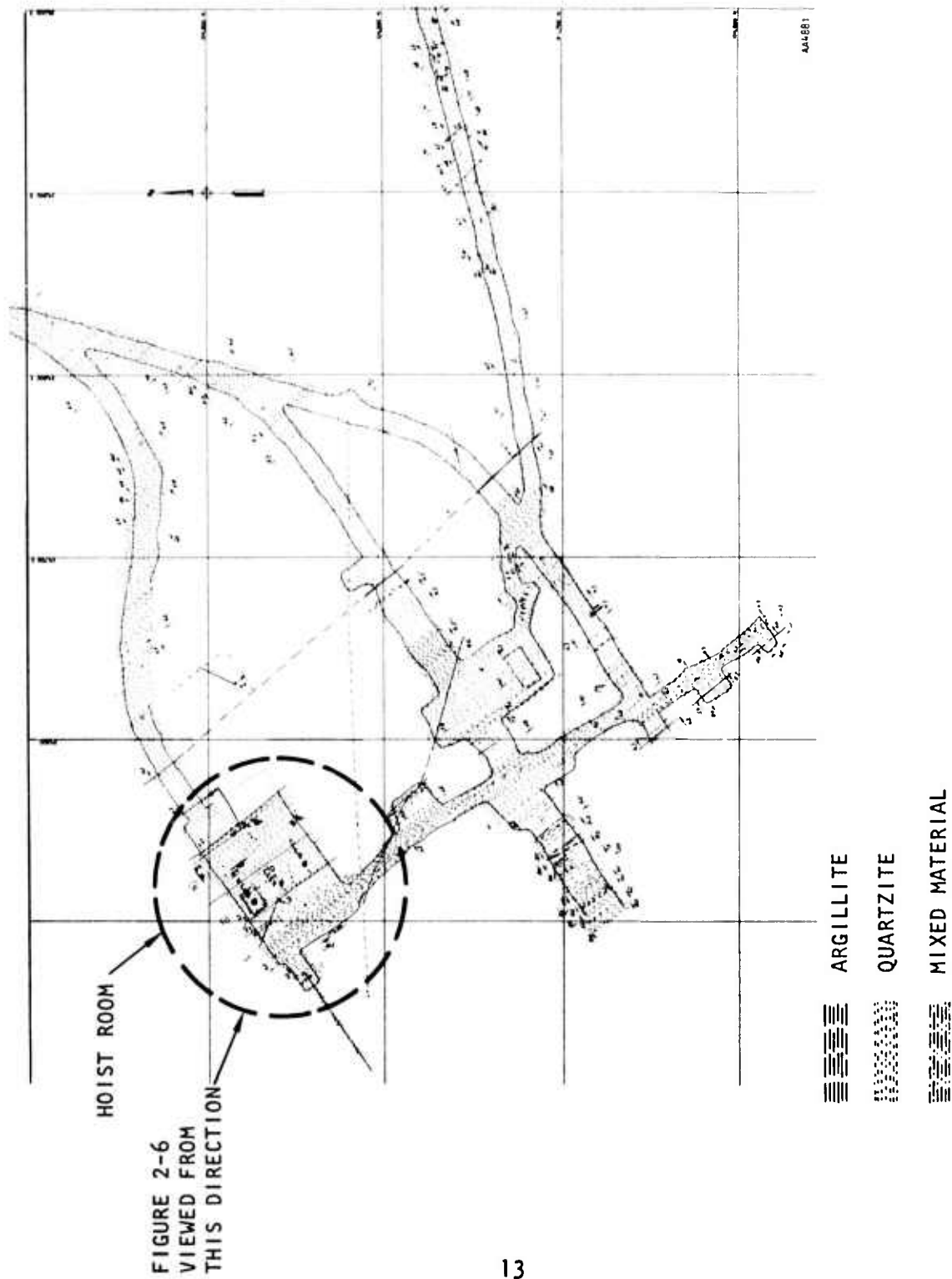


FIGURE 2-5. PLAN VIEW OF HOIST ROOM AND CONNECTING DRIFTS AT CALADAY PROJECT
SHOWING DIP OF BEDDING FAULT



R-7215-1-2701

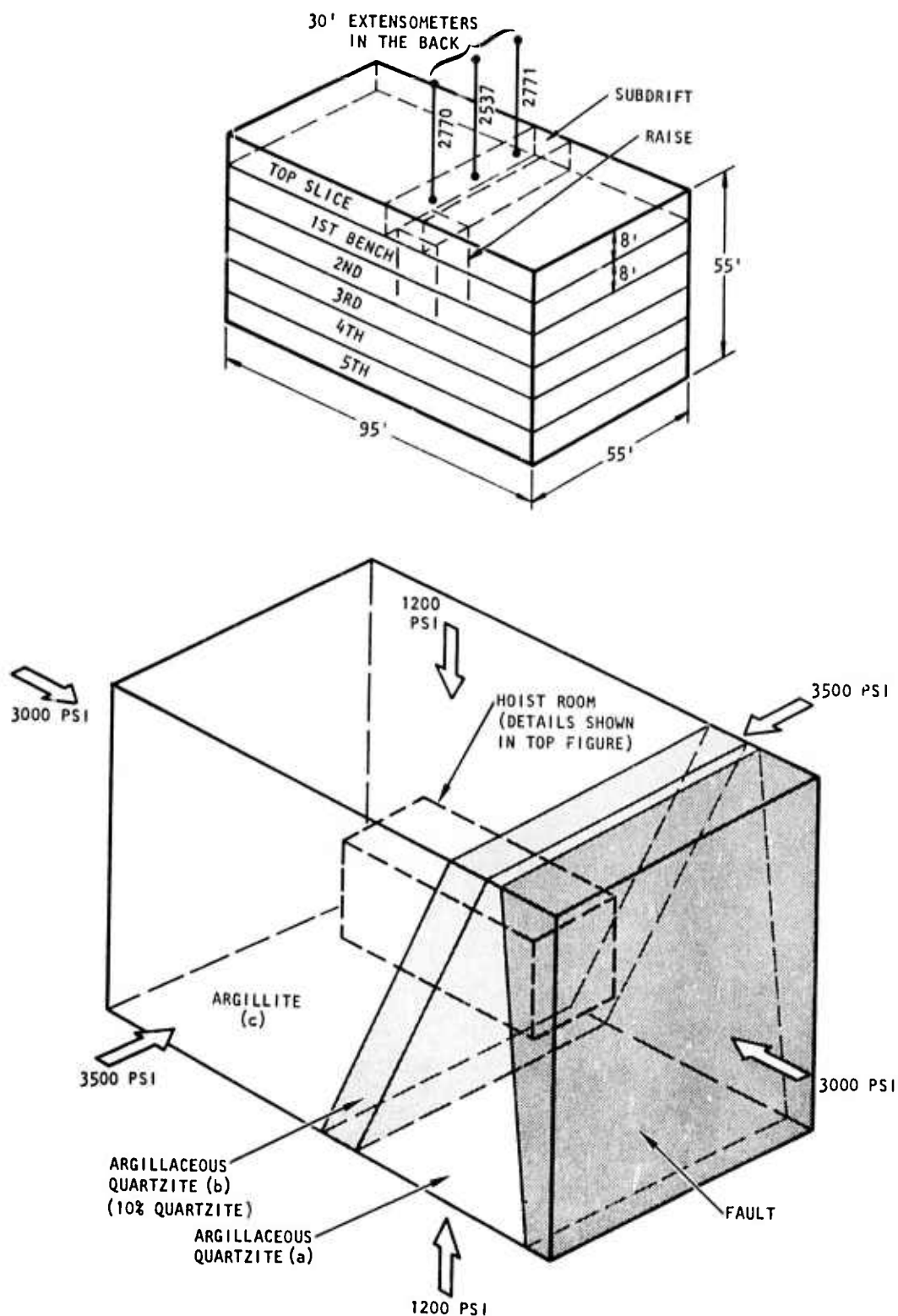


FIGURE 2-6. IDEALIZATION OF HOIST ROOM DIMENSIONS, EXCAVATION SEQUENCE AND IN SITU STRESSES

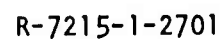


FIGURE 2-7. TIME VARIATION OF CUMULATIVE DISPLACEMENT BETWEEN TOE AND COLLAR OF EACH OF THE THREE EXTENSOMETERS INSTALLED IN THE BACK OF THE HOIST ROOM
(EXTENSION POSITIVE)



R-7215-1-2701

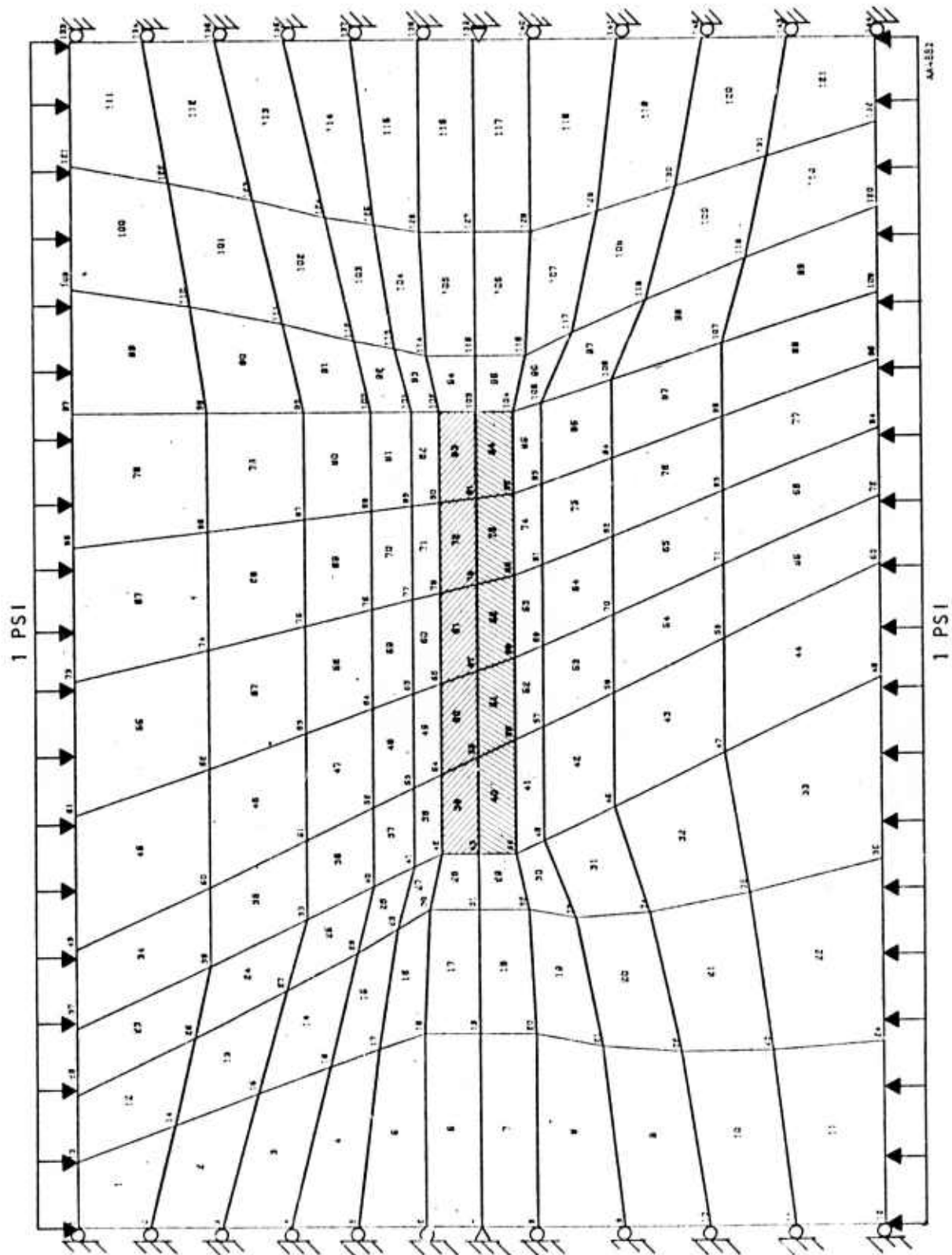


FIGURE 2.8 (a) AN AUTOMATICALLY GENERATED 2-D MESH FOR CALADAY HOIST ROOM

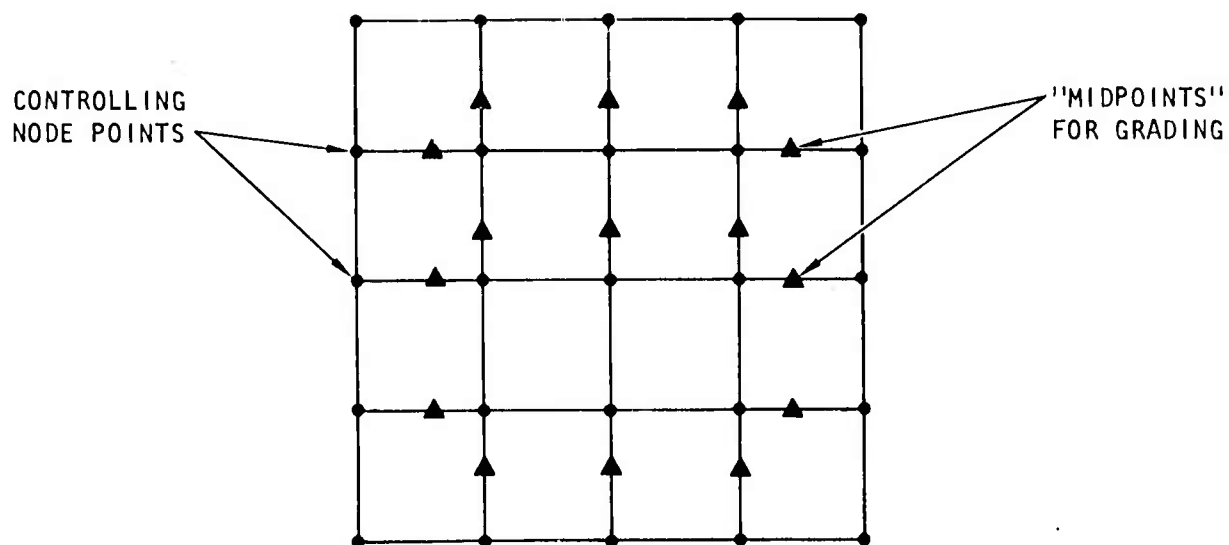


FIGURE 2.8 (b) SCHEMATIC KEY DIAGRAM FOR MESH SHOWN IN 2-8 (c)

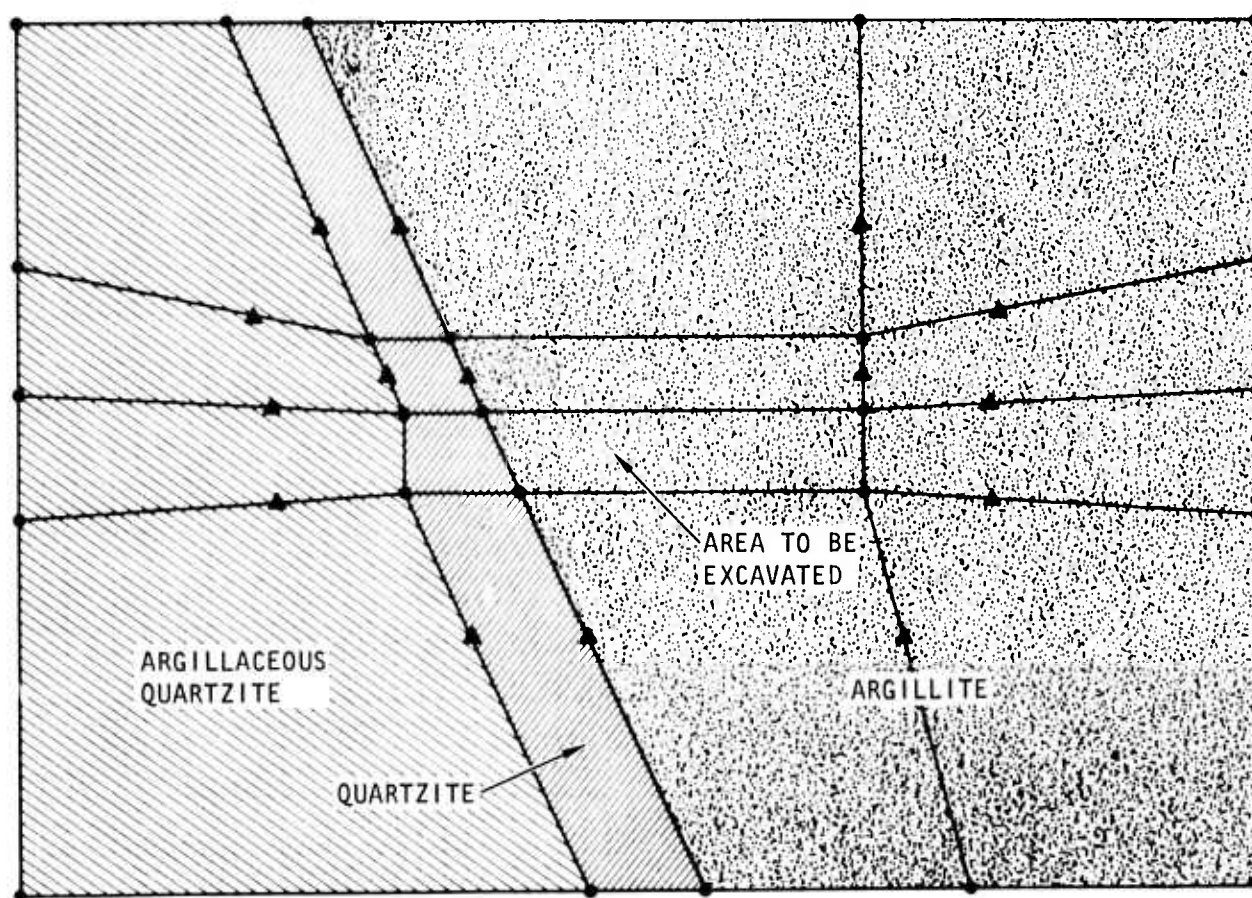


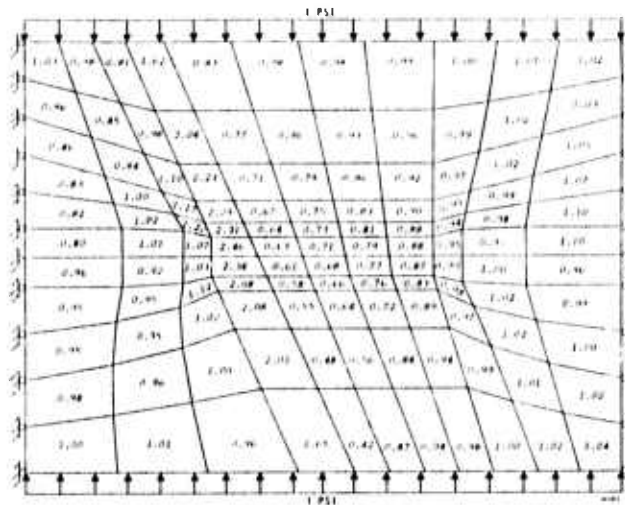
FIGURE 2-8 (c) ACTUAL KEY DIAGRAM WITH INPUT NODAL POINT COORDINATES FOR PRELIMINARY TWO-DIMENSIONAL ANALYSIS



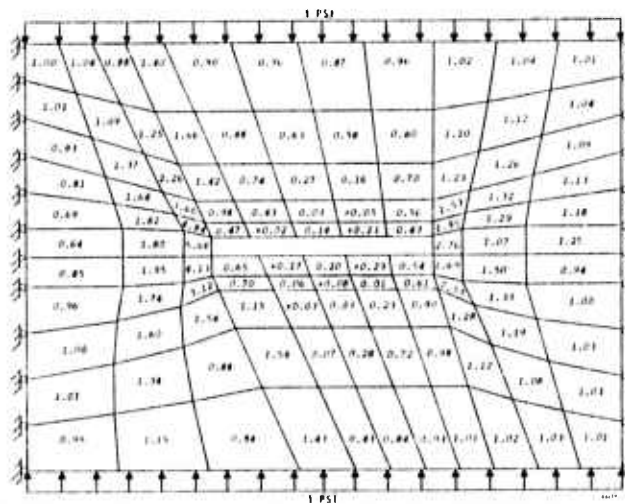
input key diagram shown in Figure 2-8(b). The so-called "key diagram" is discussed in detail in Section 5. Figure 2-8(c) shows the configuration of the key diagram when the actual coordinates of the controlling nodal points are taken into account. The key diagram has been so planned that Elements 39, 50, 61, 72, 83, and Elements 40, 51, 62, 73, and 84 outline the top slice and the first bench, respectively, and can be removed in sequence in the course of numerical calculation to simulate the actual excavation sequence.

The mathematical model is roller-supported along the left- and right-hand edges except at Nodal Points 7 and 139 which are hinged. A uniform unit pressure (1 psi) is applied along the top and bottom edges to simulate the overburden pressure. Since the model is elastic, the response to any other vertical pressure can be readily computed by scaling. These loading and supporting conditions are the result of earlier comparison studies which show that, for this plane strain idealization, applying the overburden pressure along two edges (top and bottom) is superior to applying it along one edge only (say, the top edge) and supporting the other edge (the bottom edge) as well. However, applying normal pressure to each of three orthogonal faces to represent in situ stresses is more suitable for the refined three-dimensional model described below.

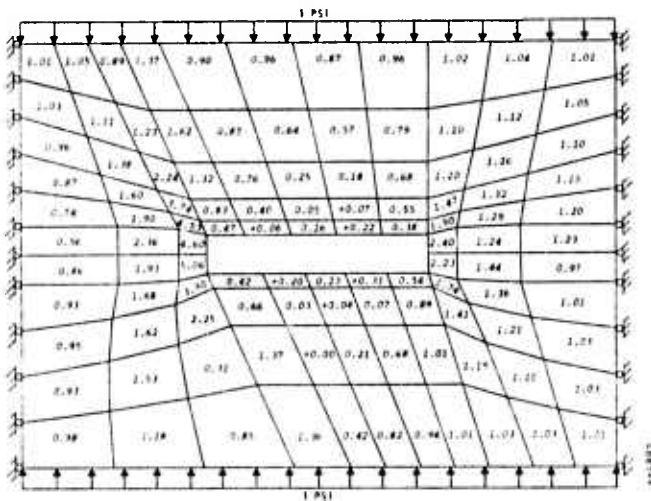
Figure 2-9 summarize the distribution of vertical normal stress determined from the preliminary plane strain analysis with idealized elastic properties. The narrow layer of argillaceous quartzite is assumed to be approximately twice as stiff as the argillaceous quartzite on the left and twenty times as stiff as the argillite on the right. Figure 2-9(a) shows the stress distribution prior to excavation. Figures 2-9(b) and 2-9(c) show the distribution following the excavation of the top slice and the first bench, respectively. The latter solutions are the result of performing four iterations following the reformulation of the global stiffness matrix to delete the stiffness of the elements corresponding to the part of the room newly excavated. Although comparison with a closed form solution cannot be made for the case of inhomogeneous rock, the familiar pattern of stress concentration around a rectangular hole is clearly seen. No attempt is made to compare the results of this computation with the extensometer



(a) DISTRIBUTION OF VERTICAL NORMAL STRESS BEFORE EXCAVATION
(ALL STRESSES ARE COMPRESSIVE)



(b) DISTRIBUTION OF VERTICAL NORMAL STRESS FOLLOWING TOP-SLICE EXCAVATION
(ALL STRESSES EXCEPT THOSE WITH POSITIVE SIGNS ARE COMPRESSIVE)



(c) DISTRIBUTION OF VERTICAL NORMAL STRESS FOLLOWING FIRST-BENCH EXCAVATION
(ALL STRESSES EXCEPT THOSE WITH POSITIVE SIGNS ARE COMPRESSIVE)

FIGURE 2-9. RESULTS OF PRELIMINARY TWO-DIMENSIONAL ELASTIC ANALYSIS



data because (a) the material coefficients used in this early study differ from those finally adopted, (b) the major fault described earlier, which would appear off the left end of the hole in the current, two-dimensional mesh, is not taken into account in this model, and (c) a two-dimensional, plane strain analysis in this case is not expected to yield a good solution especially when the plane chosen is parallel to the long axis of the hoist room. The solution is presented here as an introduction to the more complicated analyses which follow.

2.2.3 MATERIAL PROPERTIES FOR ANALYSIS OF CALADAY PROJECT HOIST ROOM

This section describes properties of the St. Regis formation argillaceous quartzite and argillite which are used in computing stresses and deformations at the Caladay hoist room. The goal of defining the properties is to determine the elastic and inelastic stiffnesses and strengths which are typical of rock masses in situ. In the analysis it is assumed that these properties are homogeneous throughout the volume of a finite element, which in the present case is about 10 to 15 feet on a side.

The material properties are selected from laboratory and in-situ measurements and by consultation with geologists and mining engineers who are familiar with the site. Due to wide variations in the types of rock present and to uncertainty in translating laboratory properties into in-situ properties, consultation is considered to be the most important element in selecting reasonable properties.

The fundamental decision which was made regarding material properties is the mathematical idealization within which the properties are represented. As explained in subsequent sections of this report, the available models include such features as anisotropy, plasticity, viscoelasticity, and viscoplasticity. The decision to use isotropic viscoelasticity is based partly on positive factors, such as recommendations from knowledgeable geologists and laboratory and in situ measurements, and partly on negative factors such as the absence of sufficient data on which to base an anisotropic model. Viscoplasticity is an attractive model for argillite and argillaceous



quartzite because both plasticity and time dependence appear to be present. Precedent for using plasticity to represent these materials is found in Reference 2-3. Clear evidence of time-dependent deformations is also found in this and in similar work (Reference 2-4). The viscoplastic model was rejected primarily for lack of data which is required to distinguish the amount of time-independent inelasticity from time-dependent inelasticity. Without rational basis for such a distinction it is better to use a simpler model with only one mechanism for inelasticity. Although an elastic/plastic model is used for the analyses of Reference 2-3, the present case involves lower in situ stresses and hence a smaller contribution to displacements from time-independent plasticity. Based on this reasoning, time-dependent elastic properties, as are represented by linear viscoelasticity, are assumed to be the dominant mechanism governing stresses and deformations around the hoist room. The model of stress/strain properties for argillite is developed according to this assumption.

In contrast to the argillite and argillaceous quartzite, the cross bed fault which passes near the hoist room is filled with clay minerals and fractured argillite. The shear strength of this material has not been measured due to the difficulty of sampling such an inhomogeneous material. It is likely, however, that the shear strength of wet fault gouge is very low. Accordingly, it would be well represented by an elastic/perfectly plastic model. The principal numerical difficulty in using such a model arises from applying stress boundary conditions, which in the present analysis represent in situ stresses. A simple calculation shows why it is not possible to specify both

- a. Shear strength of fault gouge of order 100 psi and
- b. In situ stress components of 1200, 3000, and 3500 psi

The maximum shear stress associated with the in situ stresses is $(3500 \text{ psi} - 1200 \text{ psi})/2 = 1150 \text{ psi}$, which is much larger than any reasonable shear strength for the fault gouge. Clearly the values of in situ stress which are



shown in Figure 2-6 are average or representative values which do not apply near the fault. The following are three alternatives in representing the fault within the capability of the present computer program.

- a. Move the boundaries of the mesh far beyond the fault, use elastic/plastic properties for the fault and allow plastic flow to modify the local stress field as occurs in nature.
- b. Use very low elastic moduli for the fault material, thus allowing the stiffer argillite and argillaceous quartzite to sense a flexible zone without interfering with the stress boundary conditions.
- c. Omit the fault.

Alternative (a) is rejected on account of cost. Alternative (b) is superior to Alternative (c), and hence is selected.

2.3.3.1 Viscoelastic Properties of Argillite

The viscoelastic model for argillite (zone c) is based on two assumptions which are:

- a. The argillite may be represented by three parameter solid containing a Kelvin element (spring and dashpot in parallel) in series with a spring.
- b. The elastic bulk and shear moduli of the in situ argillite rock mass can be found on the basis of laboratory tests and judgment.

The viscoelastic properties are selected such that analysis of deformation around an auxiliary shaft matches the field data. In this way the model incorporates field and laboratory measurements and engineering judgment.

TABLE 2-1. REPRESENTATIVE ELASTIC PROPERTIES OF PURE MINERALS
BASED ON LABORATORY MEASUREMENTS

Type	In Situ Young's Modulus	In Situ Poisson's Ratio
Pure Quartzite	7.0×10^6 psi	0.2
Pure Argillite	0.35×10^6 psi	0.1

E, ν in Table 2-2 are converted to K and G as follows:

$$K = \frac{E}{3(1-2\nu)} \quad (2-3)$$

$$G = \frac{E}{2(1+\nu)} \quad (2-4)$$

The viscoelastic coefficients to be determined for substitution into Equations 2-1 and 2-2 are $1/\eta_K$, $1/\eta_G$ and the K and G for the Kelvin element. This is done by parametric variation of these coefficients in a finite element analysis to match an in situ experiment.

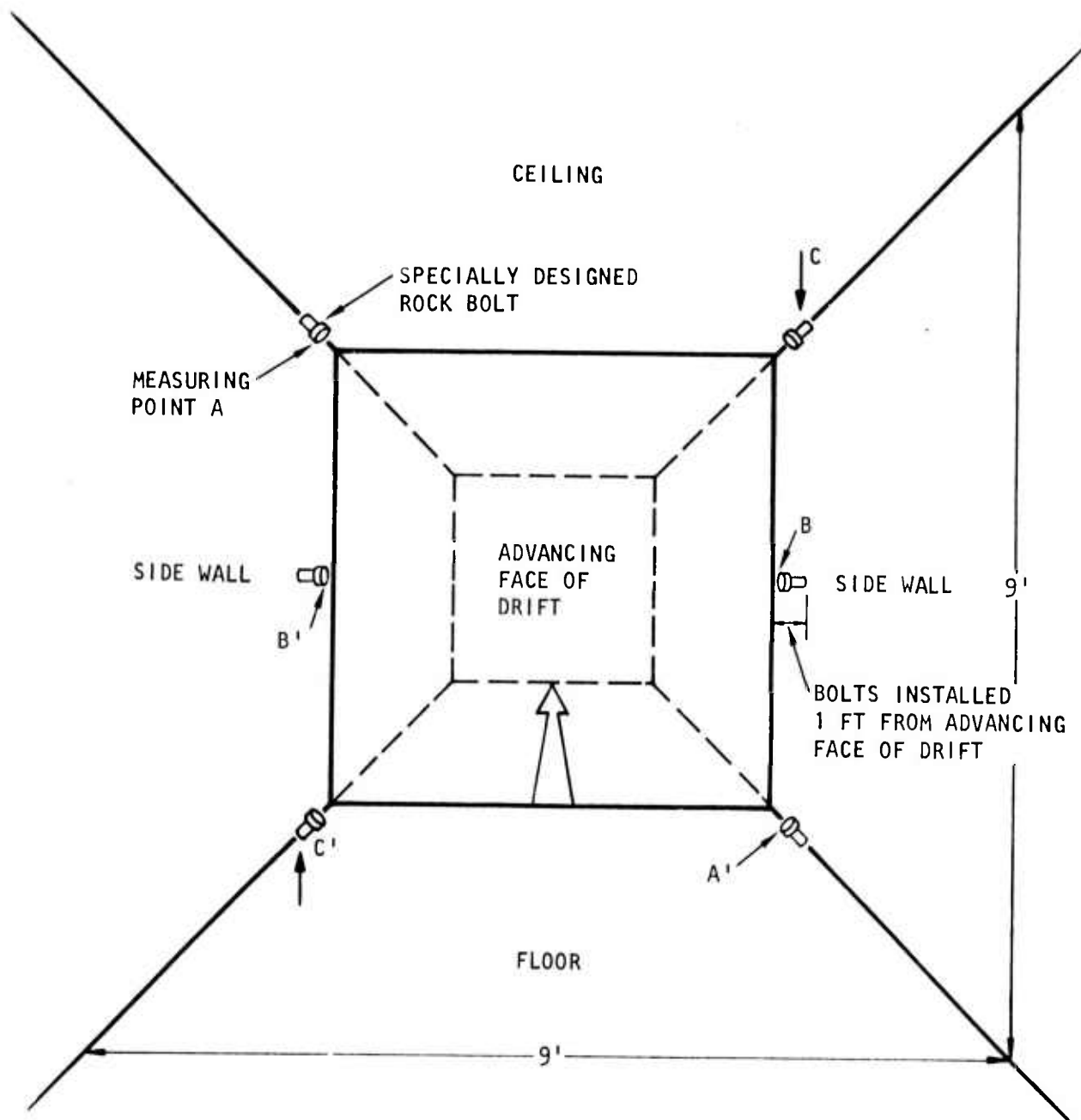
The experiment is illustrated in Figure 2-10 and is described in Reference 2-3. At a typical station, rock bolts were installed as close to the advancing face as possible. The distances BB' and CC' were measured. As excavation of the drift progressed, movements of the rock bolts were monitored by means of extensometers. The results of these measurements, reproduced from Reference 2-3, are shown in Figure 2-11. The viscoelastic coefficients were selected by assuming values for η_K and η_G , applying the measured values of in situ stresses shown in Figure 2-12 to the finite element mesh in the same figure, then changing the values until the agreement between measurement and calculation is satisfactory. In practice, the argillite in Zone C was first assumed to be elastic in bulk and viscoelastic in shear. Then it was assumed to be viscoelastic in bulk and elastic in shear. It was originally intended to assume combined viscoelasticity in shear and bulk. However, viscoelasticity in bulk alone seemed to be adequate. The viscoelastic coefficients finally selected are shown in Table 2-2. The comparison between in situ measurements and the finite element calculations using these properties is shown in Figure 2-11.



R-7215-1-2701

TABLE 2-2. PROPERTIES OF ANALYSIS OF CALADAY HOIST ROOM

Zone	Argillite, Percent	Quartzite, Percent	Argillaceous Quartzite, Percent	Viscoelastic (Kelvin) Element		Elastic Properties	
				η_K	K 10 ⁶ psi	E 10 ⁶ psi	ν
A	60	--	40			1.6	0.2
B	50	10	40			2.2	0.2
C	>90	--	<10	10 ⁹	0.75	0.35	0.1
Fault						0.05	0.3

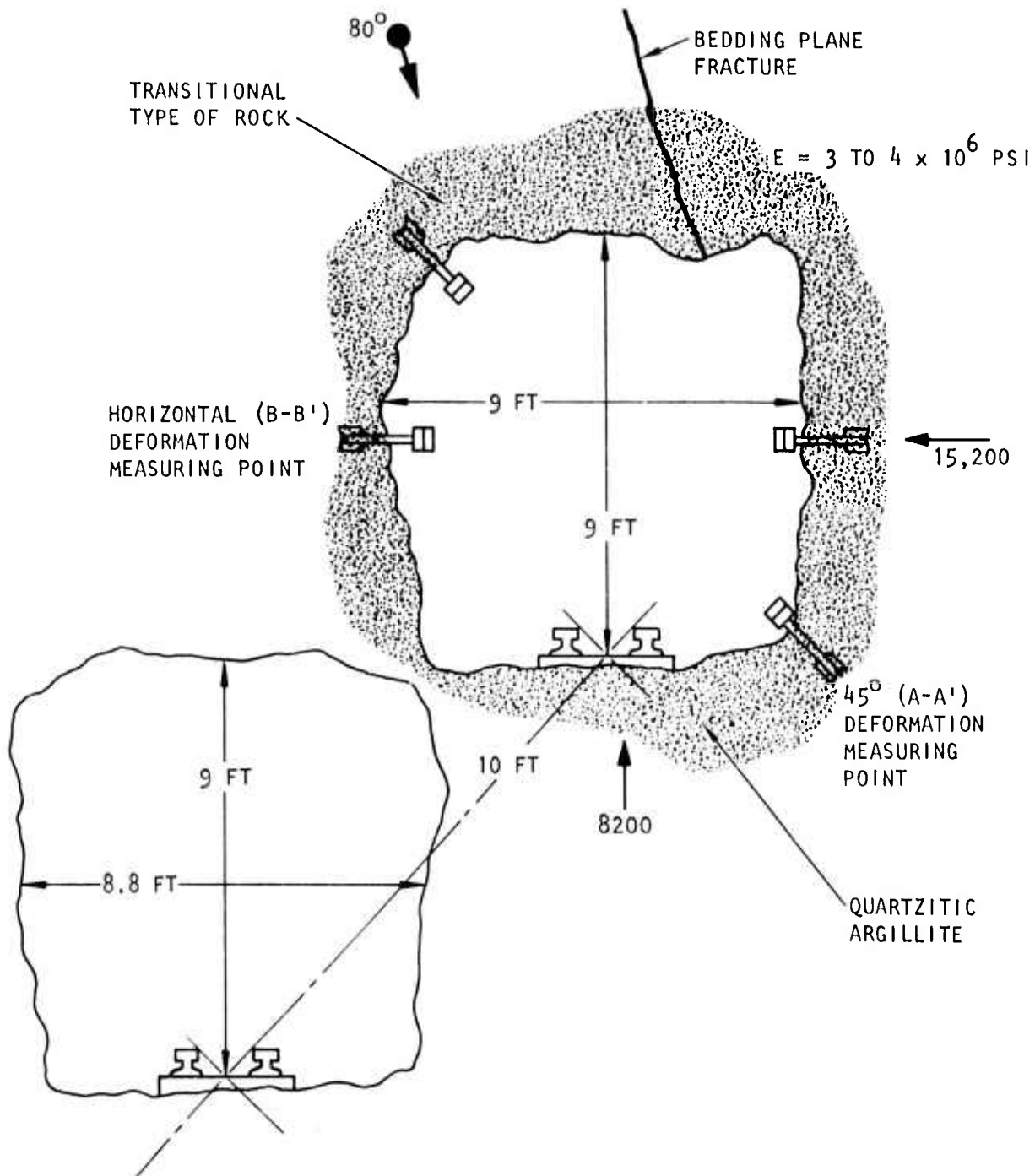


(a) LOCATION OF ROCK BOLTS SERVING AS MEASURING POINTS FOR MEASURING RELATIVE DISPLACEMENTS IN DRIFT USING EXTENSOMETER

FIGURE 2-10. AUXILIARY DRIFT IN SILVER SUMMIT MINE USED TO DETERMINE IN SITU VISCOELASTIC PROPERTIES OF ARGILLITE

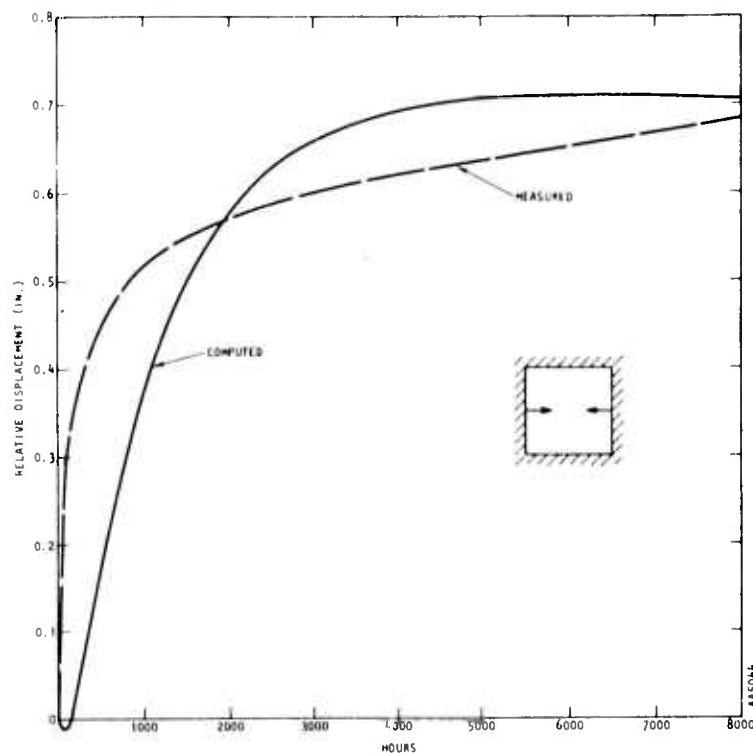


CREEP MODEL FOR ARGILLITE

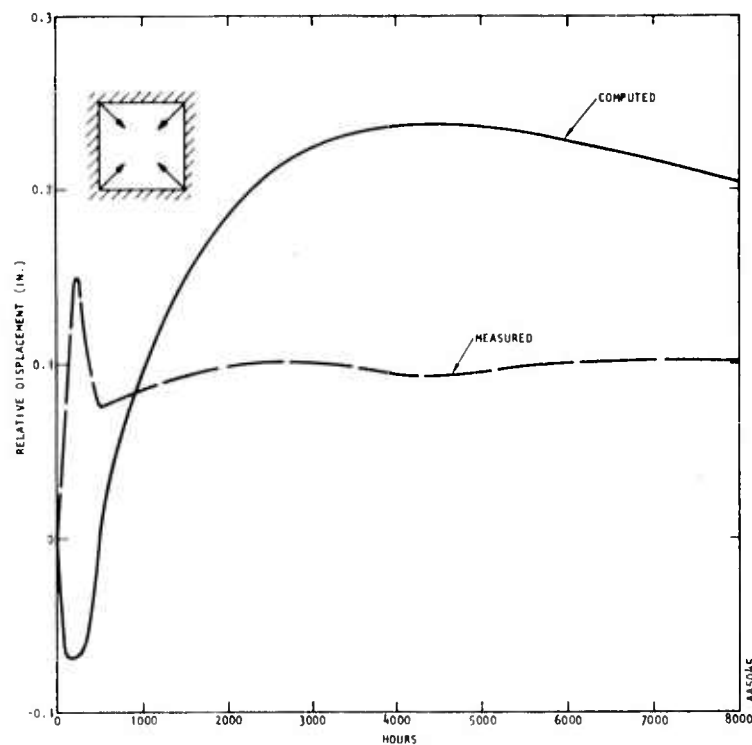


(b) A REPRESENTATIVE CROSS-SECTIONAL VIEW AT STATION SS-3 OF THE SOUTH EAST LATERAL, 4000 LEVEL, SILVER SUMMIT MINE (REFERENCE 2-5)

FIGURE 2-10. (CONTINUED)



(a) RELATIVE DEFORMATION FROM POINTS B-B'



(b) RELATIVE DEFORMATION, AVERAGE FROM POINTS A-A', C-C'

FIGURE 2-11. COMPARISON BETWEEN MEASUREMENTS AND COMPUTATION OF RELATIVE DISPLACEMENTS IN DRIFT IN ARGILLITE, SILVER SUMMIT MINE (COMPRESSION POSITIVE)



R-7215-1-2701

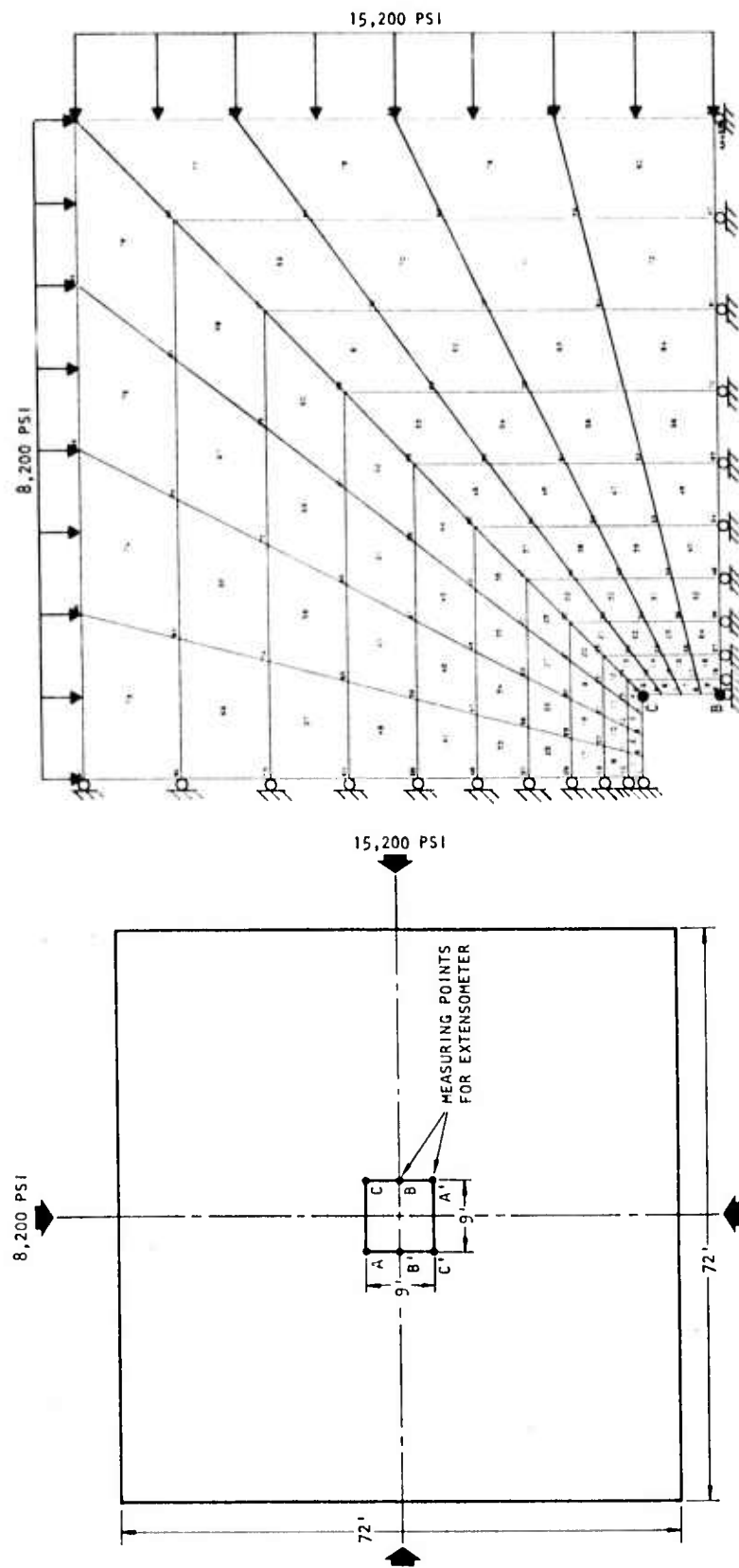


FIGURE 2-12. PLANE STRAIN FINITE ELEMENT ANALYSIS OF SECTION SS-3 IN ARGILLITE



The stress/strain relations for the Kelvin portion of the visco-elastic model are divided into two parts. One part governs volumetric behavior and a second part governs shear behavior as follows:

$$\frac{\sigma_{ii}}{3} = K \epsilon_{ii} + \eta_K \dot{\epsilon}_{ii} \quad (2-1)$$

$$\sigma'_{ij} = 2G \epsilon'_{ij} + \eta_G \dot{\epsilon}'_{ij} \quad (2-2)$$

where

ϵ_{ii} = Volumetric strain

$\frac{1}{3}\sigma_{ii}$ = Mean normal stress

ϵ'_{ij} = Deviatoric strain component

σ'_{ij} = Deviatoric stress component

K, G = Elastic bulk and shear moduli

η_K, η_G = Viscous coefficients in bulk and shear, respectively

K, G, η_K and η_G are independent coefficients. Thus, the material may be elastic in bulk and viscoelastic in shear, or vice versa, or viscoelastic in both components.

The first step in developing the model for the argillite is to determine in situ elastic moduli. Laboratory measurements of Young's moduli and Poisson's ratios are available for argillites, quartzites and mixtures of the two in Reference 2-6. Most of these data are for rocks from the St. Regis and Revett Quartzite formations. The lowest modulus for pure quartzite is about 4×10^6 psi and the highest is about 13×10^6 psi. Poisson's ratio appears to vary from about 0.05 to about 0.24. Based on these measurements and suggestions received in Reference 2-7, the properties for pure quartzite are assumed to be as shown in Table 2-1. Based on suggestions in Reference 2-7, the in situ moduli of the argillaceous quartzites in the vicinity of the hoist room are computed from the fractions of pure argillite and pure quartzite. These are indicated in Table 2-2.



2.2.3.2 Elastic Properties of Argillaceous Quartzite and Fault Zone

The properties of the argillaceous quartzite in Zones A and B are assumed to be linearly elastic as shown in Table 2-2. The elastic moduli are determined from the percentage of quartzite and argillaceous quartzite in each as described above. The judgment of experienced engineers who are familiar with the area is the most important factor in selecting these coefficients. It would have been preferable to include viscoelasticity in the models of material in Zones A and B. However, it was not possible to obtain suitable samples of the rock in time for the present analysis. Moreover, measurements on rock which was similar but which contained more quartzite showed no appreciable creep.

The moduli of material in the fault was arbitrarily assumed to be very low, as shown in Table 2-2.

2.3 THREE-DIMENSIONAL ANALYSIS OF HOIST ROOM AT CALADAY PROJECT

The physical situation of the hoist room which is shown in Figure 2-6 and the mathematical models for the various types of rocks which are described above are combined into a three-dimensional finite element analysis.

The finite element mesh for the final three-dimensional analysis of the hoist room is shown in Figure 2-13. It is an 11 x 11 x 6 mesh with 1008 nodal points and 726 elements. It is loaded on three of its six faces to simulate the in situ stress condition, and simply supported on the remaining three faces as indicated. Except for points on the simply supported faces, each point has three translational degrees of freedom so that the simultaneous solution of 2712 equations is involved in each load step. The four idealized zones having different materials are shaded in the figure. These are the same zones as shown in Figure 2-6 and Table 2-2.

For the convenience of creating plane interfaces among the different material zones, all the mesh lines running in the z-direction have been made straight and parallel to the z-axis. The mesh has been created in such a

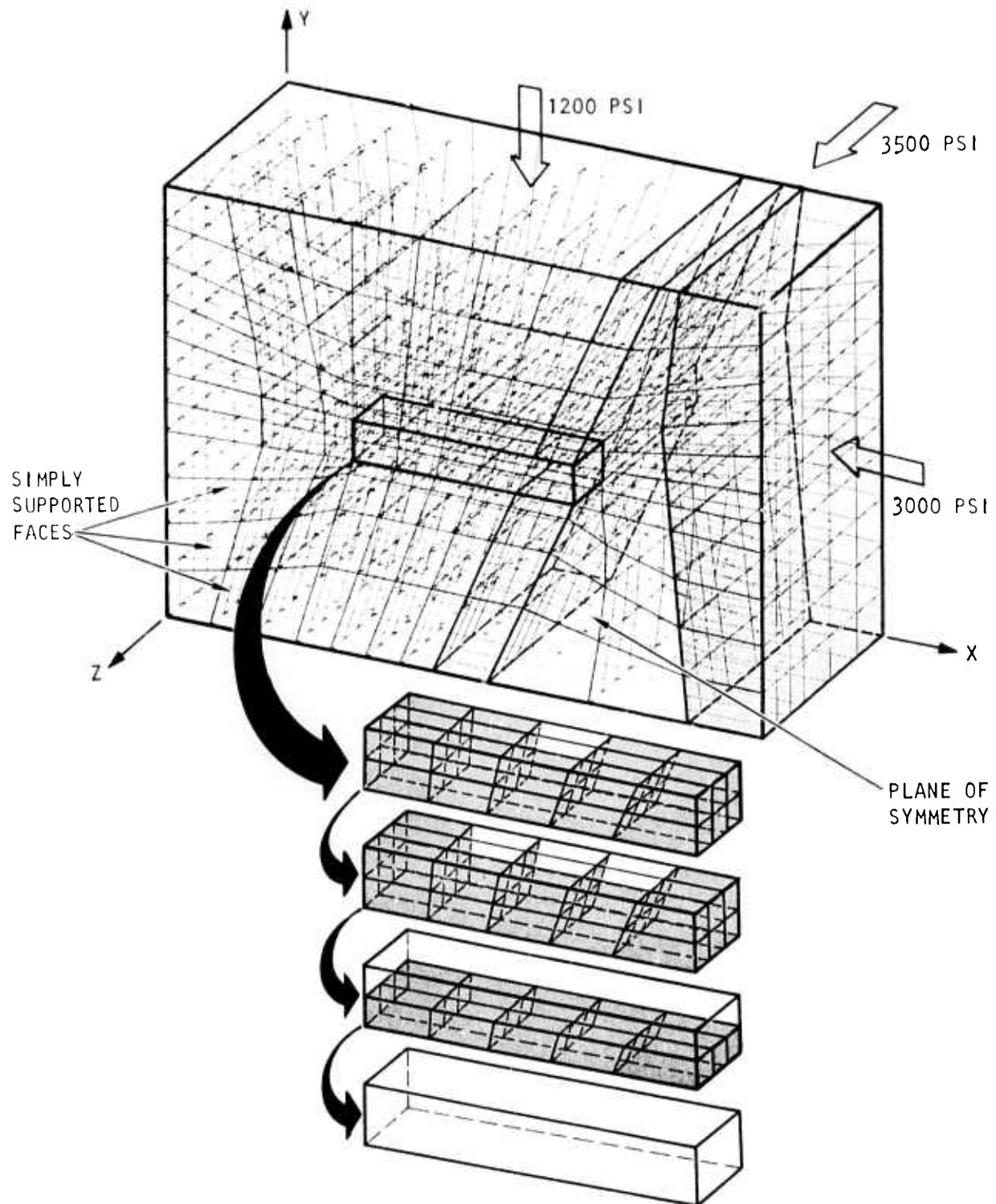


FIGURE 2-13. THREE-DIMENSIONAL FINITE ELEMENT MESH WITH ORIGINAL CONFIGURATION OF TOP SLICE AND FIRST BENCH FOLLOWED BY THREE STAGES OF EXCAVATION



manner that the rectangular cavity to be created by the excavation of the top slice and the first bench is represented by two layers of fifteen elements each. These thirty elements are "turned off" in the course of the numerical calculation in the sequence illustrated in the detailed drawing to simulate the actual excavation sequence that took place in the field. The mesh is made finer around the cavity for better stress definition and the first three layers of mesh lines over the back are located at 6 ft, 15 ft, and 30 ft above the back to facilitate the checking of extensometer readings. The mesh as designed is rather coarse; but it is as fine as is permitted by the computer budget of the present project.

Computation begins with the mesh representing solid rock except for a small cavity representing the subdrift which was driven before the extensometers were installed. The first step of the computation involves applying the in situ stresses to the mesh and finding the corresponding stress and displacement fields. The second step is an iteration to obtain an improved approximation to equilibrium conditions. In the computation, the end of Step 2 corresponds to installation of the extensometers, and hence to a zero value of relative displacement. Between Steps 2 and 3, time is assumed to elapse and viscoelastic flow occurs in the argillite. Subsequently, elements are turned off at appropriate intervals to simulate the progress of the excavation, and the real time is incremented intermittently to allow creep to take place in between the excavation steps. The entire sequence of operations is summarized in Table 2-3. The solution is iterated once following each excavation step which involves the reformulation of the global stiffness matrix. Additional iterations would be highly desirable, but were omitted to keep within the computer budget.

The result of the run is represented by the displacement components of all the node points and the stress and strain components in all the elements for each one of the twelve steps taken. It is of interest to examine the stress distribution in the mesh at the end of the second step. Since the hole that exists in the mesh at this time is still small, the stress distribution



TABLE 2-3. TWELVE STEPS TAKEN IN THE FINAL THREE-DIMENSIONAL CALCULATION

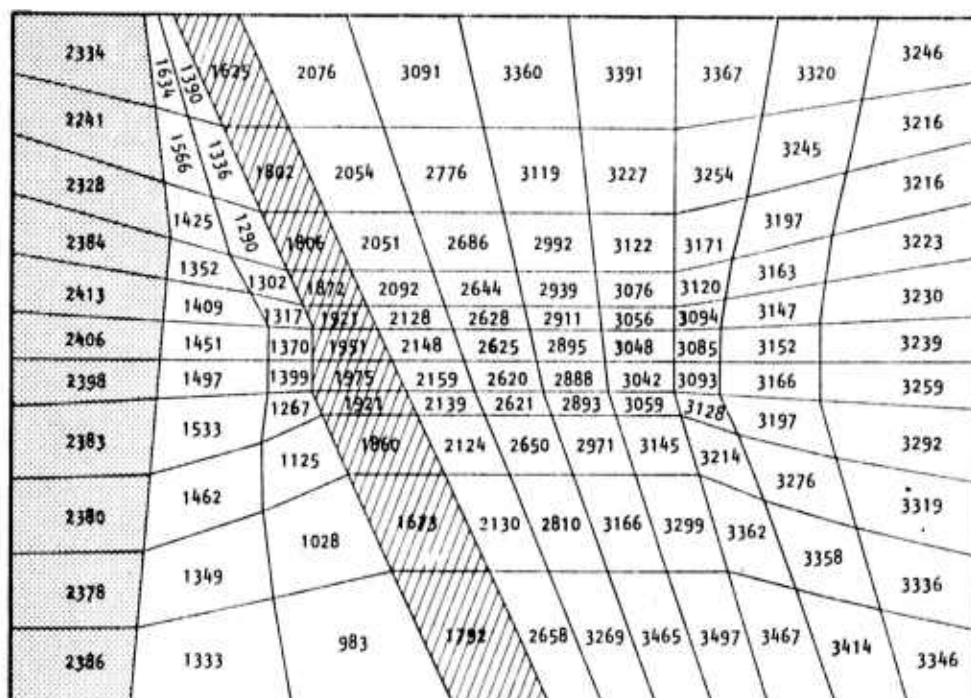
Step Number	Real Time (Days)	Purpose
1	0 (June 12)	To create the in situ stress condition with the subdrift already in place.
2	0	Iterate to stabilize the elastic solution.
3	18 (July 1)	To allow creep to take place for 18 days.
4	18	Advance top slice excavation by removing six additional elements.
5	18	To perform an iteration.
6	33 (July 15)	To allow 15 additional days of creep to take place.
7	33	Remove six more elements to complete the excavation of the top slice.
8	33	To perform an iteration.
9	49 (August 1)	To allow 16 additional days of creep to take place.
10	49	Excavate the entire first bench in one step.
11	49	To perform an iteration.
12	71 (August 22)	To allow the final 22 days of creep to take place.



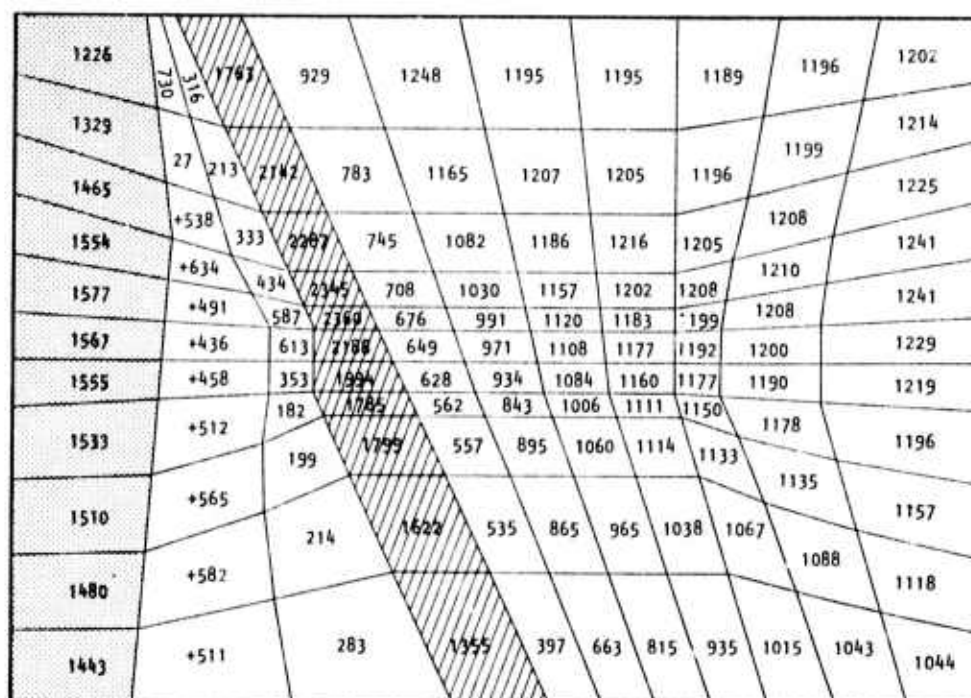
created in the mesh should be very nearly the in situ stress condition that can be realized in the mathematical model under the loading and boundary conditions adopted. Figure 2-14 summarizes the distribution of the three normal stresses in the direction of the coordinate axes in the first and the last layer of elements when the mesh is viewed from the negative z-direction.

It is noted, first of all, that the stress distribution is very irregular, with the stress values in some portions of the mesh quite unlike the homogeneous stress condition which is applied to three faces of the mesh. What is mainly responsible for this dramatic variation in the stresses is the difference among the stiffnesses of the materials involved in the four zones. Young's Modulus varies as much as two orders of magnitude from the softest to the stiffest material. Under these circumstances, there are large amounts of stress transfer from the softer to the stiffer zones, causing large shearing stresses at the material interfaces and very uneven reaction distribution over the three simply supported faces.

It is assumed in the calculation that the extensometers are installed at the end of the second step so that they are stretched only by the additional deformation created henceforth. On the basis of this assumption, the equivalent of two extensometer records have been deduced from the computer run and are plotted in Figure 2-15. Figure 2-16 shows the variation of the vertical normal stresses over the back of the room as excavation progresses sidewise from the subdrift and then downward into the first bench. Figure 2-17 shows the time history of the downward deflection of the center of the back and the upheaval of the center of the floor of the first bench during the same period. In calculating the deflections of the back and the floor during the excavations, the deflected configuration of the mesh at the end of the second step is considered as the datum. Based on this datum, the upheaval of the entire first bench floor at the end of 71 days (12th step) is pictured



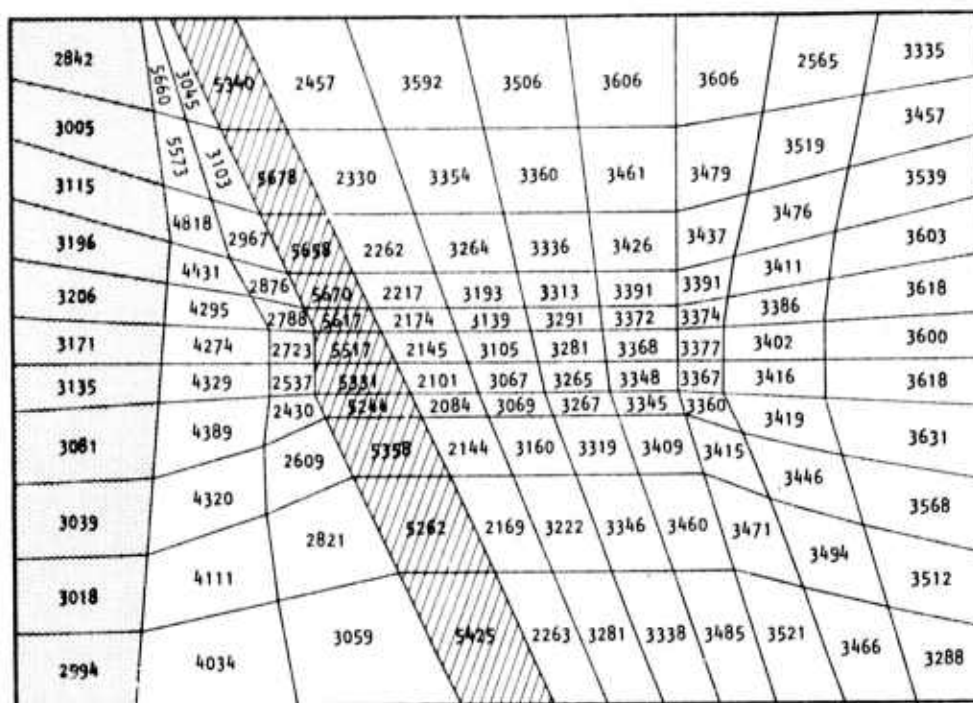
AA5048

(a) σ_x IN FRONT LAYER


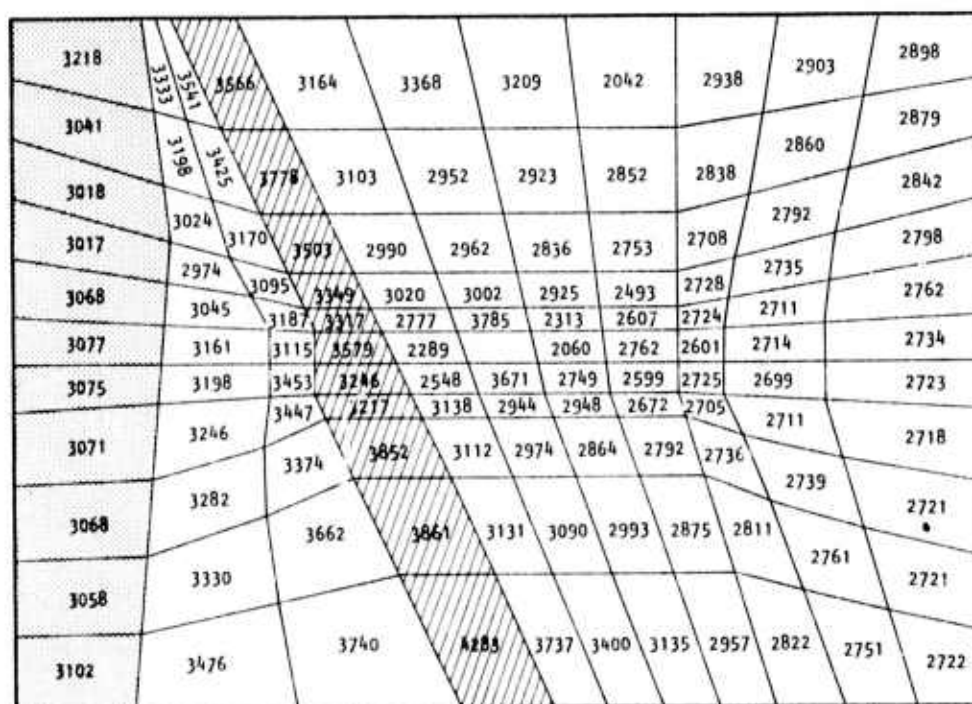
AA5049

(b) σ_y IN FRONT LAYER

FIGURE 2-14. NORMAL STRESSES IN FRONT AND BACK LAYERS OF ELEMENTS (AS VIEWED FROM THE NEGATIVE Z-DIRECTION IN FIGURE 2-13)



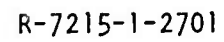
AA5050

(c) σ_z IN FRONT LAYER


AA5051

(d) σ_x IN BACK LAYER

FIGURE 2-14. (CONTINUED)



(e) σ_y IN BACK LAYER

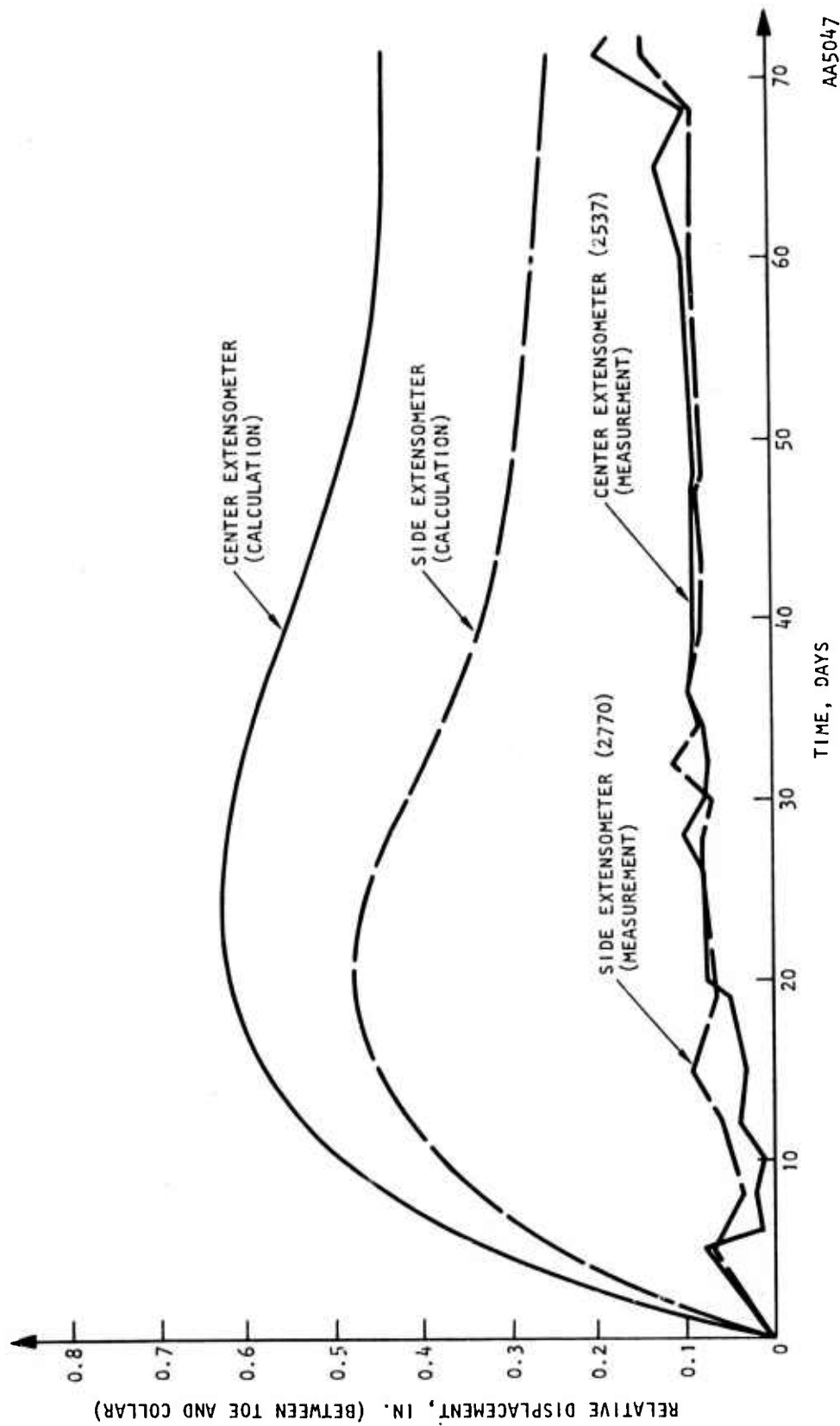


(f) σ_z IN BACK LAYER

FIGURE 2-14. (CONTINUED)



R-7215-1-2701



AA5047

FIGURE 2-15. MEASURED AND CALCULATED RELATIVE DISPLACEMENT BETWEEN ENDS OF EXTENSOMETERS LOCATED IN BACK OF HOIST ROOM VERSUS TIME (EXTENSION POSITIVE)



1347	88	1929	3570	965	780	833	1422	1102	1217	1212
1353	82	1903	3562	933	734	808	1413	1103	1215	1211
1367	52	1902	3544	911	856	939	1333	1145	1208	1210
1419	128	1799	3387	911	1035	1105	1213	1179	1197	1210
1603	91	1790	3401	839	927	1075	1153	1201	1212	1211
1577	+491	587	2360	676	992	1120	1183	1199	1208	1241

AA5054

(a) AT TIME = 0 (END OF STEP 2)

1333	82	2044	4120	707	407	573	1348	1255	1265	1217
1337	73	2030	4016	635	540	416	1295	1251	1260	1217
1354	9	2040	3957	816	290	889	1288	1253	1245	1215
1409	109	1983	3655	1036	1220	1328	1281	1236	1214	1217
1618	75	1942	3773	870	999	1147	1201	1230	1233	1211
1619	+682	697	2463	657	995	1119	1186	1203	1199	1242

AA5055

(b) AT TIME = 18 DAYS (END OF STEP 5)

FIGURE 2-16. VERTICAL NORMAL STRESSES (σ_y) IN THE ELEMENT LAYER OVER THE BACK



R-7215-1-2701

1326	197	3220	1522	+255	159	+136	601	1391	1342	1240
1350	189	2955	717	+403	33	+309	421	1325	1335	1240
1350	78	2735	3195	+383	675	631	952	1344	1305	1234
1403	158	2479	1574	1246	1527	1538	1455	1341	1251	1234
1615	76	2093	4336	963	1057	1217	1280	1277	1258	1218
1616	+762	793	2609	664	1001	1124	1190	1211	1201	1243

AA5056

(c) AT TIME = 33 DAYS (END OF STEP 8)

1326	211	3153	1107	+341	147	+255	495	1359	1310	1247
1329	192	2967	444	+435	225	+416	366	1342	1311	1245
1350	102	2653	2830	289	738	537	891	1334	1299	1240
1402	190	2574	4687	1199	1449	1463	1408	1333	1251	1242
1613	106	2108	1362	928	1004	1171	1244	1276	1269	1226
1616	+734	903	2705	669	1010	1133	1200	1226	1213	1253

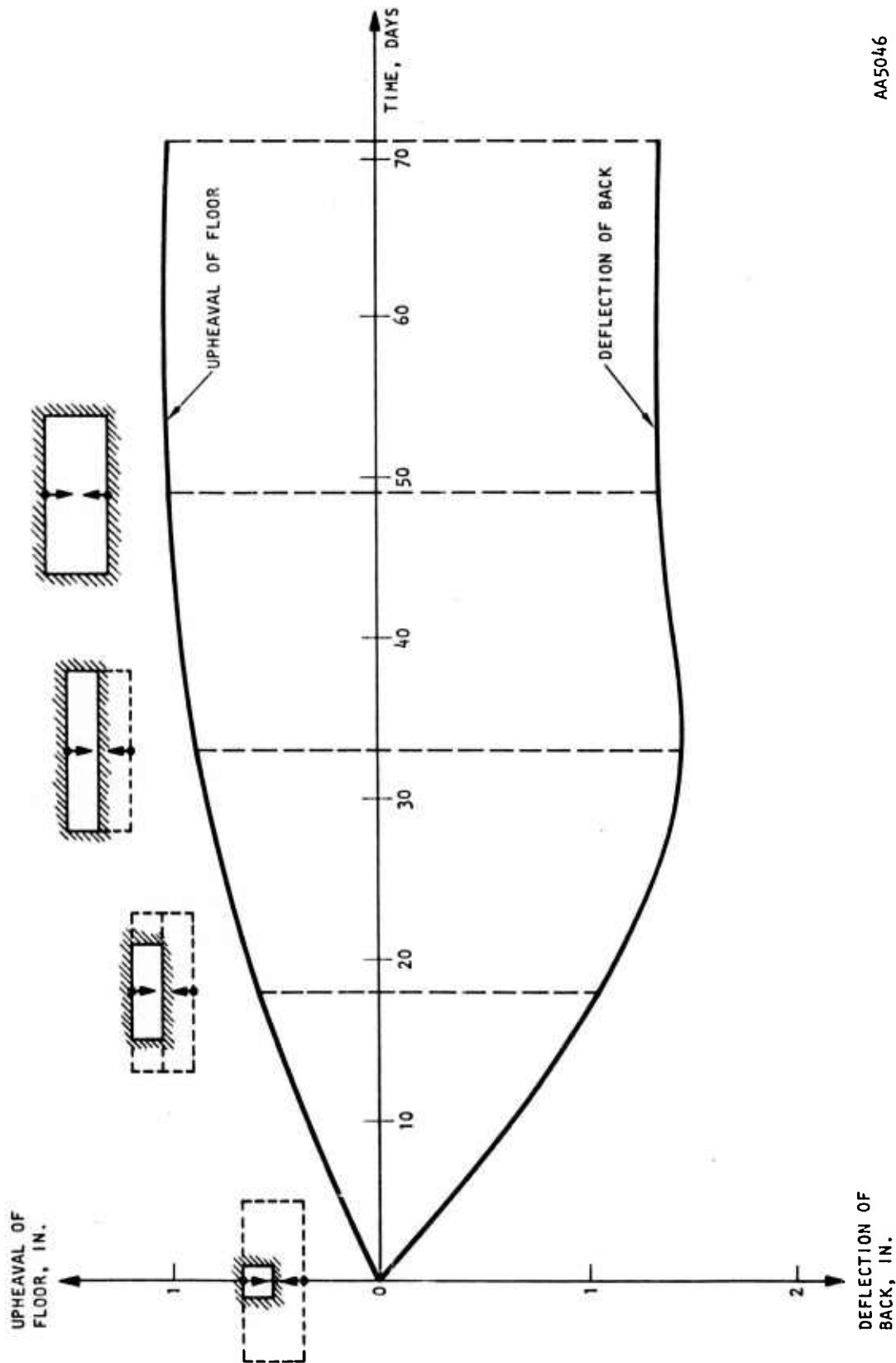
AA5057

(d) AT TIME = 49 DAYS (END OF STEP 11)

FIGURE 2-16. (CONTINUED)



R-7215-1-2701

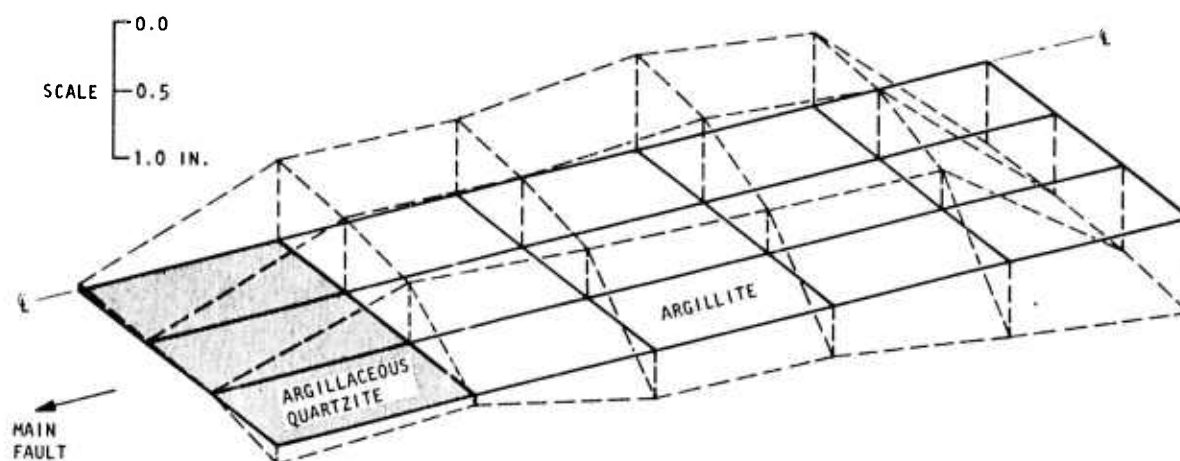


AA5046

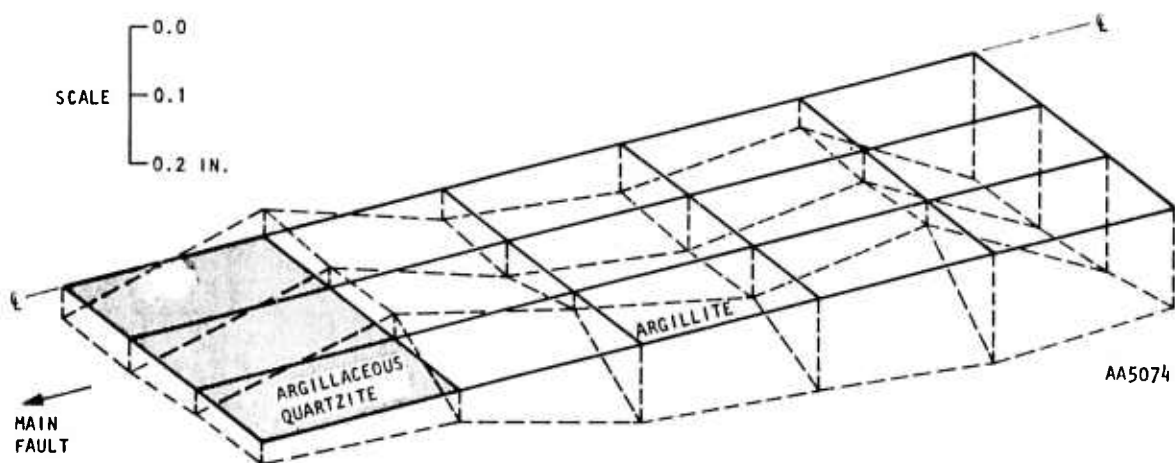
FIGURE 2-17. ABSOLUTE DEFLECTION OF CENTER OF BACK AND FIRST BENCH FLOOR



in Figure 2-18(a). Figure 2-18(b) shows the incremental deflection of the same floor from 49 to 71 days (11th to 12th step) due entirely to creep. Figure 2-18(a) is of interest only from an applied mechanics point of view, because it shows the total distortion of the plane corresponding to the first bench floor due to excavation and creep, including a part which occurred before the floor is exposed. Figure 2-18(b) is of interest to the designer who is concerned primarily with the floor heave which occurs after the floor has been cleared. If, for example, a concrete foundation were to be laid on the first bench floor at the end of 49 days, its shape at the end of 71 days would be similar to that in Figure 2-18(b). This distortion may be too great for proper operation of the hoists. One alternative would be to wait until the creep rate has become negligible before laying the foundation. A second alternative would be to anticipate the eventual shape and to compensate by digging the floor initially too deep in parts where the floor is expected to heave, and to lay the foundation when the floor reaches a stable, level condition.



(a) UPHEAVAL OF FIRST BENCH FLOOR AT THE END OF 71 DAYS (12TH STEP)



(b) FLOOR HEAVE DUE TO CREEP FROM 49 TO 71 DAYS (FOLLOWING CLEARING OF THE FIRST BENCH)

FIGURE 2-18. UPHEAVAL OF FIRST BENCH FLOOR



2.4 DISCUSSION OF RESULTS

There are three aspects of the analysis of the Caladay Project hoist room which would be modified if a second calculation were made. These are

- a. Improving the method of introducing in situ stresses
- b. Limiting the region which undergoes time-dependent deformation to the zone of influence of the hoist room
- c. Refining the finite element mesh in the vicinity of the hoist room

The present method of introducing in situ stresses is illustrated in Figure 2-13. The result is shown in Figure 2-14 and 2-16 in terms of spatial distribution of stresses at a selected stage of the calculation. This method provides that the stresses are equal to the assumed in situ stresses only near the faces where they are applied as external forces. Throughout the remainder of the finite element model, stresses are greatly affected by the relative stiffnesses and Poisson's ratios of the four layers of rock. This nonuniformity, which probably also occurs in nature but to a lesser degree, produces stress concentrations which are $1/3$ to $1/2$ as great as those due to the hole. This suggests that by applying stresses to three of the six faces of the finite element model, the user does not obtain the initial stress conditions he desires. For highly inhomogeneous models, it would be better to introduce the desired internal stresses directly, rather than attempt to find external boundary conditions which produce the desired internal stress state. A slight modification of the computer program is needed to prestress continuum elements.

There is one definite weakness in the present viscoelastic model and one possible weakness. The definite weakness is that all of the argillite in the finite element model undergoes viscoelastic volume strain. Thus, even a finite element of argillite which is so distant from the hoist room that its



stress is unaffected by the excavation nevertheless undergoes creep. This creep has no physical counterpart and hence should not be present in the mathematical model. In contrast, creep which has a physical counterpart occurs in the vicinity of the excavation. Physically, this creep is related to movement along bedding planes which accompanies changes in the local stress condition due to excavation. This picture suggests that the physical situation would be more nearly represented by assigning creep properties to a small zone of argillite in the immediate vicinity of the hoist room. However, a technique has not yet been developed for manipulating the finite element computer program such that creep occurs in this zone only in response to changes in stress from the in situ condition to a new condition related to a gradually enlarging cavity.

The possible weakness in the present viscoelastic model is that it predicts progressive shortening of the extensometers as time elapses. This is visible in the falling portion of the calculated curves in Figure 2-15. It is not clear from the measurements whether there is time-dependent extension or contraction of the extensometers. However, it appears to the present authors that the measurements indicate time-dependent extension. To change the viscoelastic model so that it agrees with the apparent creep measurements requires replacing the assumption of viscoelastic volume strain. This is because the mean normal stress in the rock between the ends of the extensometer is compressive and the viscoelastic volume strain is also required to be compressive. It appears possible that a different viscoelastic model can be found to improve agreement. For example, a Kelvin model in shear can probably be found which predicts extension of the extensometers. However, as is pointed out above, the calculated response of the Silver Summit Mine drift does not agree well with measurements when viscoelasticity in shear is assumed.

As to the finite element mesh used in the final three-dimensional calculation, some auxiliary calculations have shown that the present mesh is definitely too coarse to calculate accurately the extensometer readings and the stress concentrations in the immediate vicinity of the cavity in the early



stages of the analysis. The mesh is adequate for determining the response (deflection) of the back and the floor during latter stages of excavation. It has been conclusively shown that the large humps present in the calculated curves around the 18th day are the results of the relative coarseness of the mesh over the back in the early stage of the excavation. When Steps 4, 5, and 6 are taken, only three rows of elements have been removed so that, as seen from the z-direction (Figure 2-13), there are only three elements over the back. As a result, the mesh over the back is too coarse during this stage of the calculation to represent flexure of the back adequately.

A two-dimensional analysis along the longitudinal axis of the hoist room indicates that the calculated extensometer readings are halved by using twice as many elements over the back. The present writers consider that the same order of improvement can be achieved in the corresponding three-dimensional analysis by a similar refinement in mesh over the back.

To illustrate the effects of including the changes discussed in this section on the results of analysis, Figure 2-19 has been prepared. The shaded area shows approximately the extensometer deflections which the present writers think would be obtained. The reason for indicating a range of results rather than individual curves is that there is still some uncertainty about the elastic stiffnesses of the various rock types. It appears that the values of Young's moduli, listed in Table 2-2, have been chosen too high.

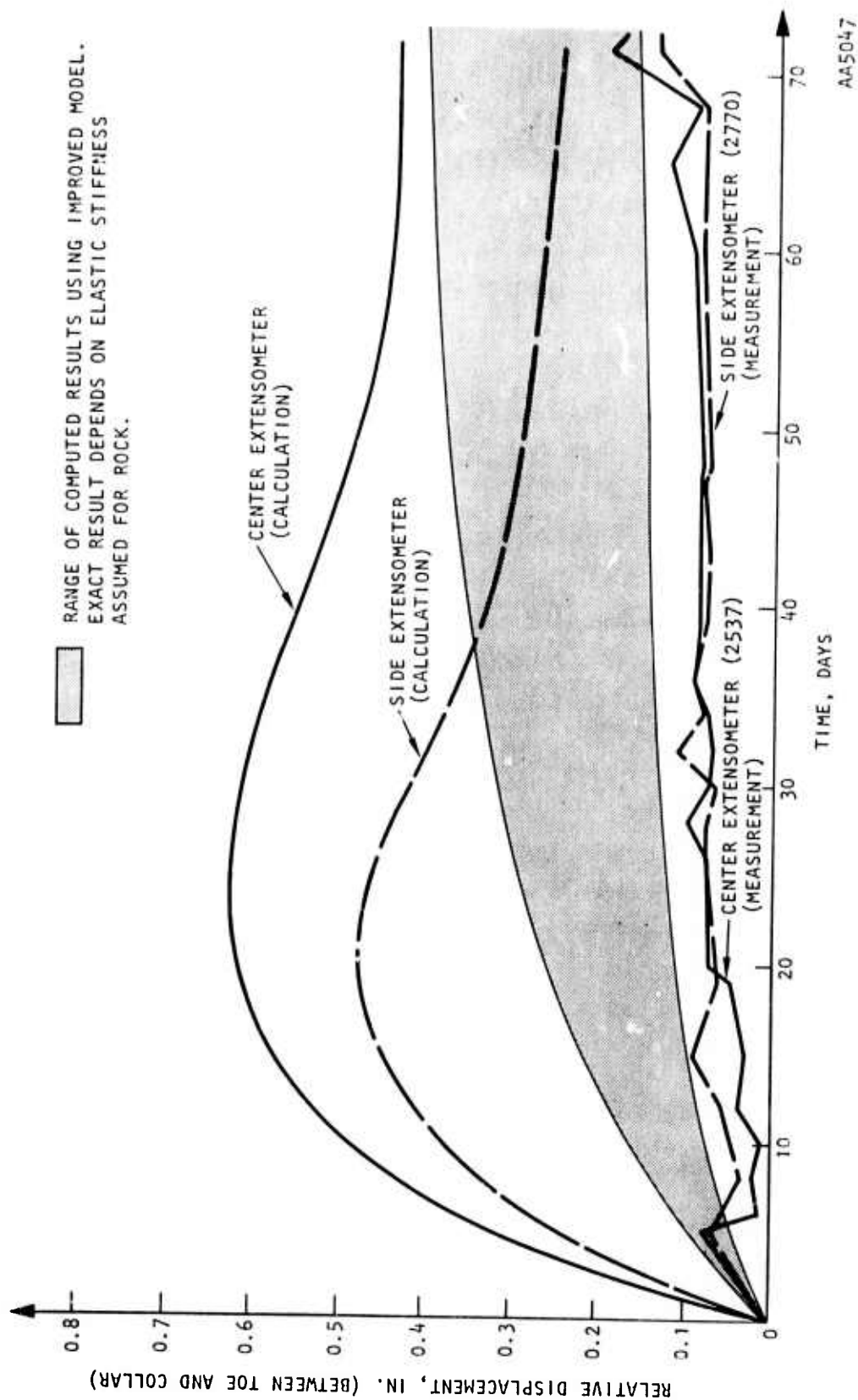


FIGURE 2-19. AUTHORS' ESTIMATE OF RESULTS WHICH WOULD BE OBTAINED IF MODEL WERE TO BE REFINED AND A SECOND ANALYSIS PERFORMED



2.5 SUMMARY AND CONCLUSIONS

One of the purposes of the analysis, which involves a three-dimensional viscoelastic model of the hoist room and neighboring rock, is to compare the measurements with calculations. Another purpose, which is considered equally important, is to indicate the procedure by which finite element models are derived from geologic maps, from laboratory and in situ measurements of rock properties, and from the judgment of geologists and mining engineers acquainted with the area. Previous comparisons between measurements and analyses which have been made by Agbabian Associates and other investigators (Reference 2-8) indicate that disagreement may exceed factors of 3 or 4. The present analysis of the Caladay Project hoist room should be evaluated in the light of this experience. As engineers involved with design and construction of mines become acquainted with the requirements of analysis, information will be developed which will improve the quality of future analyses.

There are several ways to evaluate the present study of the Caladay Project hoist room. One way is to compare the extensometer measurements in the back with calculated results, as is done in Figure 2-15. Another is to try to interpret the calculated results according to physical intuition and to state the implications of this type of analysis for design. Such evaluation is limited because there are only three extensometer measurements and because the stiffnesses of the rock types near the hoist room vary so much that physical intuition is not very helpful in explaining the outcome. The analytic model also has some shortcomings which make comparison difficult. These are considered in the following evaluation.

The present analysis of the Caladay Project hoist room involves the following steps:

- a. Represent the hoist room geometry, including idealization of continuously variable bedding and joint planes, into three or four beds with average or representative properties.



- b. Determine the stress/strain properties of each rock type using laboratory measurements, in situ measurements, and judgment. The argillite is assumed to be represented by viscoelastic properties because this is the simplest mathematical framework which apparently accounts for the little available data.
- c. Estimate the in situ stresses based on judgment and a few measurements made by the over-coring technique. In situ stresses are idealized as being uniform on the outer boundaries of the finite element mesh, but they become non-uniform in the interior due to variation in the stiffnesses of the various rock types as well as to the presence of the hoist room.

Each step requires some idealizations to obtain results within a practical budget and some assumptions to compensate for missing data. However, these idealizations and assumptions are much less restrictive than those which have been made by many previous investigators, whose work is often limited to two-dimensional or three-dimensional elastic analyses.

As shown in Figure 2-15, the analysis overestimates two of the three extensometer measurements by a factor of three to six, depending on the stage at which comparison is made. The third extensometer is considered to be influenced by the rope raises and is not included in the comparison. Factors of three to six can be attributed to uncertainties in in situ moduli, Poisson's ratio, and in situ stresses; also, the measurements contain some uncertainty which has not been evaluated. The fact that these uncertainties can be overcome to the extent represented by Figure 2-15 is moderately encouraging.

Suggestions as to how to improve the results both quantitatively and qualitatively are made in Section 2.4. The main areas in which the analysis may be improved are application of in situ stresses, definition of viscoelastic properties and refinement of the finite element mesh. These



suggestions would be applied to subsequent calculations of the Caladay Project hoist room.

- a. Replace the present method of applying boundary conditions solely by external forces with a procedure whereby elements are assigned stresses. The assigned stresses would, of course, be in equilibrium with external forces.
- b. Reduce the zone of argillite which may undergo viscoelastic deformation to a region within the zone of influence of the hoist room excavation. Consider changing the viscoelastic model such that there is time-dependent extension between nodal points corresponding to the extensometers.
- c. Refine the mesh over the back if the principal objective of the calculation is to obtain accurate deflections of the back at early stages of the analysis. The solution at later stages appears to be satisfactory.
- d. Include shotcrete over the back, which acts as a structural support and reduces deflections.

The purpose of the present project is to bring the most advanced methods of structural analysis within reach of mining engineers and designers. The analysis of the Caladay Project hoist room indicates how far the present computer program will go toward predicting stresses, roof deflections, and floor heave when used in conjunction with the kind of data which were available for this study. With more data, the analysis would be better; with less complete data, it would be worse. In any case, there will be some important aspects of response, such as stability, which must be assessed by noting where stress, strain and deflections exceed allowable values. The designer may use the computer program to evaluate several candidate designs on the basis of deflections and stress concentration, from which he may infer that rockfalls are more likely with one design than another. However, the final decisions are still based on the experience of the designer, of which calculations such as the Caladay Project hoist room may be considered a part.



REFERENCES

- 2-1. Hobbs, S., et al., *Geology of the Coeur d'Alene District*, U.S. Geol. Survey Prof. Paper 478, Shoshone County, Idaho, 1965.
- 2-2. Personal Communication: James B. Robison, Senior Engineer, Callahan Mining Corporation to Dr. William J. Karwoski, Mining Engineer, U.S.B.M., Spokane Mining Research Center.
- 2-3. Chan, S. S. M., *A Case Study of In Situ Rock Deformation Behavior for the Design of Ground Support Systems*, UIBMR-3, University of Idaho Bureau of Mining Research, January 31, 1972.
- 2-4. Waddell, G. G., *Technique of Measuring Initial Deformation Around an Opening. Analysis of Two Raise-Bore Tests*, Bureau of Mines Report of Investigations 7505, April 1971.
- 2-5. Personal Communication: John D. Smith, Consultant to George Beattie, Caladay Project Manager, Callahan Mining Corporation, Osburn, Idaho, Nov. 17, 1970.
- 2-6. Chan, S. S. M., *Engineering Properties of Mine Rocks and Rock Masses, Coeur d' Alene Mining District*, Interim Technical Report to Spokane Mining Research Center.
- 2-7. Personal Communication: Bob Gordon (Callahan Regional Geologist) to Dr. William J. Karwoski, Spokane Mining Research Center, January 2, 1972.
- 2-8. Chang, C. -Y, and K. Nair, *A Theoretical Method for Evaluating Stability of Openings in Rock*, Woodward-Lundgren and Associates, Final Report on U. S. Bureau of Mines Contract No. H0210046, April 12, 1972.



SECTION 3

APPLICATION OF FINITE ELEMENT THEORY

This section discusses the present formulation of equations of equilibrium. The provisions to extend this formulation to large deformations is also described. Then the types of elements, including truss, beam, plane strain and axisymmetric, three-dimensional and thick shell elements are described. In addition, a new element for representing slip and debonding along planar joints is described.

3.1 SOLUTION OF NONLINEAR EQUATIONS OF EQUILIBRIUM

The matrix equation of equilibrium for a structural system with material nonlinearity is:

$$\underline{K}(\underline{u}) \underline{u} = \underline{P} \quad (3-1)$$

where the instantaneous stiffness matrix (K) is a nonlinear function of the displacement vector (u). P is the vector containing external loads. There exist numerous methods of solving the above system of nonlinear equations. In general, these methods can be divided into two classes: iterative methods and incremental methods.

Iterative methods apply the total load initially and approach the solution by modifying the stiffness matrix and/or modifying the load vector. Modification of the stiffness matrix in general accelerates the convergence but is computationally costly. The optimum may be achieved by occasional stiffness reformulation.



In incremental methods the loads are applied in several steps and an incremental form of the Equation 3-1 is solved.

$$\underline{K}_n \Delta \underline{u}_{n+1} = \Delta \underline{P}_{n+1} \quad (3-2)$$

where

$$\Delta \underline{u}_{n+1} = \underline{u}_{n+1} - \underline{u}_n$$

$$\Delta \underline{P}_{n+1} = \underline{P}_{n+1} - \underline{P}_n$$

It is important to note that the stiffness matrix \underline{K}_n can only be formed based on the displacement vector from the previous step \underline{u}_n which creates some step-wise error. In this simple incremental technique the step-wise errors can accumulate and lead to considerable total error. To prevent this accumulation of the step-wise error, a modified form of the load vector is used.

$$\underline{K}_n \Delta \underline{u}_{n+1} = \underline{P}_{n+1} - \underline{F}_n \quad (3-3)$$

where

$$\underline{P}_{n+1} = \text{Total load vector at the end of the } (n+1)^{\text{th}} \text{ step}$$

$$\underline{F}_n = \text{Vector of the internal resisting forces at the end of the } n^{\text{th}} \text{ step}$$

By using this method of load vector correction the equilibrium is satisfied at the beginning of each incremental step and thereby the accumulation of the step-wise error is prevented. Satisfaction of equilibrium is assured in spite of errors or approximations in the stiffness matrix and, therefore, the reformulation of the stiffness matrix is not required at every step. However, the error in each step is directly dependent on the approximation of instantaneous stiffness matrix.



An alternative method is to apply the total force from the beginning, in which case the load in Equation 3-3 will be

$$P_n = P_{\text{total}} \quad (n=1, \dots, N)$$

It should be noted that the application of the total loads makes this method equivalent to an iterative scheme with load vector correction which was previously discussed. However, the loads in general have a specified history dictated by the sequence of application, sequence of construction and excavation, and the time phenomenon associated with the viscous material properties. In most practical problems, the specified history of loading is a series of step functions. This is true in case of construction and excavation which can be considered as a discontinuity in force-displacement relation and an abrupt change in the instantaneous stiffness matrix.

An efficient scheme is to apply the total of the step-wise loading at each stage and then carry out several iterations with occasional stiffness reformulation to accelerate the convergence. This scheme is summarized in the following steps.

For each step:

- a. Compute $u_n = u_{n-1} + \Delta u_n$ (for first step; $u_0 = 0$)
- b. Compute the strains (ϵ_n) or strain increments ($\Delta \epsilon_n$) using the derivatives of the shape functions for each element which have been initially computed and stored
- c.
 1. For time-independent materials compute the stress (σ_n) and the instantaneous stress-strain relations (C_n) (see section on material properties)
 2. For visco-elastic elements
 - i. Compute stresses $\sigma_n = C (\epsilon_n - \epsilon_{n-1}^C)$ where C is the elastic stress-strain matrix, ϵ_n is the total strain and ϵ_{n-1}^C is the total creep strain



ii. Using the stresses, compute $\bar{\epsilon}_n^C$ which is the total creep strain at the end of the time step (see section on material properties)

iii. Compute effective stress

$$\bar{\sigma}_n = C (\bar{\epsilon}_n - \bar{\epsilon}_n^C)$$

- d. Compute the internal resisting forces from the stresses (effective stresses for viscoelastic elements). If it is stiffness update cycle, compute stiffness matrix.
- e. Solve Equation 3-3 to obtain Δu_{n+1} . Compute $\gamma = \|\Delta u_{n+1}\|$.
- f. If a specified number of iteration has been reached or if $\gamma \leq \epsilon$ (ϵ is a specified quantity), go to Step g; otherwise, go to Step a and repeat the iteration.
- g. Apply the next loading step and go to Step a.

3.2 EQUATIONS OF EQUILIBRIUM FOR LARGE DEFORMATIONS

The method of large deformation finite element analysis to be used in the present computer program was initially introduced by Sharifi and Yates, Reference 3-1.

The matrix equations of equilibrium (or motion) are derived from an incremental virtual work expression and the original configuration of the finite element system is taken as the reference configuration. This choice of the reference state eliminates the need for updating of the coordinates of the nodal points which is computationally a costly operation.



The incremental virtual work expression is

$$\begin{aligned} \int_{A_0} (t_n + \Delta t_n) \delta \Delta U_n dA_0 - \int_{V_0} S_{ij} \delta \Delta \epsilon_{ij} dV_0 &= \int_{V_0} S_{ij} \delta \Delta \eta_{ij} dV_0 \\ + \int_{V_0} \Delta S_{ij} \delta \Delta \epsilon_{ij} dV_0 \end{aligned} \quad (3-4)$$

where

- u_k = Component of displacement vector
- Δu_k = Incremental component of displacement vector
- t_k = Component of traction vector
- Δt_k = Incremental component of traction vector
- S_{ij} = Component of Piola stress tensor
- ΔS_{ij} = Incremental component of Piola stress tensor
- $\Delta \epsilon_{ij}$ = Linear component of incremental strain tensor
- $\Delta \eta_{ij}$ = Nonlinear component of incremental strain tensor

The stresses and traction are referred to the area and the coordinates of the original configuration:

$$\Delta \epsilon_{ij} = \Delta u_{i,j} + \Delta u_{j,i} + u_{k,i} \Delta u_{k,j} + u_{k,j} \Delta u_{k,i} \quad (3-5a)$$

$$\Delta \eta_{ij} = \Delta u_{k,i} \Delta u_{k,j} \quad (3-5b)$$

The total and incremental displacements within each element can be expressed in terms of the nodal point values of the displacements through shape functions



$$u_i = H U_i \quad (3-6a)$$

$$\Delta u_i = H \Delta U_i \quad (3-6b)$$

where H is the vector of the shape functions and U_i and ΔU_i are the vectors of the total and incremental displacements of the element nodes.

Without loss of generality the remaining part of this section will be devoted to the derivation of the appropriate matrices for the two-dimensional quadrilateral element.

Substituting the Equation 3-6 into Equation 3-5 will result in the following expressions for the strain increments in terms of the nodal point displacements:

$$\begin{aligned} \Delta \epsilon_{xx} &= H_{,x} \Delta U_x + (H_{,x} U_x) (H_{,x} \Delta U_x) + (H_{,x} U_y) (H_{,x} \Delta U_y) \\ \Delta \epsilon_{yy} &= H_{,y} \Delta U_y + (H_{,y} U_x) (H_{,y} \Delta U_x) + (H_{,y} U_y) (H_{,y} \Delta U_y) \\ \Delta \epsilon_{xy} &= H_{,x} \Delta U_y + H_{,y} \Delta U_x + (H_{,y} U_x) (H_{,y} \Delta U_x) + (H_{,y} U_y) \\ &\quad (H_{,x} \Delta U_y) + (H_{,x} U_x) (H_{,y} \Delta U_x) + (H_{,y} \Delta U_y) \end{aligned} \quad (3-7)$$

The above equations can be written as matrix form

$$\Delta \epsilon = B (\underline{I} + \underline{E}) \Delta U = \tilde{B} \Delta U \quad (3-8)$$

where \underline{I} is the identity matrix and



$$\underline{\epsilon} = \begin{Bmatrix} \epsilon_{xx} \\ \epsilon_{yy} \\ \epsilon_{xy} \end{Bmatrix} \quad \Delta \underline{U} = \begin{Bmatrix} \Delta U_x \\ \Delta U_y \end{Bmatrix} \quad (3-9)$$

$$\underline{B} = \begin{bmatrix} \underline{H}_{,x} & 0 \\ 0 & \underline{H}_{,y} \\ \underline{H}_{,x} & \underline{H}_{,y} \end{bmatrix} \quad \underline{E} = \begin{bmatrix} \underline{U}_x \underline{H}_{,x} & \underline{U}_y \underline{H}_{,x} \\ \underline{U}_x \underline{H}_{,y} & \underline{U}_y \underline{H}_{,y} \end{bmatrix} \quad (3-10)$$

\underline{B} is the usual strain-displacement matrix for infinitesimal deformation and \underline{E} is the large deformation contribution.

The linear and geometric stiffness matrices and the load correction vector are

$$\underline{k}_e = \int_{v_m} \underline{\tilde{B}}^T \underline{C} \underline{\tilde{B}} dv_m \quad (3-11)$$

$$\underline{k}_g = \int_{v_m} \underline{B}^T \underline{S} \underline{B} dv_m \quad (3-12)$$

$$\underline{f} = \int_{v_m} \underline{\tilde{B}}^T \underline{S} dv_m \quad (3-13)$$

where v_m is the area of each element in original configuration, and \underline{C} is the instantaneous stress-strain relation

$$\Delta \underline{S} = \underline{C} \Delta \underline{\epsilon} \quad (3-14)$$

Finally, the matrix equation of equilibrium is

$$(\underline{k}_e + \underline{k}_g) \Delta \underline{U} = \underline{R} - \underline{F} \quad (3-15)$$



It is important to note that for the computation of the above matrices only the derivatives of the shape functions H_x and H_y at original geometry of each element is required. Therefore, these derivatives at integration points, can be computed in the first part of the program.

3.3 STRUCTURAL FINITE ELEMENTS

A description of the structural elements incorporated in this computer program are given here. The beam and thick shell elements have linear elastic properties. All other elements are capable of representing nonlinear properties.

3.3.1 THREE-DIMENSIONAL TRUSS ELEMENTS

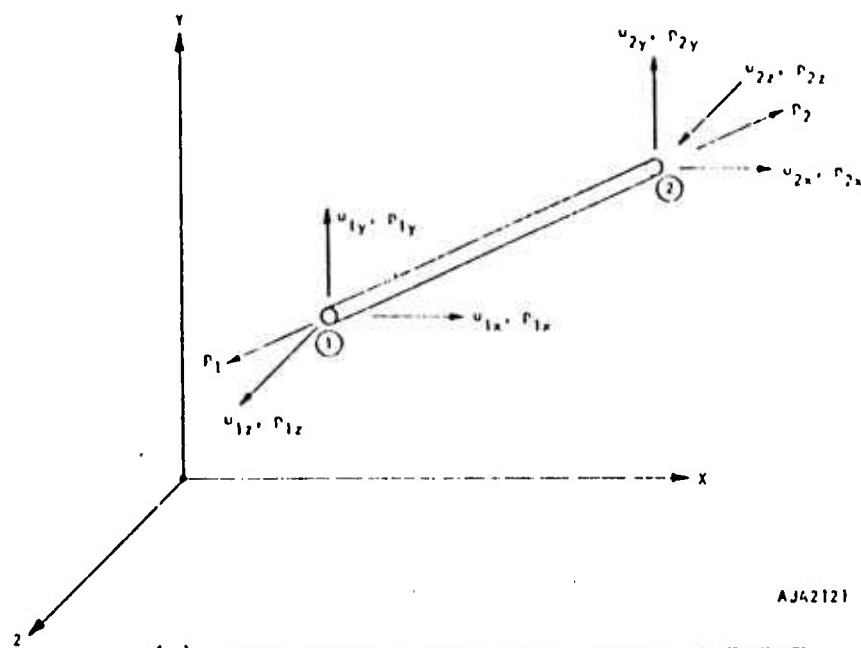
The truss element is the conventional space truss member which can resist compression or tension along its axis. It can also be used to model bolts. The truss member is subject to three translations at each end of the member as shown in Figure 3-1a. The member stiffness matrix is of order 6×6 . The material and geometrical properties are defined by the tangent Young's modulus, and the cross-sectional area of the element.

3.3.2 THREE-DIMENSIONAL BEAM ELEMENTS

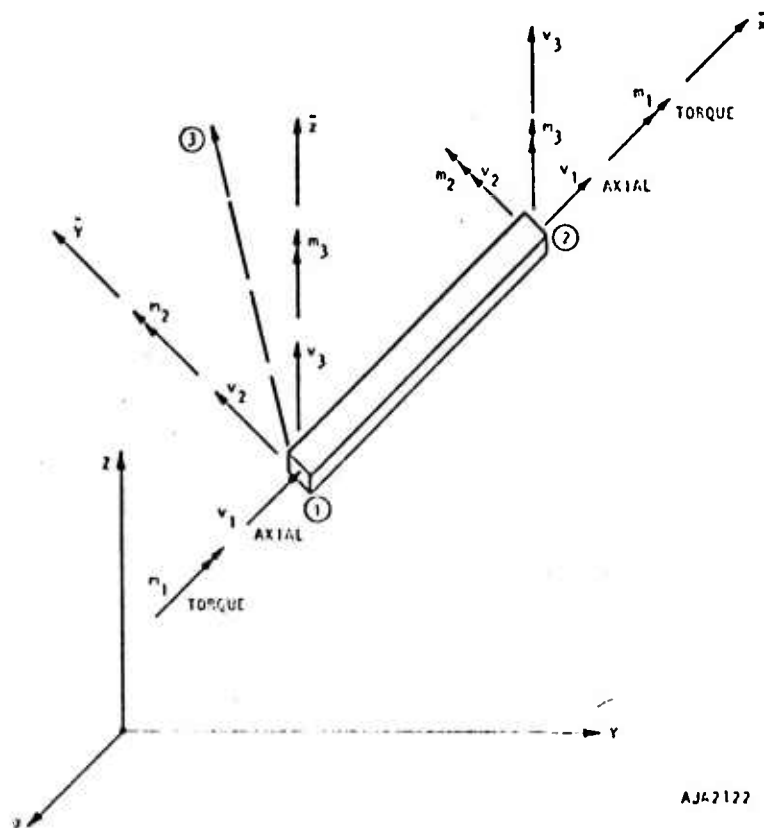
The three-dimensional beam element is subject to three translations and three rotations at each end of the member. The generalized forces and the generalized displacements associated with the six-degrees-of-freedom (DOF) at each end are shown in Figure 3-1b.

The geometrical properties of the beam element are specified by an axial and two shear areas and three principal moments of inertia, two associated with bending and one with torsion. Young's modulus and Poisson's ratio are required to define the material properties of the beam element.

The element stiffness matrix is of order 12×12 and is obtained from the classical beam theory including the effects of the shear deformations.



(a) THE THREE-DIMENSIONAL TRUSS ELEMENT



(b) THE THREE-DIMENSIONAL BEAM ELEMENT.

FIGURE 3-1. TRUSS AND BEAM ELEMENT



It is important to note that for the computation of the above matrices only the derivatives of the shape functions H_x and H_y at original geometry of each element is required. Therefore, these derivatives at integration points, can be computed in the first part of the program.

3.3 STRUCTURAL FINITE ELEMENTS

A description of the structural elements incorporated in this computer program are given here. The beam and thick shell elements have linear elastic properties. All other elements are capable of representing nonlinear properties.

3.3.1 THREE-DIMENSIONAL TRUSS ELEMENTS

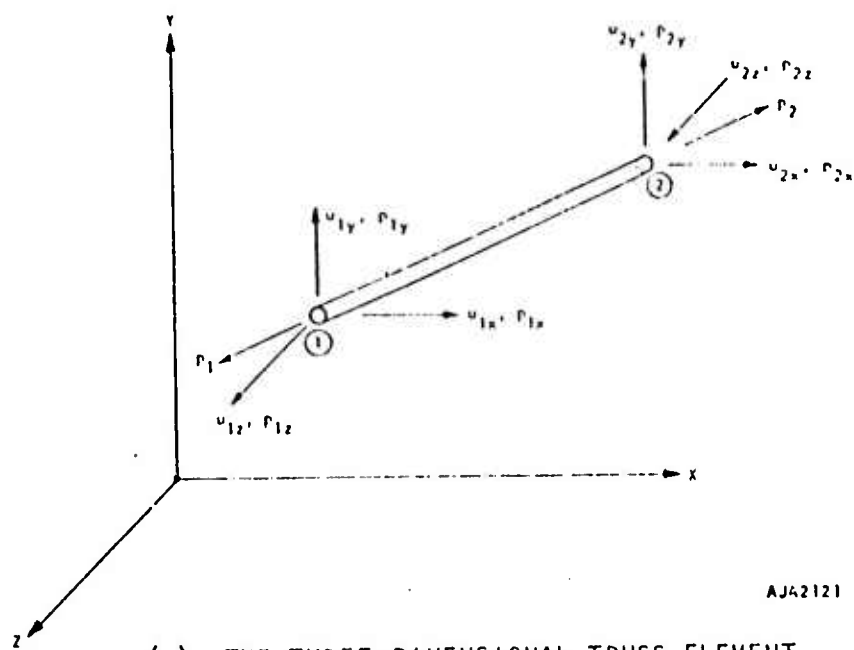
The truss element is the conventional space truss member which can resist compression or tension along its axis. It can also be used to model bolts. The truss member is subject to three translations at each end of the member as shown in Figure 3-1a. The member stiffness matrix is of order 6×6 . The material and geometrical properties are defined by the tangent Young's modulus, and the cross-sectional area of the element.

3.3.2 THREE-DIMENSIONAL BEAM ELEMENTS

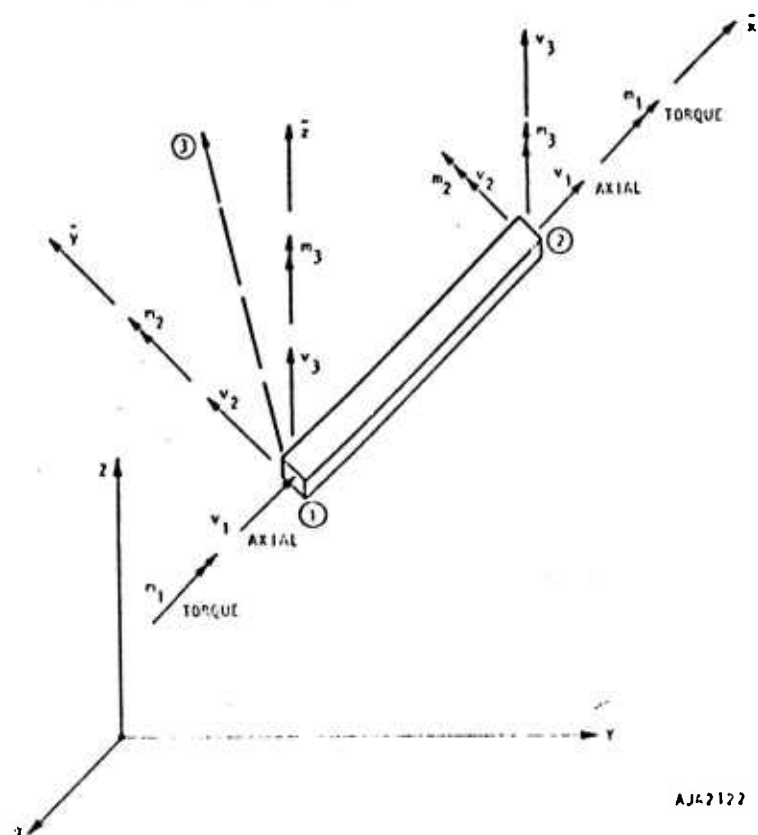
The three-dimensional beam element is subject to three translations and three rotations at each end of the member. The generalized forces and the generalized displacements associated with the six-degrees-of-freedom (DOF) at each end are shown in Figure 3-1b.

The geometrical properties of the beam element are specified by an axial and two shear areas and three principal moments of inertia, two associated with bending and one with torsion. Young's modulus and Poisson's ratio are required to define the material properties of the beam element.

The element stiffness matrix is of order 12×12 and is obtained from the classical beam theory including the effects of the shear deformations.



(a) THE THREE-DIMENSIONAL TRUSS ELEMENT



(b) THE THREE-DIMENSIONAL BEAM ELEMENT.

FIGURE 3-1. TRUSS AND BEAM ELEMENT



A provision for the member end boundary conditions accounts for hinges and other releases.

3.3.3 TWO-DIMENSIONAL PLANE STRAIN AND AXISYMMETRIC ELEMENTS

Quadrilateral isoparametric elements will be used in the computer program. For a general quadrilateral element, as shown in Figure 3-2, the local and global coordinate systems are related by

$$\begin{aligned}x &= \sum_{i=1}^4 h_i x_i \\y &= \sum_{i=1}^4 h_i y_i\end{aligned}\tag{3-16}$$

where the interpolation functions are given by

$$\begin{aligned}h_1 &= 1/4 (1-s) (1-t) \\h_2 &= 1/4 (1+s) (1-t) \\h_3 &= 1/4 (1+s) (1+t) \\h_4 &= 1/4 (1-s) (1+t)\end{aligned}\tag{3-17}$$

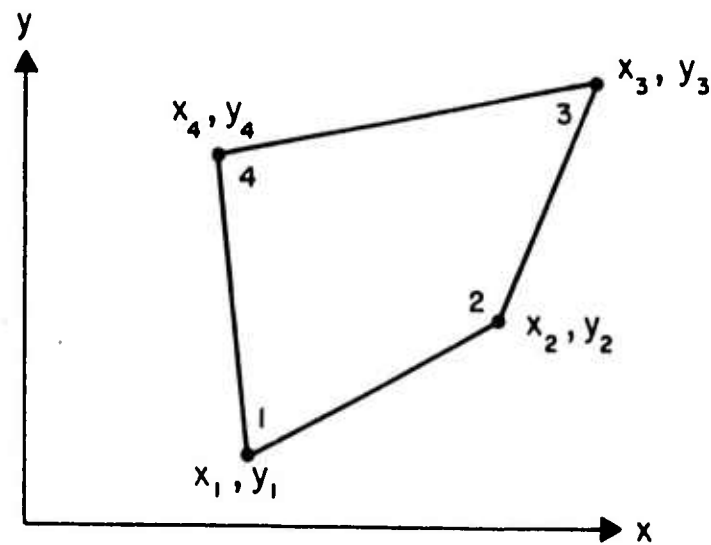
The same interpolation functions are used in the displacement approximation.

$$\begin{aligned}u_x (s,t) &= \sum h_i u_{xi} + h_5 \alpha_1 + h_6 \alpha_2 \\u_y (s,t) &= \sum h_i u_{yi} + h_5 \alpha_3 + h_6 \alpha_4\end{aligned}\tag{3-18}$$

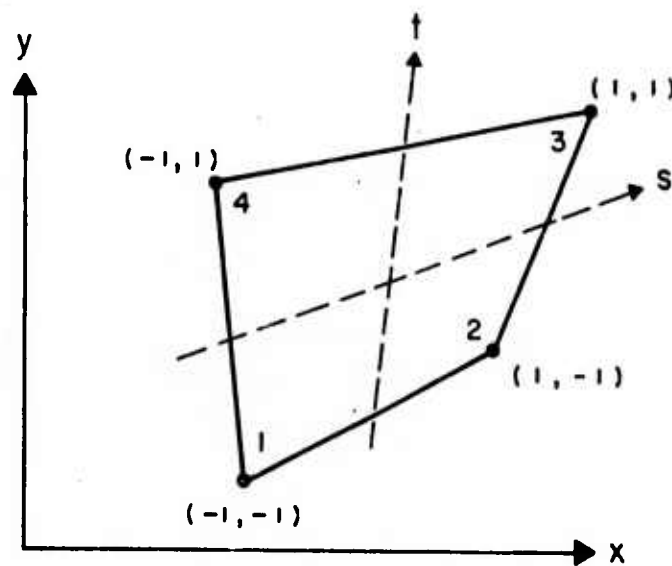
where

$$\begin{aligned}h_5 &= (1-s^2) \\h_6 &= (1-t^2)\end{aligned}$$

h_5 and h_6 are the incompatible interpolation functions.



a. GLOBAL SYSTEM



b. LOCAL SYSTEM

FIGURE 3-2. TWO-DIMENSIONAL ISOPARAMETRIC ELEMENT



For two-dimensional analysis the strain-displacement equations are

$$\begin{aligned}\epsilon_{xx} &= \frac{\partial u_x}{\partial x} = \sum h_{i,x} u_{xi} + h_{5,x} \alpha_1 + h_{6,x} \alpha_2 \\ \epsilon_{yy} &= \frac{\partial u_y}{\partial y} = \sum h_{i,y} u_{yi} + h_{5,y} \alpha_3 + h_{6,y} \alpha_4 \\ \epsilon_{xy} &= \frac{\partial u_x}{\partial y} + \frac{\partial u_y}{\partial x} = \sum h_{i,y} u_{xi} + \sum h_{i,x} u_{yi} + h_{5,y} \alpha_1 + h_{6,y} \alpha_2 + h_{5,x} \alpha_3 + h_{6,x} \alpha_4\end{aligned}\quad (3-19)$$

Or Equation 3-19 can be written in matrix form as

$$\underline{\epsilon} = \underline{B} \underline{U} = \begin{bmatrix} \underline{H}_{,x} & 0 \\ 0 & \underline{H}_{,y} \\ \underline{H}_{,y} & \underline{H}_{,x} \end{bmatrix} \begin{bmatrix} \underline{U}_x \\ \underline{U}_y \end{bmatrix} \quad (3-20)$$

In this case the three strains are related to the eight nodal point displacements and four coefficients of incompatible displacement functions by a 3 x 12 matrix. The submatrices in Equation 3-20 are given by

$$\begin{aligned}\underline{H}_{,x} &= [h_{1,x} \ h_{2,x} \ h_{3,x} \ h_{4,x} \ h_{5,x} \ h_{6,x}] \\ \underline{H}_{,y} &= [h_{1,y} \ h_{2,y} \ h_{3,y} \ h_{4,y} \ h_{5,y} \ h_{6,y}]\end{aligned}\quad (3-21)$$

The element stiffness matrix is given by the following equation:

$$\underline{k} = \int_V \underline{B}^T \underline{C} \underline{B} \, dv \quad (3-22)$$



where \underline{C} is the stress-strain matrix. The above equation is integrated numerically

$$\underline{k} = \sum_i \underline{B}_i^T \underline{C} \underline{B}_i \quad (3-23)$$

This stiffness matrix which is 12×12 is reduced to 8×8 by elimination of the four incompatible modes before assembling in the global stiffness matrix.

3.3.4 THREE-DIMENSIONAL ELEMENT

For an arbitrary eight-point brick element shown in Figure 3-3, the appropriate displacement approximations are

$$\begin{aligned} u_x &= \sum_{i=1}^8 u_{xi} + h_9 \alpha_{x1} + h_{10} \alpha_{x2} + h_{11} \alpha_{x3} \\ u_y &= \sum_{i=1}^8 u_{yi} + h_9 \alpha_{y1} + h_{10} \alpha_{y2} + h_{11} \alpha_{y3} \\ u_z &= \sum_{i=1}^8 u_{zi} + h_9 \alpha_{z1} + h_{10} \alpha_{z2} + h_{11} \alpha_{z3} \end{aligned} \quad (3-24)$$



R-7215-1-2701

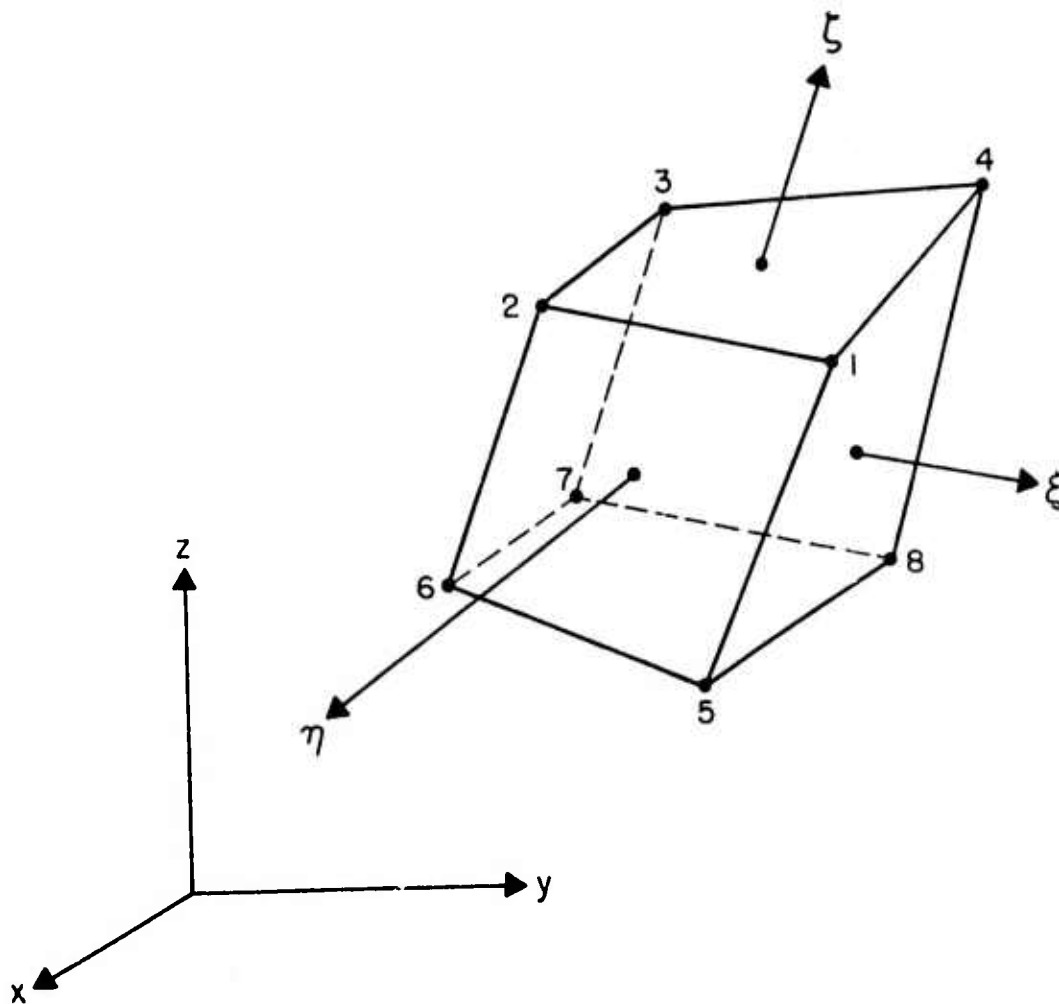


FIGURE 3-3. EIGHT-POINT THREE-DIMENSIONAL ELEMENT



where

$$\begin{aligned}h_1 &= 1/8 (1 + \xi) (1 + \eta) (1 + \zeta) \\h_2 &= 1/8 (1 - \xi) (1 + \eta) (1 + \zeta) \\h_3 &= 1/8 (1 - \xi) (1 - \eta) (1 + \zeta) \\h_4 &= 1/8 (1 + \xi) (1 - \eta) (1 + \zeta) \\h_5 &= 1/8 (1 + \xi) (1 + \eta) (1 - \zeta) \\h_6 &= 1/8 (1 - \xi) (1 + \eta) (1 - \zeta) \\h_7 &= 1/8 (1 - \xi) (1 - \eta) (1 - \zeta) \\h_8 &= 1/8 (1 + \xi) (1 - \eta) (1 - \zeta) \\h_9 &= (1 - \xi^2) \\h_{10} &= (1 - \eta^2) \\h_{11} &= (1 - \zeta^2)\end{aligned}\tag{3-25}$$

The first eight are the standard compatible interpolation functions. The last three are incompatible and are associated with linear shear and normal strains. The nine incompatible modes are eliminated at the element stiffness level by static condensation.

3.3.5 THICK SHELL ELEMENTS

The thick shell element described here was initially developed by Wilson, et al., Reference 3-3.

This shell element is a 16-node curved solid element shown in Figure 3-4. Each node has three unknown displacements. Therefore, if the shell is considered as a two-dimensional surface there are six unknowns per point. It is apparent that this type of formulation avoids the problems associated with the sixth degree of freedom--the normal rotation is set to zero when certain finite elements are used in the idealization of shells.

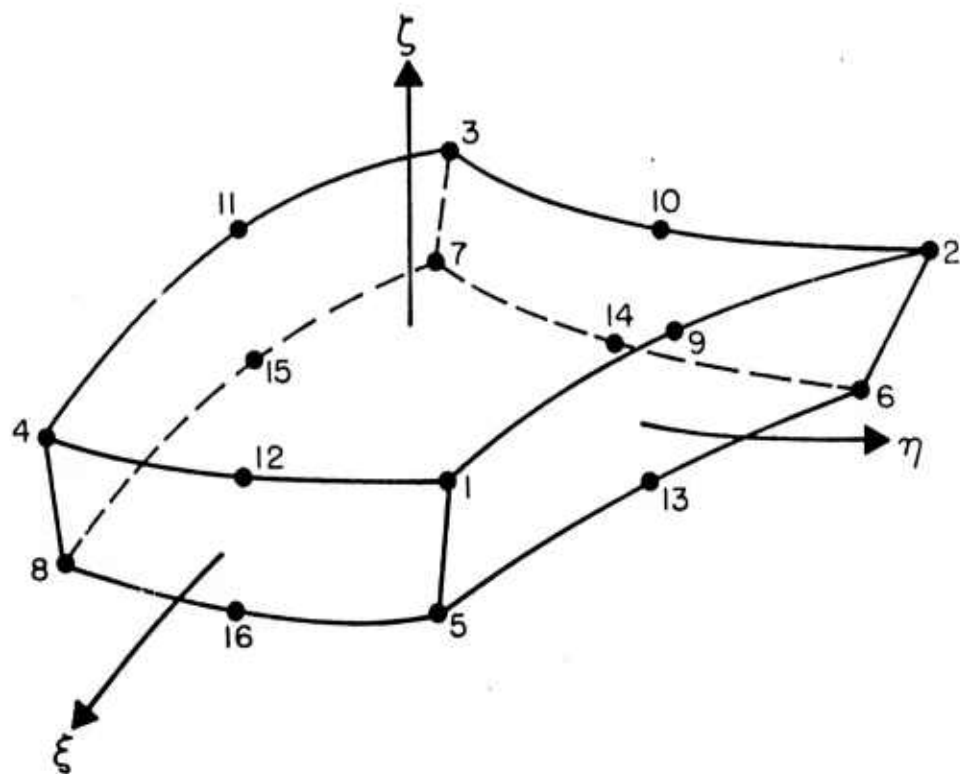


FIGURE 3-4. THREE-DIMENSIONAL THICK-SHELL ELEMENT

The locations of the nodes are defined by the orthogonal, right-handed coordinate system (x, y, z) which is referred to as a global system. Within the element a local coordinate system (ξ, η, ζ) has been chosen such that ξ, η, ζ vary from -1 to +1; $(0, 0, 0)$ is located at the centroid of the element.

The local and global coordinate systems are related through a set of interpolating functions:

$$\begin{aligned} x &= \sum_{i=1}^{16} h_i x_i \\ y &= \sum_{i=1}^{16} h_i y_i \\ z &= \sum_{i=1}^{16} h_i z_i \end{aligned} \tag{3-26}$$

where

$$\begin{aligned}
 h_1 &= 1/8 (1 + \xi) (1 + \eta) (1 + \zeta) (\xi + \eta - 1) \\
 h_2 &= 1/8 (1 - \xi) (1 + \eta) (1 + \zeta) (-\xi + \eta - 1) \\
 h_3 &= 1/8 (1 - \xi) (1 - \eta) (1 + \zeta) (-\xi - \eta - 1) \\
 h_4 &= 1/8 (1 + \xi) (1 - \eta) (1 + \zeta) (\xi - \eta - 1) \\
 h_5 &= 1/8 (1 + \xi) (1 + \eta) (1 - \zeta) (\xi + \eta - 1) \\
 h_6 &= 1/8 (1 - \xi) (1 + \eta) (1 - \zeta) (-\xi + \eta - 1) \\
 h_7 &= 1/8 (1 - \xi) (1 - \eta) (1 - \zeta) (-\xi - \eta - 1) \\
 h_8 &= 1/8 (1 + \xi) (1 - \eta) (1 - \zeta) (\xi - \eta - 1) \\
 h_9 &= 1/4 (1 - \xi^2) (1 + \eta) (1 + \zeta) \\
 h_{10} &= 1/4 (1 - \xi) (1 - \eta^2) (1 + \zeta) \\
 h_{11} &= 1/4 (1 - \xi^2) (1 - \eta) (1 + \zeta) \\
 h_{12} &= 1/4 (1 + \xi) (1 - \eta^2) (1 + \zeta) \\
 h_{13} &= 1/4 (1 - \xi^2) (1 + \eta) (1 - \zeta) \\
 h_{14} &= 1/4 (1 - \xi) (1 - \eta^2) (1 - \zeta) \\
 h_{15} &= 1/4 (1 - \xi^2) (1 - \eta) (1 - \zeta) \\
 h_{16} &= 1/4 (1 + \xi) (1 - \eta^2) (1 - \zeta)
 \end{aligned} \tag{3-27}$$

The displacements within the element are assumed to be of the following form:

$$\begin{aligned}
 u &= \sum_{i=1}^{16} h_i u_{xi} + h_{17} \alpha_{x1} + h_{18} \alpha_{x2} + h_{19} \alpha_{x3} + h_{20} \alpha_{x4} + h_{21} \alpha_{x5} \\
 v &= \sum_{i=1}^{16} h_i u_{yi} + h_{17} \alpha_{y1} + h_{18} \alpha_{y2} + h_{19} \alpha_{y3} + h_{20} \alpha_{y4} + h_{21} \alpha_{y5} \\
 w &= \sum_{i=1}^{16} h_i u_{zi} + h_{17} \alpha_{z1} + h_{18} \alpha_{z2} + h_{19} \alpha_{z3} + h_{20} \alpha_{z4} + h_{21} \alpha_{z5}
 \end{aligned} \tag{3-28}$$



where

$$\begin{aligned}h_{17} &= \xi (1 - \xi^2) \\h_{18} &= \eta (1 - \eta^2) \\h_{19} &= (1 - \xi^2) \\h_{20} &= \xi \eta (1 - \xi^2) \\h_{21} &= \eta \xi (1 - \eta^2)\end{aligned}\tag{3-29}$$

The motivation for addition of the interpolation functions h_{17} to h_{21} is to increase the capability of the element in producing closer approximations to the exact displacements under simple loadings, thereby increasing the convergence to exact solution. The incompatible interpolation functions h_{17} to h_{21} have zero values at the nodes and produce incompatibilities in displacement field along the interelement boundaries.

3.4 JOINT FINITE ELEMENT

The joint element is intended to represent the rock joints, faults, interfaces and similar discontinuities in continuum systems. The joint element has the capability of representing the main characteristics of the deformation behavior of the rock joints such as debonding and slip. The term debonding means the ability of separation of the two blocks of continuum adjacent to the joint surface which were initially in contact. Subsequent contact can also develop by the movement of the two blocks towards each other. The term slip means the relative motion along the joint surface or fault when the shearing force exceeds the shear strength of the joint.

Previous attempts have been made to develop discrete elements to represent the joint behavior. Goodman, Taylor and Brekke (Reference 3-2) developed a simple rectangular, two-dimensional element with eight degrees of freedom. This element has no thickness, and therefore the adjacent blocks



of continuum elements can penetrate into each other. Zienkiewicz, et al., (Reference 3-4) advocate the use of continuum isoparametric elements with a simple nonlinear material property for shear and normal stresses, assuming uniform strain in the thickness direction. Numerical difficulties may arise from ill conditioning of the stiffness matrix due to very large off-diagonal terms or very small diagonal terms which are generated by these elements in certain cases.

To avoid such numerical problems a new joint element is developed below, which uses relative displacements as the independent degrees of freedom. The displacement degrees of freedom of one side of the slip surface are transformed into the relative displacements between the two sides of the slip surface. The transformation relations are as follows:

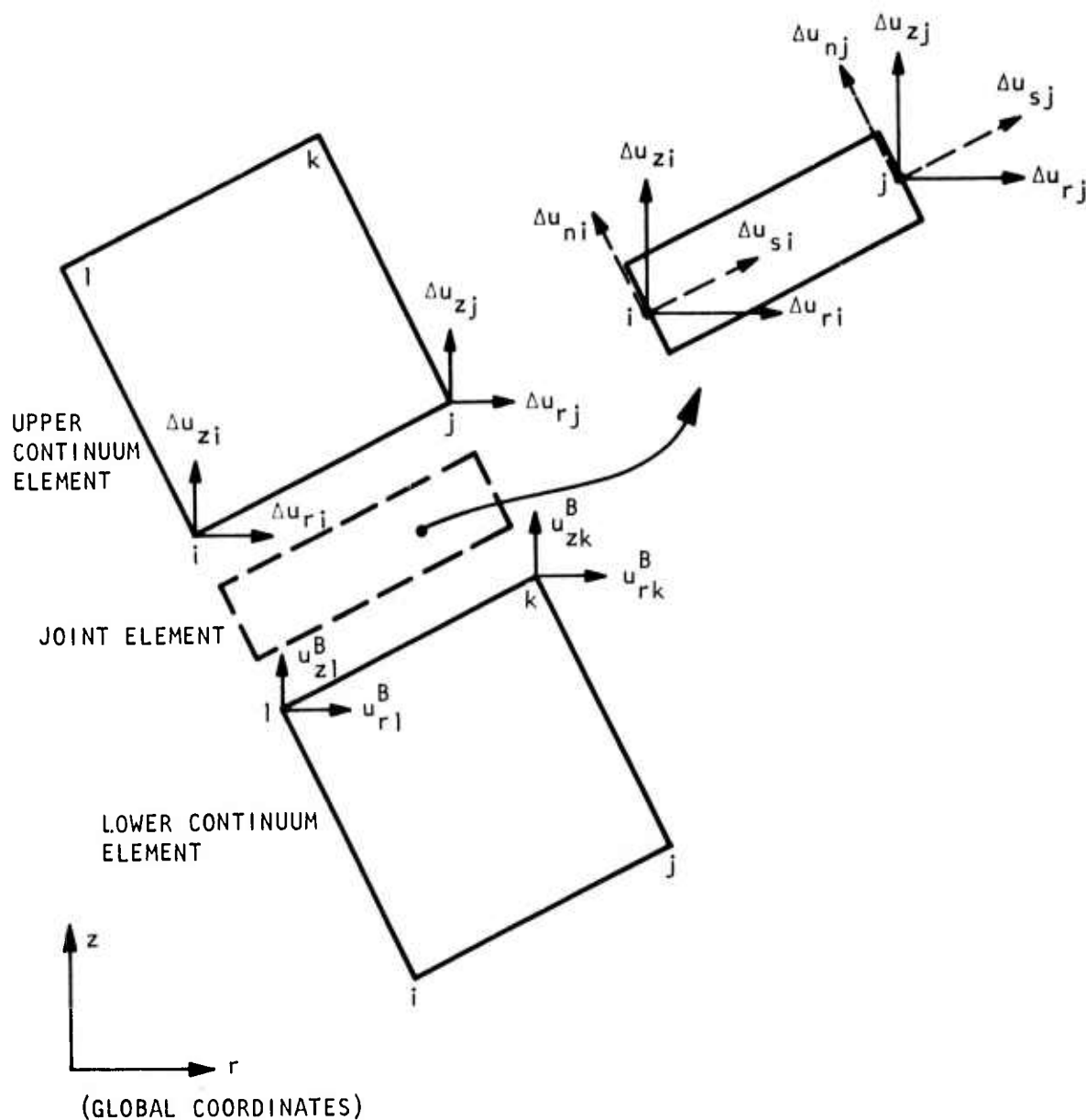
$$u_{xi}^T = u_{xi}^B + \Delta u_{xi}$$

$$u_{yi}^T = u_{yi}^B + \Delta u_{yi}$$

$$u_{xj}^T = u_{xk}^B + \Delta u_{xj}$$

$$u_{yj}^T = u_{yk}^B + \Delta u_{yj}$$

The superscripts T and B refer to the top and bottom elements with respect to the slip surface respectively. As shown in Figure 3-5, those degrees of freedom of the upper element which are on the slip surface are transformed but the degrees of freedom of the lower element are the original displacement quantities.



$$u_{ri}^T = u_{ri}^B + \Delta u_{ri}$$

$$u_{zi}^T = u_{zi}^B + \Delta u_{zi}$$

$$u_{rj}^T = u_{rj}^B + \Delta u_{rj}$$

$$u_{zj}^T = u_{zj}^B + \Delta u_{zj}$$

FIGURE 3-5. GEOMETRY OF JOINT ELEMENT



The joint element is assumed to have the relative displacements as the degrees of freedom. For example, in a two-dimensional problem the joint element will have four degrees of freedom (Figure 3-6). The relative normal and tangential displacements, Δu_n and Δu_s , are assumed to vary linearly along the element as follows

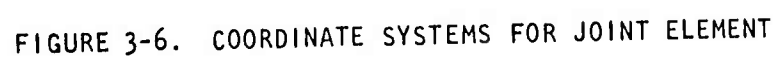
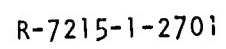
$$\begin{aligned}\Delta u_n &= h_i \Delta u_{ni} + h_j \Delta u_{nj} \\ \Delta u_s &= h_i \Delta u_{si} + h_j \Delta u_{sj}\end{aligned}\tag{3-30}$$

where the h_i and h_j are the linear interpolation functions

$$\begin{aligned}h_i &= \frac{1}{2}(1 - \xi) \\ h_j &= \frac{1}{2}(1 + \xi)\end{aligned}\tag{3-31}$$

and Δu_{ni} , Δu_{nj} , Δu_{si} and Δu_{sj} are the nodal point values of the relative displacements. The joint element is assumed to have only two strain components; ϵ_n = normal strain, and ϵ_s = shear strain. These two strain components are related to the relative displacements through the following relations.

$$\begin{aligned}\epsilon_n &= \frac{1}{t} \Delta u_n \\ \epsilon_s &= \frac{1}{t} \Delta u_s\end{aligned}\tag{3-32}$$





The substitution of Equations 3-30 and 3-31 into Equation 3-32 results in the strain-displacement relation for the element

$$\begin{Bmatrix} \epsilon_n \\ \epsilon_s \end{Bmatrix} = \frac{1}{2t} \begin{bmatrix} (1 - \xi) & 0 & (1 + \xi) & 0 \\ 0 & (1 - \xi) & 0 & (1 + \xi) \end{bmatrix} \begin{Bmatrix} \Delta u_{ni} \\ \Delta u_{si} \\ \Delta u_{nj} \\ \Delta u_{sj} \end{Bmatrix} \quad (3-33)$$

$$\underline{\epsilon} = \underline{B} \Delta \underline{U}$$

The stresses and the strains are related through the following material property matrix \underline{C} .

$$\begin{Bmatrix} \sigma_n \\ \sigma_s \end{Bmatrix} = \begin{bmatrix} C_{nn} & C_{ns} \\ C_{sn} & C_{ss} \end{bmatrix} \begin{Bmatrix} \epsilon_n \\ \epsilon_s \end{Bmatrix} \quad (3-34)$$

$$\underline{\sigma} = \underline{C} \underline{\epsilon}$$

In general the above stress/strain relationship for rock joints is nonlinear, the details of which are given in Section 4.

The stiffness matrix for the joint element is formed in n-s coordinate system;

$$\underline{k}_{ns} = \int_V \underline{B}^T \underline{C} \underline{B} dv \quad (3-35)$$



and transformed to the x-y coordinate system as follows

$$\underline{k} = \underline{I}^T \underline{k}_{ns} \underline{I} \quad (3-36)$$

where \underline{I} is the transformation matrix containing the direction cosines.

$$\underline{k} = \frac{L}{6t} \begin{bmatrix} 2(A_1 - 2B_1) & 2(A_3 + B_2) & (A_1 - 2B_1) & (A_3 + B_2) \\ & 2(A_2 + 2B_1) & (A_3 + B_2) & (A_2 + 2B_1) \\ \text{Symmetric} & & 2(A_1 - 2B_1) & 2(A_3 + B_2) \\ & & & 2(A_2 + 2B_2) \end{bmatrix} \quad (3-37)$$

where

$$\begin{aligned} A_1 &= c_{ss} a^2 + c_{nn} b^2 & B_1 &= c_{ns} ab \\ A_2 &= c_{ss} b^2 + c_{nn} a^2 & B_2 &= c_{ns} (a^2 - b^2) \\ A_3 &= (c_{nn} - c_{ss}) ab \\ a &= \frac{1}{L} (x_j - x_i) \\ b &= \frac{1}{L} (y_j - y_i) \end{aligned}$$



REFERENCES

- 3-1. Sharifi, P., and D. Yates, *Nonlinear Thermo-Elastic-Plastic and Creep Analysis by the Finite Element Method*, Missile Systems Division, Lockheed Missile and Space Company.
- 3-2. Goodman, R. E., R. L. Taylor, and T. L. Brekke, "A Model for the Mechanics of Jointed Rock," *J. Soil Mech., ASCE*, Vol. 94, SM3, 1968.
- 3-3. Wilson, E. L., et al., *Incompatible Displacement Models*, ONR Symposium on Matrix Methods in Structural Mechanics, Univ. of Illinois, Urbana, Illinois.
- 3-4. Zienkiewicz, O. C., et al., "Analysis of Nonlinear Problems in Rock Mechanics with Particular Reference to Jointed Rock Systems," *Proc. of 2nd Cong. of Int. Soc. for Rock Mech.*, Belgrade, 1970.



SECTION 4

REPRESENTATION OF PROPERTIES OF ROCK, INCLUDING ANISOTROPY,
INELASTICITY, RATE EFFECTS AND
PROPERTIES OF FAULTS OR JOINTS

The first part of this section describes homogeneous properties of rock which are available in the AA computer program. As used here, "homogeneous" refers to properties which can reasonably be averaged over several feet, which is a typical dimension of a finite element in applications to mining engineering. Inhomogeneous properties of rock masses, such as those caused by faulting, are treated by a separate procedure which is described in the second part.

The topics which are covered below include the following:

- a. Inelasticity
 - 1. Variable modulus
 - 2. Variable modulus with perfect plasticity
 - 3. Variable modulus with perfectly plastic fracture criterion and strain hardening cap
- b. Anisotropy
 - 1. Variable modulus with anisotropic fracture criterion based on the hypothesis of Jaeger (plane geometry only)
 - 2. Variable modulus with anisotropic yield criterion based on the hypothesis of Hill
- c. Rate Effects (Isotropic Only)
 - 1. Creep (series of Kelvin elements)
 - 2. Viscoplasticity (based on work of Perzyna)



d. Joint Properties

1. Dilatant
2. Nondilant

4.1 HOMOGENEOUS PROPERTIES

These models, which are also summarized in Table 4-1, afford some material descriptions which probably cannot be effectively used at present owing to the lack of experimental data on rock from particular mines. As analysis increases in effectiveness, it is expected that more data will be routinely obtained, thus enabling more sophisticated material models to be used. Advantages and disadvantages of these models are summarized in Table 4-2. Typical laboratory properties for rocks are shown in Figure 4-1.

TABLE 4-1. SUMMARY OF AVAILABLE MATERIAL PROPERTIES

Type of Model	Material Characteristics				
	Isotropic	Anisotropic	Viscoelastic	Viscoplastic	Inviscid
Constant elastic moduli	X	0	X		0
Variable moduli	X	0			X, 0
Elastic/plastic (fixed static yield surface)					
Constant moduli	X	0		X	0
Variable moduli	X	0		X	0
Cap model	X				X

X options or 0 options may be used simultaneously, but
X and 0 options may not be mixed, except where noted.



TABLE 4-2. ADVANTAGES AND DISADVANTAGES OF EACH MODEL

Advantages	Disadvantages
<u>A. Elastic-Ideally Plastic</u>	
Simple to fit to data Approximates most features of data $G = \text{Const.}$ $G = G(P_m)$ and associated flow rule theoretically correct	May not fit all available data Cannot match triaxial test Other treatments of G can lead to possible paths of energy generation For nonassociated flow rule no general uniqueness theorem
<u>B. Variable Moduli</u>	
Best fit of data Only model with repeated hysteresis within failure envelope Ideal for finite element Computationally simple Relatively easy to fit	Restricted to near-proportional loading (in shear) For nonproportional loading paths no uniqueness theorem Additional quantity must be stored at each grid point
<u>C. Cap Model</u>	
Satisfies all rigorous theoretical requirements Reasonably good fit of data Effective control of dilatancy	Indirect approach needed to fit data Relatively complicated Additional quantity, the strain hardening parameter, must be stored at each grid point
<u>D. Viscoelastic</u>	
Simple to fit to data Approximates features of data for some rocks	Requires sophisticated testing to define viscous coefficients for multi-axial loading. Does not account for deterioration in strength with time
<u>E. Viscoplastic</u>	
Approximates some features of data including shear strength, stick-slip phenomenon	Requires sophisticated testing



R-7215-1-2701

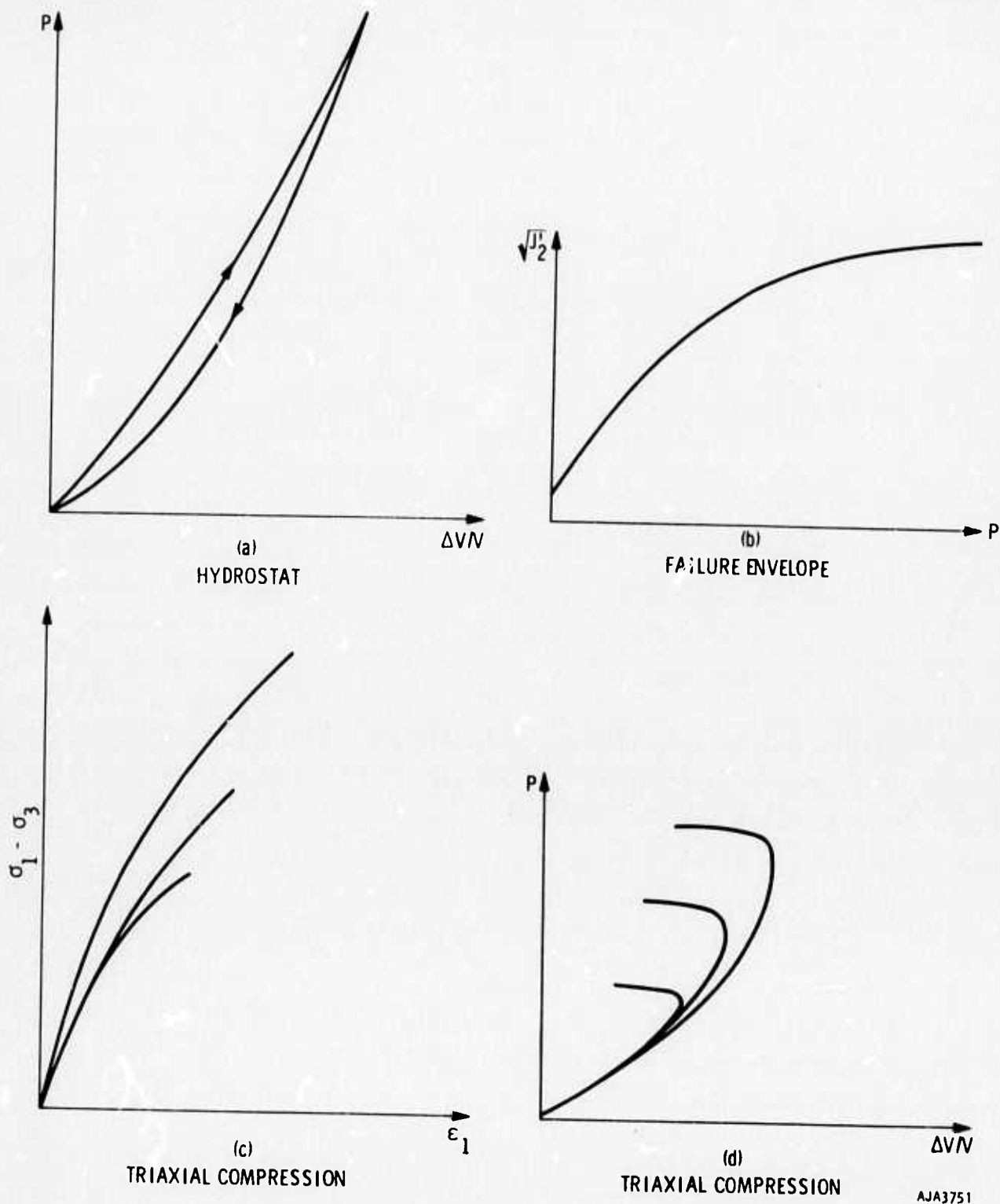


FIGURE 4-1. TYPICAL LABORATORY DATA ON ROCK FROM WHICH CONSTITUTIVE EQUATIONS ARE DERIVED



The programming of the material property subroutines is arranged to provide maximum flexibility and ease in changing properties. This is done by performing each separate function in the material properties description by a separate subroutine. Thus separate subroutines are provided for the following purposes:

Computing variable moduli

Computing derivatives of the yield functions with respect to its arguments.

Testing for yielding or fracture

Adjusting stresses for viscoelastic relaxation.

Adjusting stresses for viscoplastic relaxation.

Transforming strain increments to principal axes of orthotropy and transforming the matrix of stress/strain coefficients to the global axes.

There is considerable interdependence between the inelastic and anisotropic capabilities. Wherever possible this interdependence is used to economize on programming. Logic diagrams for each subroutine in the homogeneous material property package, are given in Appendix A.

4.1.1 INELASTICITY FOR ISOTROPIC MATERIALS--VARIABLE MODULUS

Inelasticity in isotropic materials is represented through variable bulk and shear moduli and through plasticity theory. The bulk modulus B is assumed to depend on the current value of elastic volumetric strain μ and its previous maximum value μ_{\max} .

FOR LOADING ($0 > \mu \geq \mu_{\max}$)

$$B = (B_m - B_o) \exp\left(\frac{-\mu}{\mu_1}\right) \quad (4-1)$$



FOR UNLOADING OR RELOADING ($0 < \mu < \mu_{\max}$)

$$B = B_u + (B_m - B_u) \left(\frac{\mu}{\mu_2} \right) \quad (4-2)$$

where

$$B_u = \text{the lesser of } \begin{cases} B_o + (B_m - B_o) \left(\frac{\mu_{\max}}{\mu} \right) \\ B_m \end{cases}$$

FOR LOADING OR UNLOADING/RELOADING IN TENSION ($\mu < 0$)

$$B = B_t \quad (4-3)$$

Application of this model to a granitic rock is illustrated in Figure 4-2. Specific parameters for this rock are

$$\begin{aligned} B_m &= 7.6 \times 10^6 \text{ psi} \\ B_o &= 1.205 \times 10^6 \text{ psi} \\ \mu_1 &= 0.0275 \\ \mu_2 &= 0.05 \end{aligned}$$

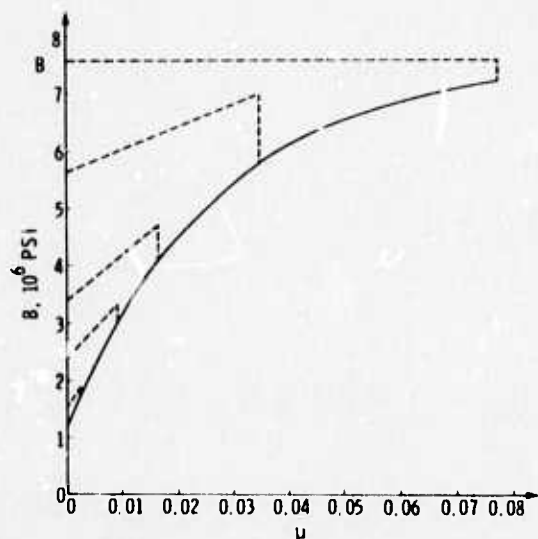
The shear modulus G is also assumed to depend on μ and μ_{\max}

FOR LOADING ($0 \leq \mu_{\max} \leq \mu$)

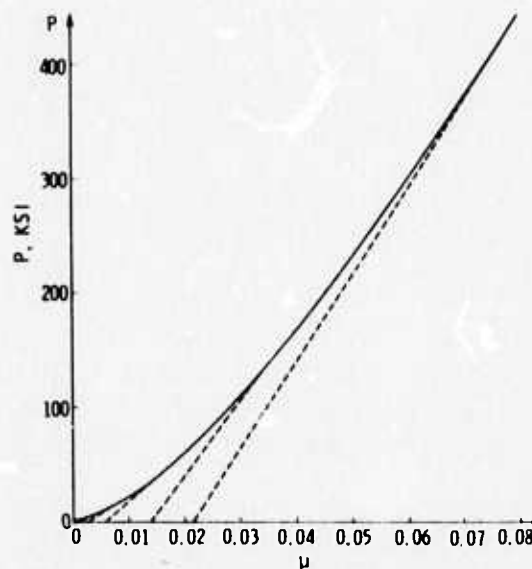
$$G = G_m - (G_m - G_o) \exp \left(\frac{-\mu}{\mu_3} \right) \quad (4-4)$$



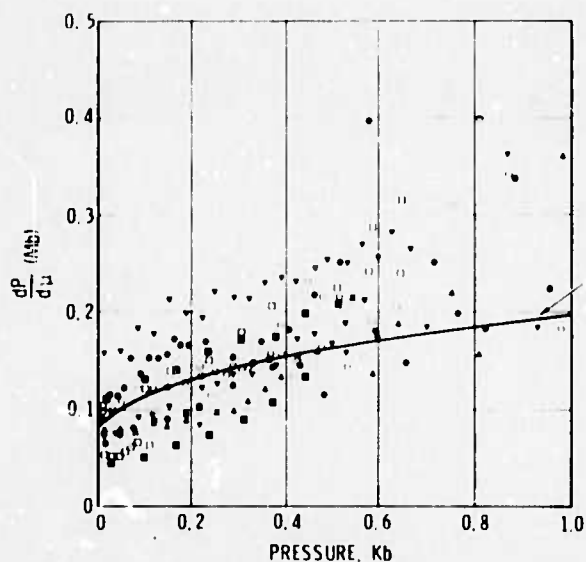
R-7215-1-2701



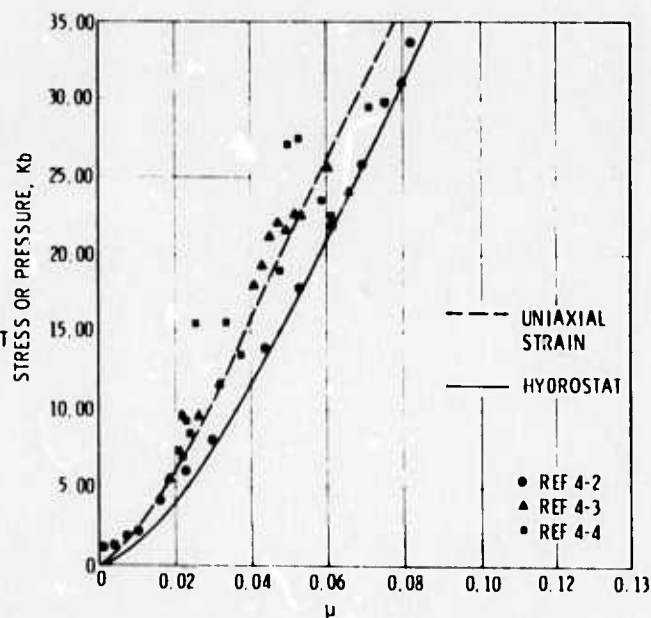
(a) MODEL BULK MODULUS FOR LOADING AND UNLOADING



(b) MODEL HYDROSTAT FOR LOADING AND UNLOADING



(c) LOW PRESSURE BULK MODULUS COMPARED WITH DATA (REFERENCE 4-1)



(d) MODEL HUGONIOT AND HYDROSTAT COMPARED WITH DATA

FIGURE 4-2. MODEL BULK MODULUS, HYDROSTAT AND YIELD POINT IN UNIAXIAL STRAIN COMPARED WITH DATA



FOR UNLOADING/RELOADING ($0 \leq \mu < \mu_{\max}$)

$$G = \text{Maximum previous value of } G \quad (4-5)$$

FOR LOADING OR UNLOADING/RELOADING IN TENSION ($\mu < 0$)

$$G = G_t \quad (4-6)$$

Application of this model to cracked and uncracked granitic rocks is illustrated in Figure 4-3. Specific parameters for these rocks are:

$$G_m = 4.35 \times 10^6 \text{ psi}$$

$$G_o = 0$$

$$\mu_3 = 0.005$$

The incremental stress $d\sigma_{ij}$ is related to the incremental component of elastic strain $d\epsilon_{ij}^e$ by the following expression:

$$d\sigma_{ij} = \left(B - \frac{2}{3} G \right) d\epsilon_{kk}^e \delta_{ij} + 2G(d\epsilon_{ij}^e) \quad (4-7)$$

where

$$\delta_{ij} = 0 \text{ if } i \neq j; = 1 \text{ if } i = j$$

Theoretical guidance on the appropriate functions for B and G is provided by Walsh (References 4-7, 4-8), who postulates that the effective modulus differs from the intrinsic modulus due to cracks and pores. As these are closed by increasing pressure, the effective modulus tends toward the consolidated value. Walsh's work contains parameters which are not retained

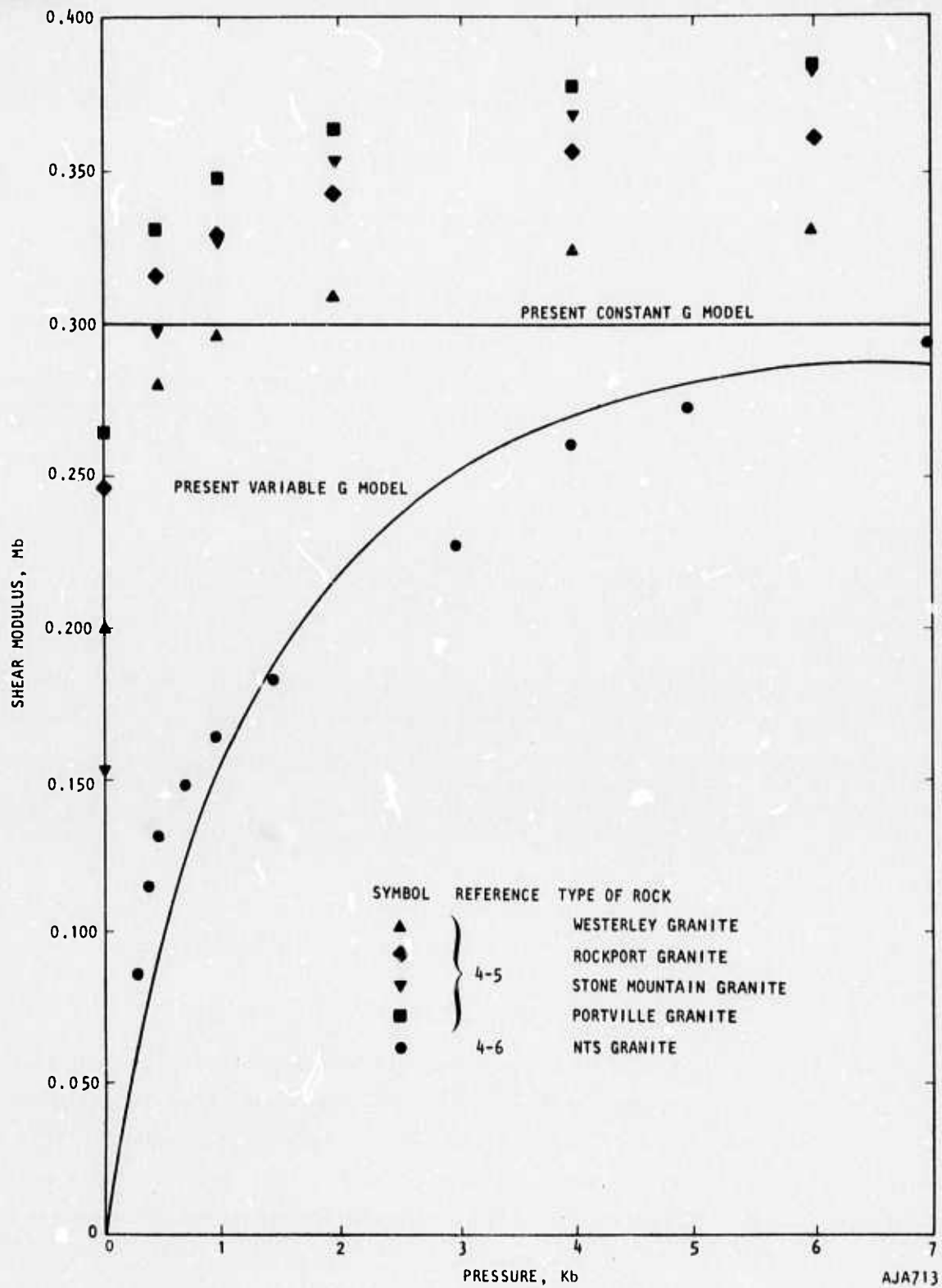


FIGURE 4-3. SHEAR MODULUS VERSUS PRESSURE FOR NTS GRANITE



in the following empirical expressions for the effective bulk modulus. However, the basic concept is retained. Also, the present model for the effective shear modulus merely follows Walsh's concept. The idea of coupling the shear stiffness to volumetric strain is proposed in Reference 4-9 and carries the danger that energy might be extracted from the model by hydrostatic compression, followed by shearing, followed by releasing the pressure and finally by releasing the shear. This danger is avoided by assuming that friction prevents cracks from reopening during unloading so that the largest value of G reached on loading is retained during subsequent unloading/reloading. Under these conditions a material may dissipate energy in shear during loading and unloading cycles but can never produce additional energy.

4.1.2 INELASTICITY FOR ISOTROPIC MATERIALS--VARIABLE MODULI WITH PLASTICITY

The present adaptation of plasticity theory is based on work of References 4-9 through 4-13. The model consists of a yield criterion

$$f(\sigma_{ij}, L) = 0 \quad (4-8)$$

where L is a function of plastic strain,

and a plastic flow rule in which f is regarded as a potential function

$$d\epsilon_{ij}^p = \lambda \frac{\partial f}{\partial \sigma_{ij}} \quad (4-9)$$

The incremental stress is related to the elastic component of incremental strain by Equation 4-7. Defining

$$d\epsilon_{ij}^e = d\epsilon_{ij} - d\epsilon_{ij}^p \quad (4-10)$$



Substituting Equations 4-9 and 4-10 into Equation 4-7 leads to

$$d\sigma_{ij} = \lambda \left(d\epsilon_{kk} - \Lambda \frac{\partial f}{\partial \sigma_{\ell\ell}} \right) \delta_{ij} + 2G \left(d\epsilon_{ij} - \Lambda \frac{\partial f}{\partial \sigma_{ij}} \right) \quad (4-11)$$

where

$$\lambda = B - \frac{2}{3} G$$

If the yield criterion is satisfied, the stress state must lie on the surface defined by f in Equation 4-8. The mathematical statement of this constraint is

$$df = \frac{\partial f}{\partial \sigma_{ij}} d\sigma_{ij} + \frac{\partial f}{\partial L} dL = 0 \quad (4-12)$$

Substituting Equation 4-11 into 4-12 permits solutions for Λ

$$\Lambda = \frac{\lambda (d\epsilon_{kk}) f_{\ell\ell} + 2G d\epsilon_{ij} f_{ij}}{\lambda f_{kk} f_{\ell\ell} + 2G f_{ij} f_{ij} + R} \quad (4-13)$$

where R is a strain-hardening function to be defined below.

Substitution of Equation 4-13 into 4-11 expresses the stress increment in terms of the strain increment.



Specific functional forms have been assumed for f . These contain empirical constants whose values can be selected to match data for a specific material. The forms are

Polynomial 1 in σ_{ij}

$$f_1(\sigma_{ij}) = \begin{cases} \sqrt{J_2'} - \sum_{n=1}^4 a_n J_1^{n-1} = 0 & J_1 > b \\ \sqrt{J_2'} - a_5 = 0 & J_1 \leq b \end{cases} \quad (4-14)$$

Polynomial 2 in σ_{ij}

$$f_1(\sigma_{ij}) = \begin{cases} \sqrt{J_2'} - \left\{ a_1 \left[1 - \left(1 - \frac{J_1}{b} \right)^2 \right] + a_2 \right\} = 0 & J_1 > b \\ \sqrt{J_2'} - (a_1 + a_2) = 0 & J_1 \leq b \end{cases} \quad (4-15)$$

Cap (to be used with Polynomial 2)

$$f_2 = (J_1 - V)^2 + P^2(J_2' - Q) = 0 \quad (4-16)$$

in which

$$V = L + P^2 X(L) X'(L) \quad (4-17)$$

$$Q = [X(L)]^2 \{ 1 + P^2 [X'(L)]^2 \} \quad (4-18)$$

and

$$X(L) = \begin{cases} A \left[1 - \left(1 - \frac{L}{B} \right)^2 \right] + C & L \leq B \\ A + C & L > B \end{cases} \quad (4-19a)$$



$$X'(L) = \begin{cases} \frac{2A}{B} \left(1 - \frac{L}{B}\right) & L \leq B \\ 0 & L > B \end{cases} \quad (4-19b)$$

The hardening parameter, L , is

$$L = \int_0^t g(J_1, \sqrt{J_2'}) \sqrt{\dot{I}_2^p} dt \quad (4-20)$$

where

$$g = W \left[1 - \frac{\sqrt{J_2'}}{\sqrt{J_2'} - f_1} \right]^2 \quad (4-21)$$

$$\dot{I}_2^p = (\dot{\epsilon}_1^p)^2 + (\dot{\epsilon}_2^p)^2 + (\dot{\epsilon}_3^p)^2 \quad (4-22)$$

The hardening parameter R is

$$R = \left(\frac{f_1^2}{(f_1 - \sqrt{J_2'})^2} \right) \left(\frac{\partial f_2}{\partial L} \right) \sqrt{\left(\frac{\partial f_2}{\partial \sigma_1} \right)^2 + \left(\frac{\partial f_2}{\partial \sigma_2} \right)^2 + \left(\frac{\partial f_2}{\partial \sigma_3} \right)^2} \quad (4-23)$$

where

$\sigma_1, \sigma_2, \sigma_3$ are principal stresses

and

$$R = 0 \text{ if } f = f_1.$$

The cap parameters and stress/strain relations produced by the cap model are shown in Figures 4-4 through 4-6. Data on strength for granite containing various degrees of cracking are shown in Figure 4-7, which illustrate the adequacy of the assumed fracture criteria.



R-721j-1-2701

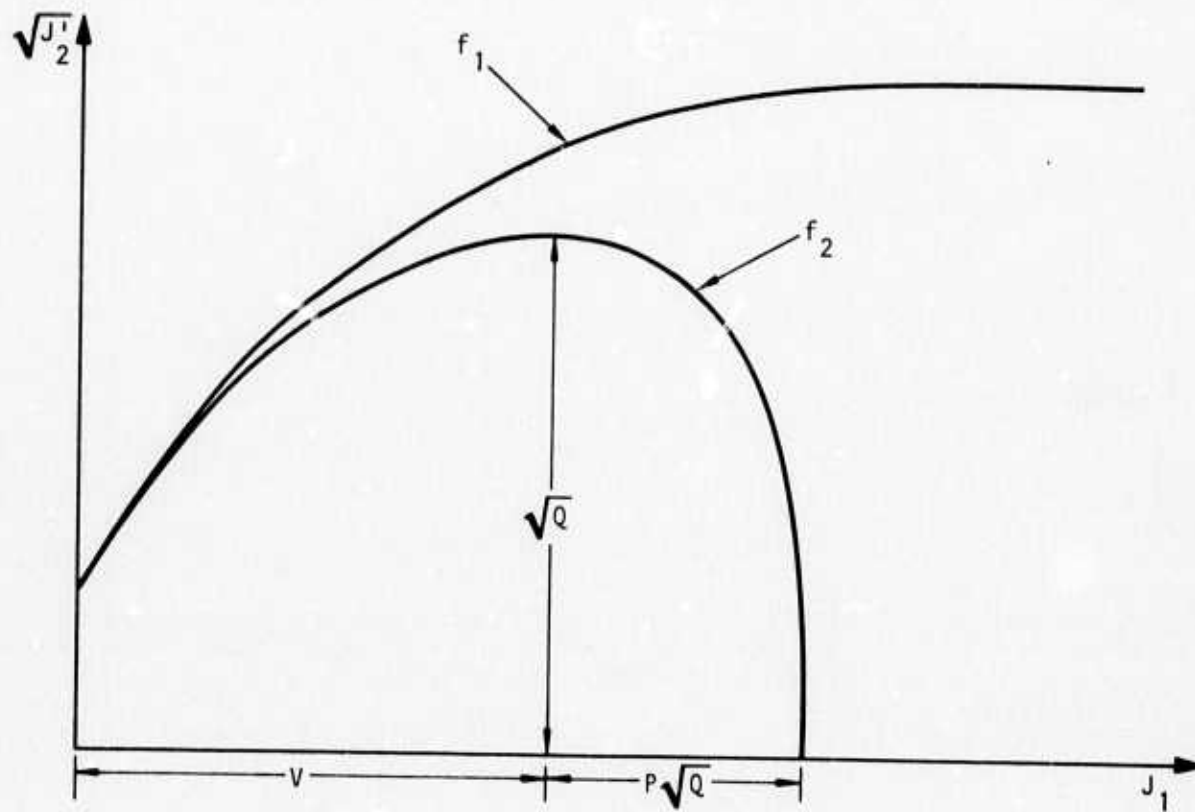


FIGURE 4-4. CAP MODEL

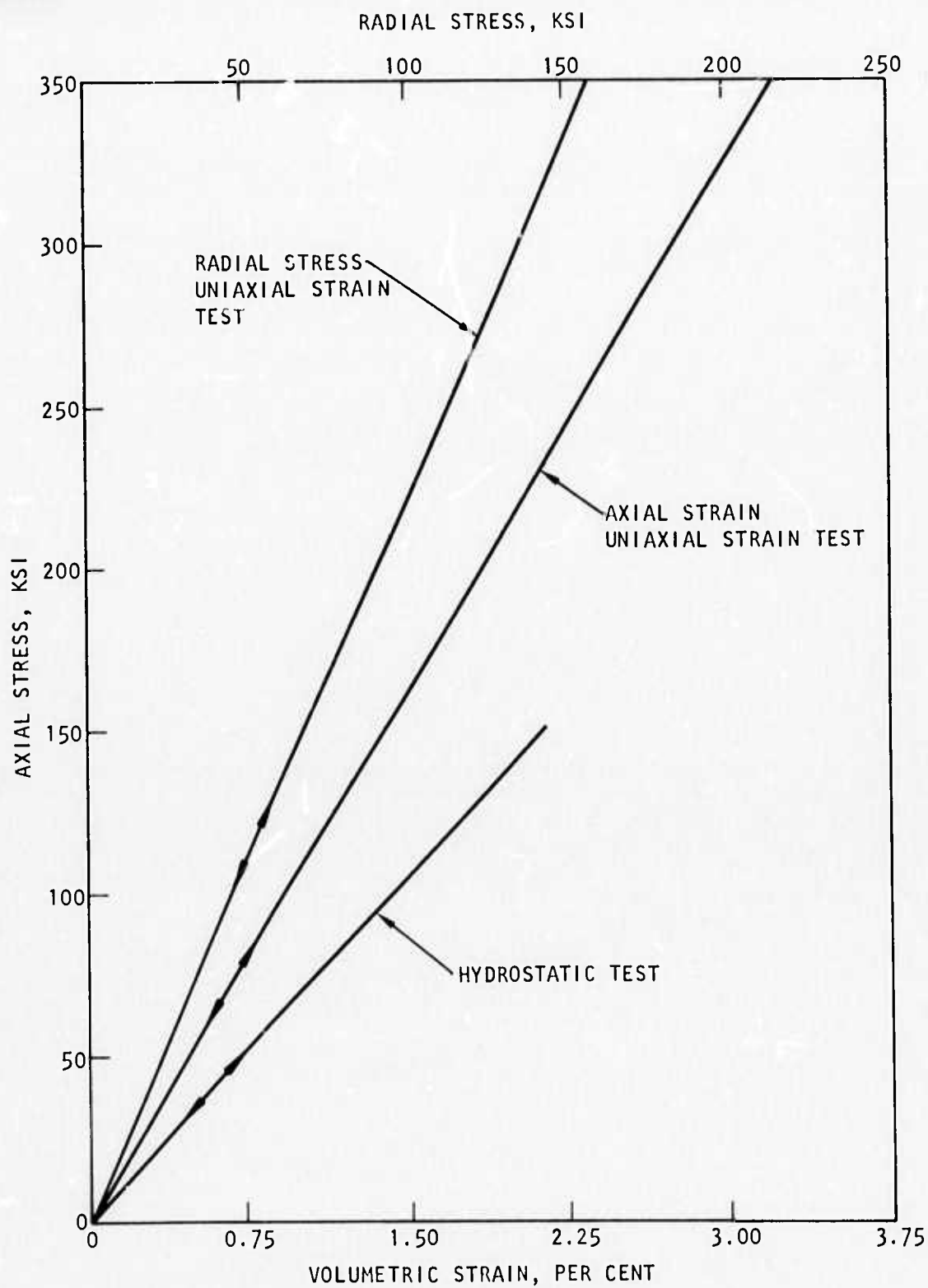


FIGURE 4-5. HYDROSTATIC AND UNIAXIAL STRAIN BEHAVIOR CAP MODEL FIT FOR GRANITIC MATERIAL

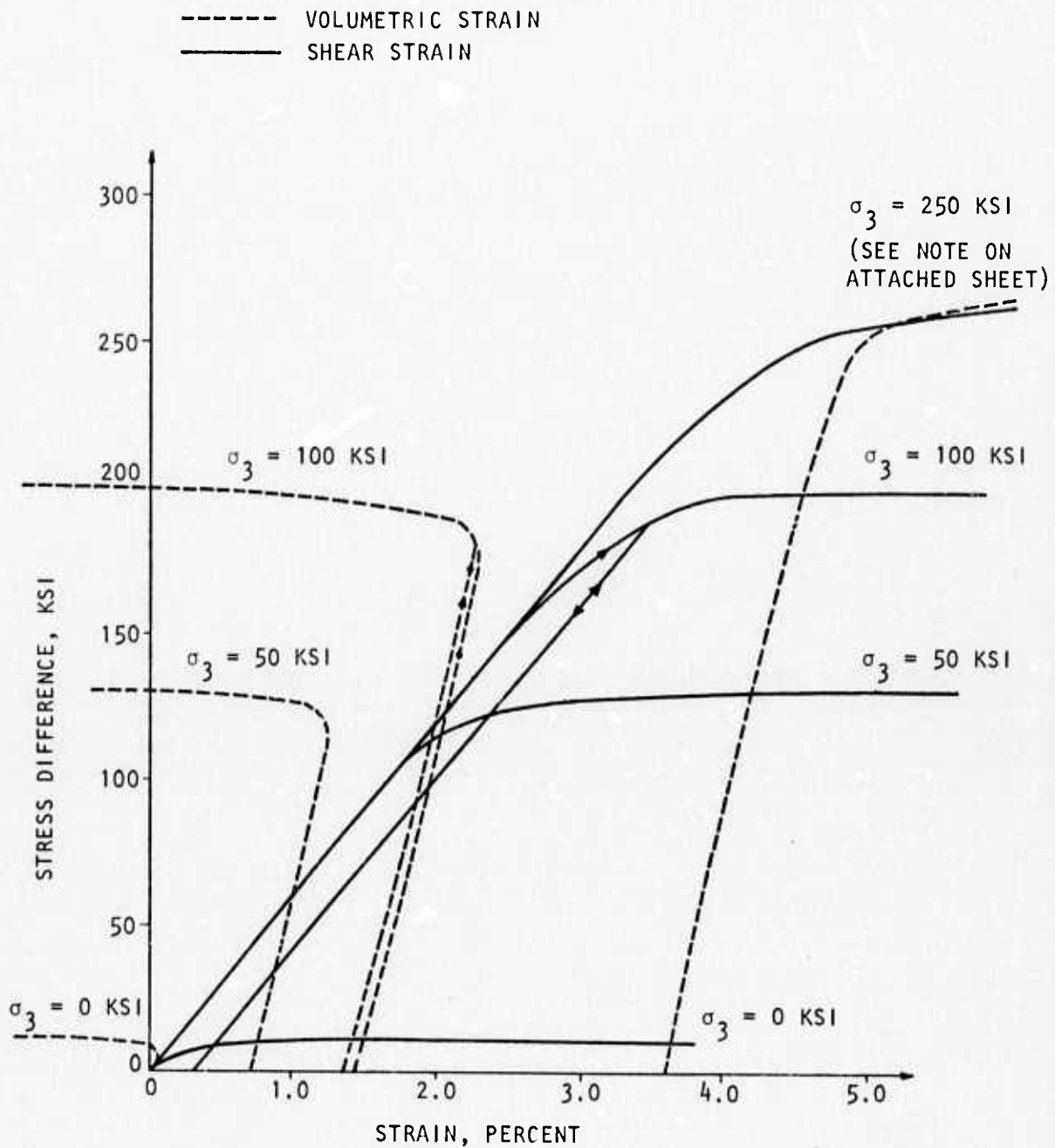


FIGURE 4-6. TRIAXIAL STRESS BEHAVIOR, CHAMBER PRESSURE = 0, 50, 100, 200 KSI, CAP MODEL FIT FOR GRANITIC MATERIAL

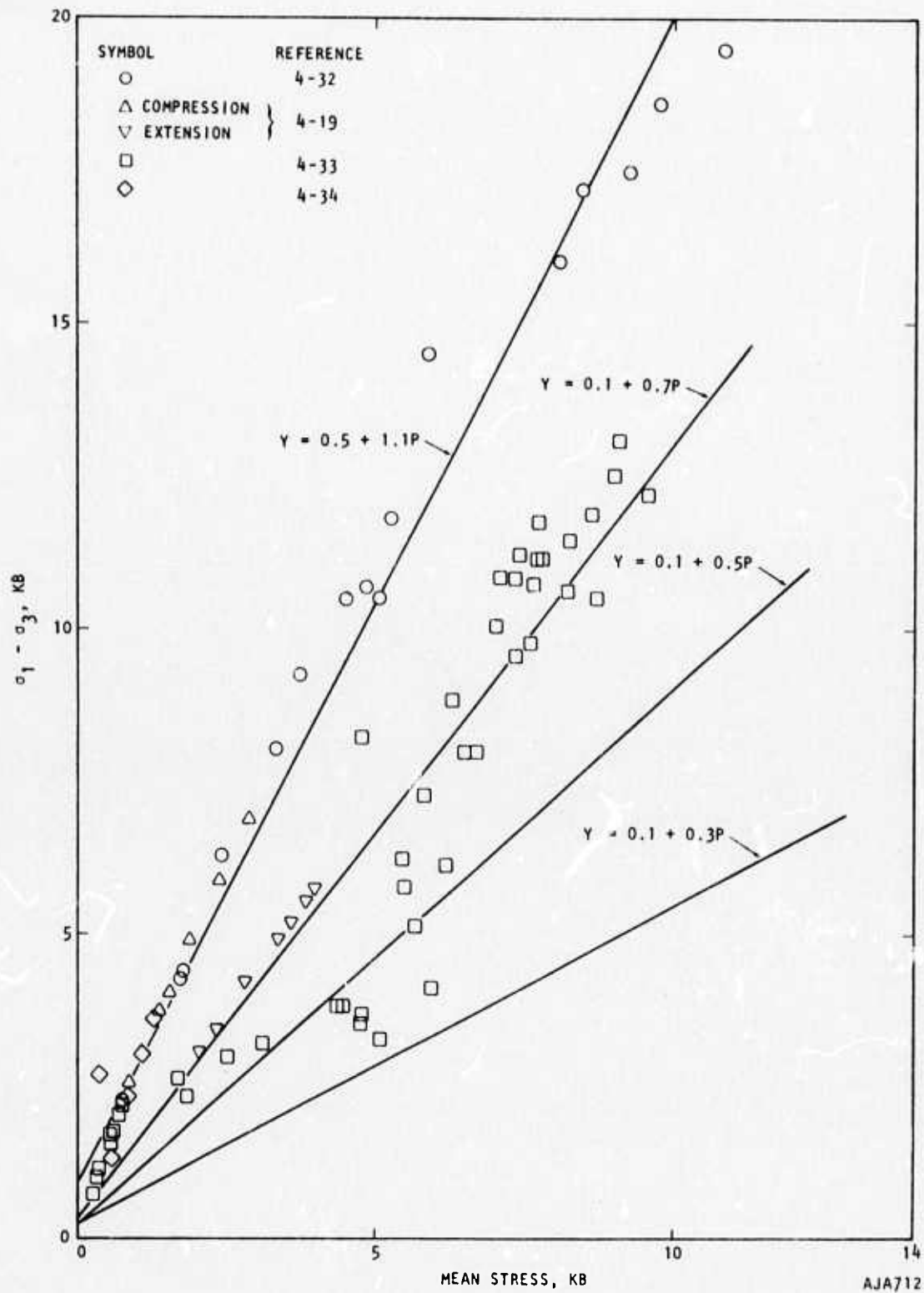


FIGURE 4-7. YIELD STRENGTH VERSUS MEAN STRESS FOR NTS GRANITE



The incremental stress/strain equations are expressed in matrix form as follows:

$$\{d\sigma\} = [C]\{d\epsilon\} \quad (4-24)$$

where $d\epsilon$ is the total increment of strain. The C matrix thus contains generalized tangent moduli and can be used in forming the element stiffness matrices. For the models described above, the C matrix is as follows:



C =

$$\begin{bmatrix} \lambda + 2G - \frac{(\lambda G + 2Gf_{11})^2}{D} & \lambda - \frac{(\lambda F + 2Gf_{22})(\lambda F + 2Gf_{11})}{D} & \lambda - \frac{(\lambda F + 2Gf_{33})(\lambda F + 2Gf_{11})}{D} & -2Gf_{12} \frac{\lambda F + 2Gf_{11}}{D} & -2Gf_{13} \frac{\lambda F + 2Gf_{11}}{D} & -2Gf_{23} \frac{\lambda F + 2Gf_{11}}{D} \\ \lambda + 2G - \frac{(\lambda + 2Gf_{22})^2}{D} & \lambda - \frac{(\lambda F + 2Gf_{22})(\lambda F + 2Gf_{33})}{D} & \lambda - \frac{(\lambda F + 2Gf_{22})(\lambda F + 2Gf_{11})}{D} & -2Gf_{12} \frac{\lambda F + 2Gf_{22}}{D} & -2Gf_{13} \frac{\lambda F + 2Gf_{22}}{D} & -2Gf_{23} \frac{\lambda F + 2Gf_{22}}{D} \\ \lambda + 2G - \frac{(\lambda + 2Gf_{33})^2}{D} & \lambda - \frac{(\lambda F + 2Gf_{33})(\lambda F + 2Gf_{11})}{D} & \lambda - \frac{(\lambda F + 2Gf_{33})(\lambda F + 2Gf_{22})}{D} & -2Gf_{12} \frac{\lambda F + 2Gf_{33}}{D} & -2Gf_{13} \frac{\lambda F + 2Gf_{33}}{D} & -2Gf_{23} \frac{\lambda F + 2Gf_{33}}{D} \\ \frac{4G^2 f_{12}^2}{D} & \frac{4G^2 f_{13}^2}{D} & \frac{4G^2 f_{23}^2}{D} & G - \frac{4G^2 f_{12}^2}{D} & \frac{4G^2 f_{13}^2}{D} & \frac{4G^2 f_{23}^2}{D} \\ \frac{4G^2 f_{13}^2}{D} & \frac{4G^2 f_{12}^2}{D} & \frac{4G^2 f_{23}^2}{D} & \frac{4G^2 f_{13}^2}{D} & G - \frac{4G^2 f_{13}^2}{D} & \frac{4G^2 f_{23}^2}{D} \\ \frac{4G^2 f_{23}^2}{D} & \frac{4G^2 f_{12}^2}{D} & \frac{4G^2 f_{13}^2}{D} & \frac{4G^2 f_{23}^2}{D} & \frac{4G^2 f_{13}^2}{D} & G - \frac{4G^2 f_{23}^2}{D} \end{bmatrix} \quad (4-25)$$

Symmetric

where

$$\begin{aligned} D &= F^2 + 2GX - R \\ F &= \frac{3f}{3\sigma_{11}} + \frac{3f}{3\sigma_{22}} + \frac{3f}{3\sigma_{33}} = f_{11} + f_{22} + f_{33} \\ X &= f_{11}^2 + f_{22}^2 + f_{33}^2 + 2f_{13}^2 + 2f_{12}^2 + 2f_{23}^2 \end{aligned}$$



The C matrix is clearly composed of elastic and inelastic parts

$$C = C^e - C^p \quad (4-26)$$

The C^e and C^p matrices are computed separately. The reason for this is efficiency in treating isotropic and anisotropic materials with the same Fortran statements.

In weakly nonlinear problems it is possible to avoid time-consuming reformulation of the stiffness matrix by introducing nonlinearity through the load vector. The method is an extension of the equilibrium equations given in Reference 4-29. In the following equation, time is used as a parameter. Number of load step could be used instead.

At time τ , the total change in complimentary strain energy is equal to the change in complimentary work done by nodal point forces.

$$\sum_{\tau=0}^{\tau=t} \int_{vol} \langle \epsilon \rangle_{\tau} \{ d\sigma \}_{\tau} dV = \sum_{\tau=0}^{\tau=t} \langle u \rangle_{\tau} \{ dP \}_{\tau} \quad (4-27)$$

where

$\langle \epsilon \rangle, \{ d\sigma \}$ = Element strain and stress increment

$\langle u \rangle, \{ dP \}$ = Nodal displacement and force vector

V = Volume of finite element

τ = Arbitrary instant of time

The strain/displacement relation is

$$\{ \epsilon \} = [B] \{ u \}$$

or

$$\langle \epsilon \rangle = \langle u \rangle [B]^T \quad (4-28)$$



The stress increment in an elastic/plastic material may be expressed by rewriting Equation 4-24 as follows.

$$\{d\sigma\} = [C]\{d\epsilon\} - \{d\sigma_p\} \quad (4-29)$$

elastic correction

where now $C = C^e$

Substituting Equations 2-28 and 2-29 into Equation 2-27,

$$\sum_{\tau=0}^{\tau=t} \int_{vol} \langle u \rangle_{\tau} [B]^T \{ [C][B]\{du\}_{\tau} - \{d\sigma_p\}_{\tau} \} dV = \sum_{\tau=0}^{\tau=t} \langle u \rangle_{\tau} \{dP\}_{\tau} \quad (4-30)$$

Noting that $\langle u \rangle_{\tau}$ may be eliminated from both sides and that

$$\int_{vol} [B]^T [C] [B] dV = [K] \quad (4-31)$$

where $[K]$ is the elastic stiffness matrix, Equation 2-30 may be rewritten as

$$\sum_{\tau=0}^{\tau=t-\Delta t} \left([K]\{du\}_{\tau} - \int_{vol} [B]^T \{d\sigma_p\}_{\tau} dV \right) + [K]\{du\}_{\Delta t} - \int_{vol} [B]^T \{d\sigma_p\}_{\Delta t} dV = \sum_{\tau=0}^{\tau=t} \{P\}_{\tau} \quad (4-32)$$

where $\{du\}_{\Delta t}$, $\{d\sigma_p\}_{\Delta t}$ equal change in u and σ_p during the interval $t - \Delta t$ to t .

Performing the indicated summation, assuming stress to be constant throughout the element and defining

$$E_{\tau} = \sum_{\tau=0}^{\tau} [K]\{du\}_{\tau} \quad (4-33)$$



we have

$$[K]\{du\}_{\Delta t} - [B]^T \{d\sigma_p\}_{\Delta t} V = \{P\}_t - \{E\}_{t-\Delta t} + [B]^T \{\sigma_p\}_{t-\Delta t} V \quad (4-34)$$

For small increments of stress and time in a step-by-step integration, the second term on the left hand side is neglected.

The expression which is used for $\{E\}$ in the computer program is derived as follows. The recoverable work done on an element is equated to the elastic strain energy stored in the element by the following equation.

$$\frac{1}{2} \langle u \rangle \{E\} = \frac{1}{2} \langle \epsilon \rangle [C] \{\epsilon\} V \quad (4-35)$$

or

$$\{E\} = [B]^T [C] \{\epsilon\} V \quad (4-36)$$

Thus Equation 4-34 may be rewritten

$$[K]\{du\}_{\Delta t} = \{P\}_t - [B]^T \left\{ [C] \{\epsilon\}_{t-\Delta t} - \{\sigma_p\}_{t-\Delta t} \right\} V \quad (4-37)$$

Following Equation 4-29

$$d\sigma_{ij} = \left(\lambda d\epsilon_{kk} \delta_{ij} + 2G d\epsilon_{ij} \right) - \left(\lambda \frac{\partial f}{\partial \sigma_{kk}} \delta_{ij} + 2G \frac{\partial f}{\partial \sigma_{ij}} \right) \Lambda \quad (4-38)$$

or

$$d\sigma_{ij} = \lambda d\epsilon_{kk} \delta_{ij} + 2G d\epsilon_{ij} - d\sigma_{ij}^P \quad (4-39)$$



where

$$d\sigma_{ij}^p = \left(\lambda \frac{\partial f}{\partial \sigma_{kk}} \delta_{ij} + 2G \frac{\partial f}{\partial \sigma_{ij}} \right) \frac{\lambda d\epsilon_{kk} \frac{\partial f}{\partial \sigma_{kk}} + 2G d\epsilon_{ij} \frac{\partial f}{\partial \sigma_{ij}}}{\lambda \frac{\partial f}{\partial \sigma_{kk}} \frac{\partial f}{\partial \sigma_{kk}} + 2G \frac{\partial f}{\partial \sigma_{ij}} \frac{\partial f}{\partial \sigma_{ij}}} \quad \text{if } f = 0$$

$$= 0 \quad \text{if } f < 0$$
(4-40)

After each integration step, Δu_i is given; $d\epsilon_{ij}$ is found.

Based on $d\epsilon_{ij}$ and stress at previous time, f is checked and $d\sigma_{ij}$ is calculated according to whether material is elastic or plastic by adding contribution for elastic part to contribution from plastic part.

Stiffness is always based on elastic, parameters, i.e., λ , G . Plasticity is introduced through updating of stress increment. Hence, there is need to update stiffness matrix.

4.1.3 INELASTICITY FOR ANISOTROPIC MATERIALS--THEORY OF JAEGER

The fracture of anisotropic rocks is the subject of several failure theories. The Walsh-Brace theory (Reference 4-14) assumes that failure is tensile in nature and that it is influenced by the presence of preexisting cracks. Some of the cracks are assumed to be small and randomly oriented while others are long and have preferred directions. Extension of the cracks is postulated to occur when the Griffith criterion (Reference 4-15), as modified by McClintock and Walsh (Reference 4-16) to account for friction on the crack faces, is satisfied.

In contrast, Jaeger (Reference 4-17) assumes the material to fail in shear either along a single plane of weakness or within the matrix material according to a Mohr-Coulomb type of failure criterion of the form

$$\tau = a_0 - \sigma a_1 \quad (4-38)$$



where

- τ = Shear stress on plane of fracture
- σ = Normal stress on plane of fracture
- a_0, a_1 = Cohesion, angle of friction

The theory is expressed in terms of principal stresses by an axis rotation as follows

$$\sigma_1 - \sigma_3 = \frac{2a_0 - 2a_1\sigma_3}{a_1 - \sqrt{a_1^2 + 1}} \quad (4-39)$$

Improved agreement with experiment is obtained if a_0 is assumed to vary

$$a_0 = a_2 - a_3 \cos (2(\xi - \beta)) \quad (4-40)$$

where

- β = Counterclockwise angle from the direction of the major principal stress (σ_1) to the direction of the bedding planes
- ξ = The orientation of β at which a_0 is minimum. Usually assumed to be equal to 30 deg

The angle β is shown in Figure 4-8 along with angles relating it to global directions in the finite element formulation. McLamore and Grey (Reference 4-18) have obtained satisfactory agreement between experimental data on strengths of slates and shales using a modification of Equation 4-25 as follows:

$$\begin{aligned} a_0 &= a_2 - a_3 [\cos 2(\xi - \beta)]^n \quad \text{for } 0 < \xi < \beta \\ a_0 &= a_4 - a_5 [\cos 2(\xi - \beta)]^n \quad \text{for } \beta < \xi < 90^\circ \end{aligned} \quad (4-41)$$

Some of their results and those of Brace and Walsh are illustrated in Figure 4-9.



R-7215-1-2701

X - Y - Z = GLOBAL AXES
1 - 2 - 3 = PRINCIPAL STRESS AXES

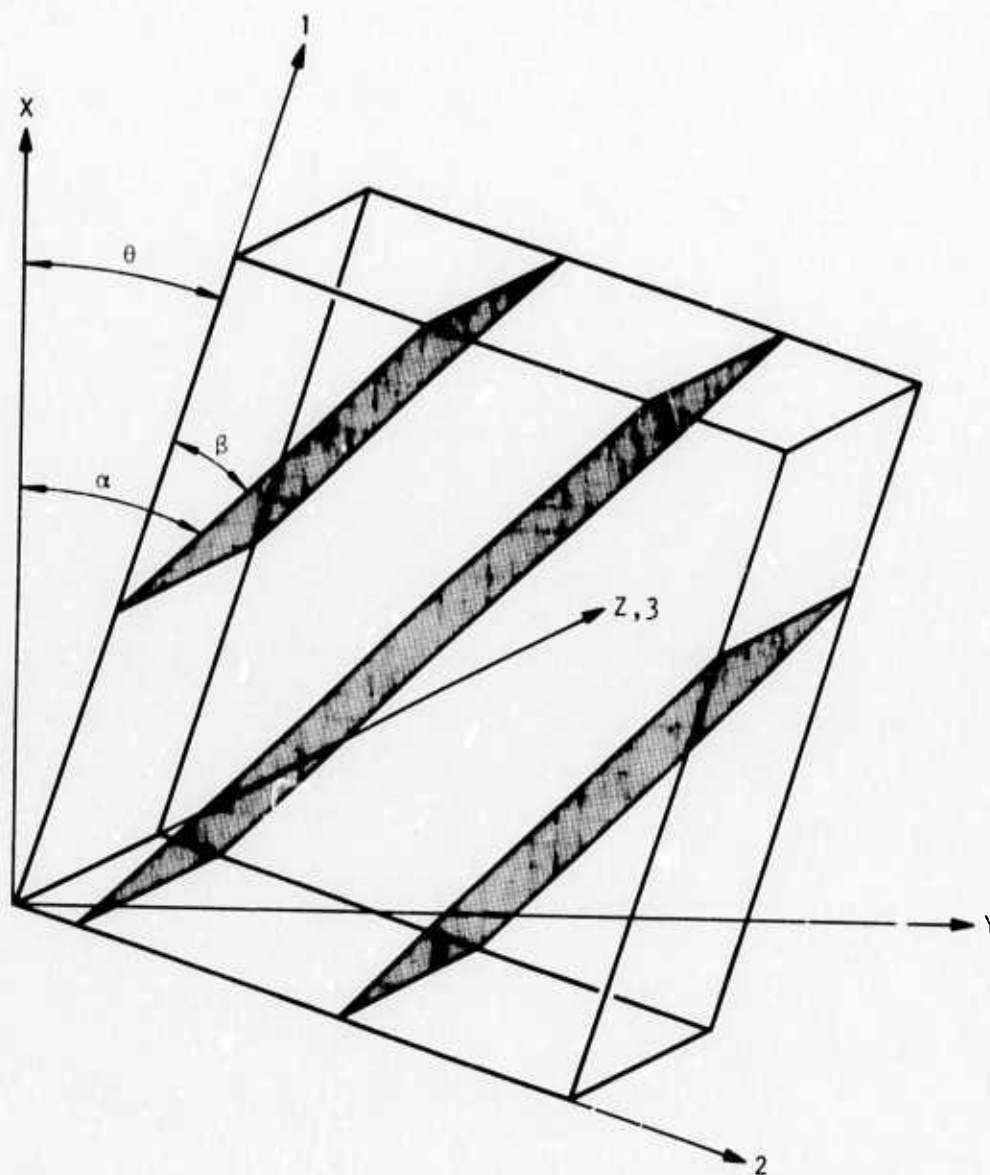
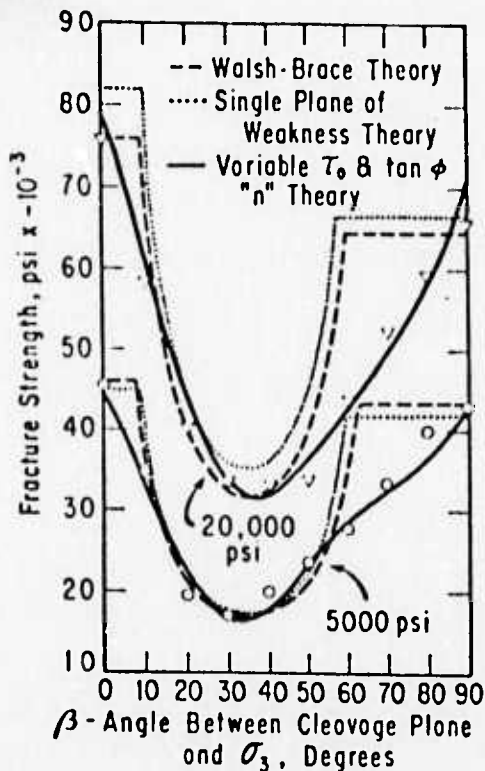
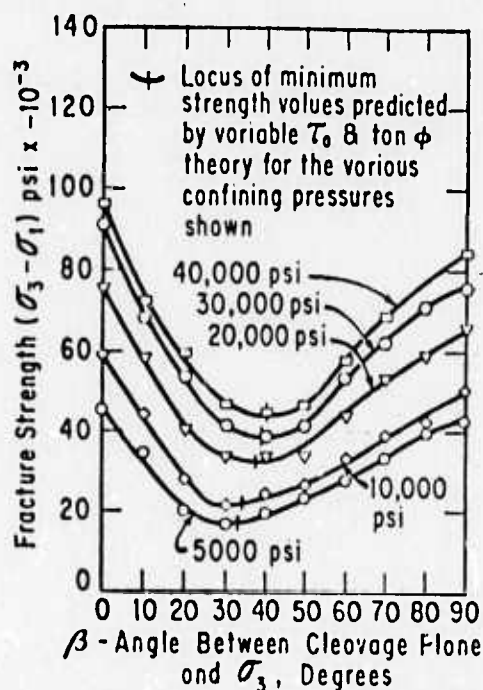


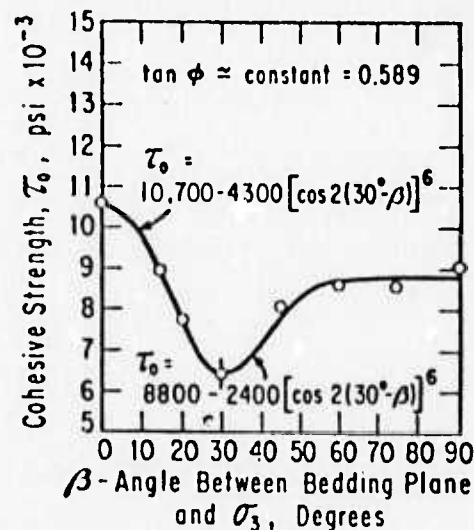
FIGURE 4-8. ORIENTATION OF PLANES OF WEAKNESS DEFINING ANISOTROPIC BEHAVIOR ACCORDING TO JAEGER



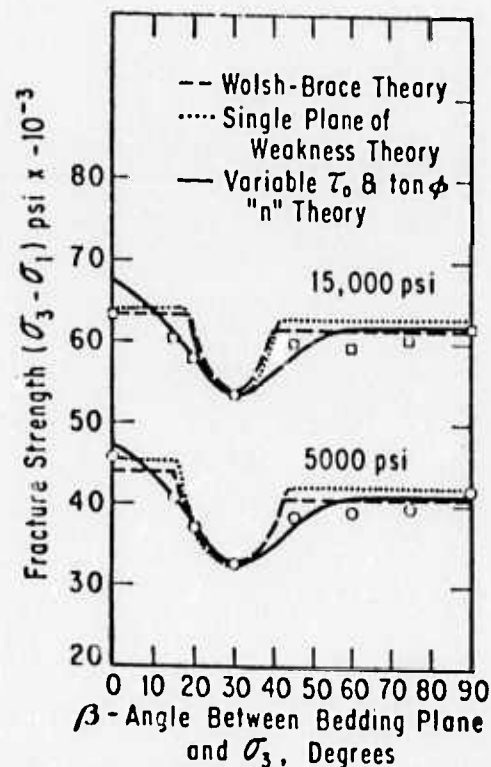
COMPARISON OF VARIOUS FAILURE THEORIES WITH SLATE DATA FOR CONFINING PRESSURES OF 5000 PSI AND 20,000 PSI



FRACTURE STRENGTH VERSUS ORIENTATION ANGLE β FOR SLATE AT VARIOUS CONFINING PRESSURES



VARIATION OF τ_0 WITH RESPECT TO β FOR GREEN RIVER SHALE-1



COMPARISON OF VARIOUS FAILURE THEORIES WITH GREEN RIVER SHALE-1 DATA FOR CONFINING PRESSURES OF 5000 PSI AND 15,000 PSI

FIGURE 4-9. COMPARISON BETWEEN FAILURE THEORIES AND EXPERIMENTAL DATA FOR ANISOTROPIC ROCK (REFERENCE 2-18)



The present application of the hypotheses in Reference 4-18 is limited to plane geometry. It does not take into account the effect of the intermediate principal stress which is shown in Reference 4-19 to play an important role in fracture of some types of rocks. More work is needed to remove these restrictions.

The first step is to determine the magnitude of the principal stresses σ_1, σ_2 and their direction as specified by θ , the counter-clockwise angle from the +X global axis.

$$\sigma_{1,2} = \frac{\sigma_{xx} + \sigma_{yy}}{2} \pm \sqrt{\left(\frac{\sigma_{xx} - \sigma_{yy}}{2}\right)^2 + \sigma_{xy}^2} \quad (4-42)$$

$$\theta = \frac{1}{2} \text{Arctan} \left(\frac{-2\sigma_{xy}}{\sigma_y - \sigma_x} \right) \quad (4-43)$$

Bilinear stress/strain relations are specified by the user in terms of Young's moduli and Poisson's ratio in directions parallel and perpendicular to the bedding planes (oriented at α relative to global axes). Thus, experimental data is required from specimens cut orthogonal to bedding plane and at angles other than 90° . The computer program transforms the various E and ν to the principal directions of stress and modifies them to account for fracture. These parameters, $E_1, \nu_{12}, \nu_{13}, E_2, \nu_{21}, \nu_{23}$, etc., are assembled into a matrix relating incremental stress and strain in principal stress axes. The relationship between incremental stress and incremental strain expressed in the principal axes of anisotropy (principal stress axes) is shown in Equation 2-24 where C is given by Equation 4-44. The matrix is then transformed through the angle θ into global coordinates for inclusion in the element stiffness matrix. An illustration of the bilinear Young's modulus approach is superposed on data in Figure 4-10.

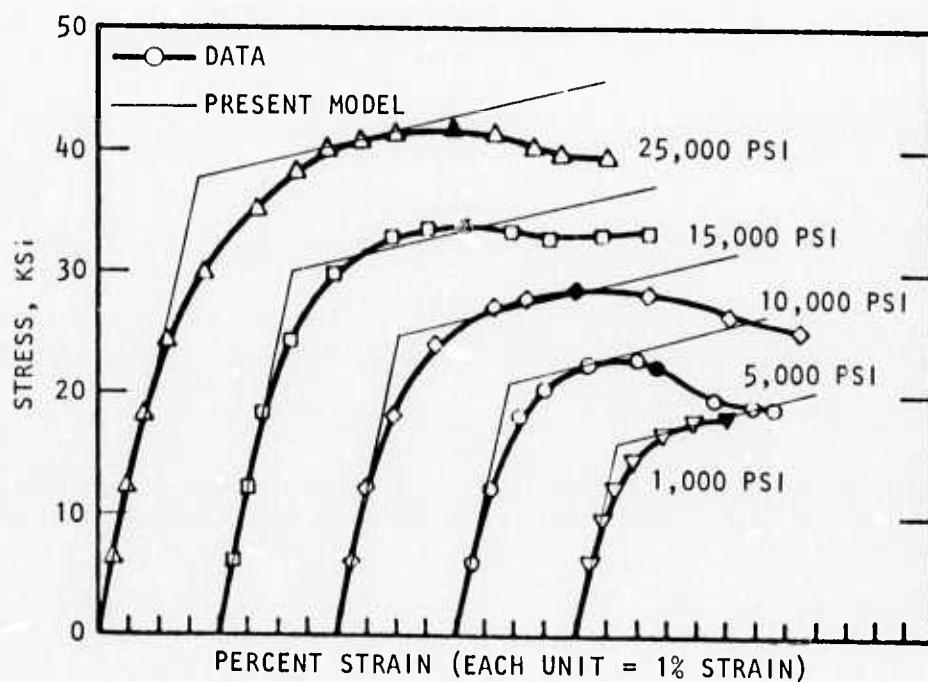


FIGURE 4-10. STRESS-STRAIN CURVES FOR GREEN RIVER SHALE-2 FOR VARIOUS CONFINING PRESSURES, $\beta = 10$ DEG (REFERENCE 2-18)



$$[c] = \frac{1}{D} \begin{bmatrix} E_1(1 - \nu_{23}\nu_{32}) & E_1(\nu_{12} + \nu_{13}\nu_{32}) & E_1(\nu_{13} + \nu_{12}\nu_{23}) \\ E_2(\nu_{21} + \nu_{23}\nu_{31}) & E_2(1 - \nu_{13}\nu_{31}) & E_2(\nu_{23} + \nu_{21}\nu_{13}) \\ E_3(\nu_{13} + \nu_{32}\nu_{21}) & E_3(\nu_{32} + \nu_{31}\nu_{12}) & E_3(1 - \nu_{12}\nu_{21}) \end{bmatrix} \quad (4-44)$$

DG_{12}
 DG_{13}
 DG_{23}

where

$$D = 1 - \nu_{23}\nu_{32} - \nu_{12}\nu_{21} - \nu_{13}\nu_{31} - \nu_{12}\nu_{23}\nu_{31} - \nu_{13}\nu_{21}\nu_{32}$$

4.1.4 INELASTICITY FOR ANISOTROPIC ROCK--THEORY OF HILL

Hill (Reference 4-9) has proposed a yield criterion for anisotropic materials whose form is compatible with the isotropic plasticity theory described above. If the stress components are expressed in the principal axes of anisotropy (not necessarily principal stress axes), the yield criterion can be expressed by

$$f(\sqrt{J_2^{**}}, J_1^*) = 0 \quad (4-45)$$

where

$$\sqrt{J_2^{**}} = c_1(\sigma_{\zeta\zeta} - \sigma_{nn})^2 + c_2(\sigma_{nn} - \sigma_{\xi\xi})^2 + c_3(\sigma_{\zeta\zeta} - \sigma_{\xi\xi})^2$$

$$c_4\sigma_{\zeta\xi}^2 + c_5\sigma_{n\xi}^2 + c_6\sigma_{\zeta\xi}^2$$

$$J_1^* = c_7\sigma_{\zeta\zeta} = c_8\sigma_{nn} + c_9\sigma_{\xi\xi}$$



in which it is assumed that the ζ , η , ξ axis system coincides with the principal direction of anisotropy. f may be used as the potential function described above. Adaptation of this theory to rock is described in Reference 4-20.

The elastic behavior of the material may be prescribed to be either isotropic or anisotropic. If it is isotropic, the quantities B and G may be used. If it is anisotropic, Young's moduli and Poisson ratios E_1 , ν_{12} , ν_{13} , etc. are specified in the principal directions of anisotropy. The C matrix (Equation 4-24) which relates incremental stress to incremental strain is thus initially expressed in the principal axes of anisotropy and is subsequently transformed to global directions of the finite element mesh.

4.1.5 RATE EFFECTS--VISCOPLASTICITY

This method of incorporating rate sensitivity equations is based on Perzyna's elastic-viscoplastic model (Reference 4-21) which is a generalization of an earlier model proposed by Hohenemser and Prager (Reference 4-22). An adaptation of the cap model described above for viscoplasticity is described in Reference 4-23. The present model is taken from Reference 4-24.

A linear elastic, rate independent region is bounded by a static yield criterion

$$f(J_1, J_2') < 0 \quad (4-46)$$

within which Hooke's Law applies. If the static yield criterion is satisfied or exceeded

$$f(J_1, J_2') \geq 0 \quad (4-47)$$

A viscoplastic strain rate is assumed to develop according to the following flow rule.

$$\dot{\epsilon}_{ij}^p = \gamma \phi(f) \frac{\partial F}{\partial \sigma_{ij}} \quad (4-48)$$



where

$\phi(f)$ = A function of the static yield criterion f

F = Assumed potential function. Presently, a nonassociated flow rule is used in which $F = J_2'$ and differentiation is performed with respect to the stress deviators σ_{ij}'

γ = Empirical viscoplastic parameter

It is assumed in the present work that

$$\phi(f) = \begin{cases} \frac{\sqrt{J_2'}}{4 \sum_{n=1}^4 a_n J_1^{n-1}} - 1. & J_1 > b \\ \frac{\sqrt{J_2'}}{a_5} - 1. & J_1 \leq b \end{cases} \quad (4-49)$$

for

$$f = \begin{cases} \sqrt{J_2'} - \sum_{n=1}^4 a_n J_1^{n-1} \geq 0 & J_1 > b \\ \sqrt{J_2'} - a_5 \geq 0 & J_1 \leq b \end{cases} \quad (4-50)$$

If $f < 0$, elastic inviscid stress/strain relations apply.

Making use of Hooke's law

$$\dot{\sigma} = \lambda \dot{\epsilon}_{kk} \delta_{ij} + 2G \dot{\epsilon}_{ij}^e \quad (4-51)$$

and expressing the elastic deviatoric strain rate by

$$\dot{\epsilon}_{ij}^e = \dot{\epsilon}_{ij}' - \dot{\epsilon}_{ij}^p \quad (4-52)$$



for the case where $f \geq 0$, the stress rate may be expressed by the following equation.

$$\dot{\sigma}_{ij} = \begin{cases} \lambda \dot{\epsilon}_{kk} \delta_{ij} + 2G \left[\dot{\epsilon}_{ij} - \gamma \left(\frac{\sqrt{J_2'}}{\sum_{n=1}^4 a_n J_1^{n-1}} - 1 \right) \frac{\sigma'_{ij}}{\sqrt{J_2'}} \right] & J_1 > b \\ \lambda \dot{\epsilon}_{kk} \delta_{ij} + 2G \left[\dot{\epsilon}_{ij} - \gamma \left(\frac{\sqrt{J_2'}}{a_5} - 1 \right) \frac{\sigma'_{ij}}{\sqrt{J_2'}} \right] & J_1 \leq b \end{cases} \quad (4-53)$$

If time is considered the integration parameter and the time step is Δt , the incremental stress is

$$d\sigma_{ij} = \lambda d\epsilon_{kk} \delta_{ij} + 2G \left[d\epsilon_{ij} - \gamma \left(\frac{\sqrt{J_2'}}{a_0 + a_1 J_1} - 1 \right) \frac{\sigma'_{ij}}{\sqrt{J_2'}} \Delta t \right] \quad (4-54)$$

The absence of plastic volume strain is due to choosing a nonassociated flow rule in which J_1 does not appear in the plastic potential.

Some example calculations, which are summarized in Tables 4-3 and 4-4, are shown in Figures 4-11 through 4-13. Comparison with some data for a tonalite is shown in Figure 4-14. The comparison illustrates the ability of the model to represent increase in strength with strain rate and its inability to represent nonlinear behavior prior to yielding. It can be shown that the effects of viscoplasticity can be accounted for entirely by a correction to the load vector (Reference 4-24). The technique is similar to that described above for rate-independent plasticity and to that described below for viscoelasticity. An important consequence of this is that time-consuming reformulation of the stiffness matrix is avoided.



R-7215-1-2701

TABLE 4-3. SUMMARY OF EXAMPLE CALCULATIONS

Case	Type of Loading	Stress Ratio, σ_3/σ_1	Strain Rate,* in./in.-sec
1	Proportional loading	0.293	200.00
2	Proportional loading	0.293	2.00
3	Proportional loading	0.293	0.20
4	Proportional loading	0.293	0.02
5	Proportional loading	0.200	0.20
6	Proportional loading	0.100	0.20
7	Uniaxial strain	0.293	0.02
8	Uniaxial strain	0.293	0.20
9	Uniaxial strain	0.293	2.00
10	Uniaxial strain	0.293	200.00

*For proportional loading, these are elastic strain rates.

TABLE 4-4. PROPERTIES USED IN PRESENT EXAMPLES

Properties

Bulk modulus	B	=	1.5×10^6	psi
Shear modulus	G	=	10^6	psi
Cohesion	a_0	=	1450	
Angle of friction	a_1	=	-0.1	
Viscoplastic coefficient	γ	=	1.0	

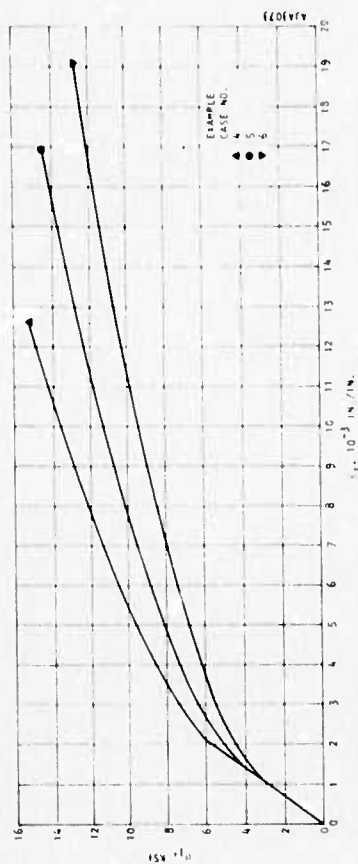


FIGURE 4-12. COMPRESSIVE STRESS/STRAIN RELATIONS FOR PRESENT MODEL SUBJECTED TO PROPORTIONAL LOADING AT DIFFERENT STRESS RATIOS

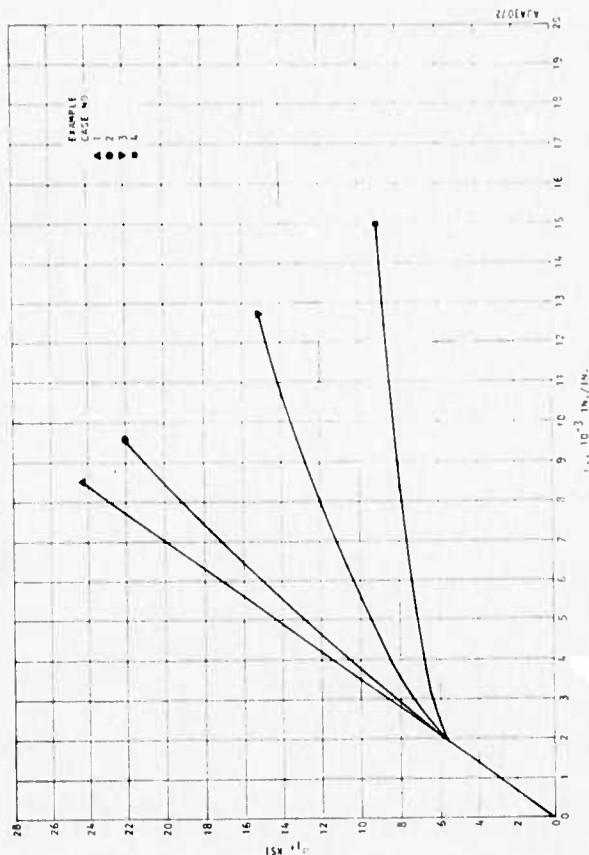


FIGURE 4-13. COMPRESSIVE STRESS/STRAIN RELATIONS FOR PRESENT MODEL SUBJECTED TO PROPORTIONAL LOADING

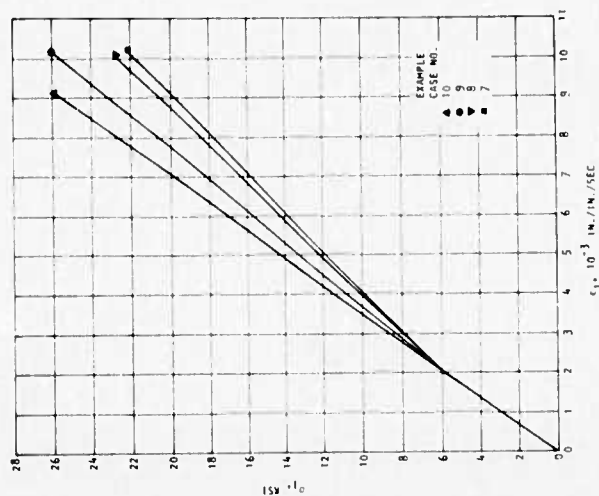


FIGURE 4-11. PRESENT MODEL SUBJECTED TO UNIAXIAL STRAIN AT VARIOUS STRAIN RATES



R-7215-1-2701

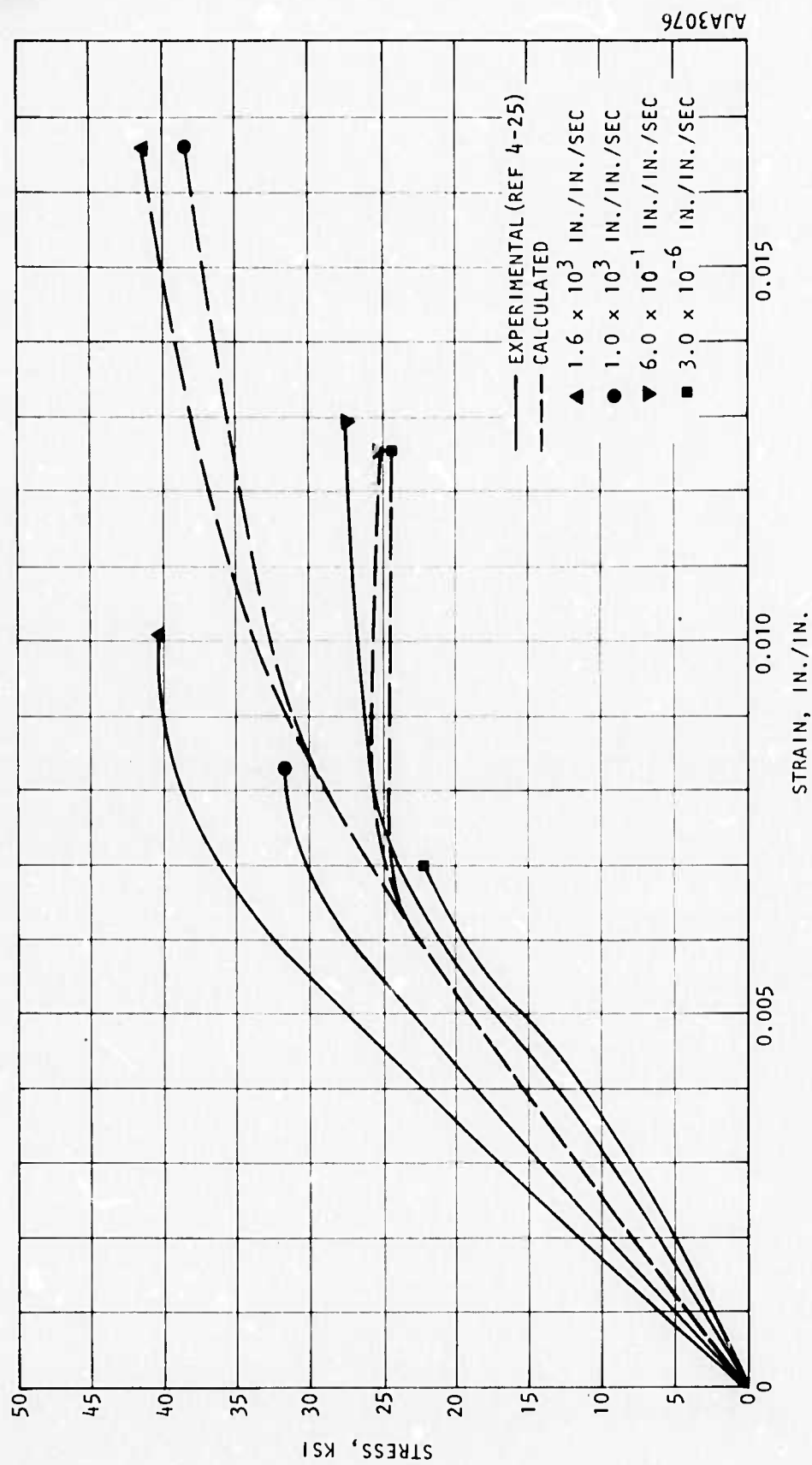


FIGURE 4-14. COMPRESSIVE STRESS/STRAIN RELATIONS FOR CEDAR CITY TONALITE AT VARIOUS STRAIN RATES



4.1.6 RATE EFFECTS--VISCOELASTICITY

The total strain is defined to be the sum of instantaneous elastic and viscoelastic parts. The strain is further divided into shear and volumetric components, which are treated separately as follows:

$$\epsilon_{ij} = \epsilon_{ij} - \delta_{ij} \epsilon_{kk} = (\epsilon_{ij}^e)^e + (\epsilon_{ij}^e)^c \quad (4-55a)$$

$$\epsilon_{kk} = (\epsilon_{kk}^e)^e + (\epsilon_{kk}^e)^c \quad (4-55b)$$

In the computer program the user may choose to have either elastic or viscoelastic shear deformation and to have either elastic or viscoelastic volumetric deformation.

Kelvin, Maxwell and three-parameter fluid models are available as shown in Figure 4-15. To simplify the following discussion, no distinction is made between volumetric and shear components. The creep rate and creep strain at $t + \Delta t$ may be expressed as follows:

KELVIN

$$\dot{\epsilon}^c + a_1 \epsilon^c = a_2 \sigma \quad (4-56a)$$

$$\epsilon_{t + \Delta t}^c = \epsilon_t^c \exp(-a_1 \Delta t) + \sigma_t \frac{a_2}{a_1} (1 - \exp(-a_1 \Delta t)) \quad (4-56b)$$

where $a_1 = \frac{E}{\eta}$ and $a_2 = \frac{1}{\eta}$, E and η are the spring and dashpot constants respectively.

MAXWELL

$$\dot{\epsilon}^c = a_1 \dot{\sigma} + a_2 \sigma \quad (4-57a)$$

$$\epsilon_{t + \Delta t}^c = \epsilon_t^c + \left[(a_2 \Delta t + a_1) \sigma_{t + \Delta t} - a_1 \sigma_t \right] \quad (4-57b)$$

where $a_1 = \frac{1}{E}$ and $a_2 = \frac{1}{\eta}$

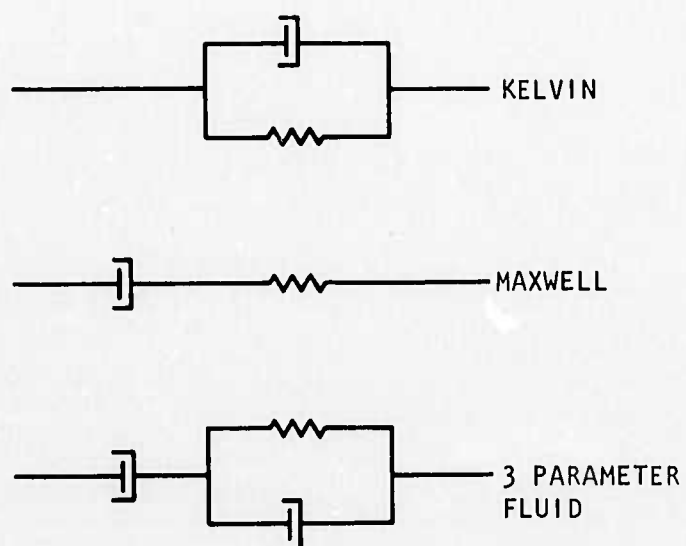


FIGURE 4-15. VISCOUS MODELS AVAILABLE IN THE PRESENT COMPUTER PROGRAM



THREE-PARAMETER FLUID

The creep strain of the three-parameter fluid is divided into two components ϵ^c_1 and ϵ^c_2 which represent the creep strain in a Kelvin model and dashpot

$$\epsilon^c = \epsilon^c_1 + \epsilon^c_2 \quad (4-58a)$$

$$\epsilon^c_{t+\Delta t} = \epsilon^c_t \exp(-a_1 \Delta t) + \sigma_t \frac{a_2}{a_1} (1 - \exp(-a_1 \Delta t)) \quad (4-58b)$$

$$\epsilon^c_{t+\Delta t} = \epsilon^c_{t+\Delta t} + \frac{\Delta t}{a_2} \sigma_t \quad (4-58c)$$

These models are illustrated in Figure 4-15. Various aspects of their properties are discussed in Reference 4-35. Equations 4-56a, -57a, and -58a are in suitable form for application to a time-marching integration procedure.

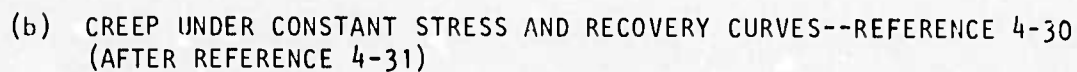
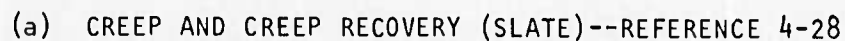
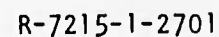
Typical creep and creep recovery data for several rocks are shown in Figure 4-16. Application of a Kelvin model to one of the rocks is shown in Figure 4-17. By suitably varying the parameters a_1 and a_2 , a range of behavior can be reproduced.

The finite element adaptation of these models uses the initial strain approach to writing the equilibrium equations based on the change in internal energy.

$$U = \int_{vol} \sigma^T \epsilon \, dV - \int_S P^T u \, dS \quad (4-59)$$

The stress/strain relations are in terms of a matrix C of elastic stress/strain coefficients

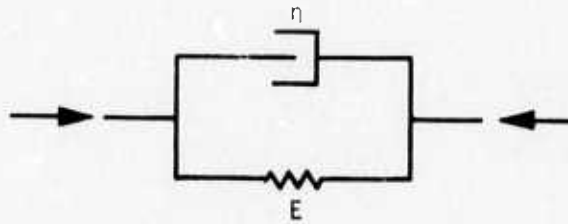
$$\{\sigma_t\} = [C] \{\epsilon_0 + d\epsilon - \epsilon_0^c\} \quad (4-60)$$



116



R-7215-1-2701



$$(a) \begin{cases} E_1 = 476.2 \\ \eta_1 = 3.950 \end{cases}$$

$$(b) \begin{cases} E = E_1 \\ \eta = 1/2 \eta_1 \end{cases}$$

$$(c) \begin{cases} E = E_1 \\ \eta = 1/4 \eta_1 \end{cases}$$

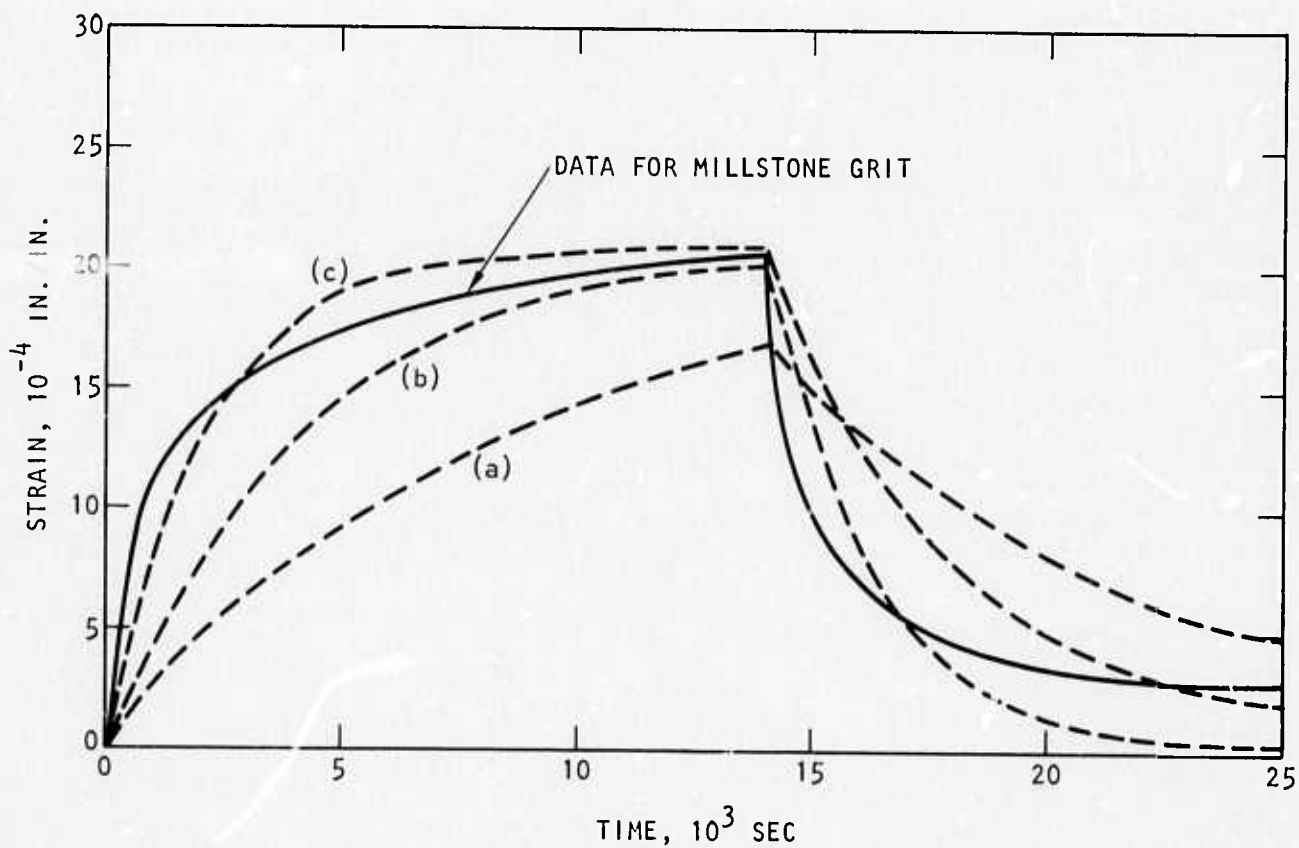


FIGURE 4-17. COMPARISON BETWEEN PRESENT CREEP MODEL AND EXPERIMENTAL DATA (REFERENCES 4-30, 4-31)



where

$\{\sigma_t\}$ = Stress at t

$\{\epsilon_o\}$ = Total strain (including creep) at $t = t_o$

$\{d\epsilon\}$ = Strain increment (including creep) during $\Delta t = t - t_o$

$\left\{\epsilon_o^c\right\}$ = Accumulated creep to $t = t_o$

An error is committed in Equation 4-60 in that $d\epsilon$ contains both elastic and viscous components, whereas it is treated as if it were entirely elastic.

Defining the strain/displacement transformation matrix B as

$$\{\epsilon\} = [B]\{u\} \quad (4-61)$$

The strain energy for an element is

$$U = du^T \int_{vol} B^T C B dV u + \int_{vol} (\epsilon_o - \epsilon_c)^T C B dV u \quad (4-62)$$

Defining

$$\int_{vol} B^T C B dV = k \quad (4-63)$$

where K is the element stiffness matrix and performing a variation with respect to the generalized displacements u results in

$$kdu = P - F_e \quad (4-64)$$

where

$$P = \int_s p^T dS$$

$$F_e = \int_{vol} (\epsilon_o - \epsilon_c)^T C B dV$$



It is significant that the element stiffness matrix consists entirely of linear elastic terms. Thus, the assemblage stiffness matrix needs to be formulated only once, resulting in great economy of computing. It is necessary to store the components of the creep strain at t_0 for use in the next step.

This approach has been adapted to finite element for rock and concrete (Reference 4-26). Some experimental work which has been performed on rock is compared in Reference 4-27 with a series of Kelvin models. Reference 4-28 discusses methods of accounting separately for volumetric and deviatoric creep strains.

4.2 MATERIAL PROPERTIES OF JOINTS

This section describes the properties which may be assigned to joints. These properties consist of the shearing and normal stiffnesses of the joints. They correspond physically to the stiffness and strength of fault gouge, to the roughness of the joints and to the angles of slip surfaces relative to the principal plane of the joint. They are classed as dilatant if shearing produces joint expansion or contraction or nondilatant if shearing and normal displacement are uncoupled. The properties are specified by the user in natural coordinates which may be directions parallel and perpendicular either to slip surfaces or to the principal plane of the joint. In either case, transformation to global directions is automatically performed by the program.

As in the case of homogeneous material properties, the joint properties are controlled by subroutines CONECT and ELPL through modular subroutines. Presently, these contain built-in joint properties. As more data become available on properties of joints and the present joint material properties become obsolete, the present model may easily be modified without disturbing the main program or any of the other material properties.



4.2.1 NONDILATANT JOINTS

This class of joints is the simplest to model mathematically since there is no volume change due to shearing strains, and therefore the shear and the normal components of deformation are uncoupled and the stress-strain relations are as follows:

$$\begin{Bmatrix} \sigma_n \\ \sigma_s \end{Bmatrix} = \begin{bmatrix} C_{nn} & 0 \\ 0 & C_{ss} \end{bmatrix} \begin{Bmatrix} \epsilon_n \\ \epsilon_s \end{Bmatrix} \quad (4-65)$$

However, C_{nn} and C_{ss} are nonlinear functions.

In stress-deformation relationship in normal direction, three distinct stages can be recognized (see Figure 4-18);

- Separation, $C_{nn} = C_{ss} = 0$ when $\epsilon_n \geq 0$
- Crushing of the surface irregularities or the compression of the material in the fault or joint, if any $C_{nn} = E_c$ ($\epsilon_n^c < \epsilon_n < 0$). For smooth surfaces this case does not exist, therefore $\epsilon_n^c = 0$.
- Contact, $C_{nn} = E_f$. ($\epsilon_n < \epsilon_n^c$)

It is important to note that very high values can be assigned to E_f without any numerical problems with the special joint element described in Section 3.

The tangential stress-strain relationship is assumed to be elastic-perfectly plastic using a Mohr-Coulomb yield criterion:

$$\begin{aligned} C_{ss} &= G & \sigma_s &< c + \sigma_n \tan \phi \\ C_{ss} &= 0 & \sigma_s &= c + \sigma_n \tan \phi \end{aligned} \quad (4-66)$$

where c and ϕ are the cohesion or the angle of friction.



R-7215-1-2701

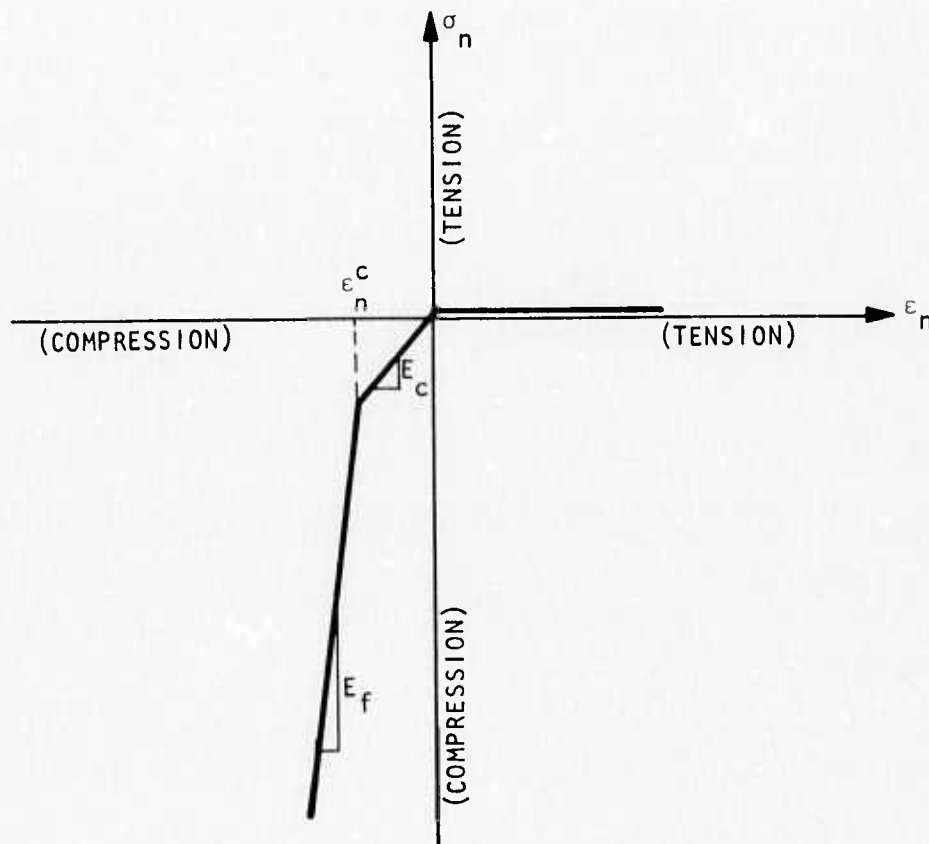


FIGURE 4-18. NORMAL STRESS-STRAIN RELATION FOR JOINTS



4.2.2 DILATANT JOINTS

Dilatancy of rock joints and faults are very complex to model mathematically; however, to include a measure of dilatancy, the procedure developed by Goodman, Dubois, and Brekke (Reference 4-36) is used here. Further data are available from Reference 4-37.

It is assumed that the deformation in p-q coordinate system shown in Figure 4-19 is nondilatant. The angle γ between the p direction and the joint surface is, therefore, defined to be a material property of the joint. The stress-strain relation in n-s coordinate is:

$$\begin{Bmatrix} \sigma_n \\ \sigma_s \end{Bmatrix} \begin{bmatrix} (c_{qq} c^2 + c_{pp} s^2) & (c_{qq} - c_{pp}) sc \\ (c_{qq} - c_{pp}) sc & (c_{qq} s^2 + c_{pp} c^2) \end{bmatrix} \begin{Bmatrix} \epsilon_n \\ \epsilon_s \end{Bmatrix} \quad (4-67)$$

where

$$c = \cos \gamma$$

$$s = \sin \gamma$$

4.2.3 DEMONSTRATION OF JOINT ELEMENT

The example problem in Figure 4-20 demonstrates the behavior of the present joint element. The problem consists of a plane system of three solid blocks and three joint planes. The system is restrained at the bottom and is subjected to lateral pressure P and vertical pressure $2P$. The joints are assumed to be filled with nondilatant material having the properties shown in Figure 4-20. The blocks are assumed to have the isotropic elastic properties shown in Figure 4-20. The material in the joints is represented by joint elements which are shown as their shaded strips. Ambiguity with respect to nodal displacements would arise at the point of the wedge-shaped block if the joint elements were to extend to the point. Ambiguity is avoided by stopping the elements short of the point. This is a good approximation to a physical



R-7215-1-2701

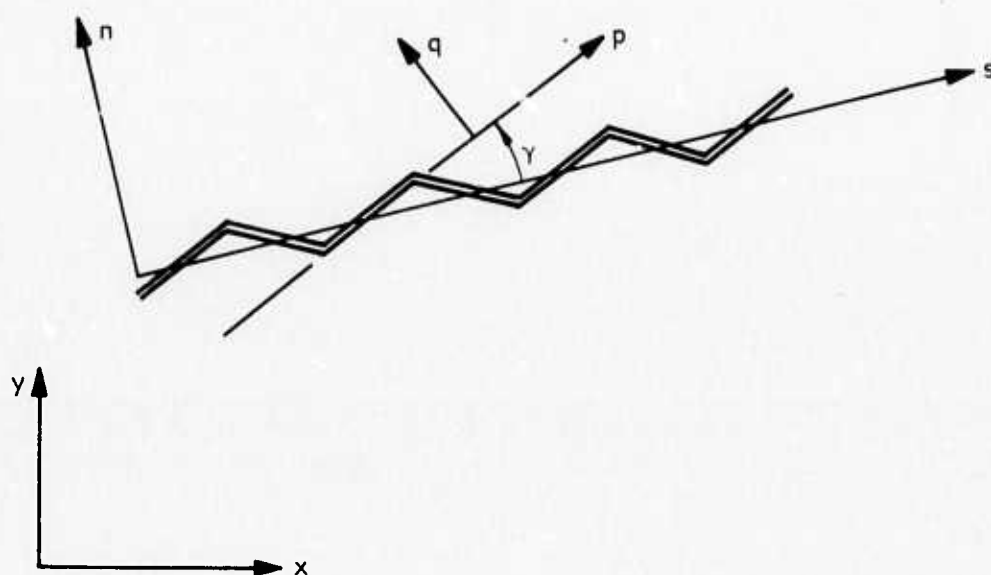


FIGURE 4-19. DILATANT JOINT

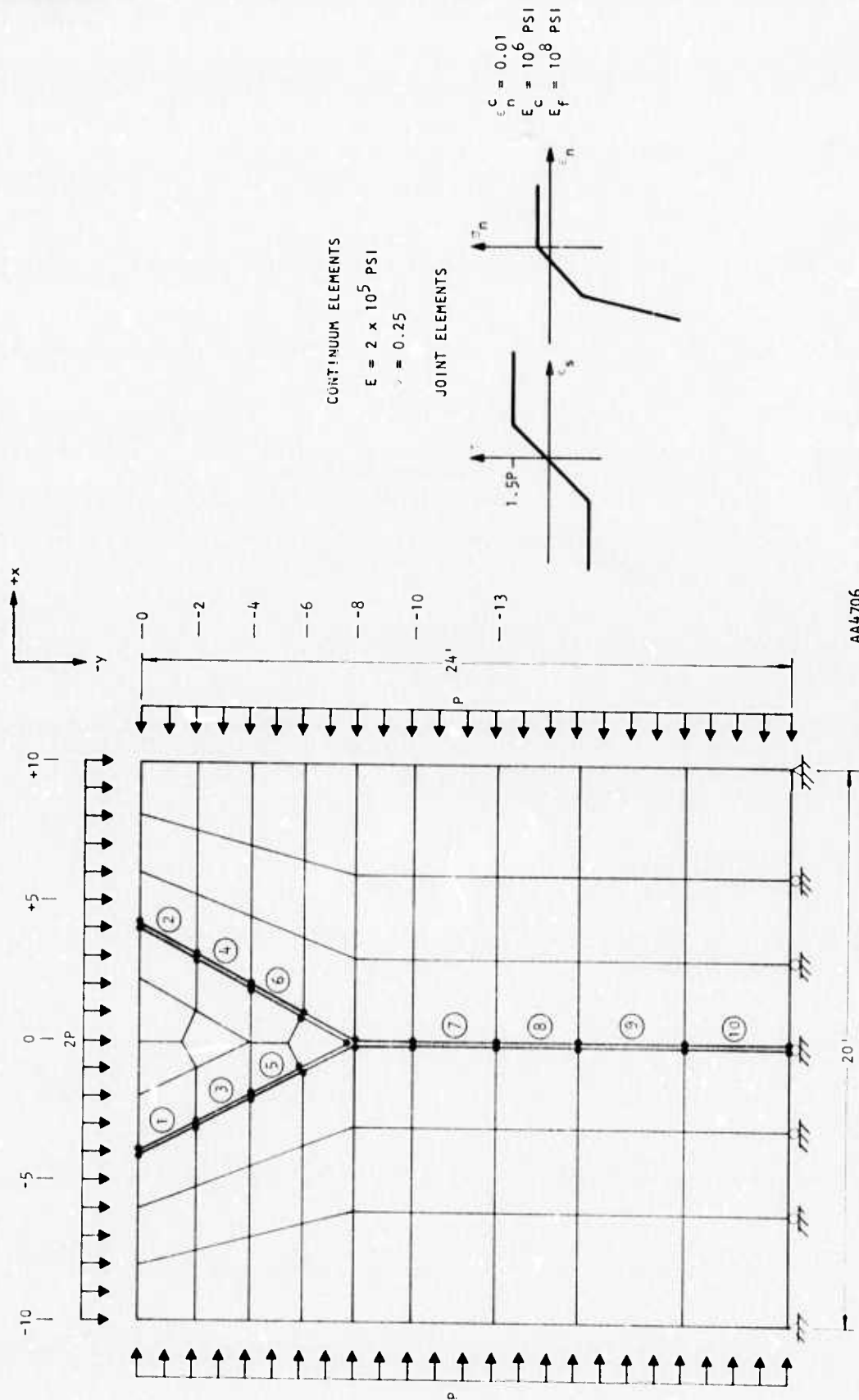


FIGURE 4-20. GEOMETRY OF EXAMPLE PROBLEM USING PLANE SLIP ELEMENT



R-7215-1-2701

system if the joint elements extend infinitesimally close to the point. In the present example, the gap is made large to illustrate how the difficulty is avoided. The blocks are represented by plane strain elements.

Results of the present example are shown in Figures 4-21 and 4-22. Figure 4-21 shows how the vertical displacement varies as a function of horizontal distance from the centerline. Each curve in Figure 4-21 corresponds to a different distance below the top surface. Figure 4-22 shows the wedge in its final position.



R-7215-1-2701

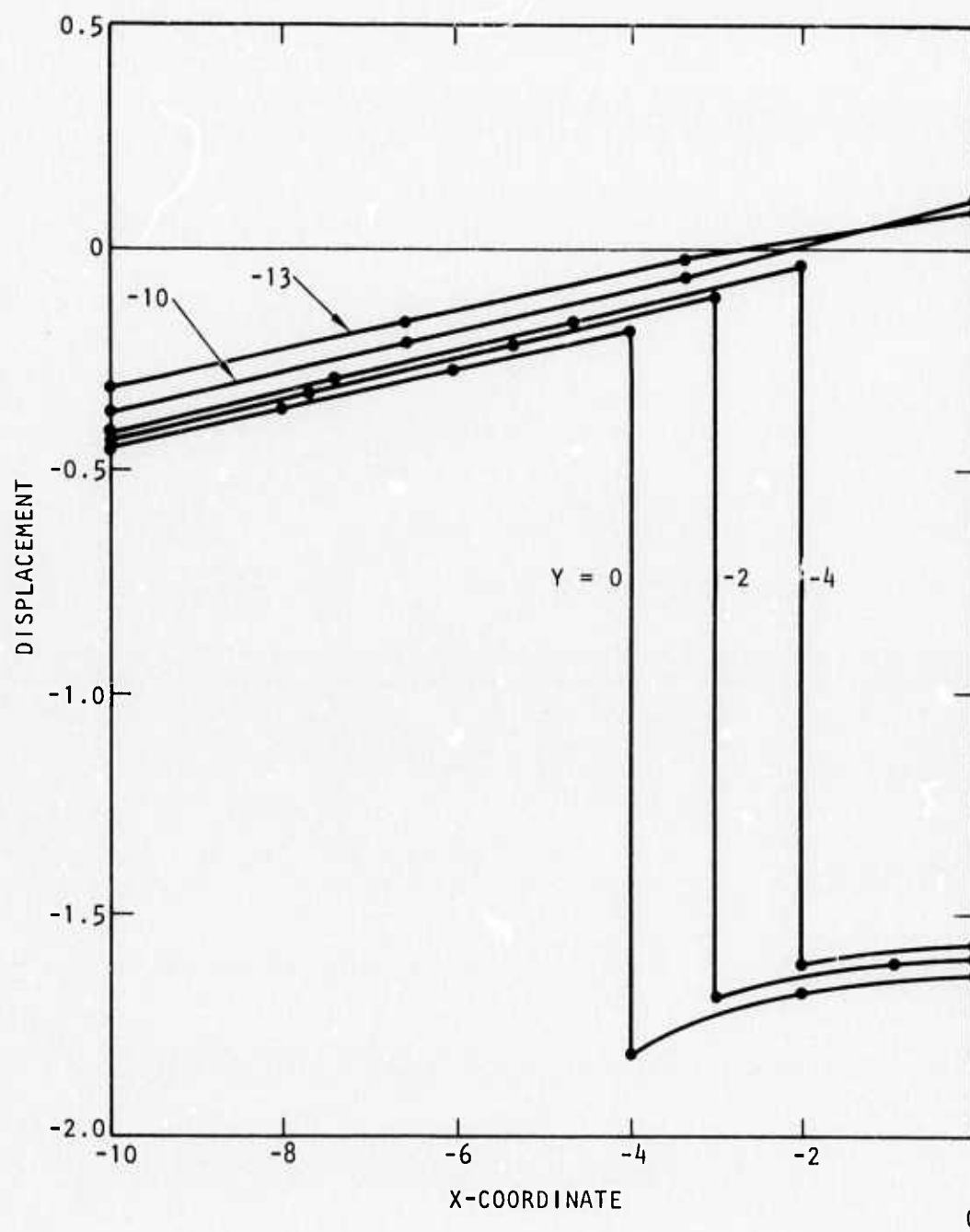


FIGURE 4-21. VERTICAL DISPLACEMENTS FOR EXAMPLE WEDGE PROBLEM



R-7215-1-2701

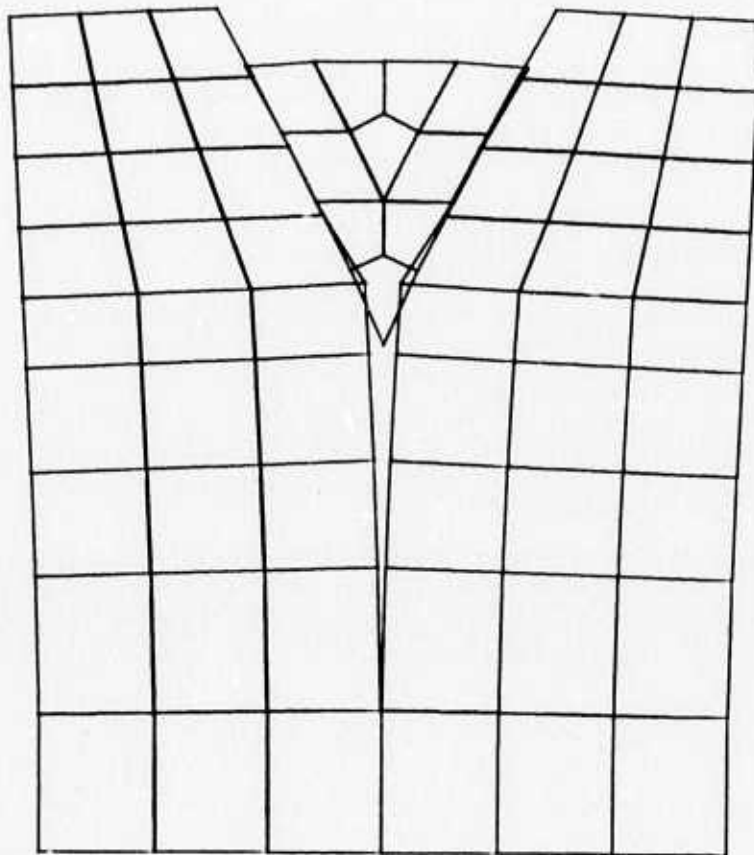


FIGURE 4-22. FINITE ELEMENT MESH IN THE DISPLACED CONFIGURATION FOR WEDGE PROBLEM IN FINAL EQUILIBRIUM STATE



REFERENCES

- 4-1. Saucier K. L., *Properties of Cedar City Tonalite*, MPC-69-9, U.S. Army Corps of Engineers, Waterways Experiment Station, June 1969.
- 4-2. LaMori, P. N., *Compressibility of Three Rocks, (A) Westerly Granite and Solenhofen Limestone to 40 Kbar and 300°C, (B) Cedar City Tonalite to 40 Kbar at Room Temperature*, DASA 2151, Battelle Memorial Institute, August 1968.
- 4-3. Jones, A. H., and N. H. Froula, *Uniaxial Strain Behavior of Four Geological Materials to 50 Kilobars*, DASA 2209, General Motors Materials and Structures Laboratory, March 1969.
- 4-4. Petersen, C. F., *Shock Wave Studies of Selected Rocks*, Stanford Research Institute, May 1969.
- 4-5. Simmons, G., "Velocity of Shear Waves in Rocks to 10 Kilobars, Part 1," *J. Geophys. Res.*, Vol. 69, No. 6, 1964, p. 1123.
- 4-6. Stephens, D. R., *Elastic Constants of Fractured Granodiorite*, UCID-15369, Lawrence Radiation Laboratory, (to be published).
- 4-7. Walsh, J. B., "The Effect of Cracks on Poisson's Ratio," *J. Geophys. Res.*, Vol. 70, No. 2, January 15, 1965.
- 4-8. Walsh, J. B., "The Effect of Cracks on Poisson's Ratio," *J. Geophys. Res.*, Vol. 70, No. 20, October 15, 1965.
- 4-9. Hill, R., *The Mathematical Theory of Plasticity*, Oxford, 1950.
- 4-10. Drucker, D. C., "A More Fundamental Approach to Stress/Strain Relations," *Proc., 1st U.S. Cong. Appl. Mech.*, ASME, 1950.
- 4-11. Drucker, D. C., "Some Implications of Work Hardening and Ideal Plasticity," *Quart. Appl. Math.*, Vol. 7, 1950, pp. 411-418.
- 4-12. Drucker, D. C., and W. Prager, "Soil Mechanics and Plastic Analysis or Limit Design," *Quart. Appl. Math.*, Vol. 10, 1952, pp. 157-175.
- 4-13. Sandler, I., and F. L. Dimaggio, *Material Model for Rocks*, DASA 2595, Paul Weidlinger Consulting Engineering, October 1970.
- 4-14. Walsh, J. B., and W. F. Brace, "A Fracture Criterion for Brittle Anisotropic Rocks," *J. Geophys. Res.*, Vol. 69, No. 16, 1964, p. 3449.
- 4-15. Griffith, A. A., "Theory of Rupture," *Proc. 1st Int. Cong. Appl. Mech.*, 1924, p. 55.



- 4-16. McClintock, F. A., and J. B. Walsh, "Friction on Griffith Cracks Under Pressure," *Proc. 4th U.S. Natl. Cong. Appl. Mech.*, 1963, pp. 1015-1021.
- 4-17. Jaeger, J. C., "Shear Failure of Anisotropic Rocks," *Geologic Magazine*, Vol. 97, 1960, pp. 65-72.
- 4-18. McLamore, R., and K. E. Grey, "The Mechanical Behavior of Anisotropic Sedimentary Rocks," *Trans.*, ASME, February 1967.
- 4-19. Mogi, K., "Effect of the Intermediate Principal Stress on Rock Failure," *J. Geophys. Res.*, Vol. 72, No. 20, October 1967, p. 5117.
- 4-20. Pariseau, W. G., "Plasticity Theory for Anisotropic Rocks and Soils," *10th Symposium on Rock Mechanics*, University of Texas, Austin, May 1968.
- 4-21. Perzyna, R., "The Constitutive Equations for Work-Hardening and Rate Sensitive Plastic Materials," *Proc. Vib. Prob.*, 3, 4, 1963. pp. 281-290.
- 4-22. Hohenemser, K., and W. Prager, *Über die Ansätze der Mechanik Isotroper Kontinua*, ZAMM, 12, 1932, pp. 216-226.
- 4-23. Dimaggio, F. L., and I. Sandler, *The Effect of Strain Rate on the Constitutive Equations of Rock*, DNA 2801T, Paul Weidlinger Consulting Engineering, October 1971.
- 4-24. Isenberg, J., and F. S. Wong, *A Viscoplastic Model with a Discussion of its Stress/Strain and Wave Propagation Properties*, R-7110-1886, Agabian-Jacobsen Associates, April 1971.
- 4-25. Perkins, R. D., and S. J. Green, *Uniaxial Stress Behavior of Porphyritic Tonalite at Strain Rates to 10^3 /Second*, DASA 2200, General Motors Manufacturing Development, February 1969.
- 4-26. Zienkiewicz, O. C., "A Numerical Method of Viscoelastic Stress Analysis," *Intl. J. Mech. Sci.*, Vol. 10, 1968, pp. 807-827.
- 4-27. Hayashi, M., and S. Hibino, "Progressive Relaxation of Rock Masses During Excavation of Underground Cavity," *Proc. Intl. Symp. on Rock Mech.*, Madrid, October 1968.
- 4-28. Soydemu, C., and W. E. Schmid, "Deformation and Stability of Viscoelastic Soil Media," *J. Soil Mech. and Found. Div.*, Proc. ASCE, Vol. 96, No. SM6, November 1970.
- 4-29. Yaghmai, S., *Incremental Analysis of Large Deformations in Mechanics of Solids with Applications to Axisymmetric Shells of Revolution*, NASACR-1350, University of California, Berkeley, June 1969.



- 4-30. Obert, L., and W. I. Duvall, *Rock Mechanics and the Design of Structures in Rock*, John Wiley and Sons, Inc., New York, 1967.
- 4-31. Evans, R. H., "The Elasticity and Plasticity of Rocks and Artificial Stone," *Leeds Philosophical and Literary Soc., Proc.*, 3, Part 3, 1966.
- 4-32. Brace, W. F., et al., "Dilatancy in the Fracture of Crystalline Rocks," *J. Geophys. Res.*, Vol. 71, No. 16, August 15, 1966.
- 4-33. Giardini, A. A., et al., "Triaxial Compression Data on Nuclear Explosion Shocked, Mechanically Shocked and Normal Granodiorite from the Nevada Test Site," *J. Geophys. Res.*, Vol. 73, No. 4, February 15, 1968.
- 4-34. Army Corps of Engineers, Missouri River Division Laboratory, *Tests for Strength Characteristics of Rock, Pile Driver Project*, MRDL-64190, 1964.
- 4-35. Flugge, W., *Viscoelasticity*, Blaisdell Publishing Co., Waltham, Mass., 1967.
- 4-36. Goodman, R. E., and J. Dubois, "Duplication of Dilatancy in Analysis of Jointed Rocks," *J. of the Soil Mechanics*, Proc. ASCE, Vol. 98, No. SM4, April 1972.
- 4-37. Goodman, R. E., et al., *Research on Strength-Deformability--Water Pressure Relationships for Faults in Direct Shear*, Final Report on ARPA Contract H0210020, University of California, April 1972.



SECTION 5

DESCRIPTION OF THE COMPUTER PROGRAM

This section describes the computer program in terms of features which are apparent to the user, such as automatic mesh generation, and in terms of its logical structure. The first part of the section describes the steps which the user takes in order to prepare the input data. The mesh generator, bandwidth reducer and plotting capability are described. The motive and logic diagrams for element renumbering are also described.

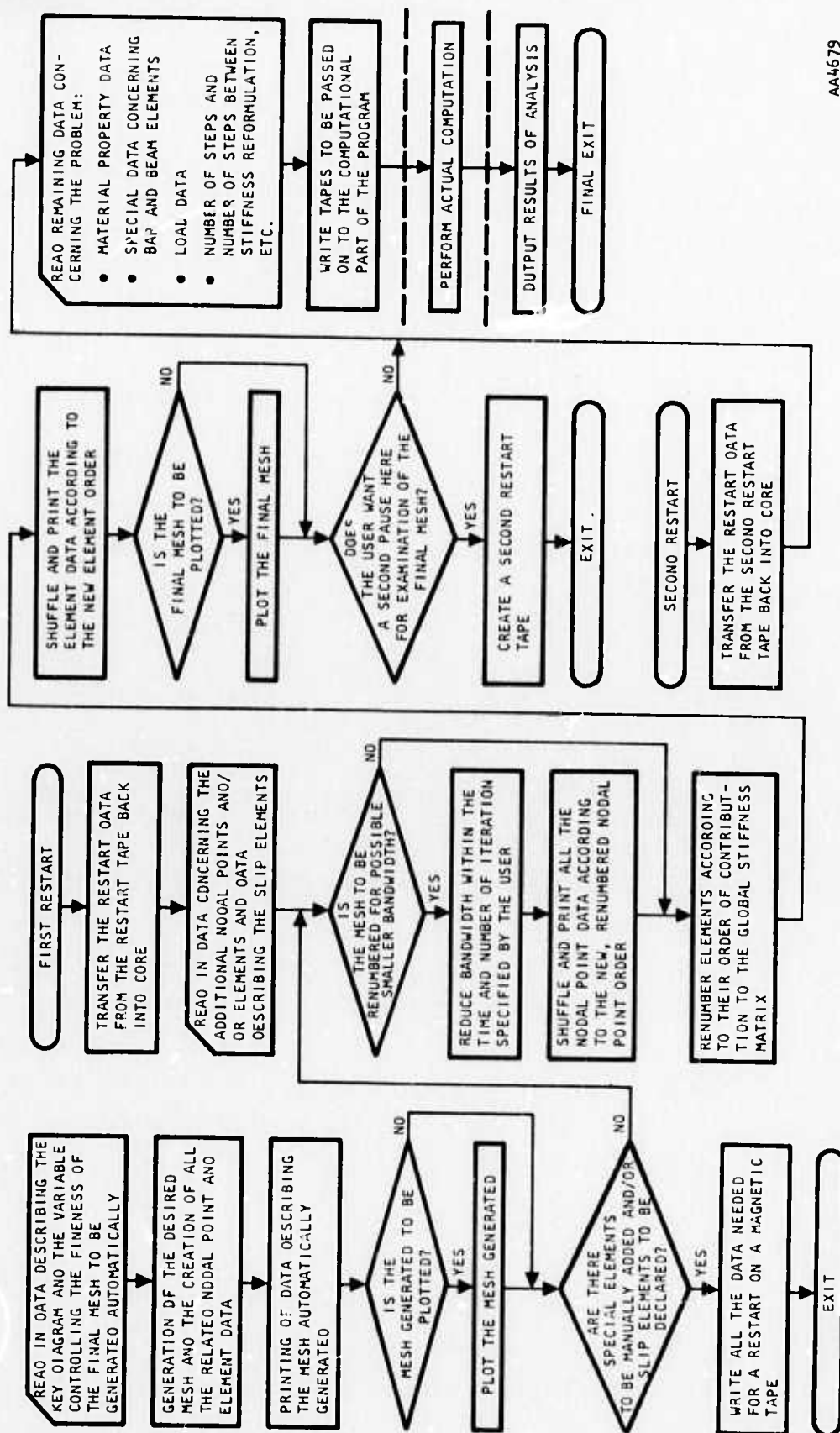
The second part of this section describes the execution part of the computer program in terms of logic diagrams. Subroutines are described which control the computation, form the global stiffness matrix and compute the load vector, form element stiffnesses and other operations. Also described is the technique of multibuffering whereby data is transferred between core and peripheral storage units at the same time that computations are being performed in core. This technique greatly improves the efficiency of the program for problems where large blocks of data are stored on peripheral memory units.

5.1 PROCESSING OF INPUT DATA

The sequence in which input data are processed is shown in Figure 5-1. There are three basic phases. The first consists of generating continuum (two- or three-dimensional) and joint elements and plotting the results. The second phase consists of adding other elements (beam, thick shell, bar, etc.) manually, reducing the bandwidth, shuffling the element numbers so that they appear in the order of contribution to the global stiffness matrix, and plotting the final mesh. The third phase consists of reading additional data such as material properties and loads.

MESH GENERATOR

The automatic mesh generation scheme incorporated in the program requires the user to provide a coarse mesh which the program refines by subdivision under the control of the user. The main goal is to minimize the



AA4679

FIGURE 5-1. OPERATIONS OF THE INPUT PORTION OF THE PRESENT COMPUTER PROGRAM



the input preparation on the part of the user. The method uses the key diagram concept described in Reference 5-1; the remainder of the present mesh generation scheme is new and original work.

The subdivision of the given, coarse mesh to obtain the final, fine mesh is carried out by subdividing each one of the mesh units, as "zones," within the coarse mesh in the following manner. Consider the simple case of a general, two-dimensional mesh, in which the basic mesh unit or zone is a parabolic quadrilateral as shown in Figure 5-2. Assume that the x and y coordinates of the four corner mesh points, 1, 2, 3, and 4, as well as those of the four midpoints, 5, 6, 7, and 8, are known. The x and y coordinates of an arbitrary point P within this zone can then be expressed conveniently in terms of the coordinates of the eight points through the use of the local, curvilinear coordinates, ξ and η , whose values range from -1 to +1 on opposite sides as indicated in Figure 5-2. Thus, one can write

$$\begin{aligned}x &= \sum_{i=1}^8 N_i x_i \\y &= \sum_{i=1}^8 N_i y_i\end{aligned}\tag{5-1}$$

in which N_i 's are the so-called "isoparametric shape functions" expressible in terms of the curvilinear coordinates as follows:

$$\begin{aligned}N_1 &= -\frac{1}{4}(1-\xi)(1-\eta)(\xi+\eta+1) \\N_2 &= -\frac{1}{4}(1-\xi)(1+\eta)(\xi-\eta+1) \\N_3 &= \frac{1}{4}(1+\xi)(1+\eta)(\xi+\eta-1) \\N_4 &= \frac{1}{4}(1+\xi)(1-\eta)(\xi-\eta-1) \\N_5 &= \frac{1}{2}(1-\xi)(1-\eta^2) \\N_6 &= \frac{1}{2}(1-\xi)(1-\eta^2) \\N_7 &= \frac{1}{2}(1-\xi^2)(1+\eta) \\N_8 &= \frac{1}{2}(1-\xi^2)(1+\eta)\end{aligned}\tag{5-2}$$



R-7215-1-2701

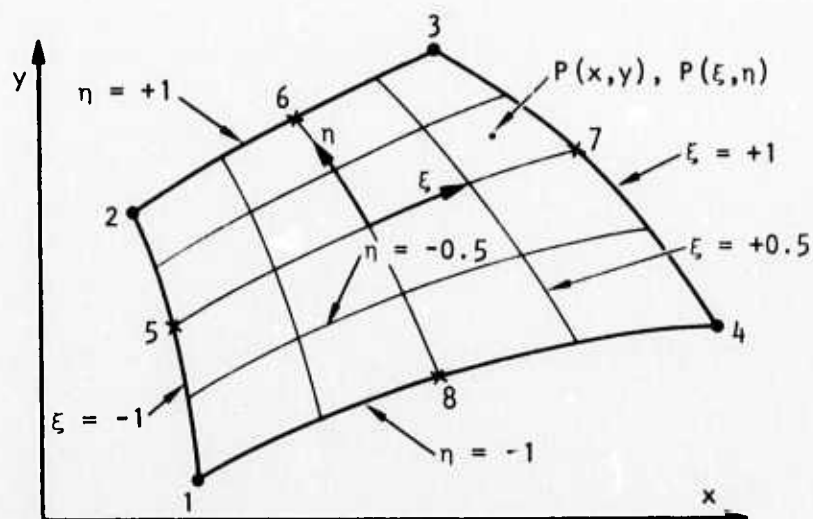


FIGURE 5-2. QUADRILATERAL ZONE, WHOSE SHAPE AND COORDINATES ARE EXPRESSED BY PARABOLIC SHAPE FUNCTIONS



Thus, for a certain set of values of the curvilinear coordinates, or "natural coordinates," the corresponding Cartesian coordinates can be easily found from Equations 5-2. Consequently, to subdivide the zone into a 4×4 mesh, for example, and establish the Cartesian coordinates of the twenty-one new mesh points, one merely substitutes into Equations 5-1 twenty-one times, each time with a different combination of values of ξ and η which are incremented successively by 0.5.

This technique can be used to treat each one of the zones in a given, coarse mesh of any configuration. The only restriction that has to be observed is that the number of subdivisions between any two adjoining zones must match. This is to satisfy the fundamental connectivity requirement of the finite element method. To satisfy this continuity requirement and to facilitate the preparation of the input that defines the basic coarse mesh, it is convenient to introduce the so-called "key diagram."

A key diagram, in general, is a rectangular grid resembling a checker-board. It has no physical dimensions. Its purpose is to present, or define, the connectivity of the zones in the coarse mesh and to facilitate defining the position of a mesh point in the form of row and column numbers in the coarse mesh. Another purpose of the key diagram is to help define the extent of subdivision of a zone, for, to satisfy the aforementioned connectivity, a newly introduced mesh line has to extend across all the zones located in the same row or column in the key diagram.

Figure 5-3 illustrates the generation of a simple finite element mesh representing a dam and part of its foundation. The domain has been blocked into three zones which are connected as shown in the accompanying key diagram. The final mesh is the result of subdividing the first and the last zone into two subdivisions and the second into three subdivisions in the vertical direction, and all three zones into three subdivisions in the horizontal direction.



R-7215-1-2701

KEY DIAGRAM

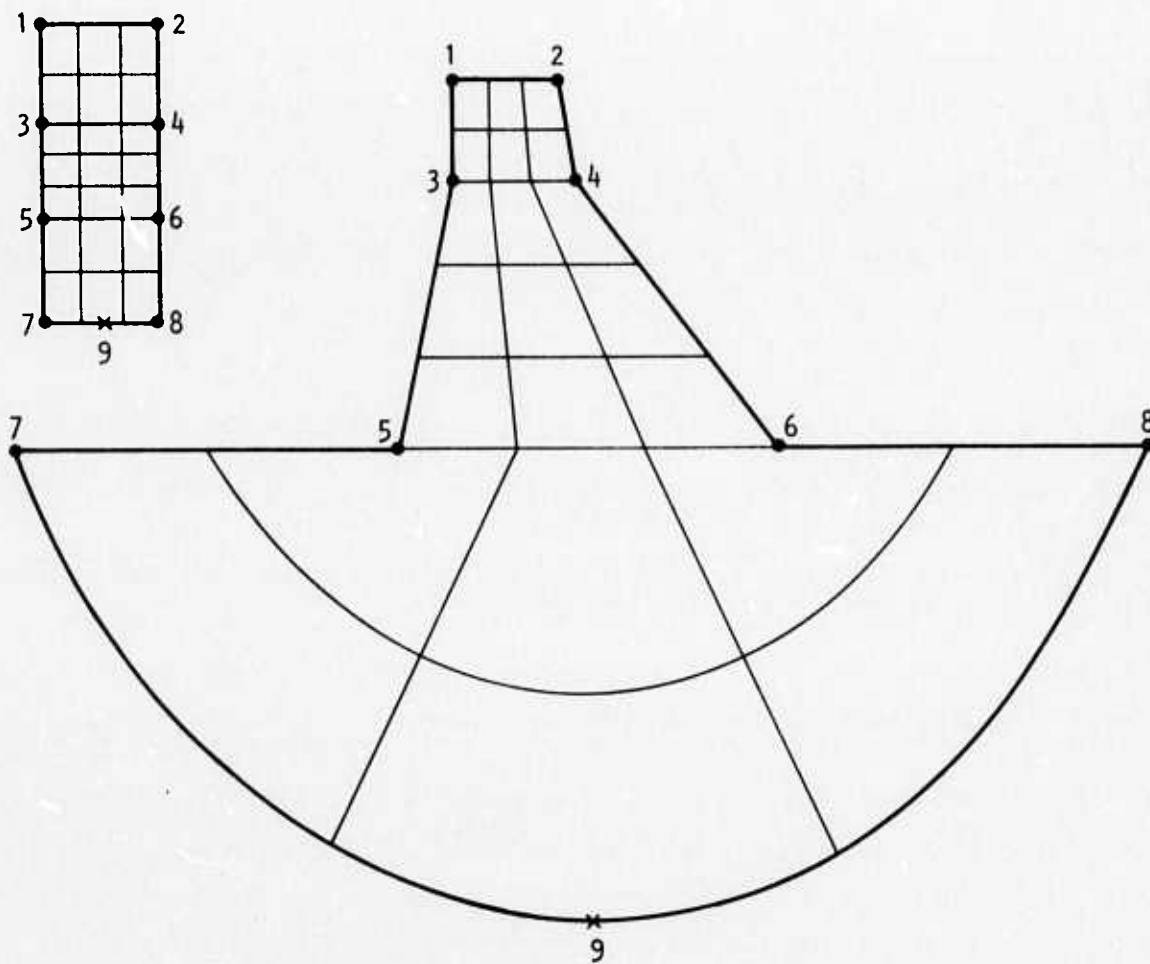


FIGURE 5-3. KEY DIAGRAM AND RESULTING FINITE ELEMENT MESH FOR A DAM AND FOUNDATION



The input to the program for this particular example would consist of the following:

- a. A statement that the key diagram, or the original coarse mesh, is 3 by 1.
- b. The rectangular coordinates of the given, eight mesh points and those of the single midpoint that define the lower boundary on a curve.
- c. Three material numbers to associate the first two zones with concrete and the third with the soil medium.
- d. The three numbers, 2, 3 and 2, that specify the number of subdivisions in the vertical direction, and the number 2 for the horizontal direction.

The computer program would assign the material number for a zone to all of the elements that are created in the zone, and number the nodal points and elements in the final mesh column-wise, from the top to the bottom, from the left toward the right by referring to the key diagram. The curved mesh lines in the third zone are meant only to emphasize the fact that nodal points are generated on a second degree curve because of the nature of the shape function; the actual mesh line is always a straight line between two neighboring mesh points.

In the previous example, if the user is not satisfied with the refinement of the final mesh or with that in any one of the zones, he can quickly rerun the problem by modifying the four integers mentioned in Item d without having to change any of the data mentioned in the first three items which define the given, coarse mesh. This is perhaps the most important feature of this particular mesh generation scheme.

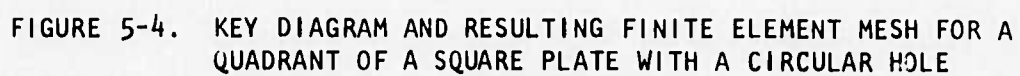
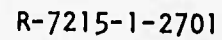


Aside from being used to define an edge of a zone on a curve, a midpoint can also be used to imply a mesh grading. The mesh shown in Figure 5-4 is the result of specifying the three midpoints, M_1 , M_2 and M_3 , purposely off-centered and toward the edge of the circular hole. Midpoints M_1 and M_2 are there merely to form the edge of the hole on a curve. In this particular example, number of subdivisions of 5 and 5 in the vertical direction (in the key diagram) and of 16 in the horizontal direction were specified.

Another feature that makes the scheme versatile and powerful is the provision for the user to prescribe a zone as void merely by assigning zero for the material number of that zone. With this provision, one can easily generate a mesh around a notch or a cutout. The mesh around a tunnel shown in Figure 5-5 is such an example.

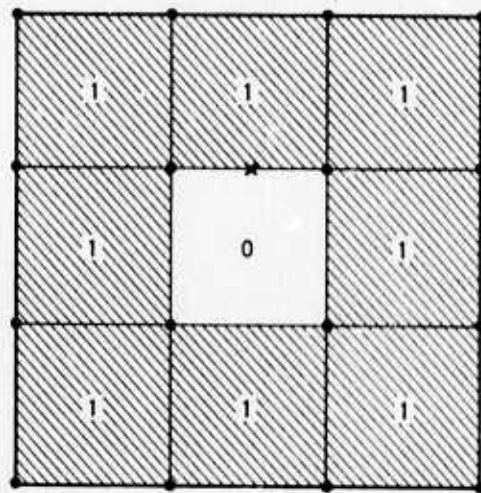
The final feature to be mentioned here is the program's ability to join any two edges in the key diagram. This makes it possible to produce the meshes shown in Figures 5-6 and 5-7. The user may prefer the type of mesh shown in Figure 5-7 over that shown in Figure 5-5 for the radiating pattern of the mesh lines which makes it easier to make a finer mesh around the edge of the tunnel.

The same scheme can be used to generate a three-dimensional mesh. The necessary changes are to replace the two-dimensional shape function and key diagram by their three-dimensional counterparts, and to introduce the third Cartesian coordinate. The basic "zone" or "block" in this case is a general, six-sided body with parabolic edges. It has eight corner nodes and twelve midpoints as shown in Figure 5-8, and the Cartesian coordinates at an arbitrary point P within the block having the natural coordinates ξ , η and ζ are expressible in terms of the Cartesian coordinates of the twenty controlling points as follows:

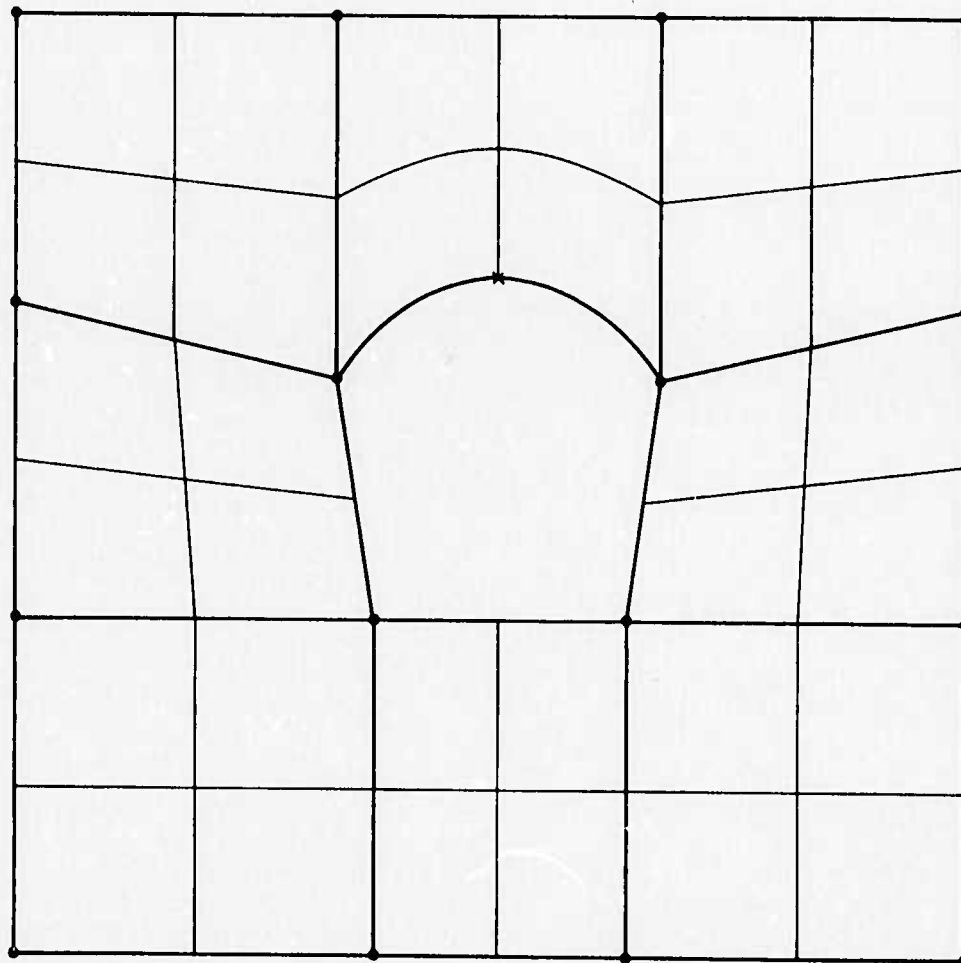




R-7215-1-2701



KEY DIAGRAM



AA4680

FIGURE 5-5. KEY DIAGRAM AND RESULTING FINITE ELEMENT MESH FOR A TUNNEL

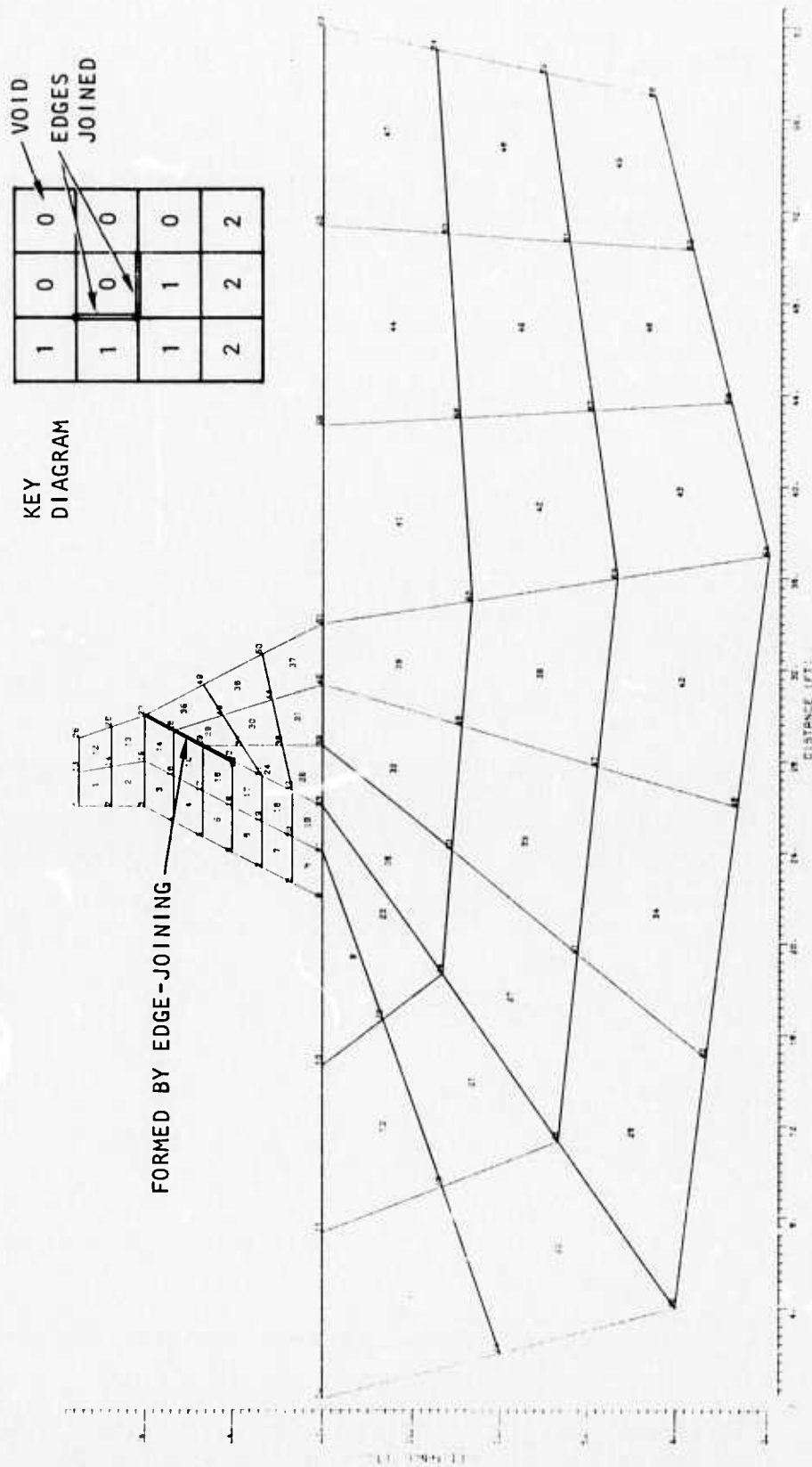


FIGURE 5-6. KEY DIAGRAM AND RESULTING FINITE ELEMENT MESH FOR A DAM ON FOUNDATION, ILLUSTRATING CAPABILITY TO JOIN ANY TWO EDGES IN THE KEY DIAGRAM

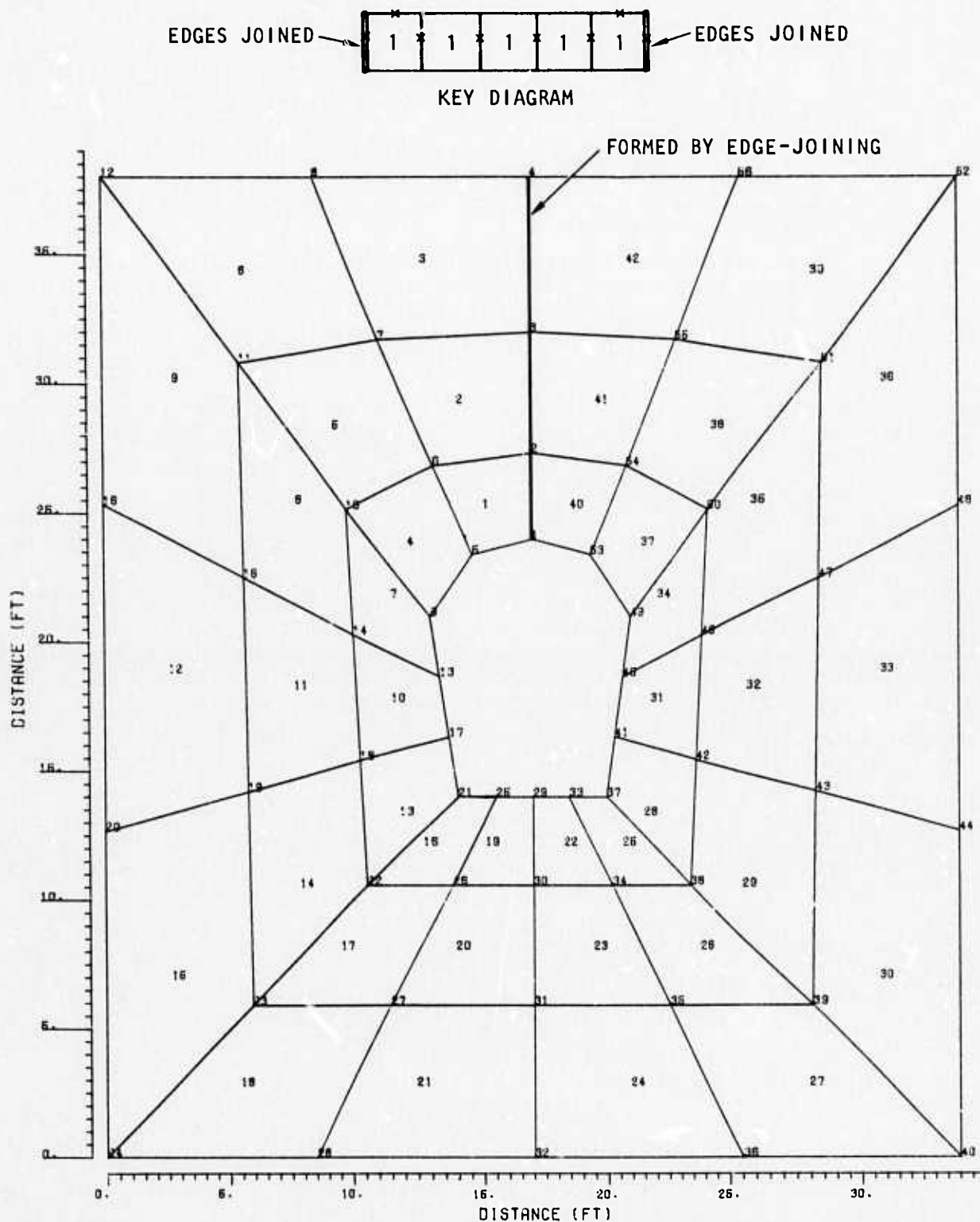


FIGURE 5-7. KEY DIAGRAM AND RESULTING FINITE ELEMENT MESH FOR A TUNNEL, ILLUSTRATING CAPABILITY TO JOIN ANY TWO EDGES IN THE KEY DIAGRAM



R-7215-1-2701

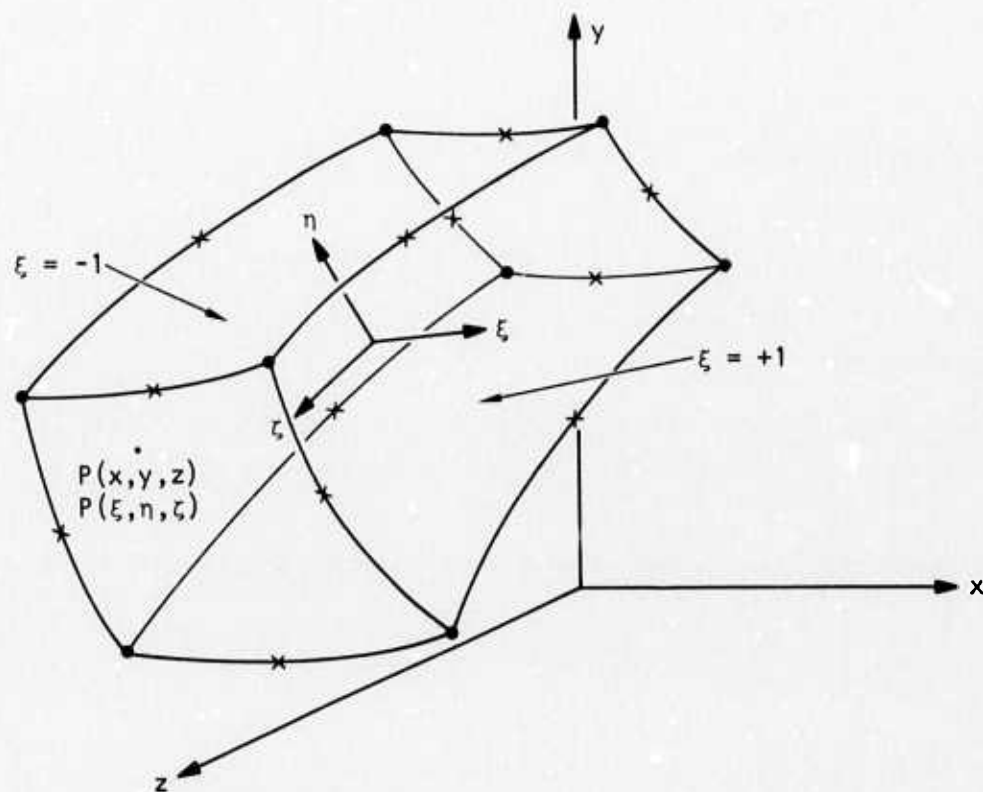


FIGURE 5-8. THREE-DIMENSIONAL ZONE WHOSE SHAPE AND COORDINATES ARE EXPRESSED BY PARABOLIC SHAPE FUNCTIONS



$$\begin{aligned}x &= \sum_{i=1}^{20} N_i x_i \\y &= \sum_{i=1}^{20} N_i y_i \\z &= \sum_{i=1}^{20} N_i z_i\end{aligned}\tag{5-3}$$

where, for corner points,

$$N_i = \frac{1}{8} (1 + \xi_i \xi) (1 + \eta_i \eta) (1 + \zeta_i \zeta) (\xi_i \xi + \eta_i \eta + \zeta_i \zeta - 2) \tag{5-4}$$

and for midpoints,

$$N_i = \frac{1}{4} (1 - \xi^2) (1 + \eta_i \eta) (1 + \zeta_i \zeta) \quad \text{for points with } \xi_i = 0$$

$$N_i = \frac{1}{4} (1 + \xi_i \xi) (1 - \eta^2) (1 + \zeta_i \zeta) \quad \text{for points with } \eta_i = 0$$

$$N_i = \frac{1}{4} (1 + \xi_i \xi) (1 + \eta_i \eta) (1 - \zeta^2) \quad \text{for points with } \zeta_i = 0$$

As before, zero can be used as material number to imply void or cavity, and a midpoint can be so specified as to imply a curved edge as well as a mesh grading along the edge. Instead of joining two edges, one can now join any two interfaces as long as the meshes on them are compatible. Some three-dimensional meshes automatically generated in this manner are illustrated in Figures 5-9 and 5-10.

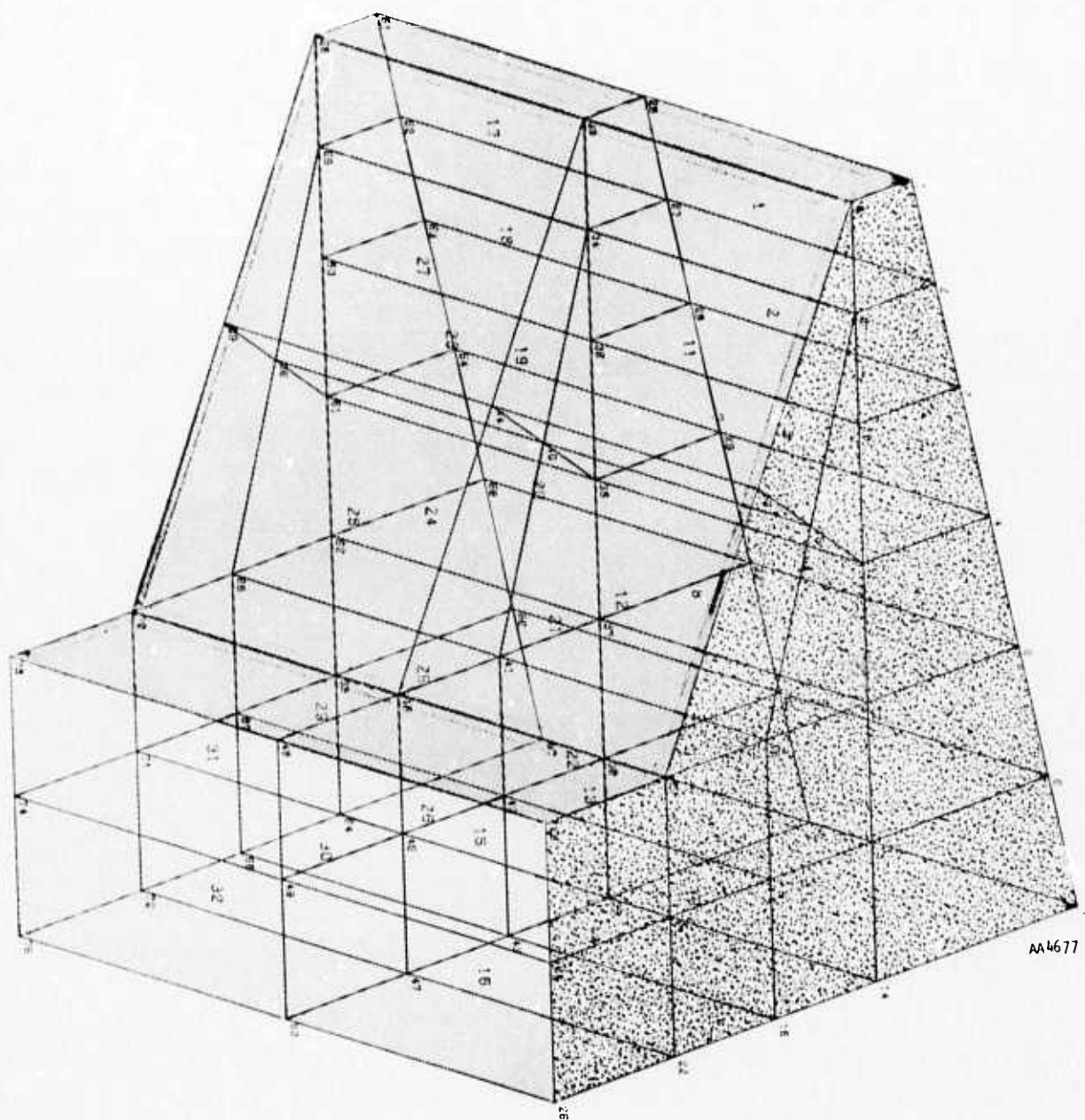


FIGURE 5-9. AUTOMATICALLY GENERATED THREE-DIMENSIONAL MESH

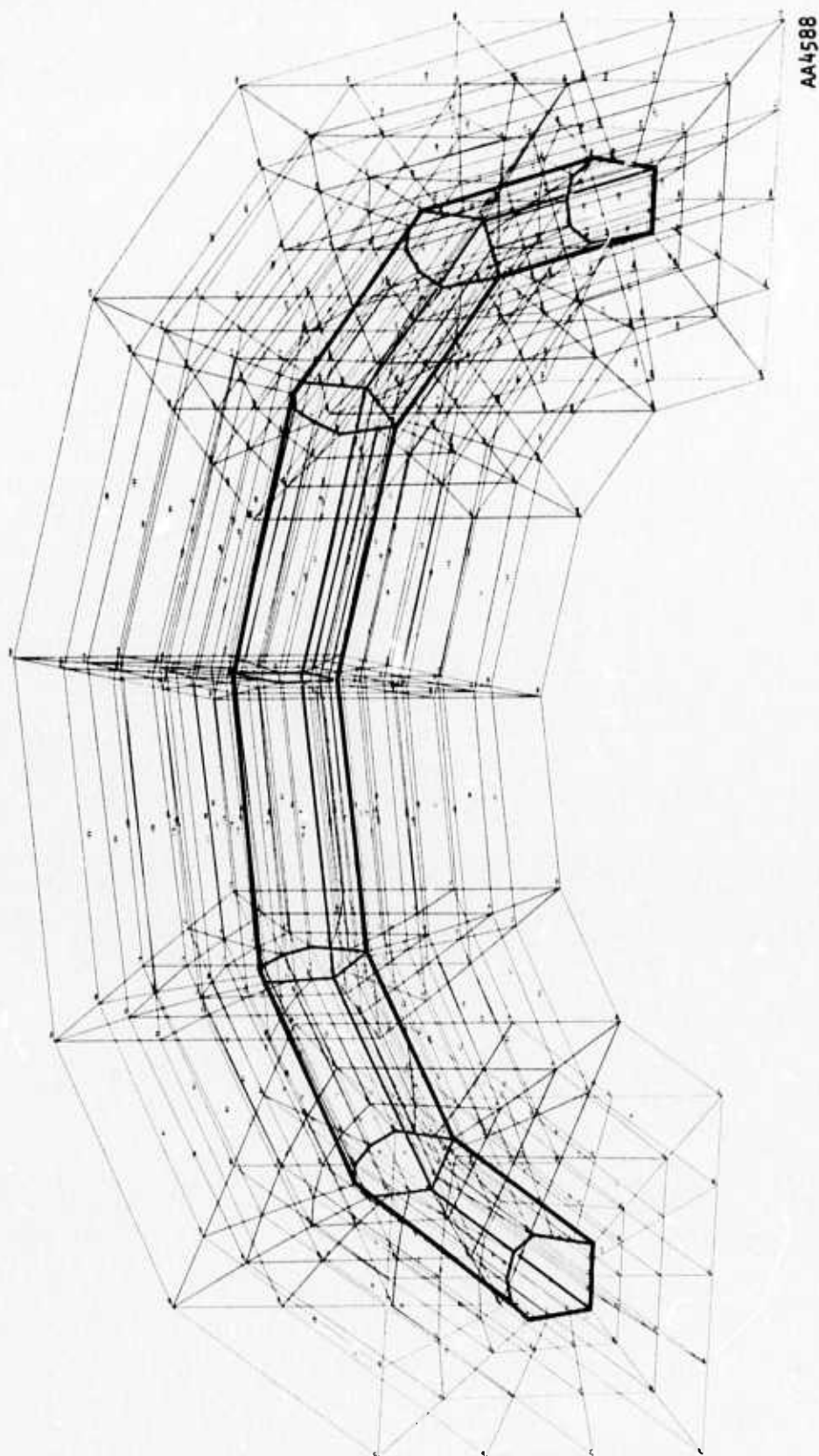


FIGURE 5-10. THREE-DIMENSIONAL FINITE ELEMENT MESH REPRESENTING A TUNNEL (PREPARATION TIME, INCLUDING FURTHER REFINEMENT OF ANY SECTION--ABOUT 1 HOUR)



BANDWIDTH REDUCER

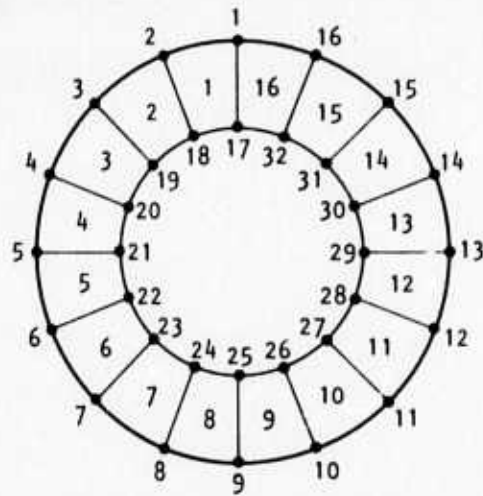
The computer time required to perform a computation is approximately proportional to the square of the bandwidth. Thus it is important to aim for a minimum bandwidth when numbering nodal points. However, when the finite element mesh is generated automatically by the technique described above, no attention whatever is paid to minimizing bandwidth. The user can influence the bandwidth to some extent by judicious choice of key diagram. Nevertheless, it is very likely that the bandwidth so generated will not be optimum. The situation will often be made worse when elements are added manually. To help alleviate this difficulty and thus encourage the user to use the automatic mesh generator, a bandwidth reducer is included in the present computer program.

The function of the bandwidth reducer is shown in Figure 5-11. The INPUT NODAL POINT configuration is typical of the mesh which would be generated automatically for which the maximum difference in nodal point numbers for any element is 31. This configuration was submitted to the bandwidth reducer. The result, after 2 sec of computation time by the bandwidth reducer is the REDUCED NODAL POINT configuration, for which the maximum difference in node numbers is 6. That this configuration is not optimum is shown by the IDEAL configuration for which the maximum difference is 5. Thus, the technique is not optimum because it does not always converge to the minimum bandwidth in the computer time which the user has selected. Also, the technique operates on nodal point numbers rather than on degree of freedom numbers. Thus, when several types of elements are mixed, the configuration corresponding to minimum difference in node numbers does not necessarily correspond to minimum bandwidth.

Logic diagrams for the bandwidth reducer are shown in Figures 5-12 and 5-13.

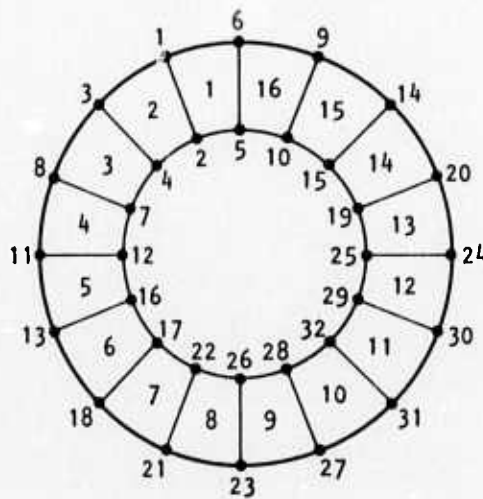
ELEMENT NUMBERING

In addition to renumbering nodal points to reduce the bandwidth of the global stiffness matrix, the elements are numbered in the order of their contribution to the global stiffness matrix. In this way, the strain/



INPUT NODAL POINT CONFIGURATION

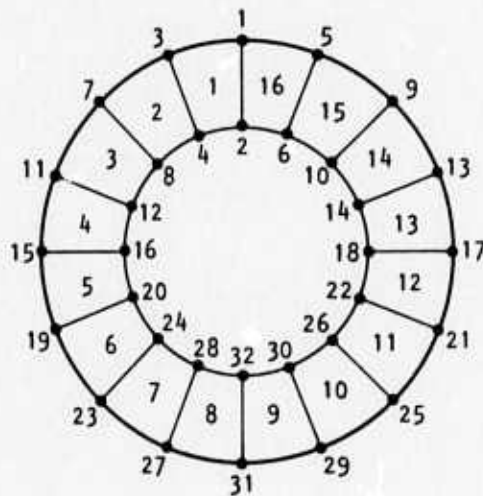
MAXIMUM NODAL POINT DIFFERENCE = 31



REDUCED NODAL POINT CONFIGURATION

MAXIMUM NODAL POINT DIFFERENCE = 6

SOLUTION TIME = 2 SECONDS



IDEAL CONFIGURATION

MAXIMUM NODAL POINT DIFFERENCE = 5

AA4681

FIGURE 5-11. EXAMPLE OF BANDWIDTH REDUCER

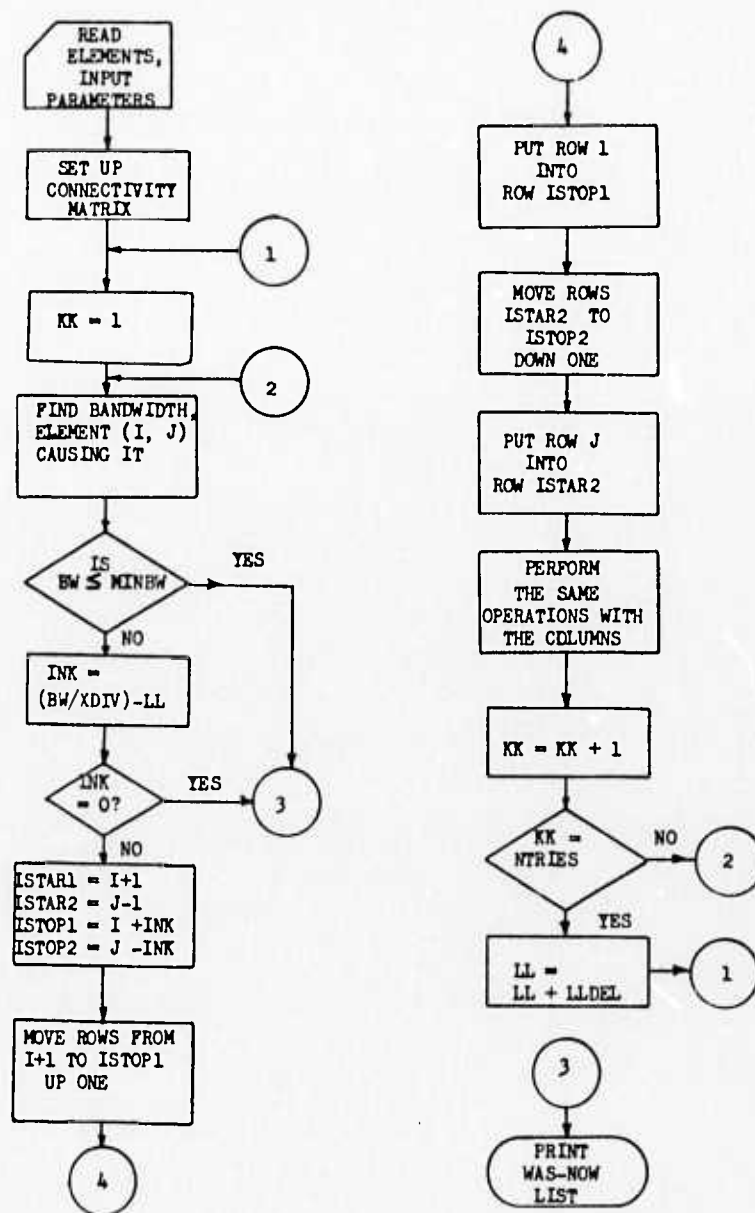
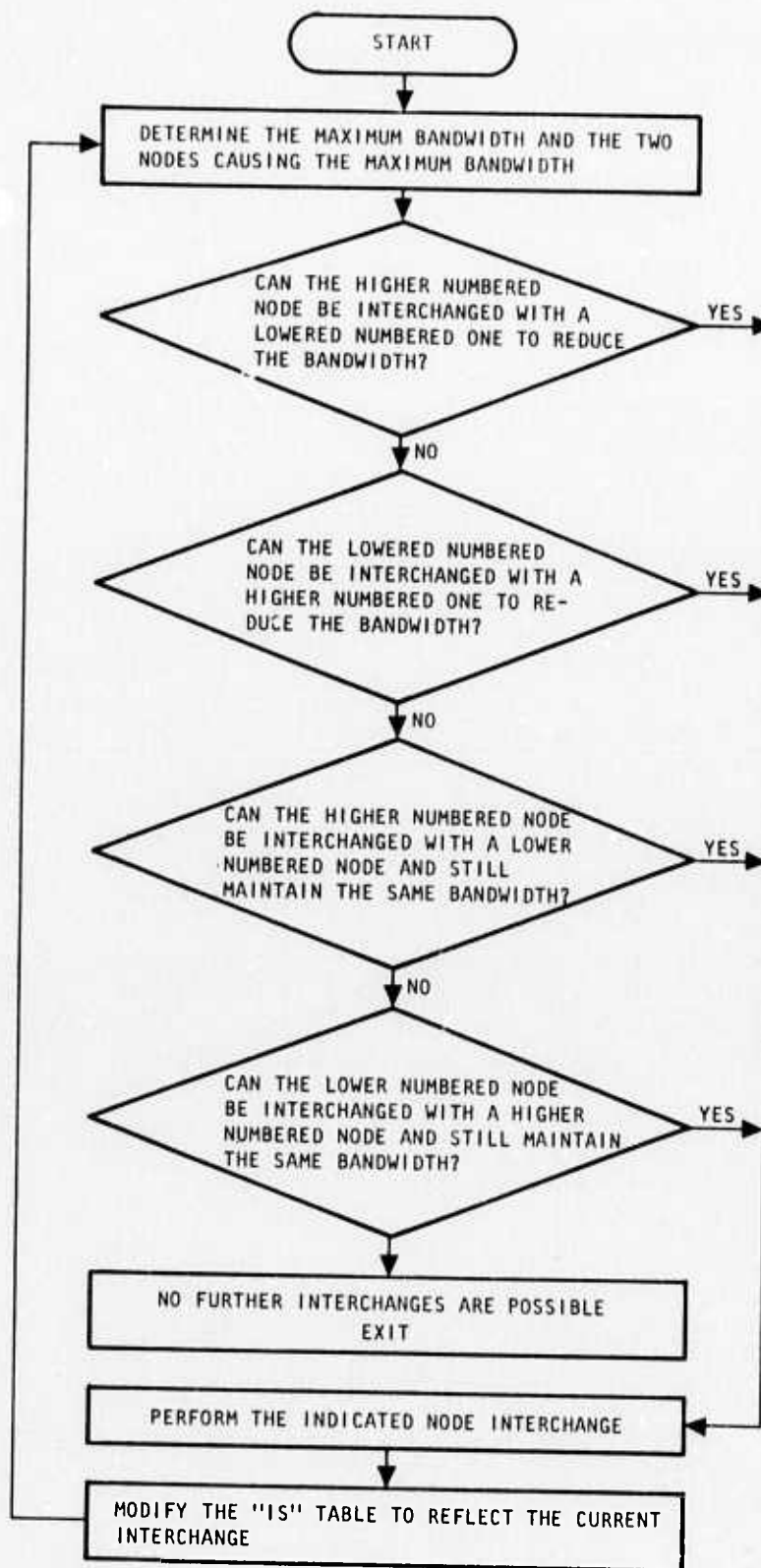


FIGURE 5-12. PROCEDURE USED IN BANDWIDTH REDUCER (REFERENCE 5-2)



AA4659

FIGURE 5-13. PROCEDURE USED IN BANDWIDTH REDUCER (REFERENCE 5-3)



stiffness matrixes can be retrieved from peripheral storage in the least time. Since the element data are used in the basic operations of forming the global stiffness matrix and effective load vector, the efficiency gained by performing these complicated operations is essential.

The element numbers assigned by the mesh generator and the user are revised such that

$$\begin{aligned} \min(\text{LM}(I)) \text{ for the } n^{\text{th}} \text{ element} &\leq \\ \min(\text{LM}(I)) \text{ for the } n+1^{\text{th}} \text{ element} \end{aligned}$$

where

$\text{LM}(I)$ = Array of degree of freedom members for the element

Element data are stored sequentially on peripheral storage units such that the data for Element 1 is at the head of the unit, and then in sequence

$$\text{Element Number} = 1 \leq \dots n, n+1 \dots \leq \text{NUMEL}$$

where

NUMEL = Total number of elements

In order to modify the effective load vector F , to obtain the matrix C of stress/strain coefficients and to obtain element stresses and strains, an array containing the previous loads F , the displacements u and the incremental displacements du is brought into core as shown in Figure 5-15. Also required are data stored on the element data tape such as the strain/displacement transformation matrixes and LM arrays for the elements of interest. As shown in Figure 5-14, all degrees of freedom to which Element n contributes are found in a sequence of F , u , du array one bandwidth (MBAND) long. Thus it is possible to process to F , u , du array by reading the element data tape only once.

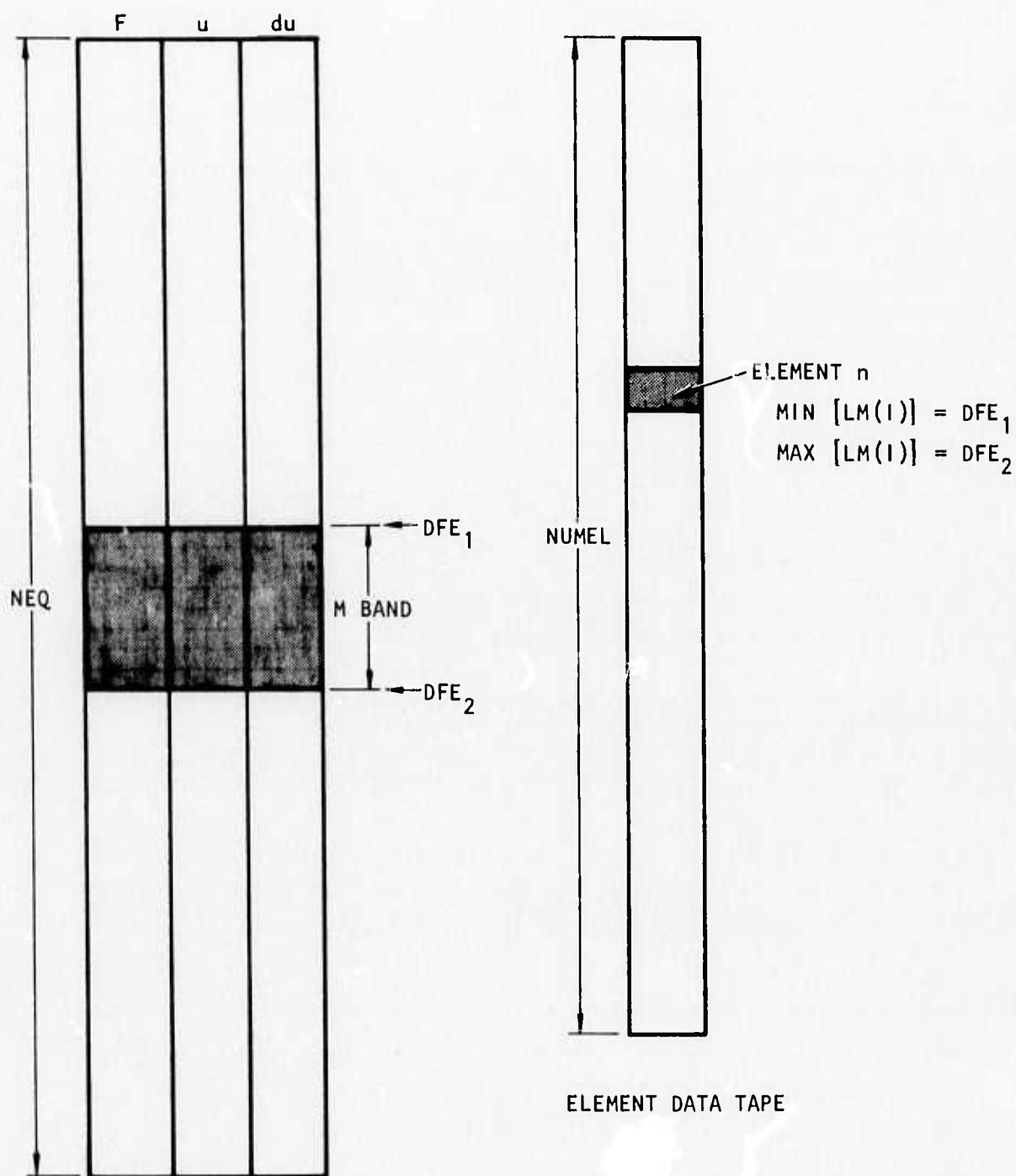


FIGURE 5-14. OPERATION ON FORCE, DISPLACEMENT AND INCREMENTAL DISPLACEMENT ARRAYS



In order to assemble the global stiffness matrix, which is stored in blocks, Block nn is brought into core as shown in Figure 5-15. At the same time, data from Element n is made available from the element data tape. Element n fits entirely into Block nn . Elements n , $nn + 1$, etc. are processed so long as

$$DFE_1 \geq DFK_2$$

and

$$DFE_2 \leq DFK_2$$

In this event, element stiffness is directly added to the appropriate rows and columns of Block nn . If

$$DFE_1 \geq DFK_2$$

and

$$DFE_2 > DFK_2$$

it signifies that Element n contributes to Block nn and to Block $nn + 1$. In this event, those contributions which can be made to Block nn are made, and the stiffnesses and LM arrays of those elements which contribute also to Block $nn + 1$ are written temporarily on storage unit T1 for subsequent insertion into Block $nn + 1$. Elements are processed and their stiffnesses are added to Block nn and or accumulated on T1 until

$$DFE_1 > DFK_2$$

This signifies that Block nn of the global stiffness matrix is prepared except for data stored on unit T0, which contains element data overlapping Blocks $nn - 1$ and nn . This data is read into core and that part for which

$$DFE_1 < DFK_1$$



R-7215-1-2701

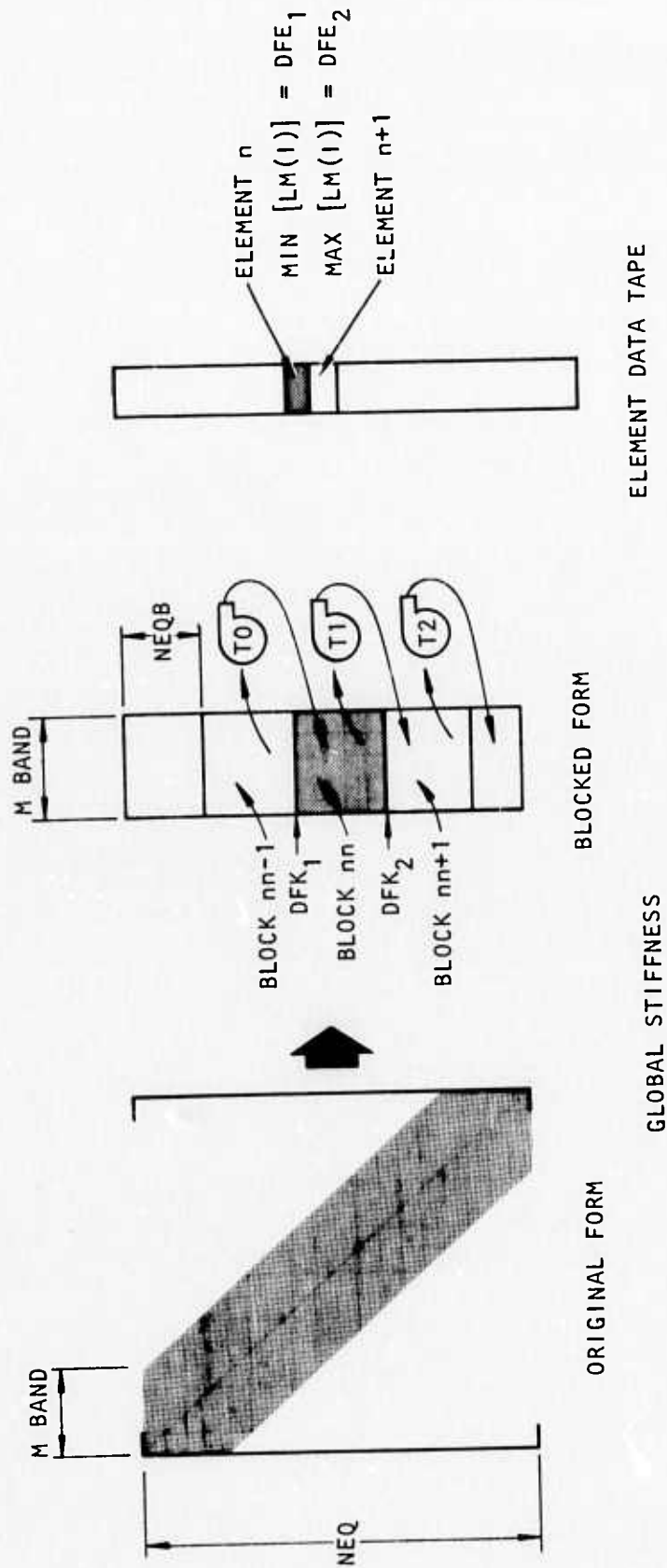


FIGURE 5-15. GENERATION OF GLOBAL STIFFNESS MATRIX FROM ELEMENT DATA



is added to Block nn . Now Block nn is completely prepared and is moved out of core while Block $nn + 1$ is brought into core. Block $nn + 1$ is filled in the same way as Blocks $nn - 1$ and nn , which is by passing sequentially through the element data array. When all direct contributions to Block $nn + 1$ have been made and all data which contributes to Block $nn + 2$ has been stored on unit T2, the data stored on unit T1 is read into core and added to Block $nn + 1$. This block is now completely prepared and is transferred to peripheral storage.

SIMULATION OF THE CONSTRUCTION AND EXCAVATION SEQUENCE

The construction and excavation sequence will be represented by modification of the material properties of the elements involved. Initially elements will be assigned to the regions to be constructed or excavated later. A flag will indicate the time of the addition or subtraction of each element. In case of excavation, the elements of that region will have the appropriate material properties and will contribute to the global stiffness of the system up to the indicated time, beyond which the contribution of these elements to the global stiffness of the system will be zero. The reverse of this procedure will be applied to the elements of the regions to be constructed later. All these operations will be performed in the element package.

SELF-LOADING

The initial state of the system will be assumed to be stress free. Then the dead load, if any, will be applied in a specified number of increments prior to the application of the external load. It is necessary to apply the self-loading incrementally due to the fact that the system is, in general, nonlinear.



5.2 EXECUTION PHASE OF PROGRAM

The execution phase of the program is summarized in Figures 5-16 through 5-21. The controlling program is BMCALC, Figure 5-16. The first main operation is to form the effective load vector and global stiffness matrix, which is performed by Subroutine KFORM, Figure 5-17. The assembly of the global stiffness from the element stiffnesses is performed by Subroutine BSTIF, Figure 5-18. Subroutines FWRT, TDRUM and FILLFU transfer data from peripheral storage to core.

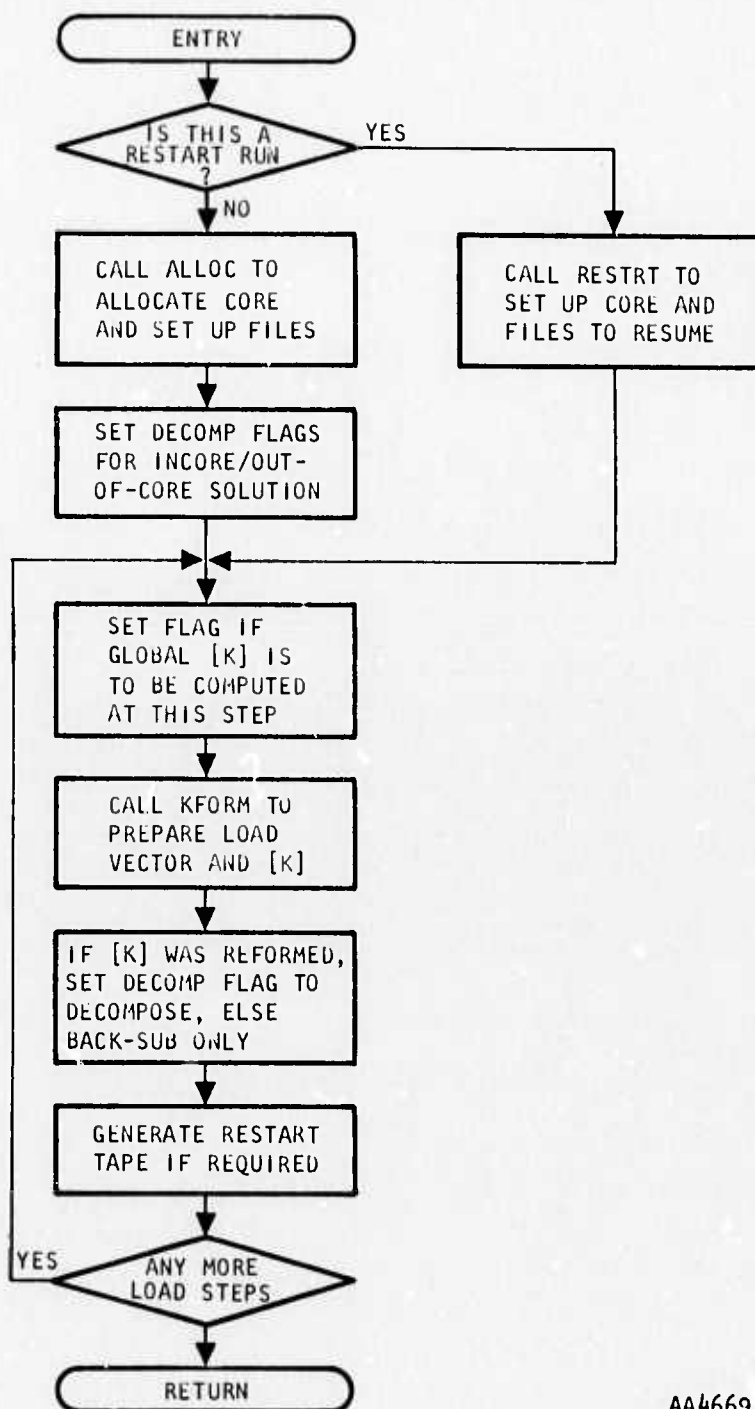
5.2.1 MULTIBUFFERING TECHNIQUE

Multibuffering is a technique whereby central processor wait time for all binary Read/Write operations involving the peripheral storage of data is minimized. (Formatted I/O operations such as card reading, punching, and printing are not included in this discussion.) The reason for using multibuffering techniques is that data moves faster between core locations than between peripheral storage and core.

The problem which multibuffering overcomes is the standard I/O feature of higher level programming languages, such as FORTRAN, which requires that when an I/O operation (READ or WRITE) is initiated, computation ceases until the I/O operation is completed. This feature assures the user that data he may wish to use is in core before he tries to use it. The amount of time the program must wait for completion of I/O operations depends on (1) the access time and (2) the data transfer time. These times depend on the type of peripheral device being used and the amount of data to be transferred. Thus, as the amount of peripheral storage increases, the time spent waiting for completion of I/O operations increases and for large volumes of data the I/O time may control overall run times. Multibuffering minimizes the wait time of these I/O operations by allowing computations to proceed *at the same time data transfer from peripheral storage is occurring*. This requires standard FORTRAN I/O operations to be replaced. This is possible on most large scale scientific computers by the use of special machine-dependent



R-7215-1-2701

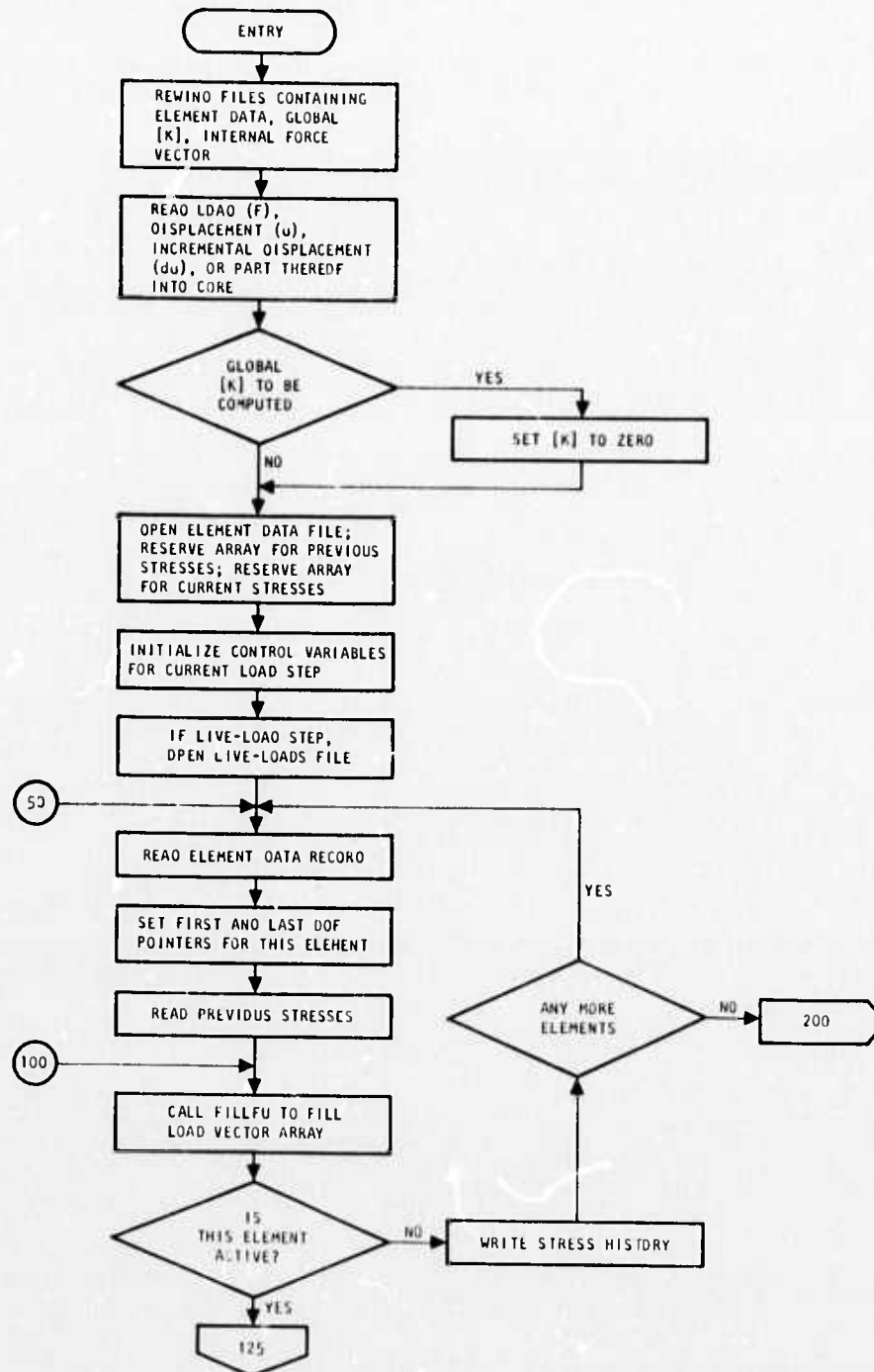


AA4669

FIGURE 5-16. PROGRAM BMCALC--CONTROLS MAIN OPERATIONS OF THE COMPUTATION SECTION



R-7215-1-2701

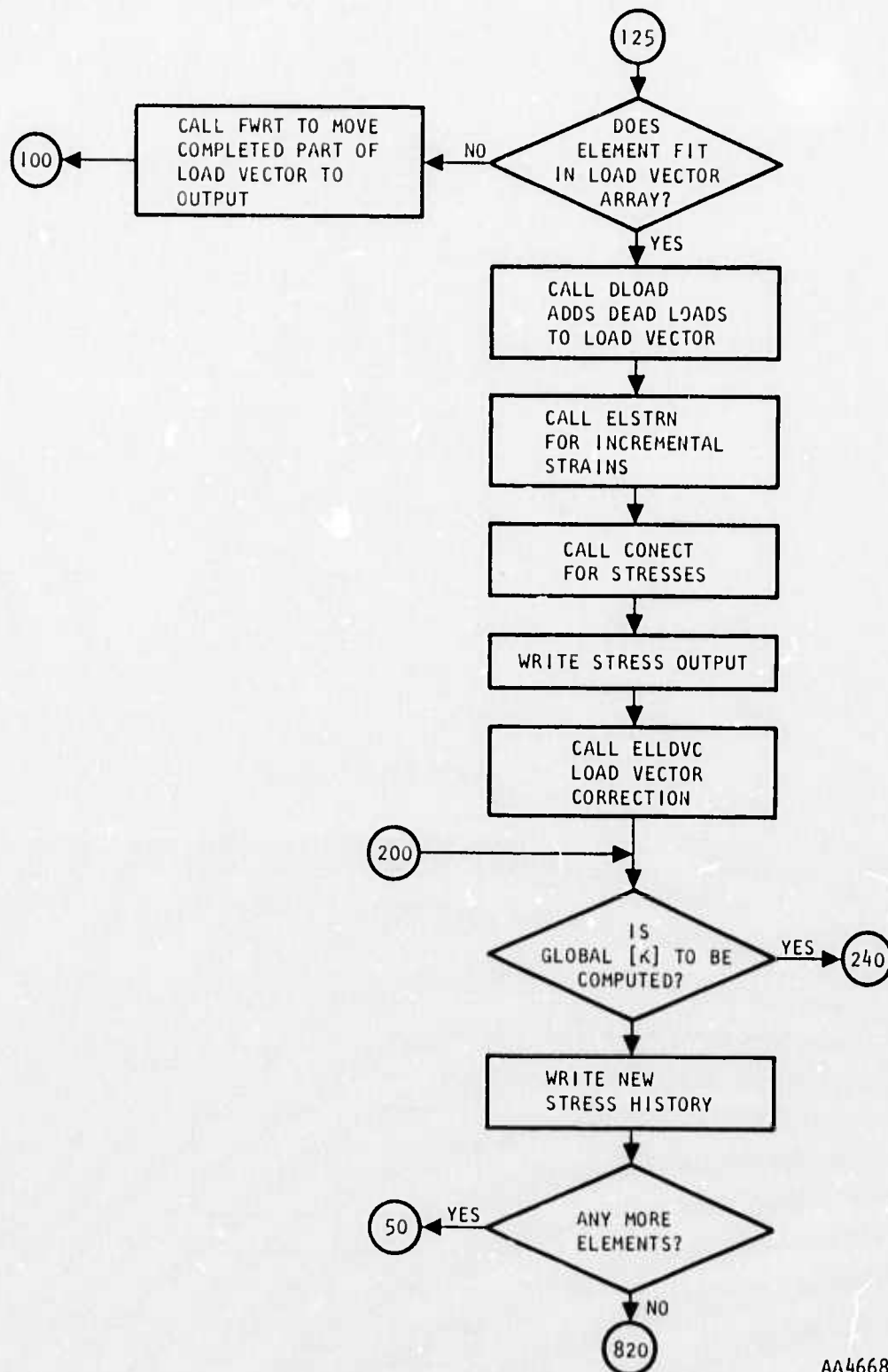


AA4664

FIGURE 5-17. SUBROUTINE KFORM--CALLS SUBROUTINES TO COMPUTE THE LOAD VECTOR AND GLOBAL STIFFNESS

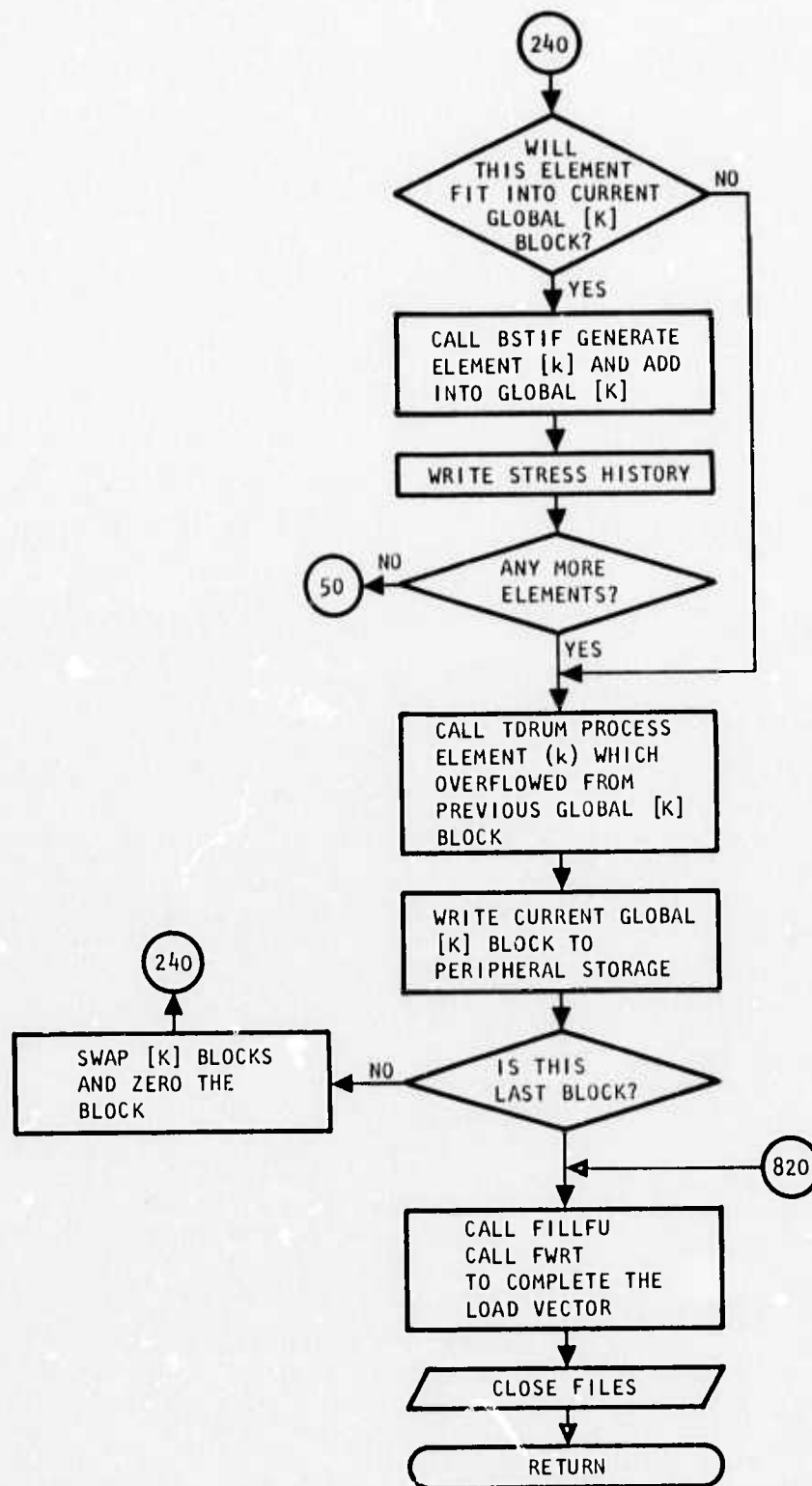


R-7215-1-2701



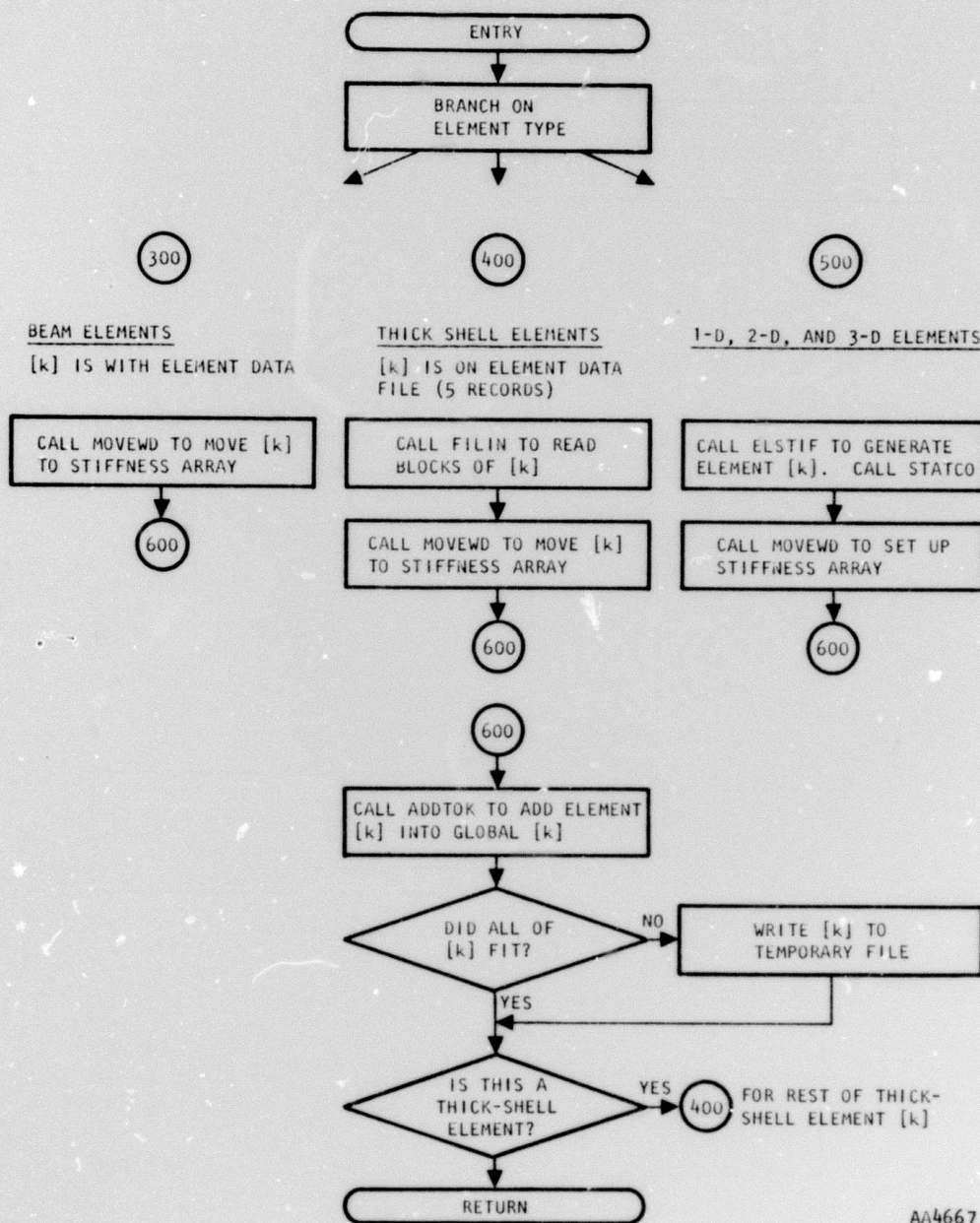
AA4668

FIGURE 5-17. (CONTINUED)



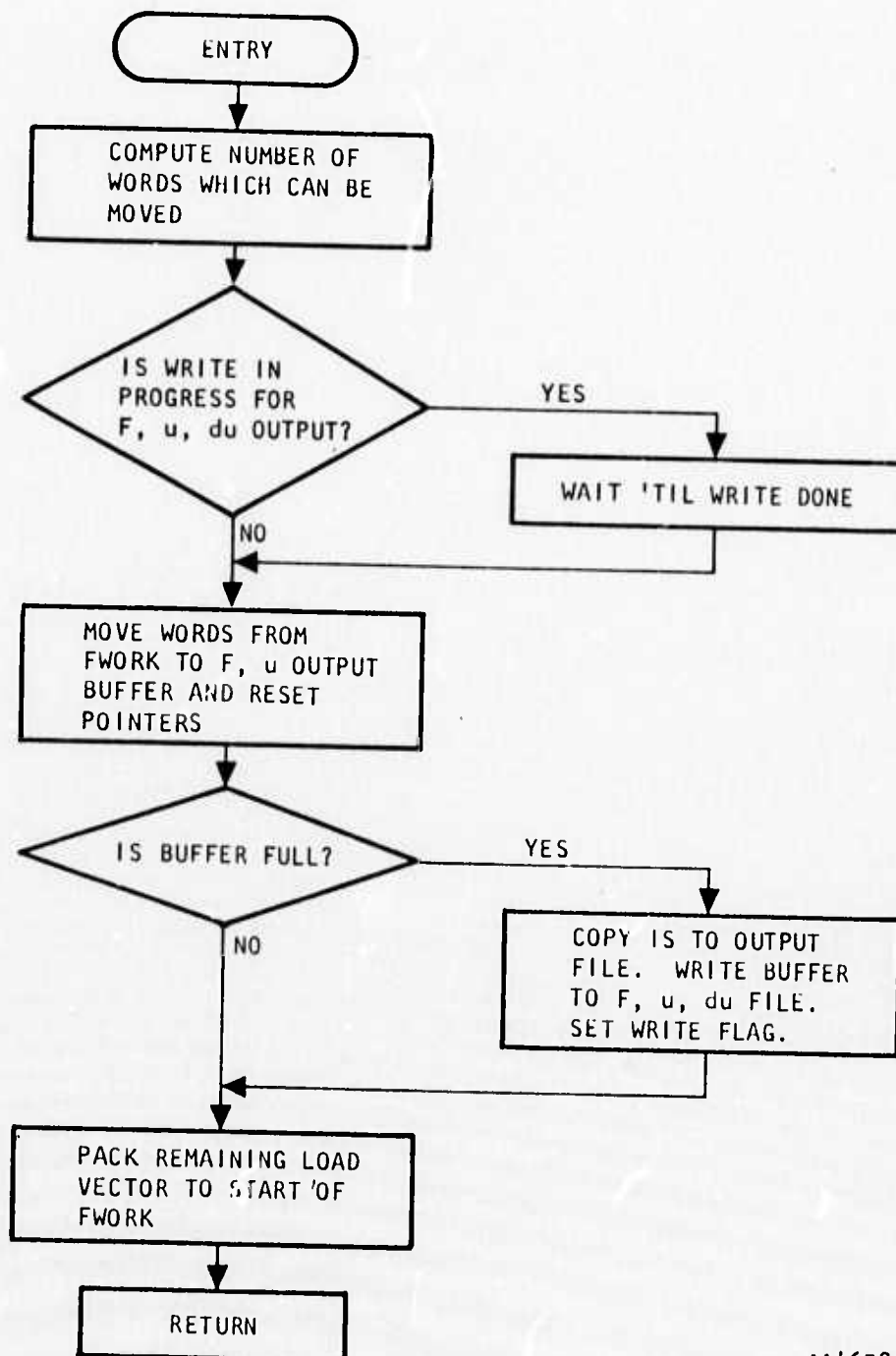
AA4671

FIGURE 5-17. (CONTINUED)



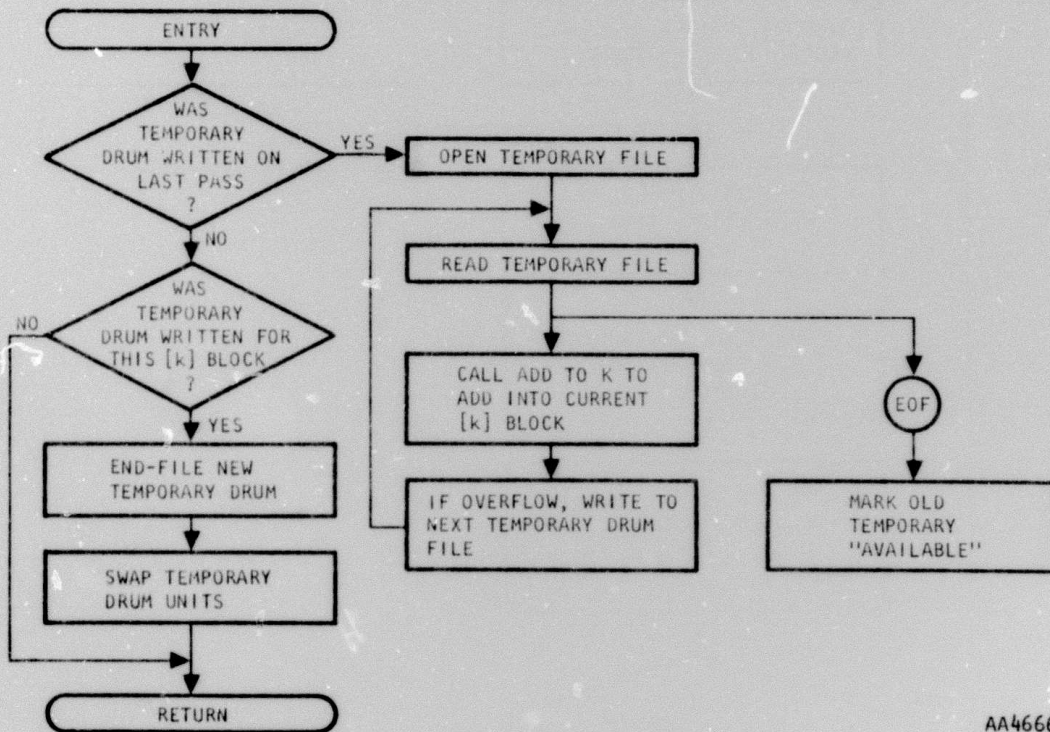
AA4667

FIGURE 5-18. SUBROUTINE BSTIF--COMPUTER ELEMENT STIFFNESS [k] AND ADDS TO GLOBAL [k]



AA4658

FIGURE 5-19. SUBROUTINE FWRT--MOVES DATA FROM LIVE LOAD VECTOR (FWORK) TO F, u, du OUTPUT BUFFER AND TO u OUTPUT FILE



AA4666

FIGURE 5-20. SUBROUTINE TDRUM--ADDS IN ELEMENT [k] WHICH OVERFLOWED FROM PREVIOUS BLOCK OF [k]

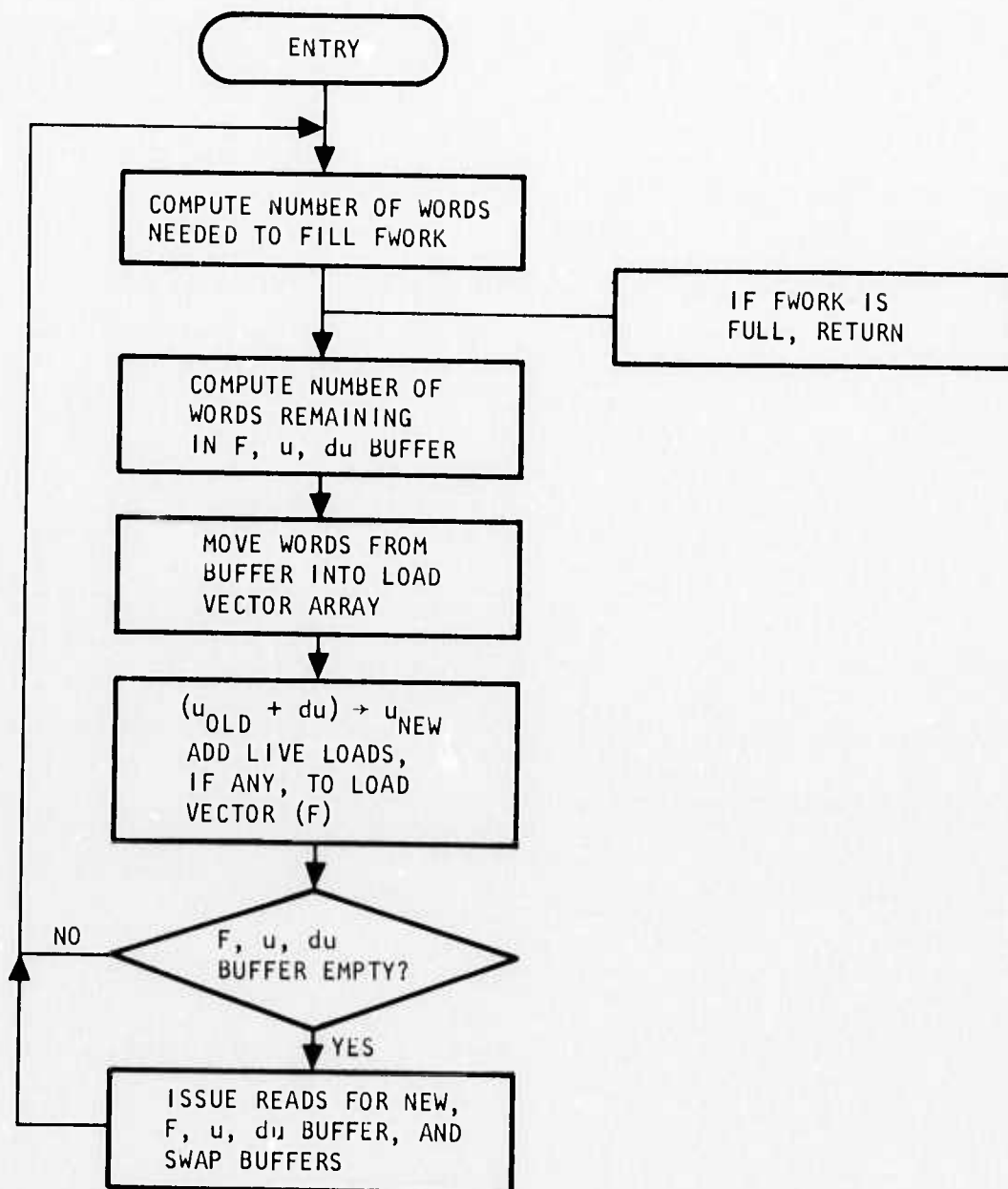


FIGURE 5-21. SUBROUTINE FILLFU--ADDS LIVE LOADS TO LOAD VECTOR, UPDATES DISPLACEMENTS, FILLS BUFFER AREA WITH F, u, du ARRAY



statements or subroutines. These interface routines are generally different on each machine and, unless care is exercised, a program may become machine dependent. This danger is avoided in the present application of multibuffering by isolating all I/O statements in one subroutine which may easily be modified when moving the program to a different machine.

A general multibuffering scheme to perform computations on a set of data stored on peripheral devices is shown in Figure 5-22. This scheme, which is incorporated in the present computer program, requires either the amount of main storage used for buffers to be increased or the size of each buffer to be decreased relative to the buffer size that might be used with standard FORTRAN I/O procedures. Since most of the main storage is already used in determining buffer sizes, the latter alternative is employed. Extensive testing and previous experience have shown that, although the number of I/O operations increases, multibuffering results in substantial overall reduction in computer run time for a given problem. Savings increase with the problem size and thus the volume of data on peripheral storage increases.

5.2.2 BAND SOLVER

The solution of large structural systems requires the solution of a set of linear simultaneous equations of the form

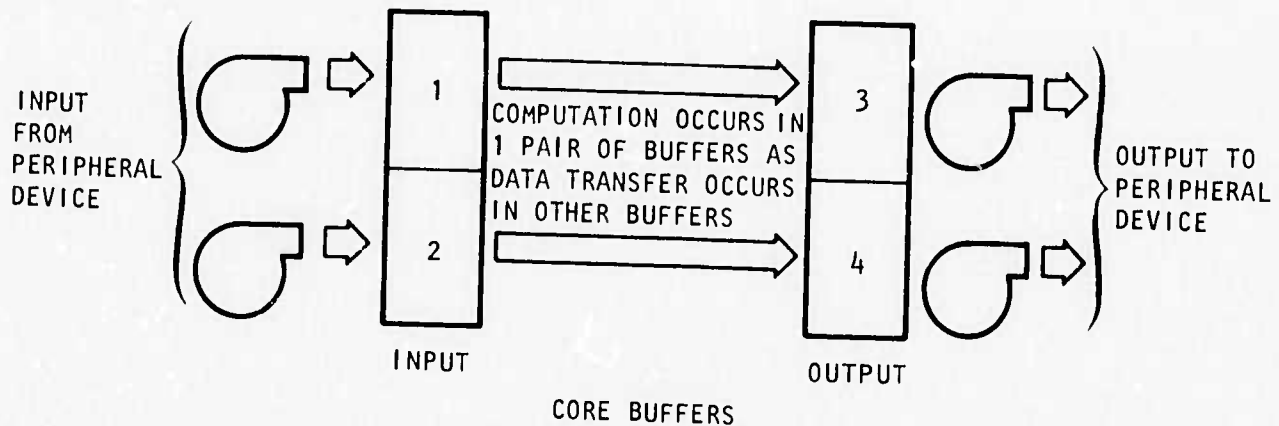
$$\{F\} = [K] \{u\} \quad (5-5)$$

where

$\{F\}$ is a vector of applied loads

$\{u\}$ is a vector of unknown displacements or, as in the present case, displacement increments

$[K]$ is the global stiffness matrix. In the present case it is banded and positive definite



- a. Initiate read of data into (1)
- b. Test for completion of Step a data transfer
- c. Initiate read of data into (2)
- d. Perform computation on data in (1) storing results of computation in (3)
- e. Initiate write of data in (3)
- f. Test for completion of Step c data transfer; if incomplete, stop computation until completed.
- g. Initiate read of data into (1)
- h. Perform computation on data in (2) storing results in (4)
- i. Test for completion of Step e data transfer
- j. Initiate write of data in (4)
- k. Test for completion of Step g data transfer
- l. Loop to Step c until all data has been processed
- m. Test for completion of final buffer operation

FIGURE 5-22. TYPICAL OPERATION OF MULTIBUFFERING TECHNIQUE



Many methods of obtaining a solution to Equation 5-5 are available. A frequently used method is the Choleski Decomposition Method. Defining

$$[K] = [L] [D] [L]^T \quad (5-6)$$

where

[L] is a lower triangular matrix with ones on the diagonal terms

[D] is a diagonal matrix

then substituting Equation 5-6 into Equation 5-5

$$\{F\} = [L] [D] [L]^T \{u\} \quad (5-7)$$

and defining

$$\{Z\} = [D] [L]^T \{u\} \quad (5-8)$$

Equation 5-7 becomes

$$\{F\} = [L] \{Z\} \quad (5-9)$$

There are many algorithms for solving Equations 5-8 and 5-9. The algorithms used in this code are (Reference 5-4).

$$L_{ij} = \frac{1}{D_j} \left[K_{ij} - \sum_{m=1}^{i-1} L_{im} D_m L_{jm} \right] \quad i > j \quad (5-10)$$

$$D_j = K_{jj} - \sum_{m=1}^{j-1} D_m L_{jm}^2 \quad (5-11)$$

$$Z_i = F_i - \sum_{m=1}^{i-1} L_{im} Z_m \quad (5-12)$$

$$U_j = \frac{Z_j}{D_j} - \sum_{m=j+1}^n L_{mj} U_m \quad (5-13)$$



where

n = Total number of equations

i, j = Row and column indices

The use of Equations 5-10 and 5-11 to obtain the $\{L\}$ and $\{D\}$ matrices in the most general case of a block-by-block solution is illustrated in Figures 5-23 through 5-25. Figure 5-23 shows a typical banded stiffness matrix with the arrangement of the terms in each core block. Although shown as a two-dimensional array, the actual locations of storage may be consecutive. Figure 5-24 shows a method of assigning core storage to allow the double buffering scheme of Section 5.2.1 to be used. The indicated Scratch Core area may be of any size (it must be at least four words in length) and is used as a buffer area to save columns of the reduced stiffness matrix needed for reduction, i.e., decomposition of future stiffness blocks. All I/O operations between the scratch area of core and peripheral devices use the technique of Section 5.2.1. Thus storage and retrieval of intermediate data required for the computation of $\{L\}$ and $\{D\}$ may in the optimum case be performed at core speed. Only a single output buffer is shown in Figure 5-24. This presents no contradiction to the double buffering scheme. Figure 5-25 shows that between initiation of the write and storage of new data in the output buffer many calculations are performed. Tests have shown that this calculation time is greater than the data transfer time thus allowing a single output buffer to be used. Figure 5-25 shows the sequence of operations in decomposing the stiffness matrix. The generation of $\{Z\}$ (from Equation 5-12) may be performed at the same time $\{L\}$ and $\{D\}$ are generated.

After completing decomposition of the stiffness matrix and generating the $\{Z\}$ matrix, the displacements $\{u\}$ are computed by Equation 5-13. Figure 5-26 shows the sequence of operations in computing the $\{u\}$ matrix.



R-7215-1-2701

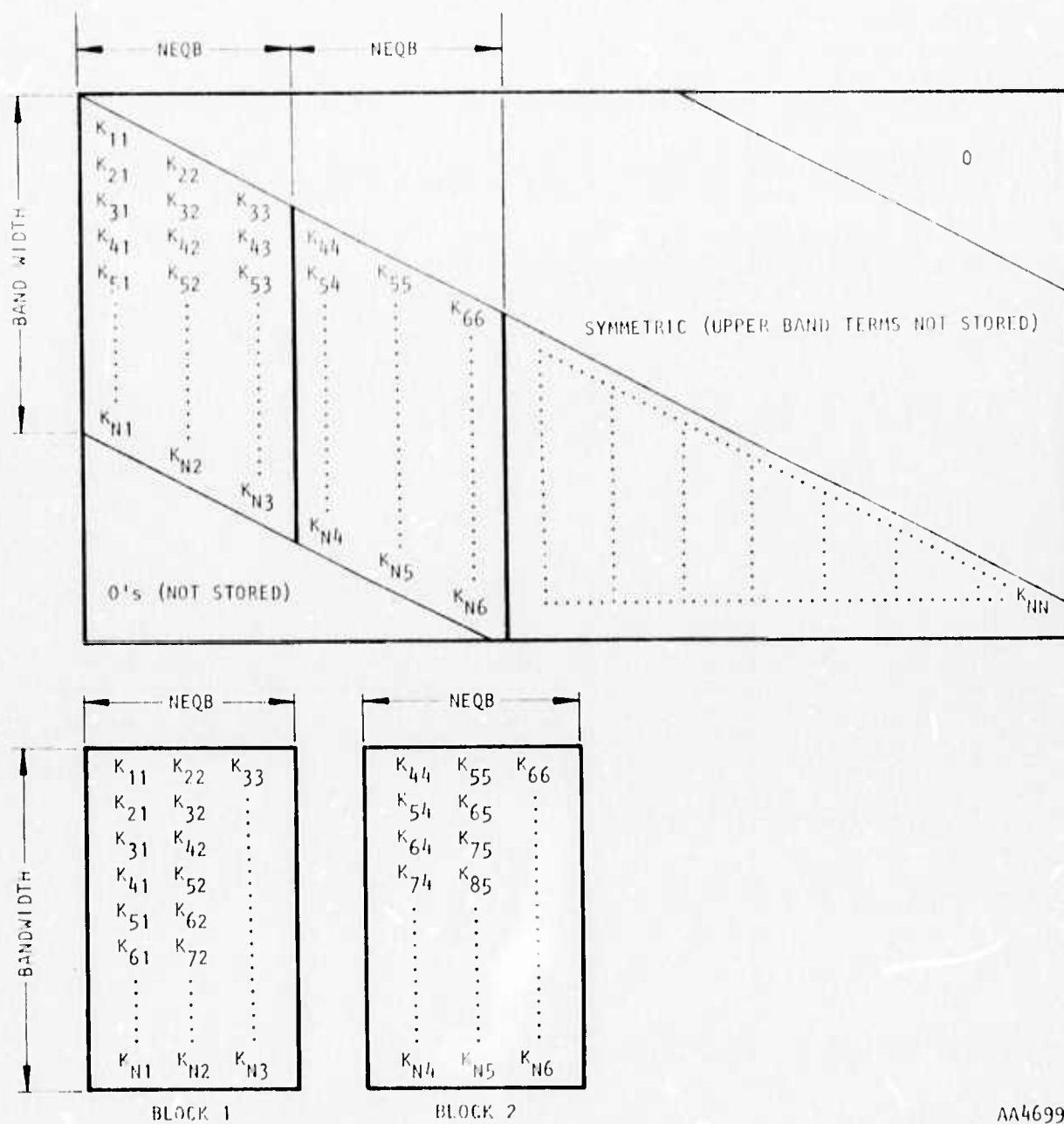


FIGURE 5-23. METHOD OF STORING STIFFNESS MATRIX USED IN PRESENT PROGRAM



R-7215-1-2701

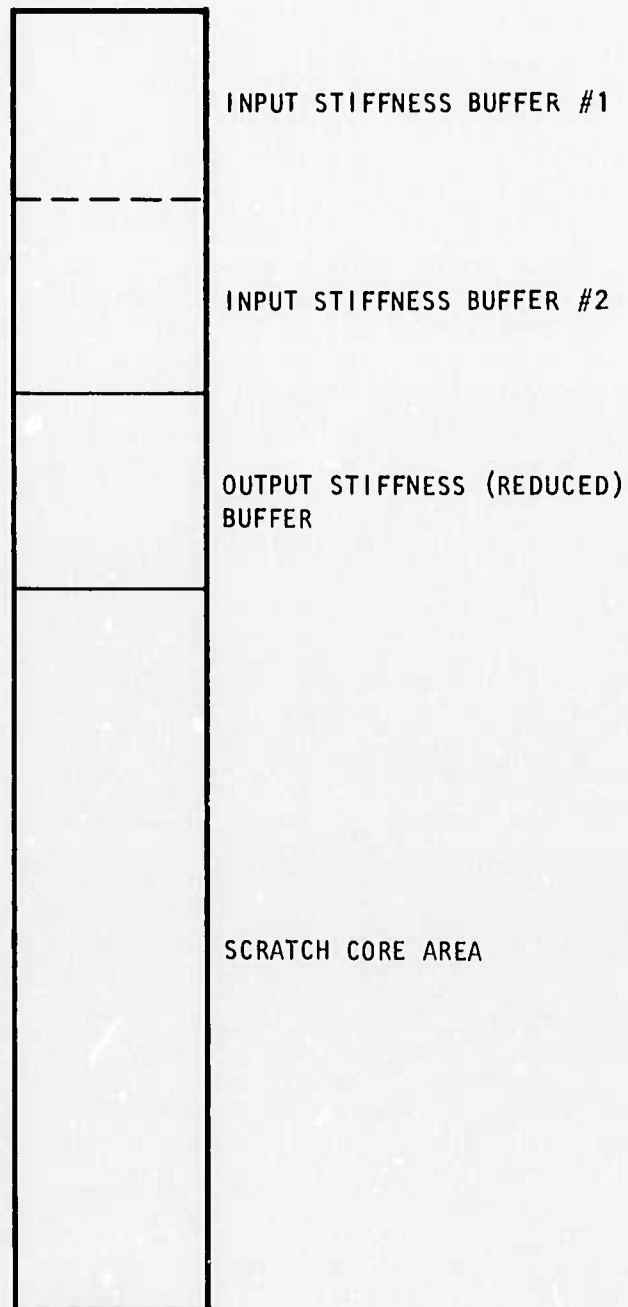
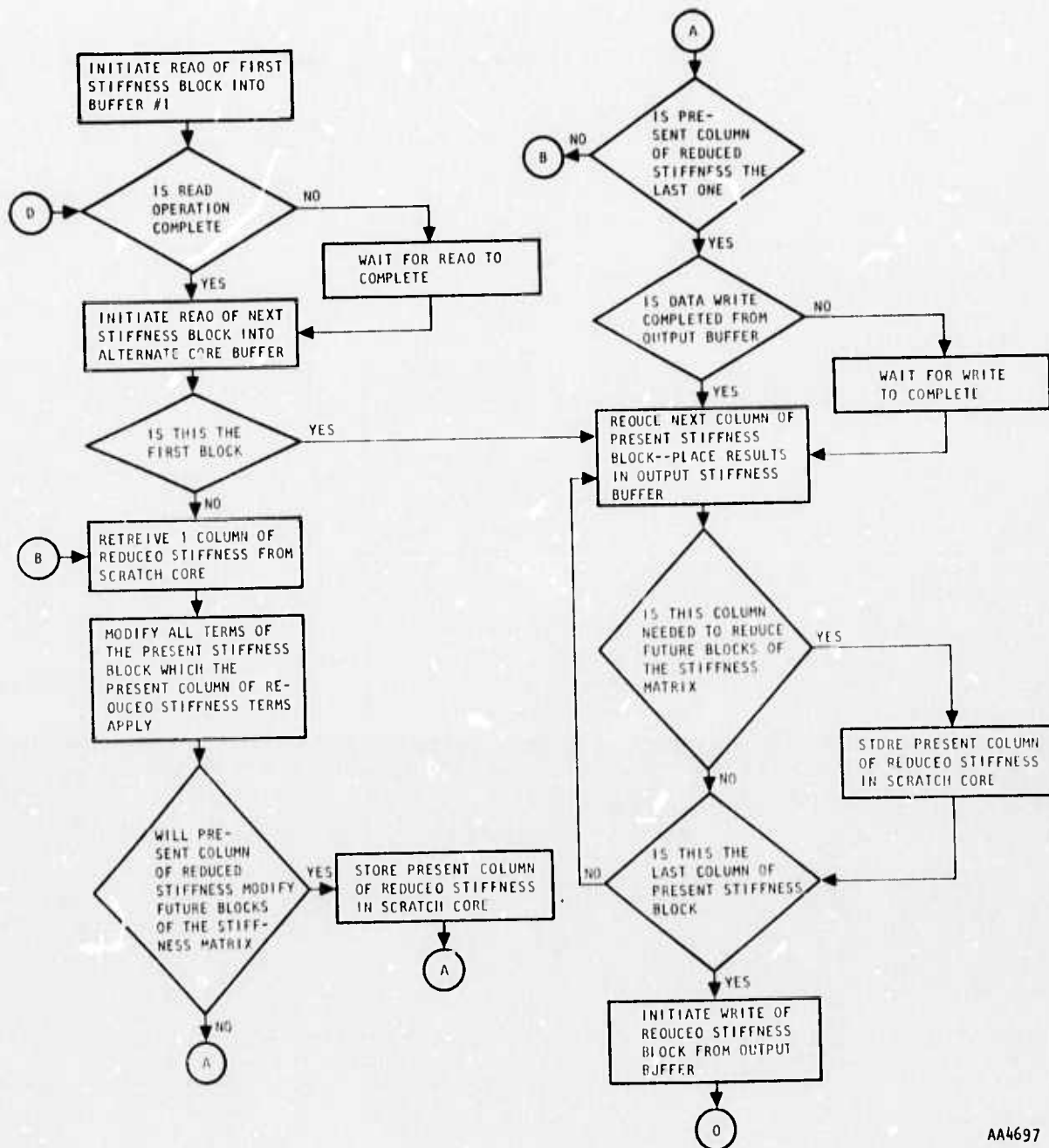


FIGURE 5-24. CORE BUFFERS FOR STIFFNESS MATRIX DECOMPOSITION



R-7215-1-2701



AA4697

FIGURE 5-25. SCHEMATIC DIAGRAM OF STIFFNESS MATRIX DECOMPOSITION

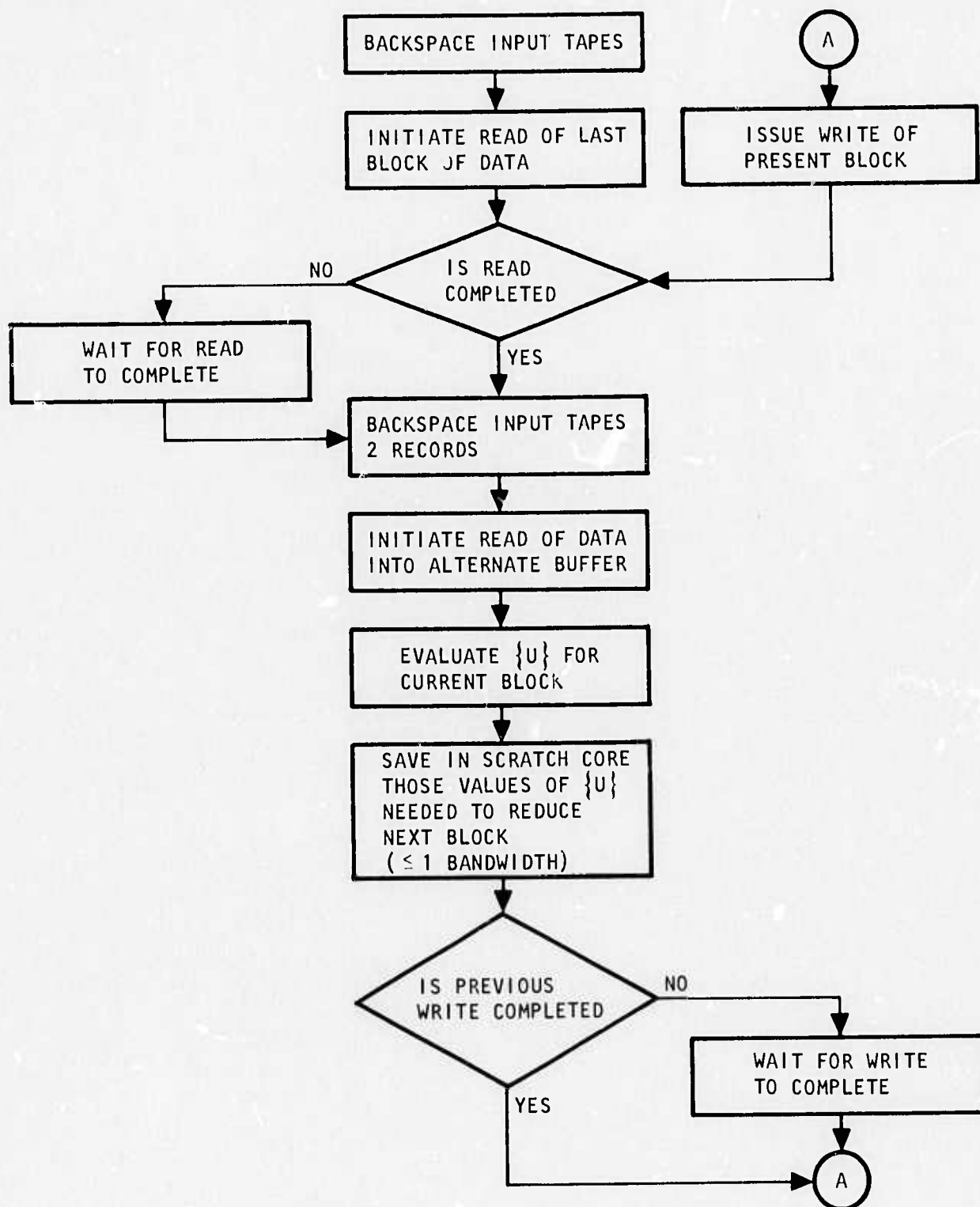


FIGURE 5-26. SCHEMATIC DIAGRAM OF SOLUTION VECTOR EVALUATION



R-7215-1-2701

REFERENCES

- 5-1. Zienkiewicz, O. C., and D. V. Phillips, "An Automatic Mesh Calculation Scheme for Plane and Curved Surfaces by Isoparametric Coordinates," *Numerical Methods in Engineering*, Vol. 4, No. 3, October-December 1971.
- 5-2. Grooms, H. R., "Algorithm for Matrix Bandwidth Reduction," *J. of the Structural Division*, Proc. ASCE, Vol. 98, No. ST1, January 1972.
- 5-3. Rosen, R., "Matrix Bandwidth Minimization," Proc. 1968 ACM National Conference.
- 5-4. Rubinstein, M. F., and R. Rosen, "Structural Analyses by Matrix Decomposition," *J. of Franklin Institute*, Vol. 286, No. 4, October 1968.



SECTION 6

COMPARISON WITH CLOSED-FORM ANALYTIC SOLUTIONS

6.1 SAMPLE PROBLEMS

To investigate the numerical accuracy of the present computer program and to determine the computer time required to solve problems of various size and complexity, several example problems have been formulated and their numerical solutions compared with closed-form, analytic solutions. One-, two-, and three-dimensional linear elastic solutions are considered as well as one- and two-dimensional elastic/plastic and two-dimensional visco-elastic solutions. These are listed in Table 6-1.

Problem 1--Stress Around a Circular Hole

The geometry of Problem No. 1 is illustrated in Figure 6-1. The finite element mesh is illustrated in Figure 6-2. The solution is shown in Figure 6-3 in terms of principal stresses at $\theta = 5.7$ and 42.1° . It does not depend on the material properties of the plate.

Problem 2--Stress and Displacement in an Elastic Thick-Walled Cylinder Under Internal Pressure

The geometry of Problem No. 2 is illustrated in Figure 6-4. The finite element mesh is also shown. The solution is shown in Figure 6-5 in terms of radial and tangential stresses.

Problem 3--Stress in an Elastic, Perfectly Plastic Thick-Walled Cylinder Under Internal Pressure

The geometry of Problem No. 3 is the same as that of Problem No. 2 and is shown in Figure 6-4. For this problem, an additional material property, the Mises yield criterion, is specified as follows:

$$f = \sqrt{J_2} - a_1 \leq 0 \quad (6-1)$$

The analytic solution is shown in Figure 6-6.



R-7215-1-2701

TABLE 6-1. PROBLEMS SOLVED BY FINITE ELEMENT
AND CLOSED-FORM METHODS

<u>Number</u>	<u>Description</u>	<u>Geometry</u>	<u>Material Property</u>	<u>Closed-Form Solution</u>
1	Stress around a circular hole	Two-dimensional (plane)	Elastic	Reference 6-1
2	Stress in a thick walled cylinder under internal pressure	One-dimensional (axisymmetric)	Elastic	Reference 6-2
3	Stress in a thick walled cylinder under internal pressure	One-dimensional (axisymmetric)	Elastic, perfectly plastic	Reference 6-2
4	Stress in a reinforced thick walled cylinder	One-dimensional (axisymmetric)	Viscoelastic	Reference 6-3
5	Stress concentration around a cylindrical hole in a semiinfinite body	Three-dimensional	Elastic	Reference 6-4

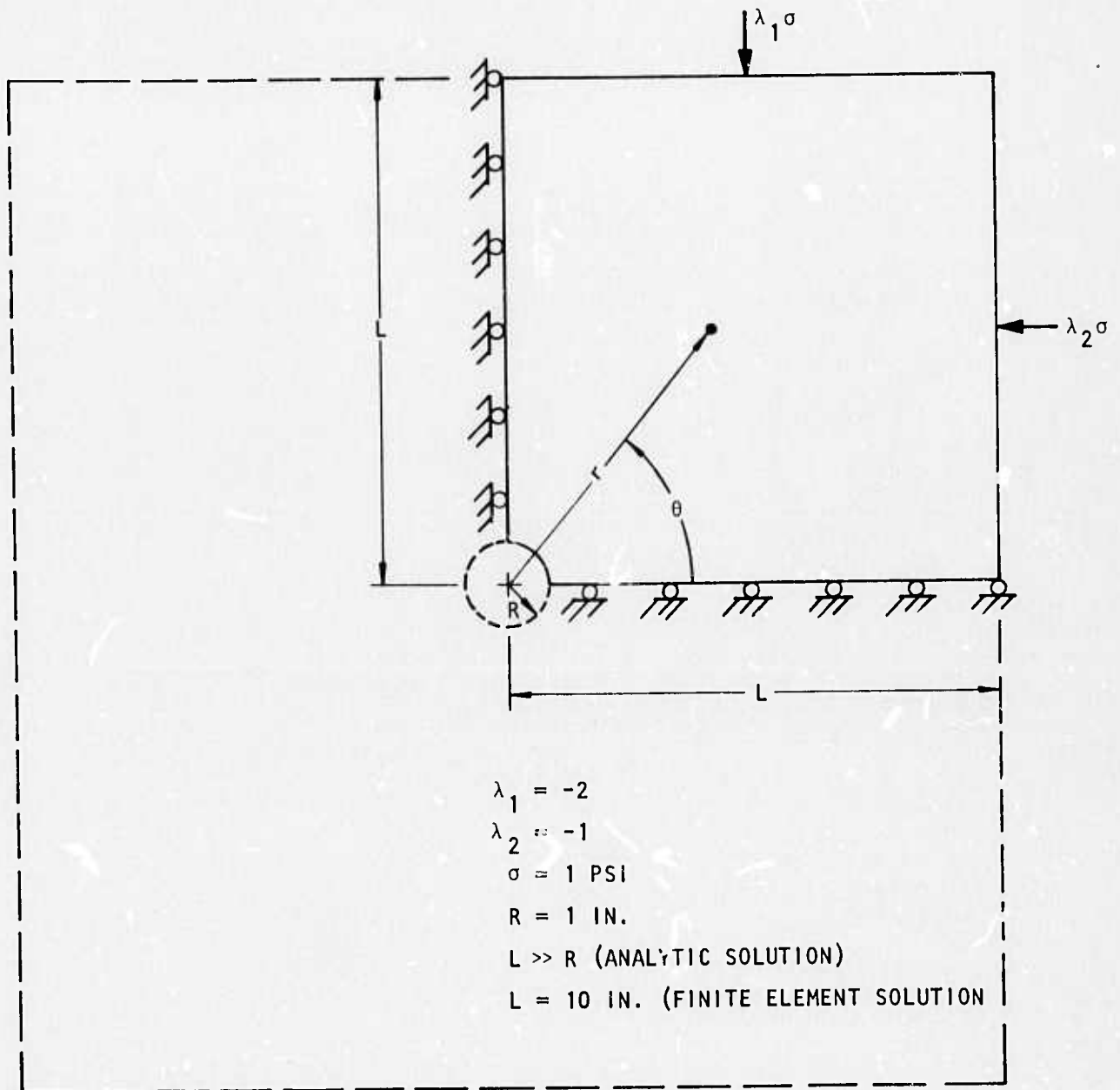


FIGURE 6-1. PROBLEM 1--STRESSES AROUND A CIRCULAR HOLE



R-7215-1-2701

SQUARE PLATE (20 IN. X 20 IN.)

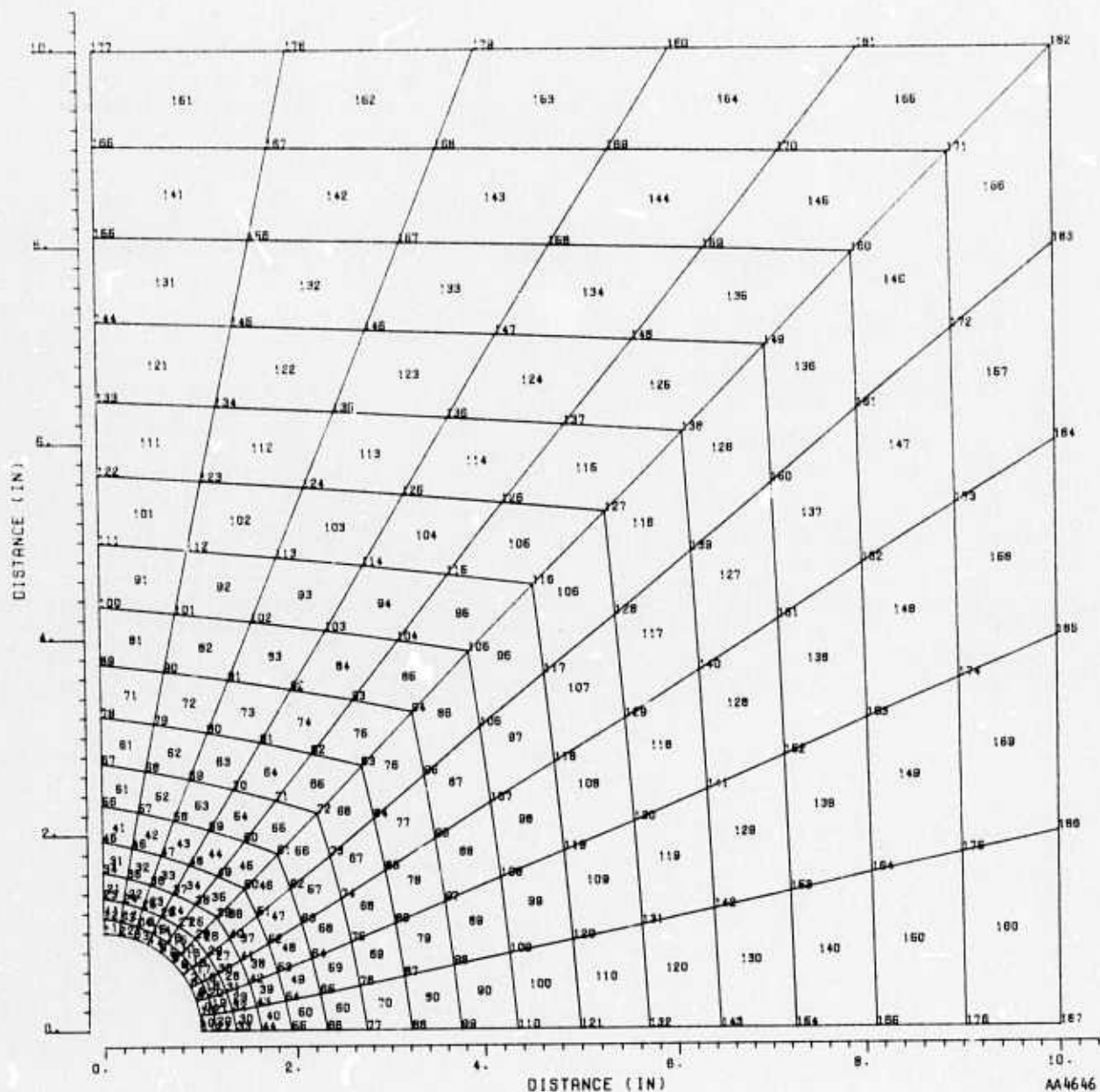
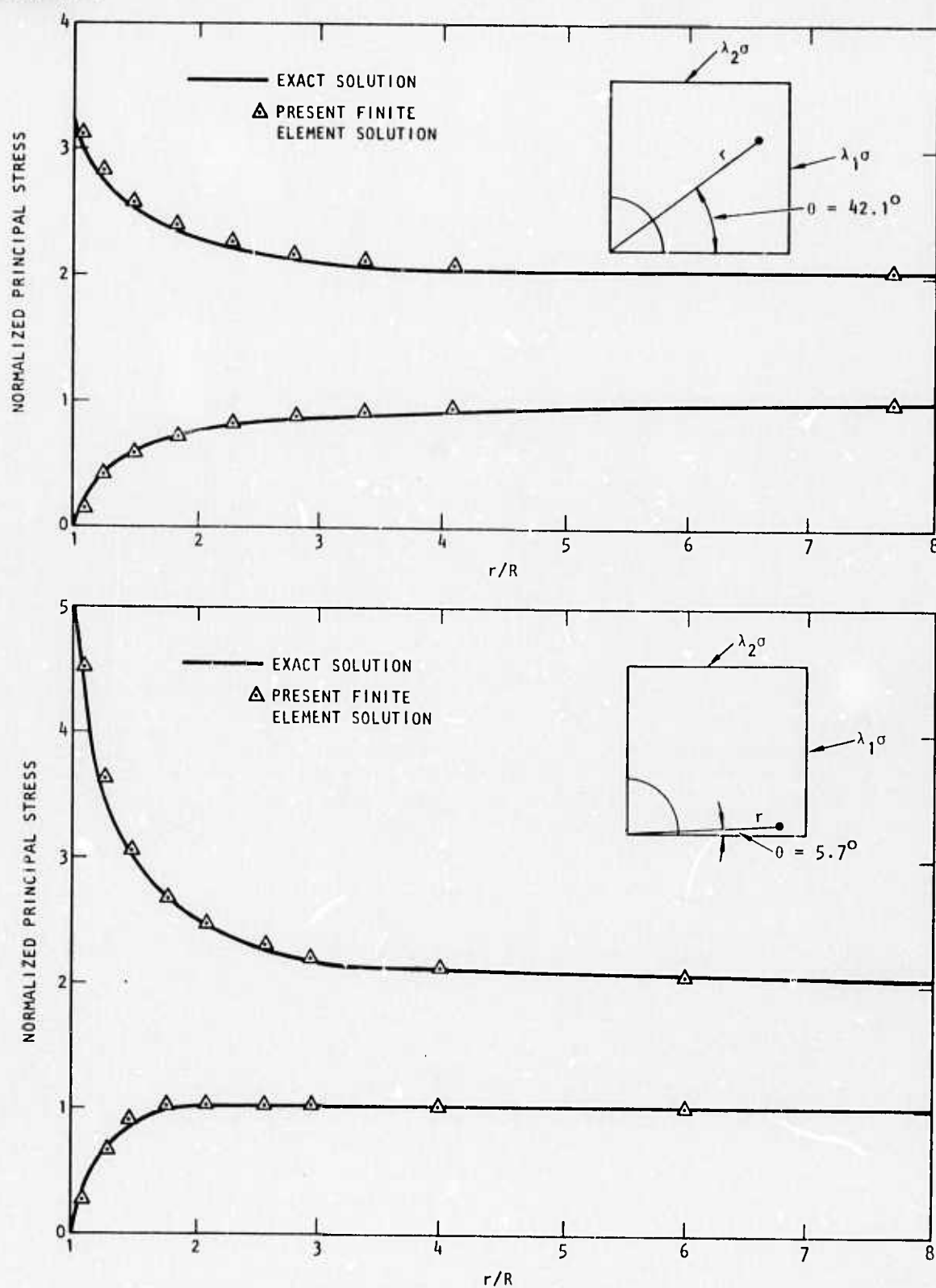


FIGURE 6-2. FINITE ELEMENT MESH FOR STRESS CONCENTRATION AROUND CIRCULAR HOLE



AA4673

FIGURE 6-3. COMPARISON BETWEEN PRESENT FINITE ELEMENT SOLUTION AND ANALYTIC SOLUTION FOR PROBLEM 1, STRESSES AROUND A CIRCULAR HOLE



R-7215-1-2701

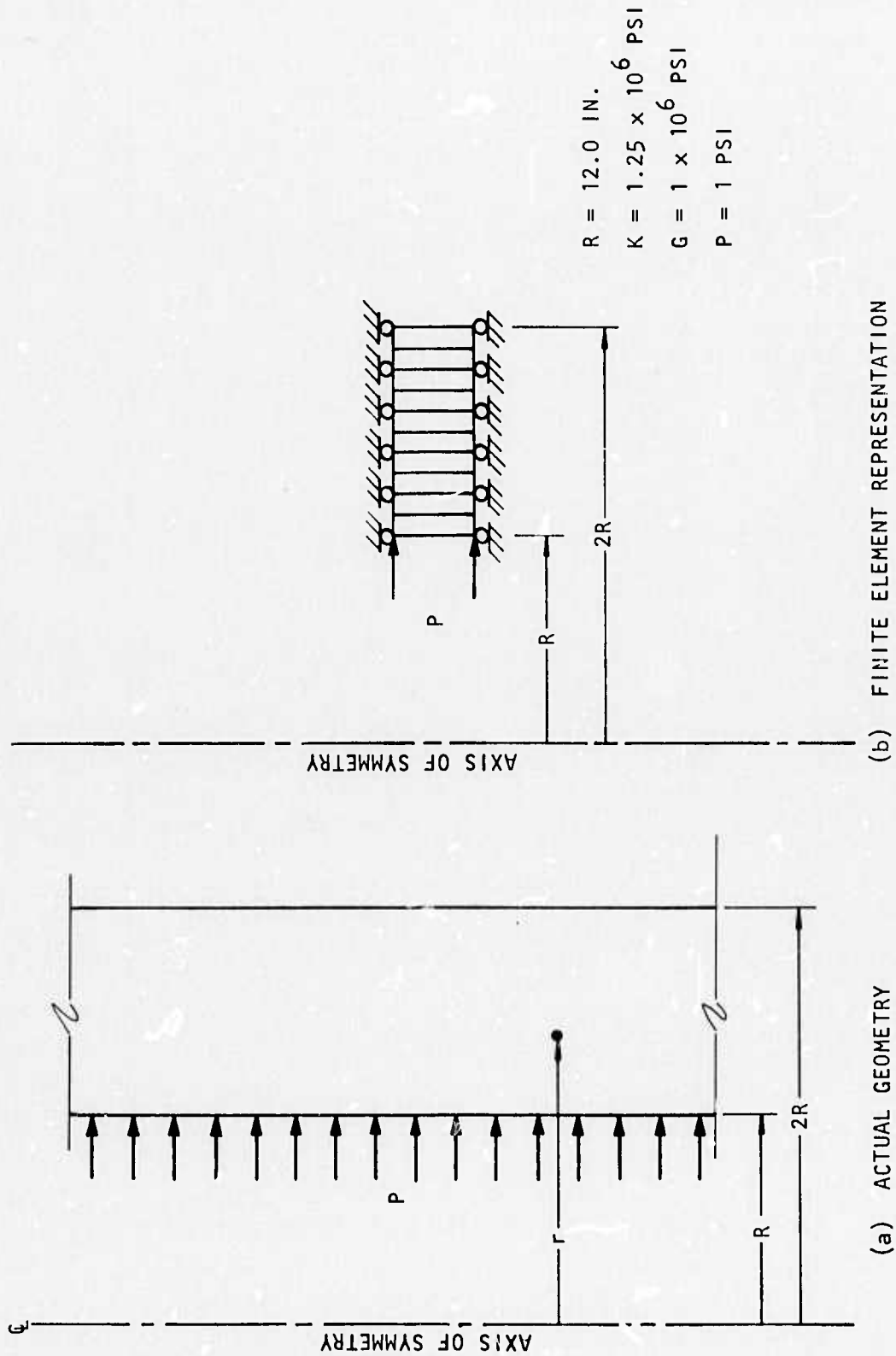


FIGURE 6-4. PROBLEM 2--INFINITELY LONG, THICK ELASTIC CYLINDER SUBJECT TO INTERNAL PRESSURE

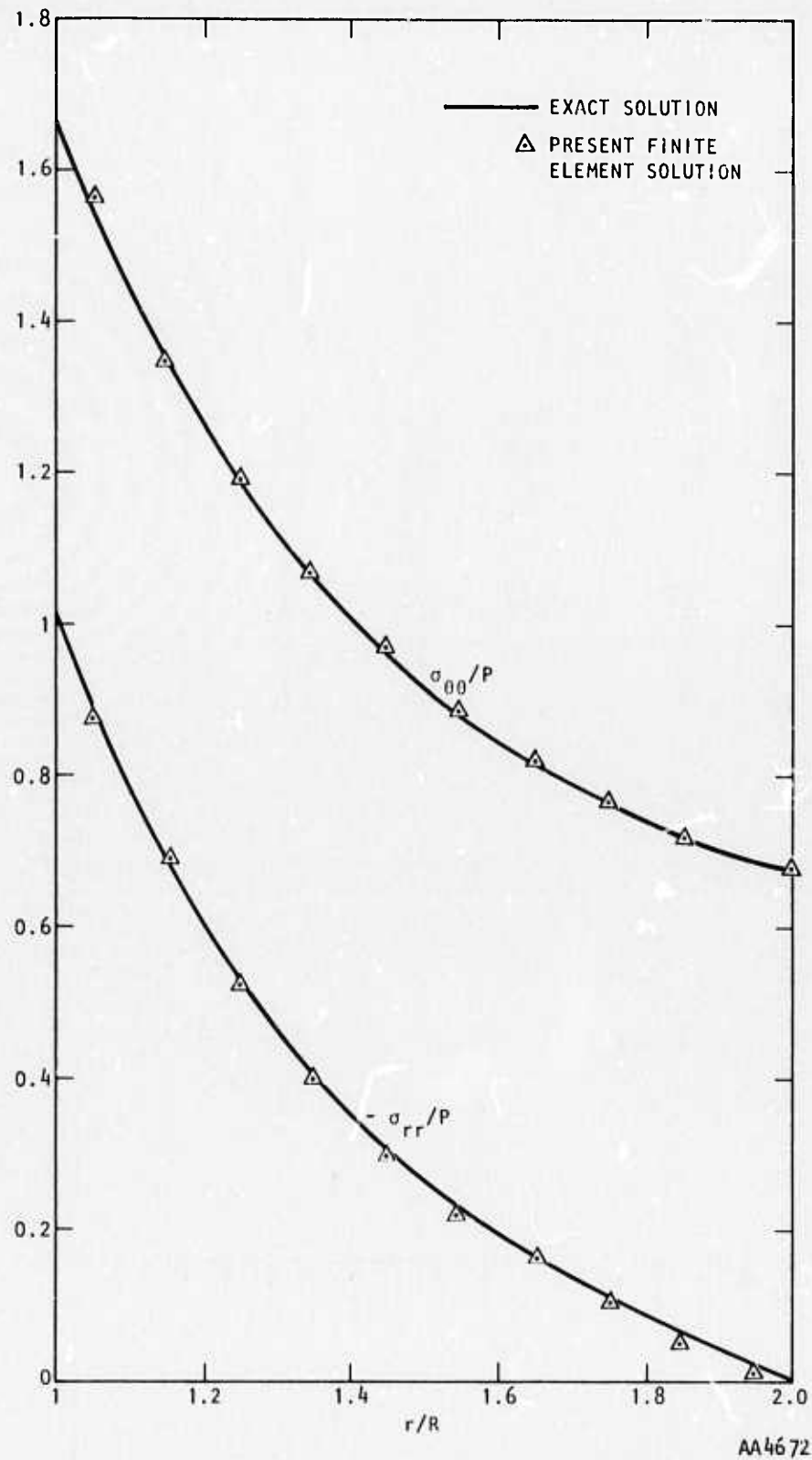


FIGURE 6-5. COMPARISON BETWEEN PRESENT FINITE ELEMENT SOLUTION AND ANALYTIC SOLUTION FOR PROBLEM 2, THICK ELASTIC CYLINDER SUBJECT TO INTERNAL PRESSURE

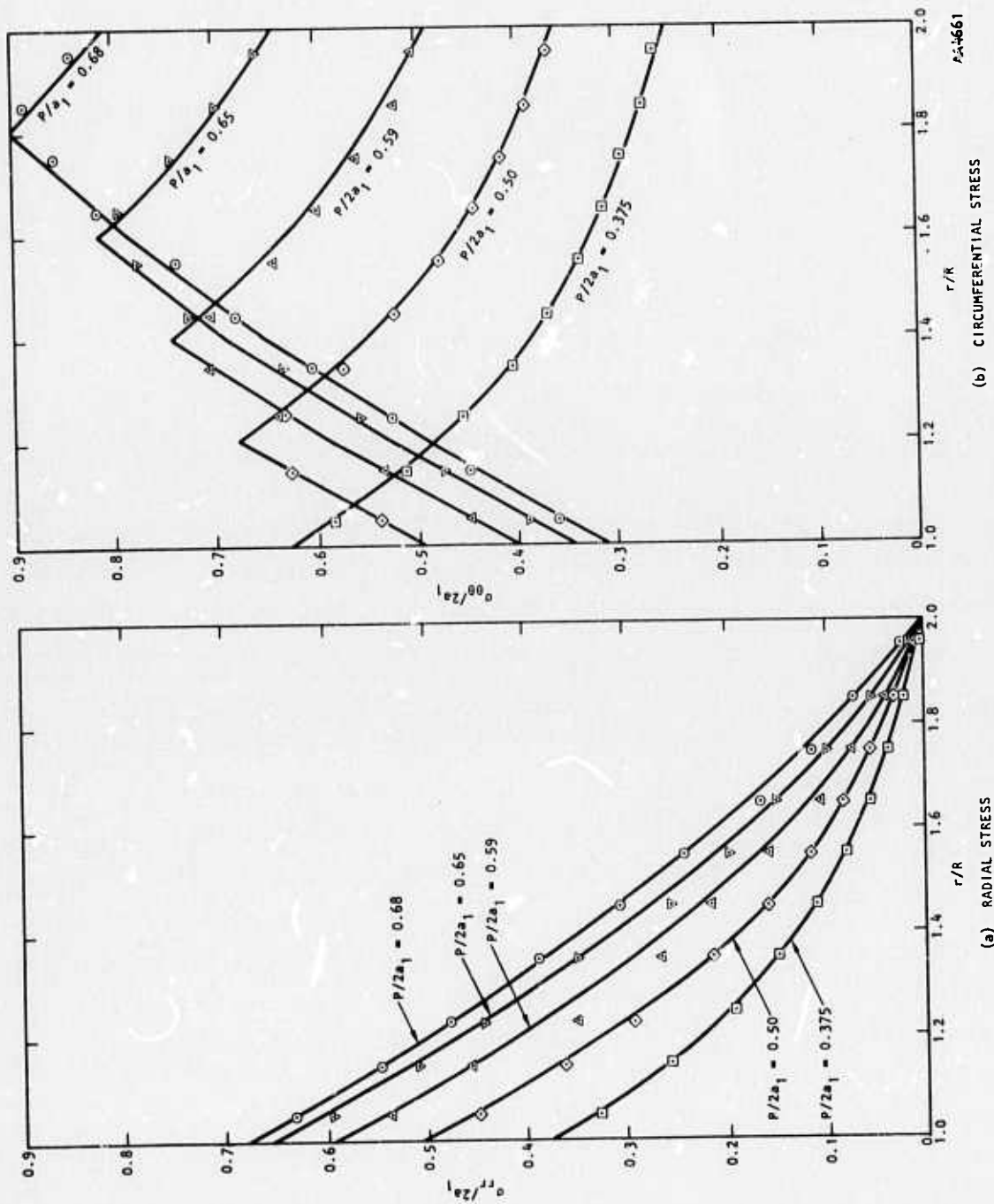


FIGURE 6-6. COMPARISON BETWEEN PRESENT FINITE ELEMENT SOLUTION AND ANALYTIC SOLUTION FOR PROBLEM 3, ELASTIC/PLASTIC CYLINDER SUBJECT TO INTERNAL PRESSURE



Problem 4--Stress in a Visco-Elastic, Reinforced
Cylinder Under Internal Pressure

The geometry of Problem No. 4, shown in Figure 6-7, is similar to that of Problems 2 and 3. The main difference is a steel reinforcing ring around the outer circumference. The material of the cylinder is assumed to be governed by a Maxwell-type law as follows:

$$\sigma_{ij} = 2G(\epsilon'_{ij}) \exp(-t/B) \quad (6-2)$$

where

ϵ'_{ij} = Component of deviatoric strain tensor

G = Elastic shear modulus

t = Time in units of $B = \eta/G$ where η = viscoelastic parameter)

Volumetric deformation of the cylinder and all deformations of the reinforcing ring are assumed to be linearly elastic inviscid. The variation of radial and circumferential stresses are shown as functions of radius and time in Figure 6-8.

Problem 5--Three-Dimensional Stress Concentration Around a
Cylindrical Hole in a Semiinfinite Elastic Body

The geometry of Problem No. 5 is illustrated in Figure 6-9. The stress distribution around the hole near the stress free face ($X_1 - X_2$ plane) is appropriate to plane stress, while in the interior there is axial stress along the axis of the hole. The finite element mesh is shown in Figure 6-10. The loading condition selected for this example is uniaxial stress parallel to the X_2 -axis. Thus the faces parallel to the X_2 - p plane are stress free as is one face parallel to the X_2 - X_1 plane. The finite element solution is compared with the analytic solution in Figure 6-11.



R-7215-1-270

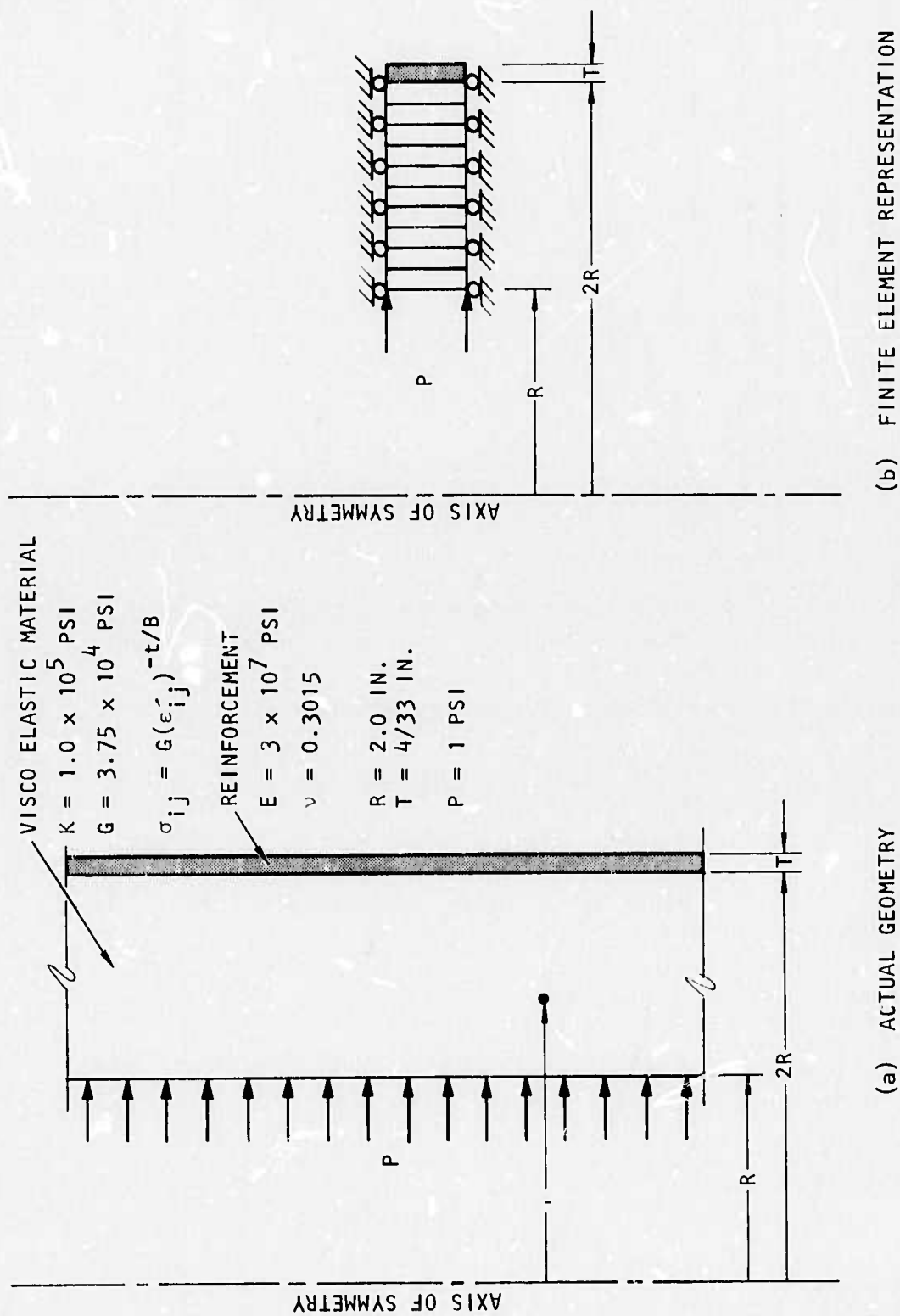


FIGURE 6-7. PROBLEM 1--INFINITELY LONG REINFORCED THICK VISCOELASTIC CYLINDER
SUBJECTED TO INTERNAL PRESSURE



R-7215-1-2701

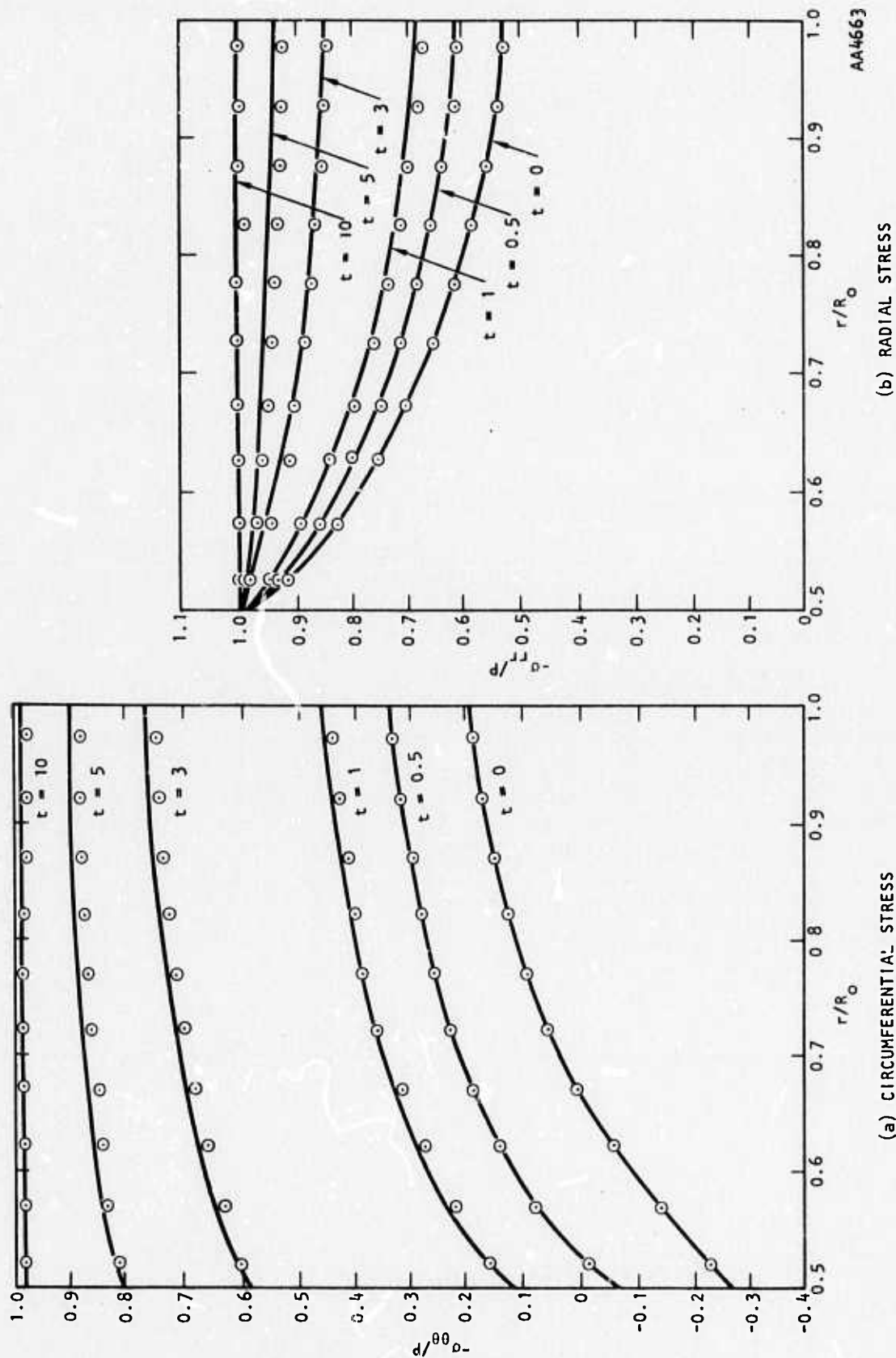


FIGURE 6-6. PROBLEM 4--REINFORCED VISCOELASTIC CYLINDER SUBJECTED TO INTERNAL PRESSURE (REFERENCE 6-4)

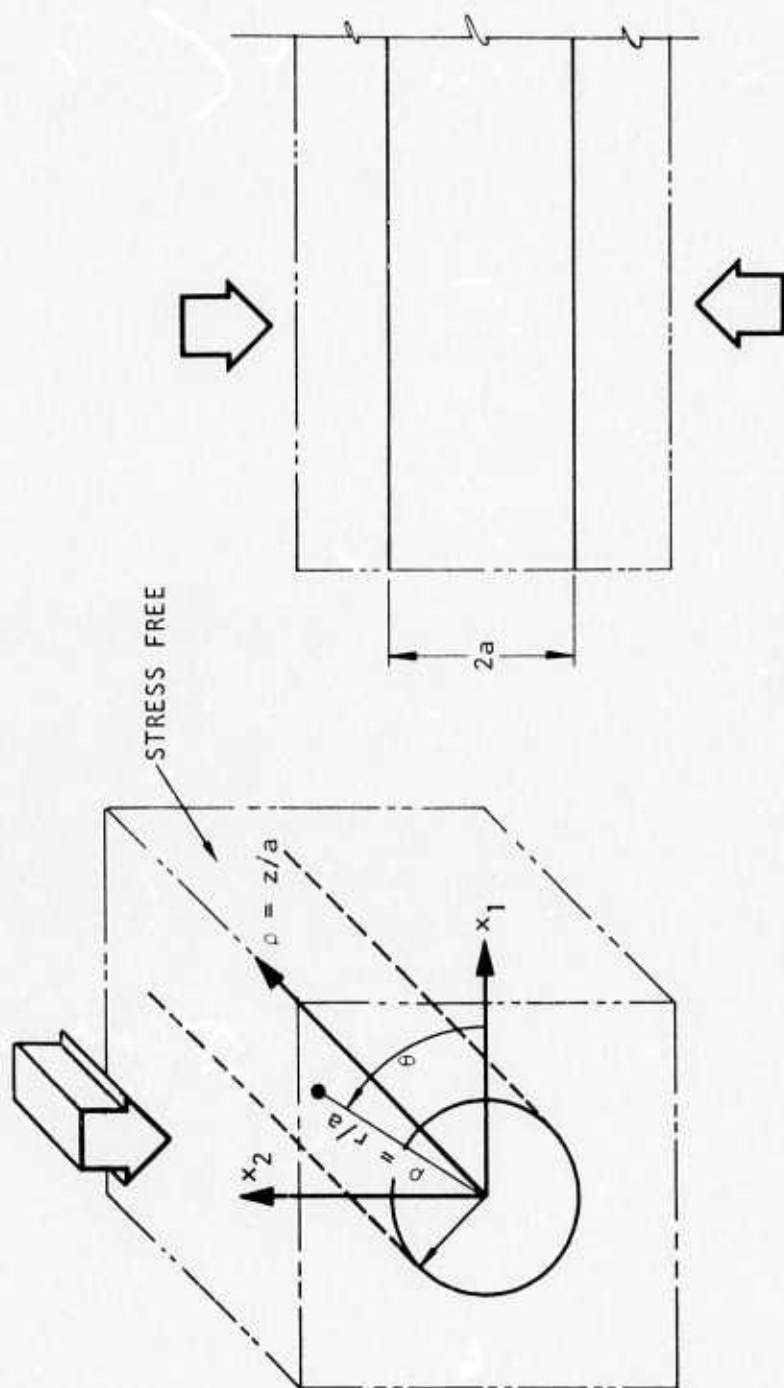


FIGURE 6-9. PROBLEM 5--THREE-DIMENSIONAL STRESS CONCENTRATION AROUND A CYLINDRICAL HOLE IN A SEMIINFINITE ELASTIC BODY

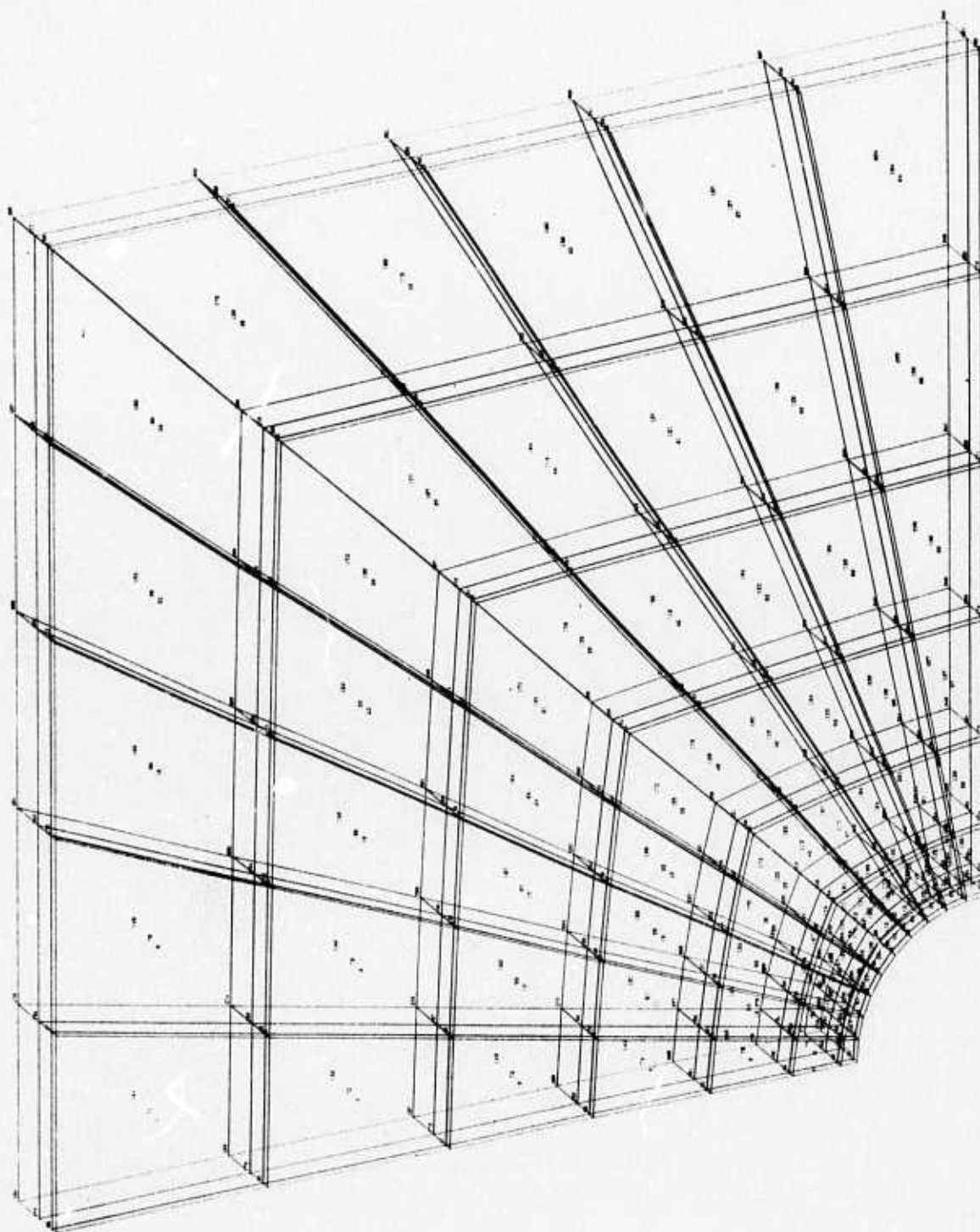
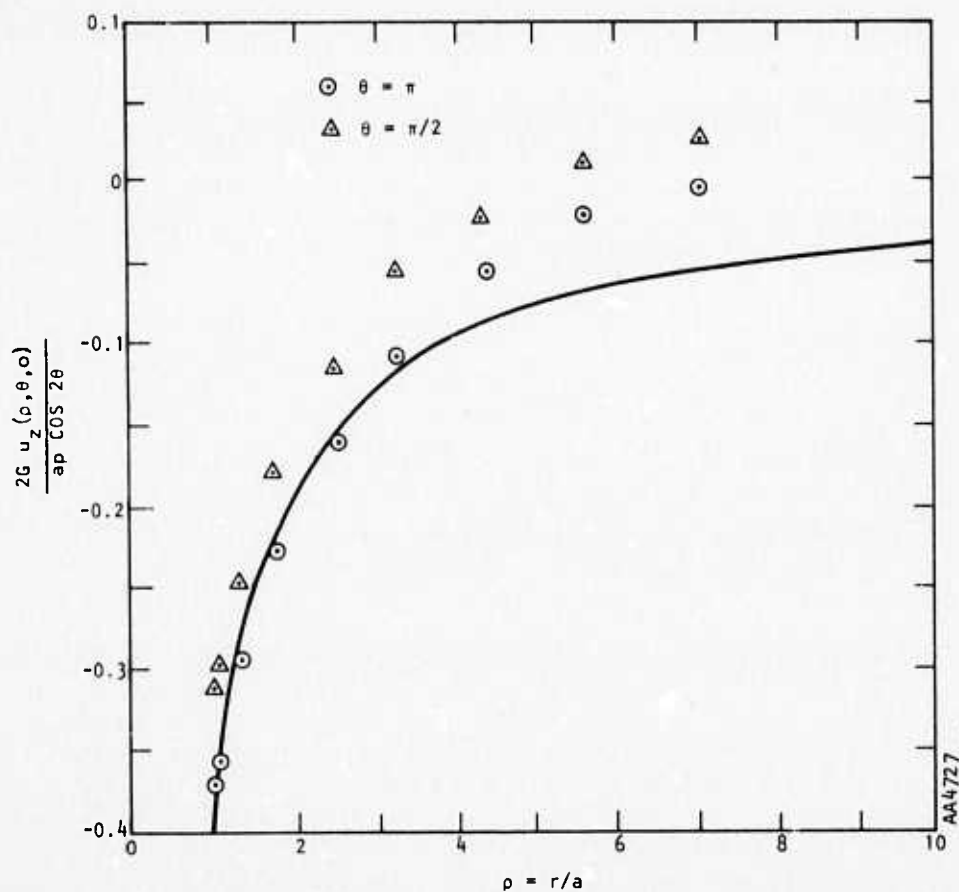
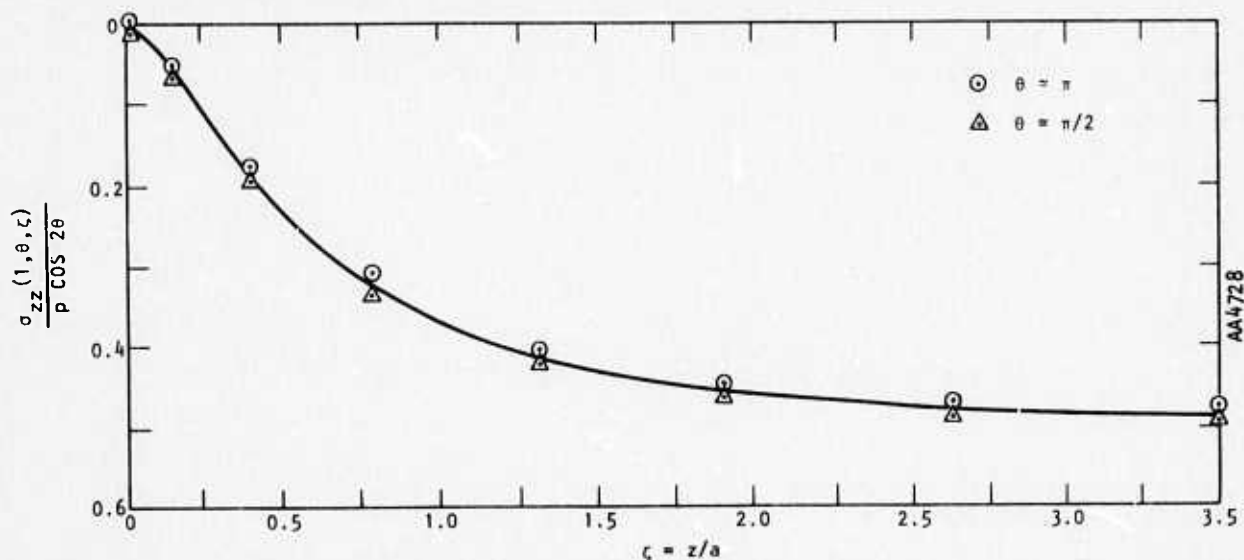


FIGURE 6-10. PROBLEM 5--FINITE ELEMENT MESH (ONLY FIRST THREE LAYERS ARE SHOWN FOR CLARITY. COMPLETE MESH CONTAINS EIGHT LAYERS.)

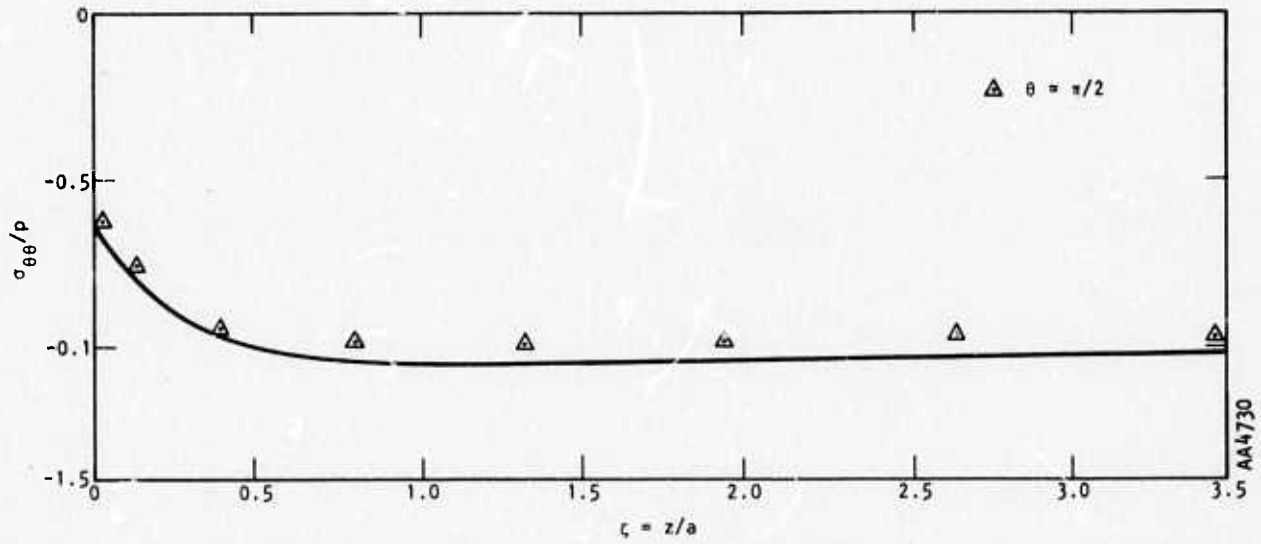


(a) AXIAL DISPLACEMENT ON THE STRESS FREE PLANE $\rho = 0$ (NOTICE THAT THE FINITE ELEMENT SOLUTION WHICH ENCOMPASSES A FINITE DOMAIN DIVERGES FROM THE ANALYTIC SOLUTION, WHICH CONSIDERS AN INFINITE DOMAIN, AS THE FINITE BOUNDARY IS APPROACHED)

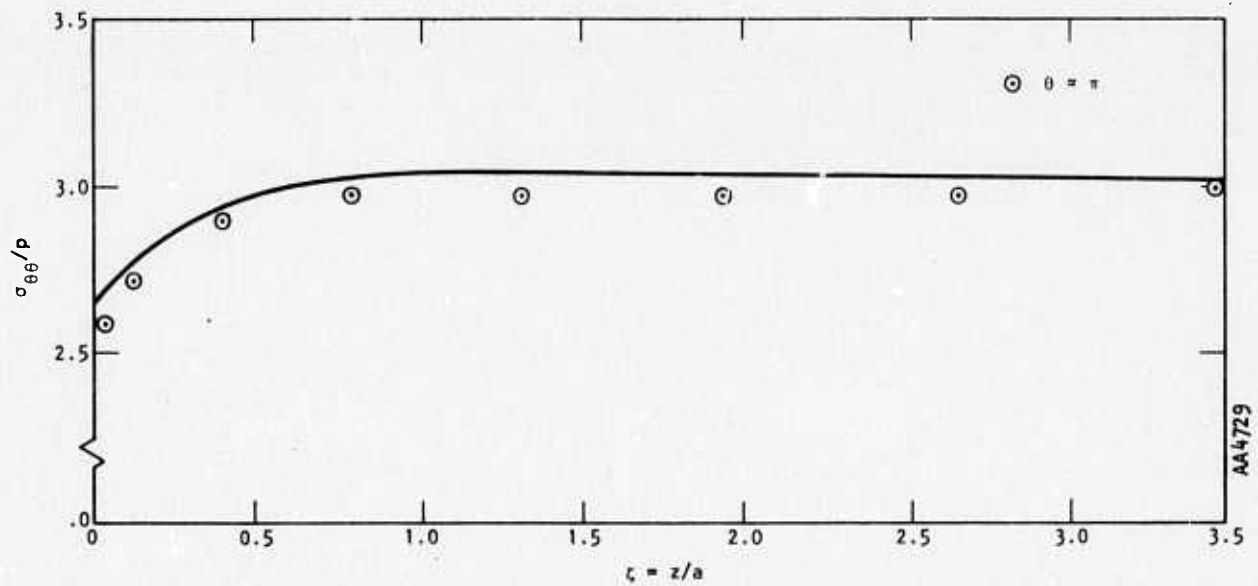


(b) AXIAL STRESS AT EDGE OF THE HOLE

FIGURE 6-11. PROBLEM 5--THREE-DIMENSIONAL STRESS CONCENTRATION (REFERENCE 6-4)



(c) TANGENTIAL STRESS AT EDGE OF HOLE (CROWN)



(d) TANGENTIAL STRESS AT EDGE OF HOLE (SPRING LINE)

FIGURE 6-11. (CONTINUED)



6.2 COMPUTING TIME REQUIRED FOR SOLUTION

The computing time required to solve Problem 5 and several small problems on a Univac 1108 with 65,000 words of core is shown in Table 6-2. More data on time to solve various sizes of problems will be gathered during the second phase of the contract.



TABLE 6-2. COMPUTING TIME REQUIRED FOR SOLUTIONS

	Number of Equations	Bandwidth	Number of Blocks for Global Stiffness	Number of Equations/Block	Number of Elements	Time to Form Global Stiffness, sec	Triangularize, sec	Back-sub, sec	Compute Stress, sec
1	2112	312	87	28	640	540	2178	180	30
2*	2144	278	86	25	560	2400	--	260	30
3 [†]	496	278	16	31	80	61	333	--	3
4 [†]	558	312	20	28	80	72	464	--	4
5 [†]	168	42	1	168	21	17	3.7	--	1.1
6	168	42	14	12	21	24	8	1	5.5
7	168	42	56	2	21	37	20	3	3.7
8*	2712	259	130	21	726	2308	--	197	--

*Global stiffness matrix triangularized as formed; forward reduction of load vector included in backsubstitution.

[†]Triangularization includes backsubstitution time.

Number 2 is Example Problem No. 5 (three-dimensional stress concentration)

Number 8 is Caladay Project Hoist Room



REFERENCES

- 6-1. Savin, G. N., "Stress Concentration Around Holes," *Pergamon Press*, New York, 1961.
- 6-2. Prager, W. and P. G. Hodge, Jr., *Theory of Perfectly Plastic Solids*, John Wiley & Sons, Inc., New York, 1951
- 6-3. Zienkiewicz, O. C., et al., "A Numerical Method of Viscoelastic Stress Analysis," *Int. J. Mech. Sci.*, Pergamon Press, 1968, pp. 807-827.
- 6-4. Youngdahl, C. K., and E. Sternberg, *Three-Dimensional Stress Concentration Around a Cylindrical Hole in a Semi Infinite Elastic Body*, Argonne National Laboratory, ANL-7097, September 1965.



R-7215-1-2701

APPENDIX A
LOGIC DIAGRAMS
FOR MATERIAL PROPERTIES

Logic diagrams for subroutines in the material property package are shown below. Subroutine CONECT connects the package to the main program. Subroutine ELPL controls all the other subroutines.



R-7215-1-2701

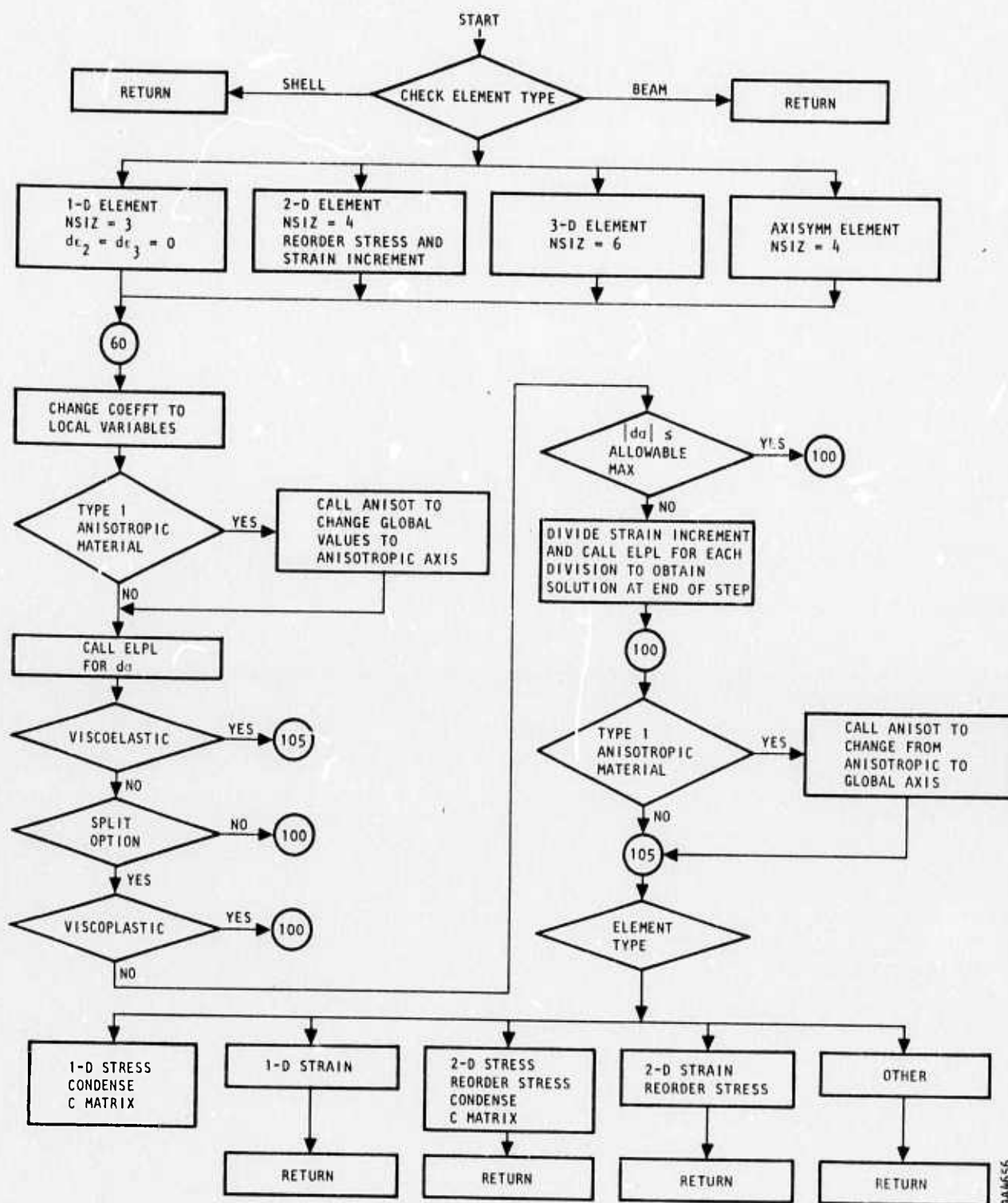
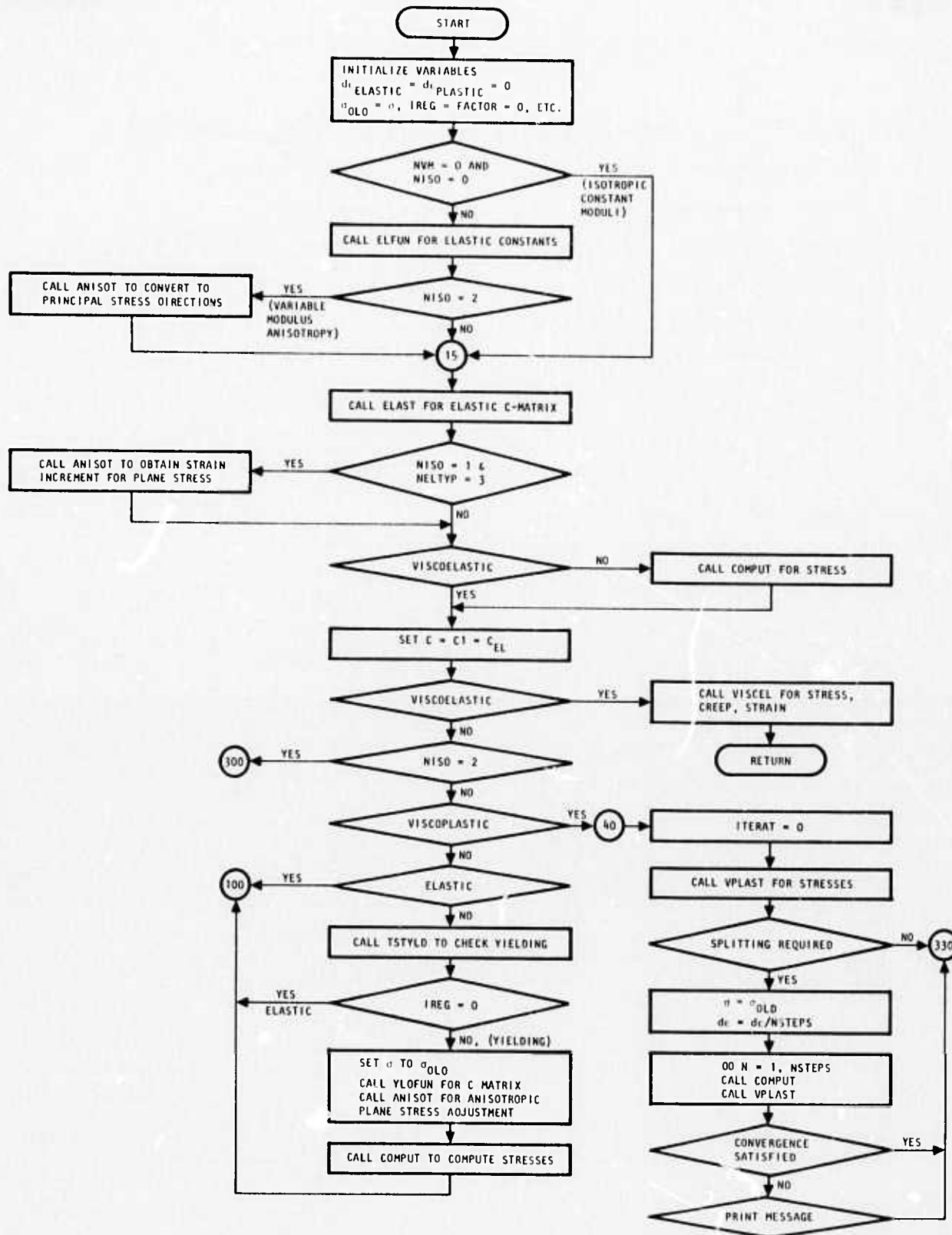
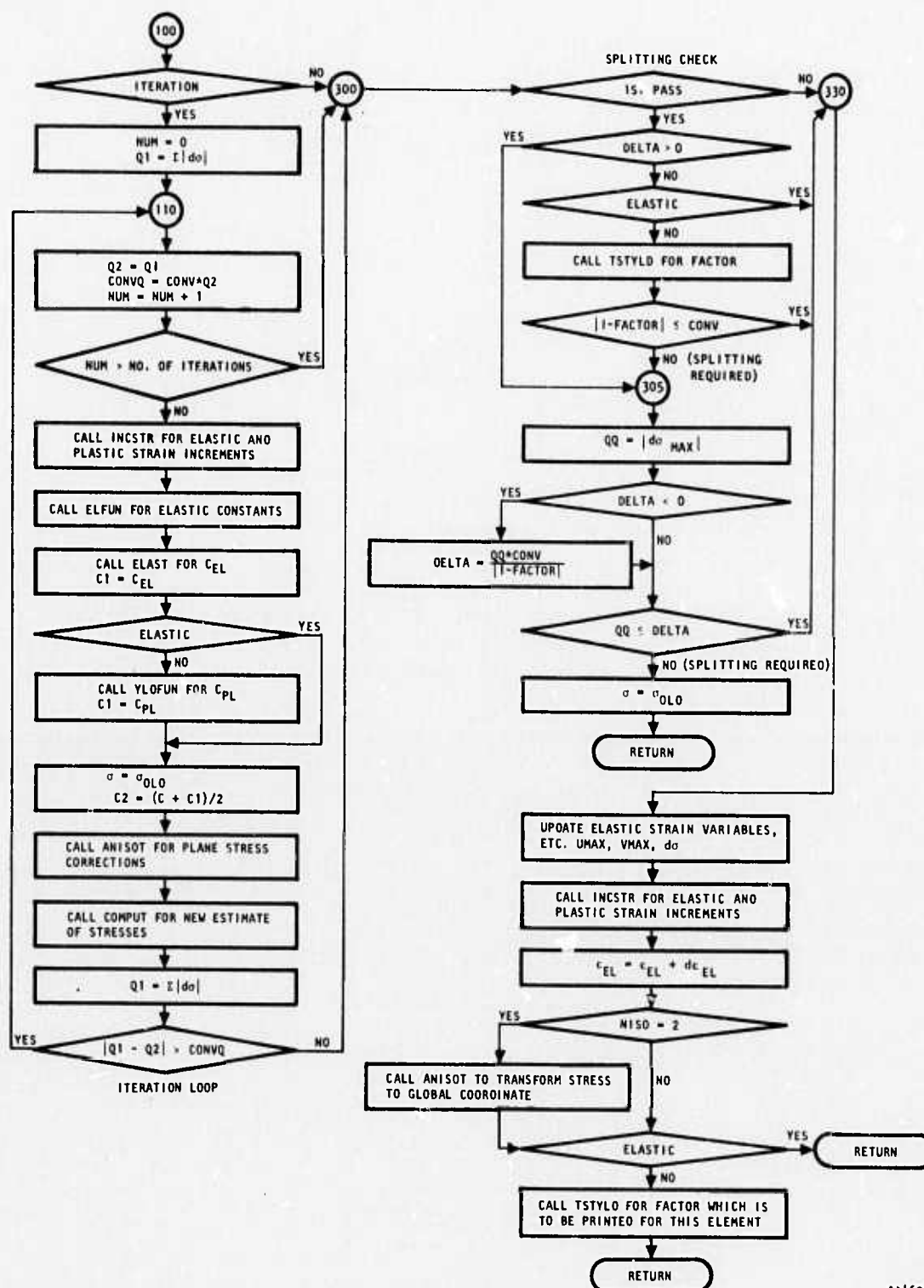


FIGURE A-1. CONECT--SUBROUTINE CONECT LINKS MAIN LINE PROGRAM TO MATERIAL PACKAGE ELPL



AA4692

FIGURE A-2. SUBROUTINE ELPL CONTROLS MATERIAL PROPERTY SUBROUTINES, TRANSFERS AXES FOR ANISOTROPIC MATERIALS, PERFORMS TESTS FOR STRAIN SPLITTING AND ITERATION.



A4693

FIGURE A-2 (CONTINUED)

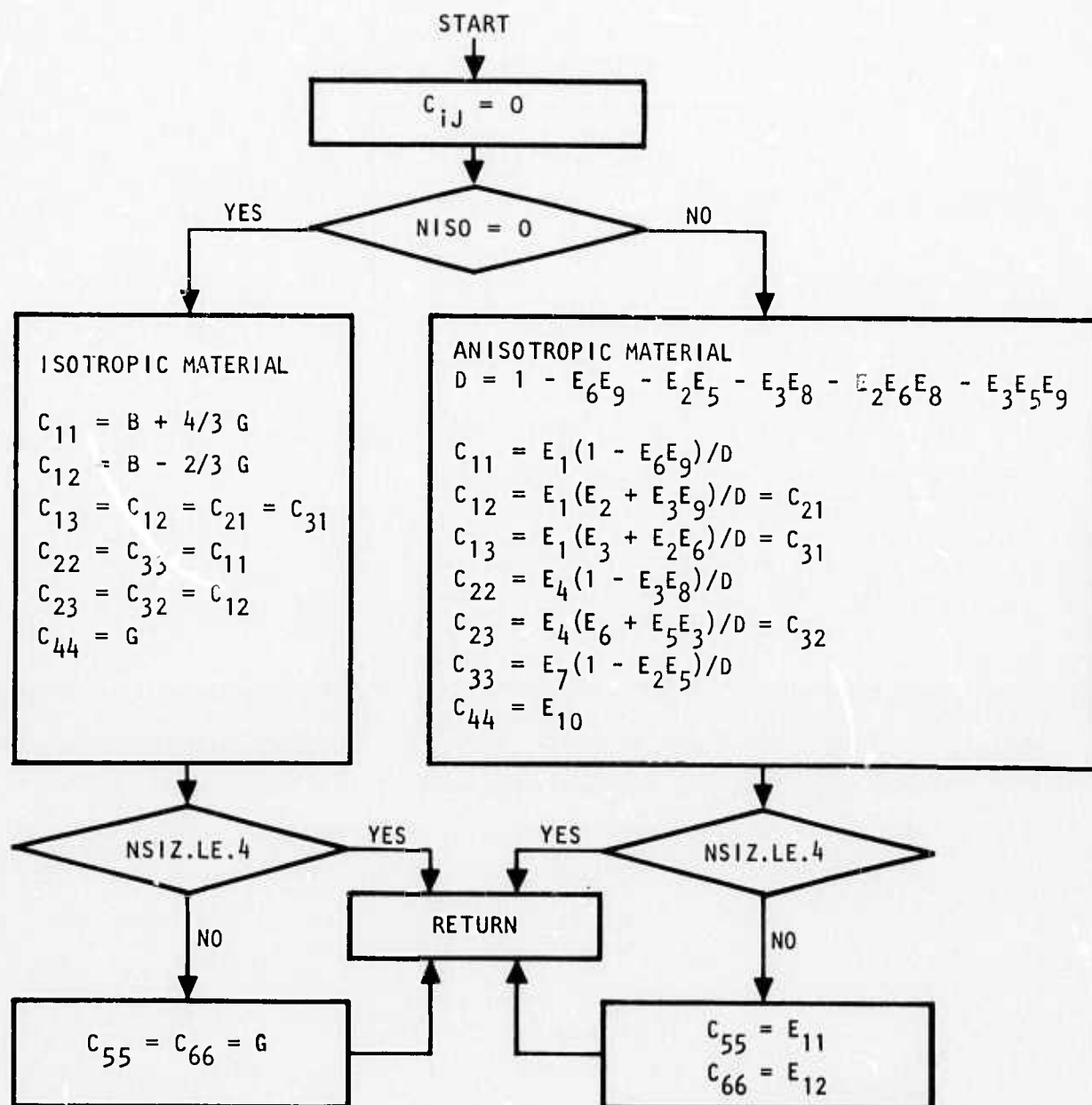


FIGURE A-3. SUBROUTINE ELAST--ELAST FORMULATES C-MATRIX USING COEFFICIENTS FOR EITHER ISOTROPIC OR ANISOTROPIC MATERIALS GENERATED BY ELFUN

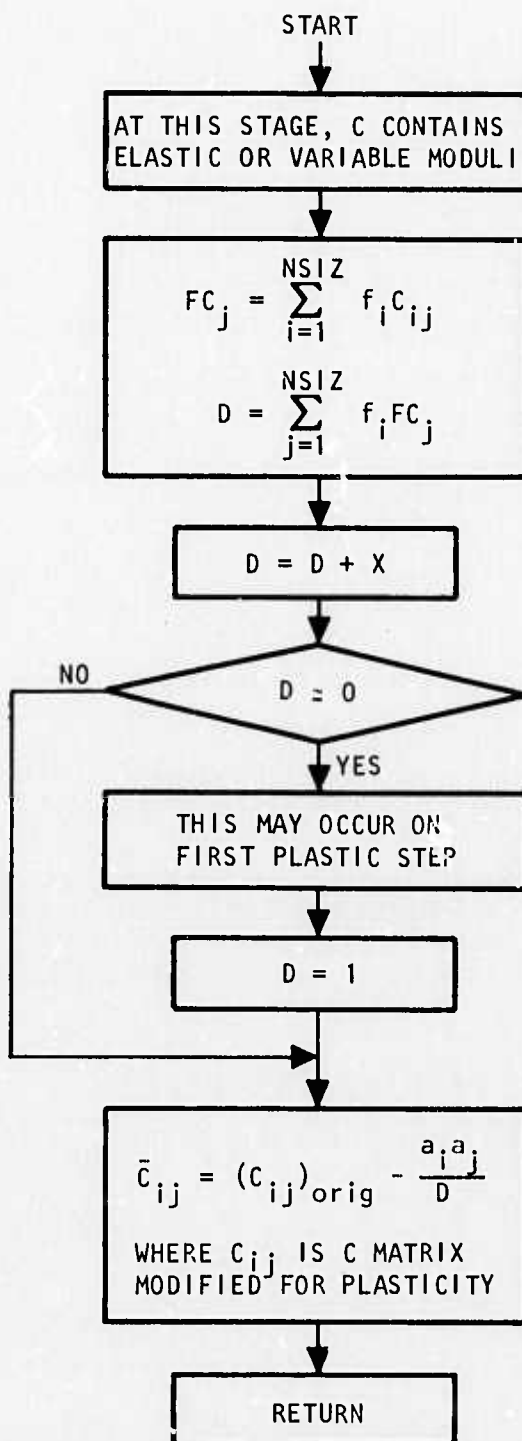
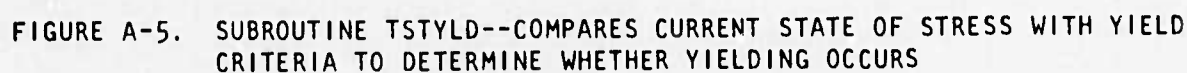
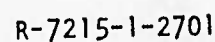


FIGURE A-4. SUBROUTINE PLAST--THIS SUBROUTINE MODIFIES C MATRIX GENERATED BY SUBROUTINE ELAST IN ORDER TO ACCOUNT FOR PLASTICITY. THE BASIC QUANTITIES FOR THIS MODIFICATION ARE DERIVATIVES OF THE YIELD FUNCTION WITH RESPECT TO THEIR ARGUMENTS AND ARE COMPUTED IN YLDFUN.





R-7215-1-2701

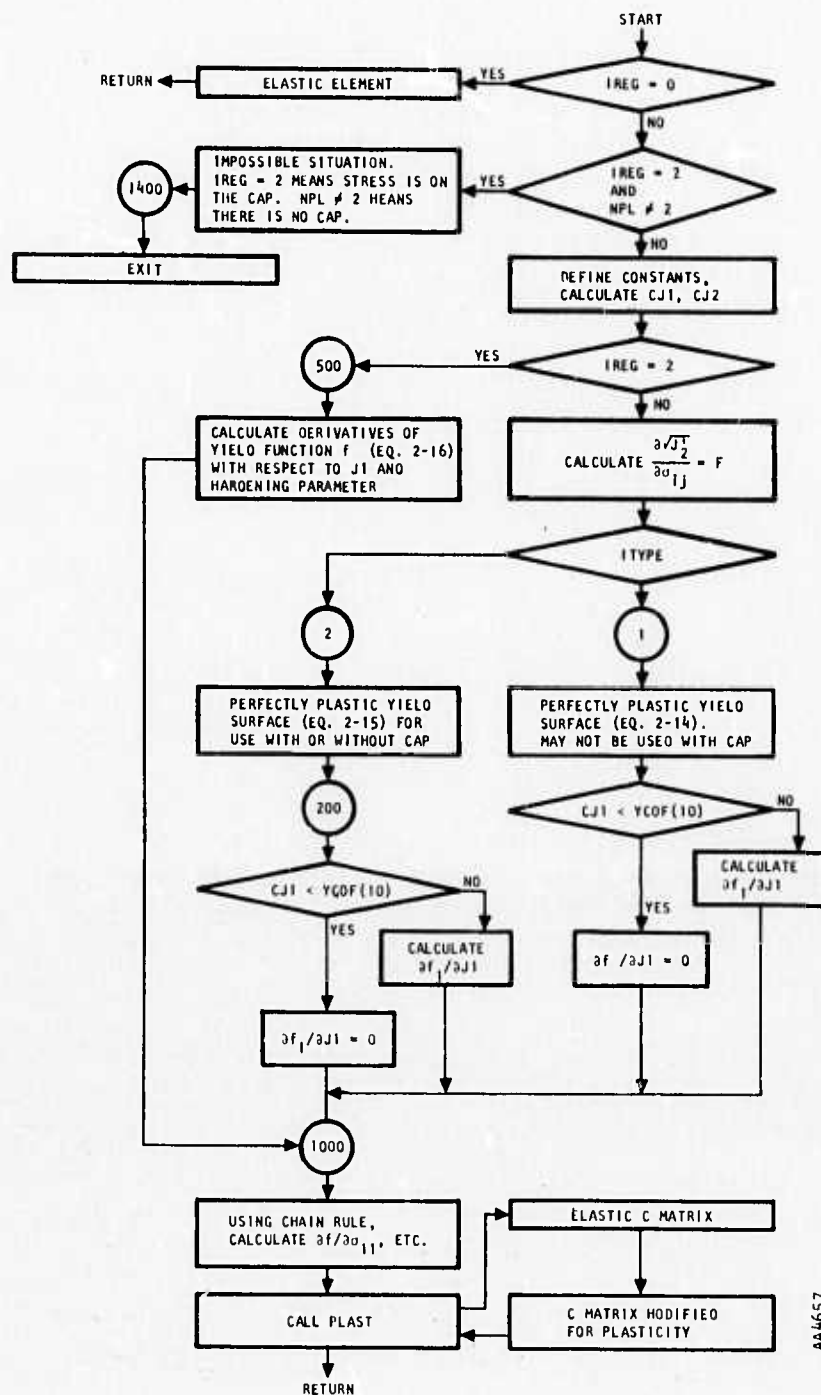


FIGURE A-6. SUBROUTINE YLDFUN--THIS SUBROUTINE CALCULATES THE DERIVATIVES OF THE YIELD FUNCTION WITH RESPECT TO THE STRESS COMPONENTS. THE YIELD FUNCTION WHOSE DERIVATIVES ARE COMPUTED IS DETERMINED BY THE INDICES IREG (SET IN (TSTYLD) AND ITYPE (SET BY INPUT))

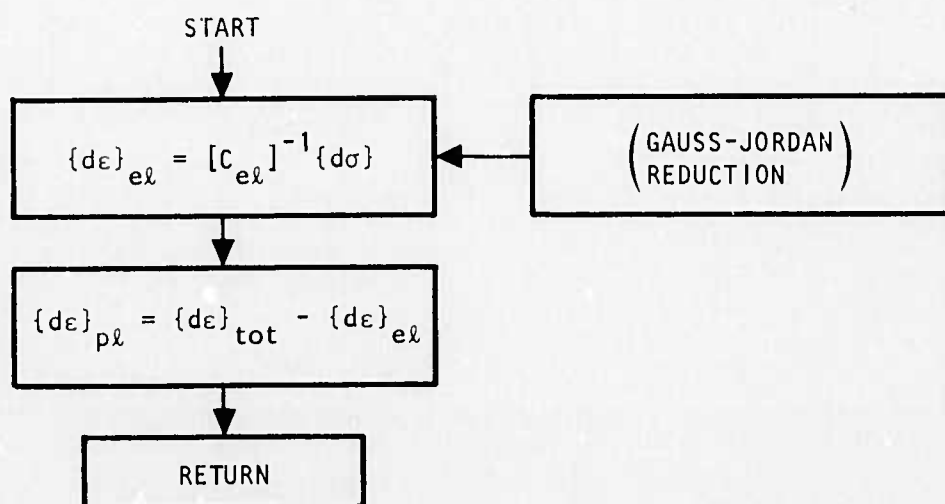
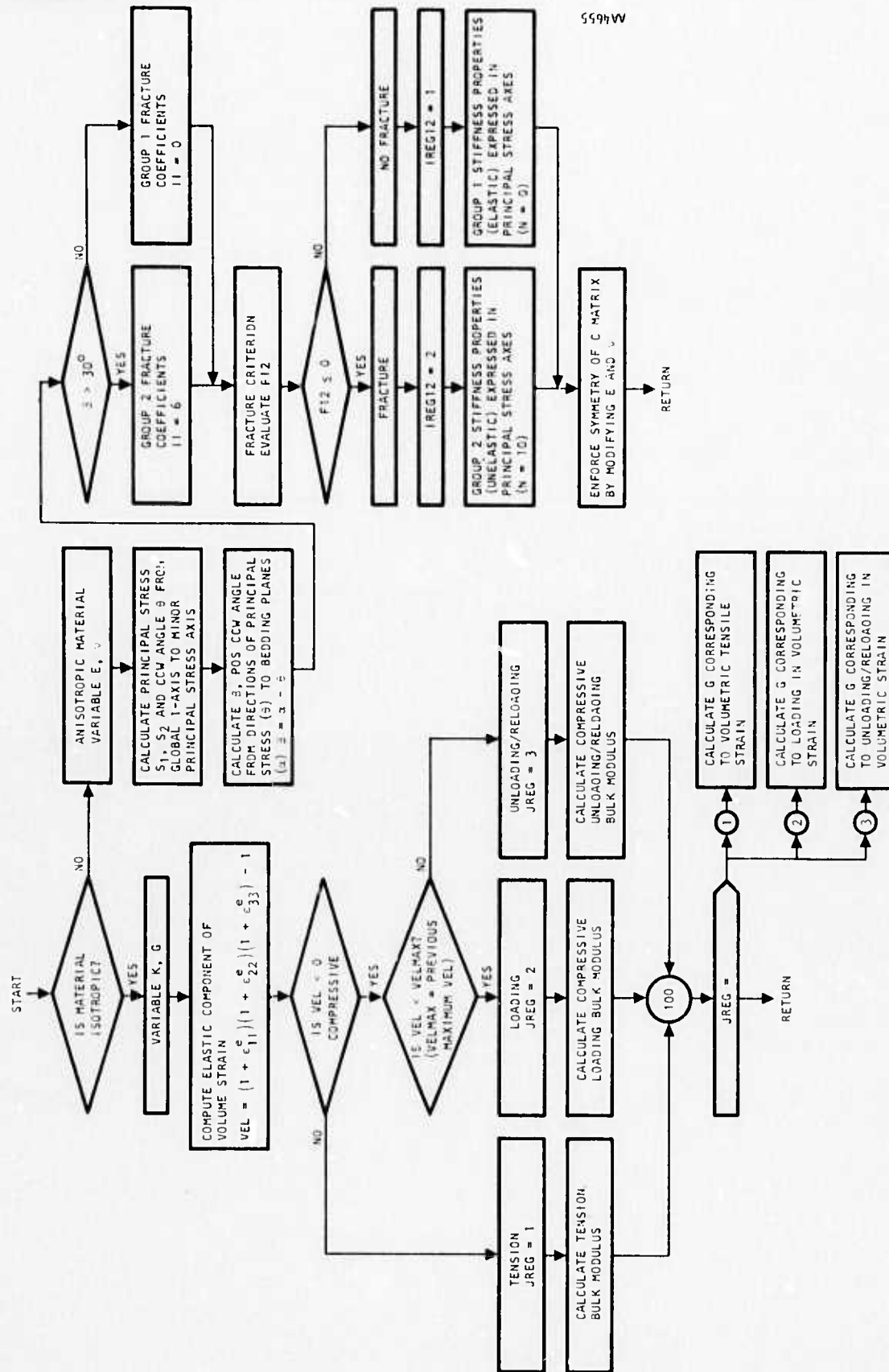


FIGURE A-7. SUBROUTINE INCSTR--INCSTR COMPUTES ELASTIC AND PLASTIC STRAIN INCREMENTS)

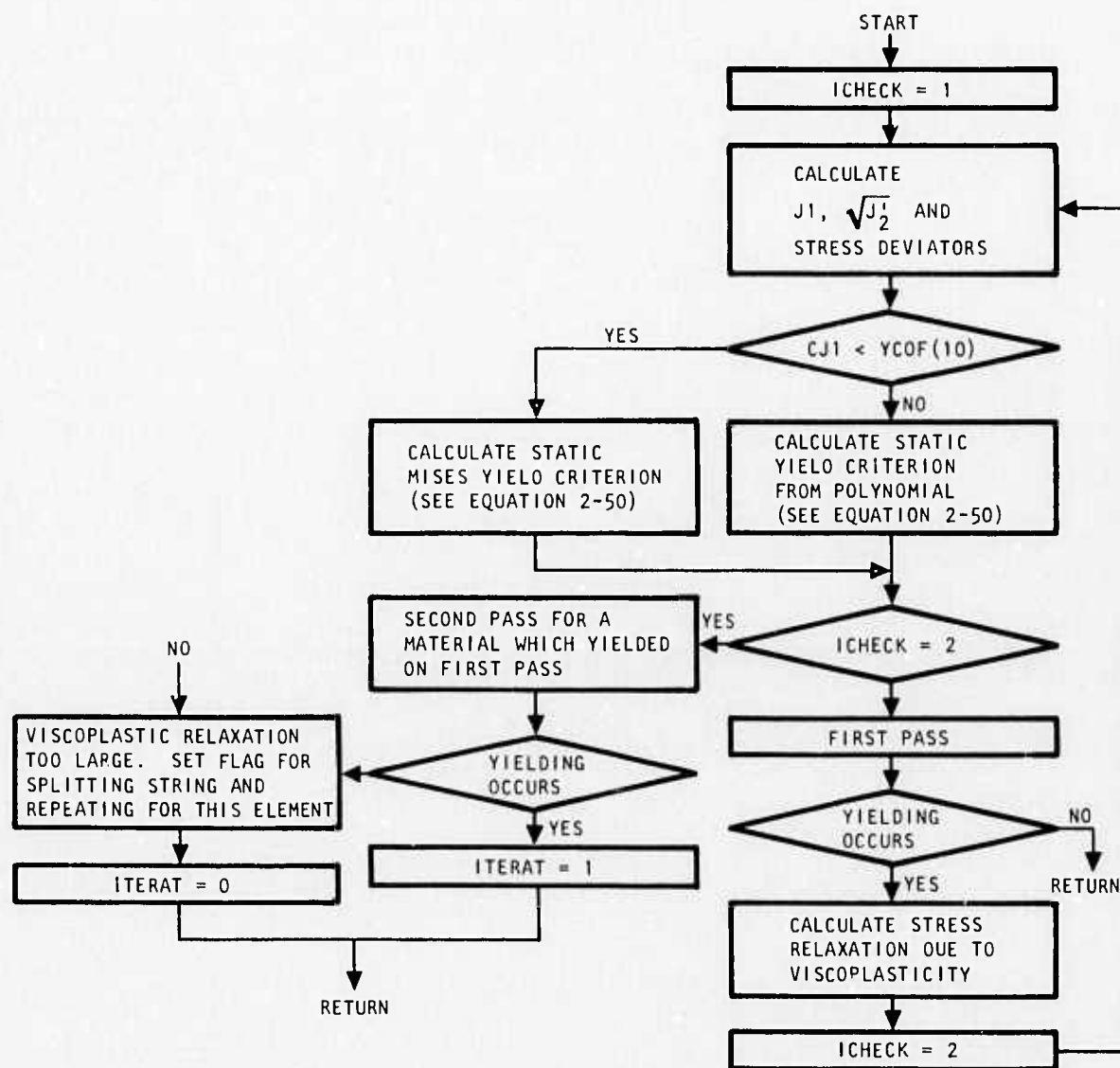


R-7215-1-2701



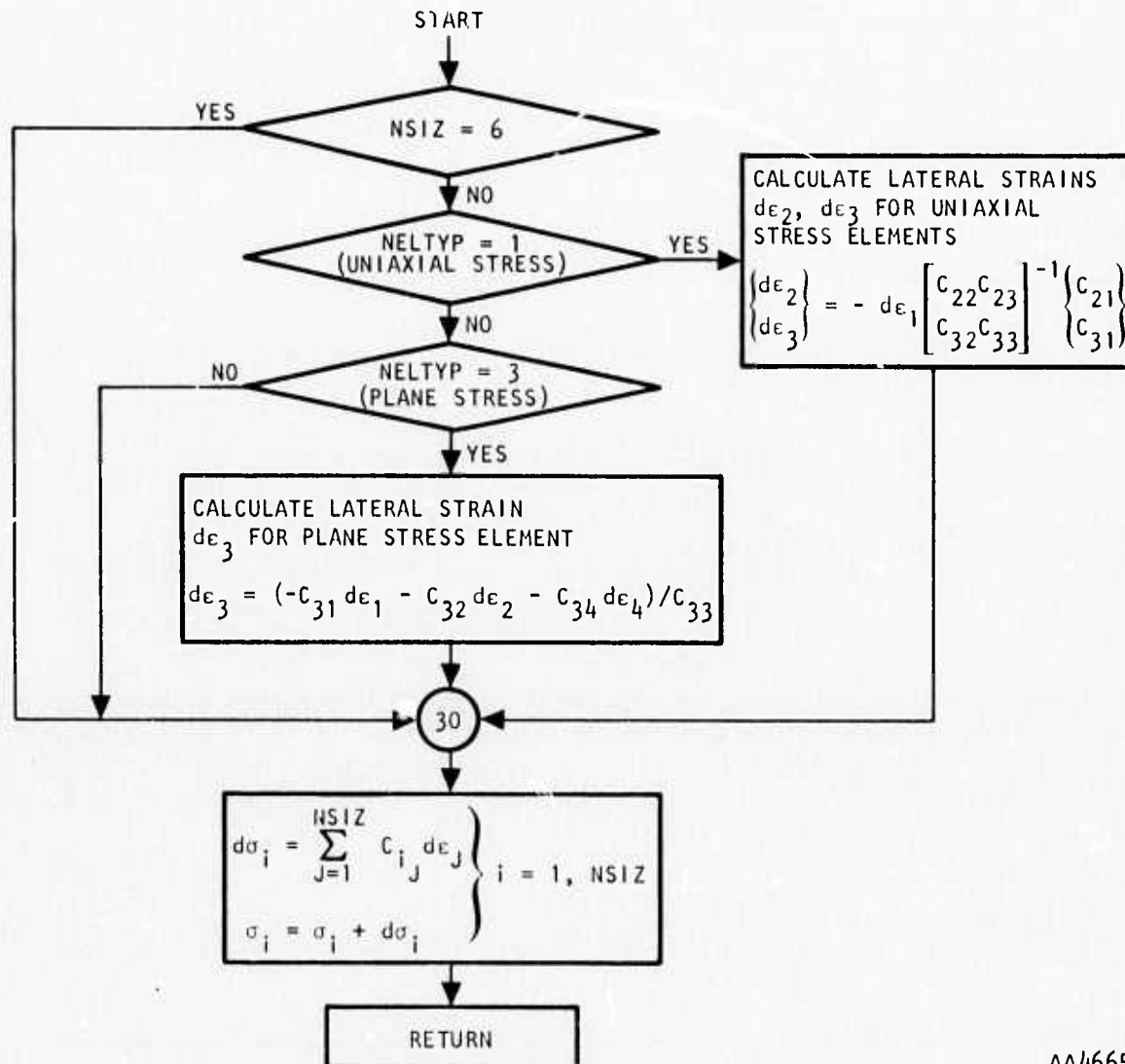
M4655

FIGURE A-8. SUBROUTINE ELFUN--THIS SUBROUTINE CALCULATES VALUES OF VARIABLE ELASTIC MODULI (K, G FOR ISOTROPIC MATERIAL, E, ν FOR ANISOTROPIC MATERIAL). INPUT FOR ISOTROPIC MATERIAL IS CURRENT AND PREVIOUS MAXIMUM VALUES OF ELASTIC VOLUME STRAIN. INPUT FOR ANISOTROPIC MATERIAL IS CURRENT VALUE OF STRESSES.



AA4660

FIGURE A-9. SUBROUTINE VPLAST--THIS SUBROUTINE IS USED FOR A VISCOPLASTIC MATERIAL. IT CALCULATES THE STATIC YIELD CRITERION, DETERMINES WHETHER YIELDING OCCURS AND, IF YIELDING OCCURS, MODIFIES THE STRESSES TO ACCOUNT FOR VISCOPLASTIC STRESS RELAXATION.



AA4665

FIGURE A-10. SUBROUTINE COMPUT--COMPUT CALCULATES STRESS INCREMENTS AND ADDS THEM TO OLD STRESSES TO OBTAIN NEW STRESSES. STRAINS CORRESPONDING TO ZERO STRESSES (PLANE STRESS, UNIAXIAL STRESS) ARE COMPUTED.